The characterisation of fossil bone

Turner-Walker, Gordon Howard

The Characterisation of Fossil Bone

Gordon Turner-Walker

This research presents a multi-disciplinary approach to the analysis of ancient bones, in which many different chemical and physical analytical techniques were applied to a relatively small sample of human and animal bones from different depositional environments. The results of these analyses indicate that the principle mechanisms responsible for diagenetic alteration of buried bones are chemical hydrolysis of bone collagen and microscopic tunnelling by saprophytic micro-organisms. These mechanisms, either independently or together, result in an increase in the porosity of the bone at a microscopic scale from a value of approximately 20 percent in fresh bone up to as much as 65 percent in some archaeological bones. There is no evidence that the hydrolysis of collagen in buried bones directly affects the mineral component of bone, although the breaking of the intimate association between the collagen molecules and the bone apatite crystallites exposes the crystallites to potential dissolution and recrystallization by percolating ground water. Disruption of the collagen-apatite bond has been recognised in optical microscopy of thin sections by loss of the characteristic birefringence seen in unaltered bone when viewed in polarised light. The birefringence in histologically normal bone results from the strongly anisotropic orientation of the bone mineral crystallites imposed by their association with the highly organised collagen fibrils. Loss of birefringence as a result of diagenetic activity is attributed to a randomising of the orientation of crystallites after hydrolytic degradation of the collagen molecule. With progressive loss of collagen the relative calcium and phosphorus contents of fossil bones have been found to increase in proportions close to those of stoichiometrically correct hydroxyapatite. Microscopic and mineralogical studies have suggested that changes in the crystallinity of buried bones may be attributed to the presence of well-ordered crystals of hydroxyapatite in the pore structures of the bones and that these derive from dissolution and re-precipitation of the original bone apatite. However the elemental and isotopic composition of these re-precipitated apatites may not reflect that of the original biomineral due to the incorporation of strontium, uranium fluoride *etc.* from the environment. Dissolution of bone mineral can, in most cases, be associated with the action of micro-organisms, many of which are known to favour low pHs and secrete organic acids as a by-product of their metabolism. Although micro-organisms isolated from buried bones produce collagen degrading enzymes (collagenases) these enzymes are too large to enter the spaces between the bone apatite crystallites and are therefore unable to attack the collagenous matrix of undegraded bone. Before micro-organisms can utilise bone collagen, the bone matrix must first be demineralized to expose the collagen fibrils *or* the collagen must be degraded by hydrolysis into shorter lengths that then escape *via* disrupted regions of the surrounding crystallites. Analysis of the strengths of modern and fossil bones has demonstrated a near logarithmic relationship between tensile strength and porosity. In addition, plots of strength vs porosity and strength vs nitrogen content are bimodal, indicating that two mechanisms are involved in the degradation of fossil bones. The microscopic and chemical analyses suggest that these mechanisms are chain scissioning of collagen and tunnelling by micro-organisms. Microscopic studies show that surface adsorption of 'humic acids' and metal ions are responsible for the colouration of fossil bones. Analysis of the total lipid extract of fossil bones contain cholesterol and cholesterol degradation products. Fossil cholesterol represents a potentially important and unique resource for palaeodietary studies. Conversely, this research has demonstrated that studies of ancient DNA are compounded by inhibition by compounds from the soil and contamination by modern DNA. Fossil bones in anoxic or waterlogged soils are readily colonised by sulphate-reducing bacteria and these bacteria are responsible for the deposition of iron sulphide in the form of pyrite framboids in pore spaces in the bone. On exposure to atmospheric oxygen, these pyrite framboids oxidise to sulphuric acid which in turn attacks bone apatite, resulting in the formation of vivianite ($Fe_3(PO_4)_2.8H_2O$) and gypsum ($CaSO_4.2H_2O$). Crystallization and hydration of these minerals frequently disrupt the physical integrity of the bone specimens. Finally this research indicates potential regimes for the conservation of fossil bone specimens together with the archaeological or environmental evidence preserved within them.

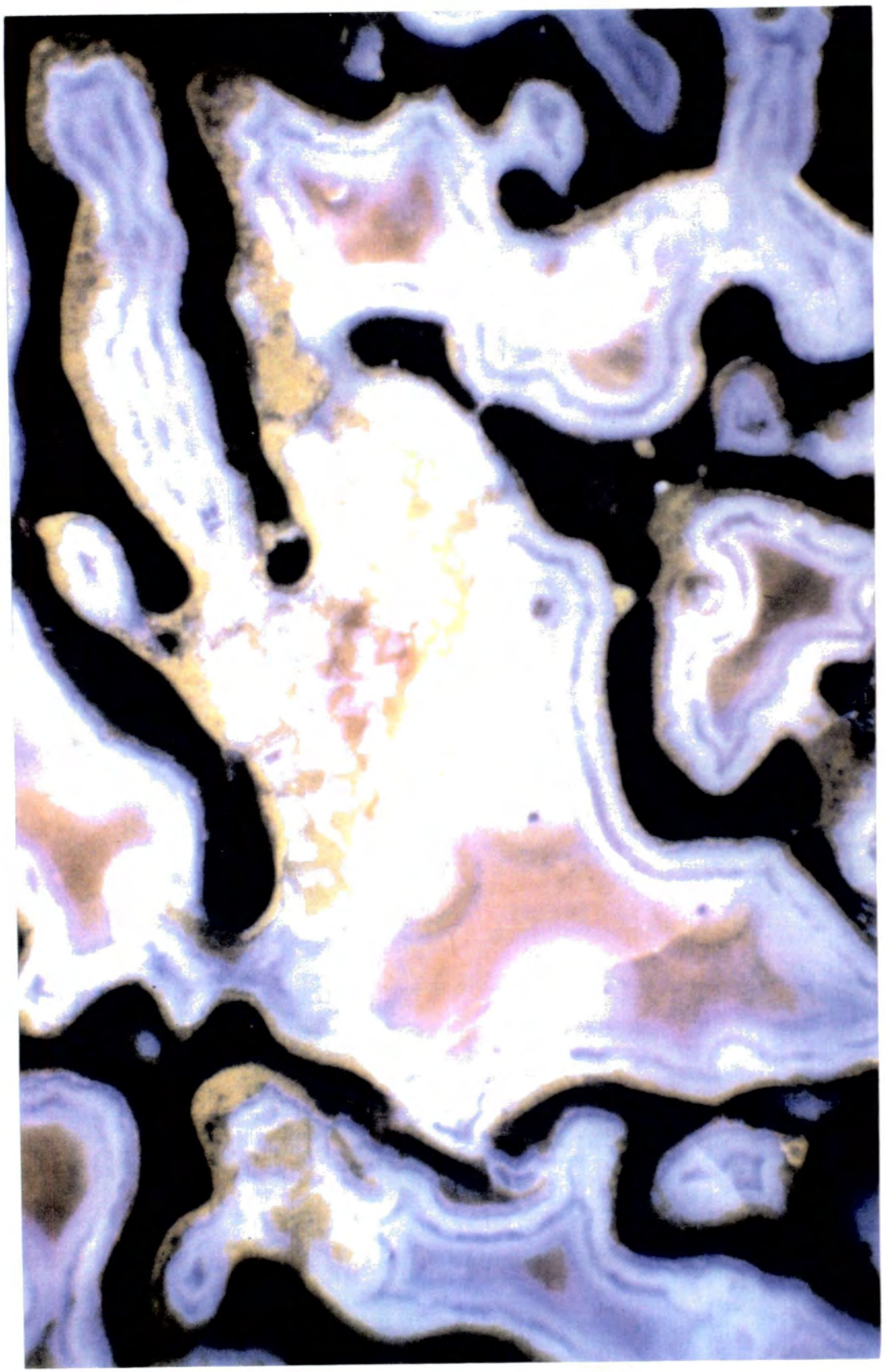

Frontispiece Polished section of unidentified dinosaur bone. The dark material represents the original bone and the coloured material is siliceous mineral infilling the pore spaces between the trabeculae (field approximately 4mm x 6mm)

The Characterisation of Fossil Bone

Gordon Howard Turner-Walker

Thesis Submitted for Doctor of Philosophy

University of Durham
Department of Archaeology

September 1993

Contents

List of Tables

List of Figures

Page

List of Plates

No part of the work in this thesis has been submitted for a degree in this or any other university and , except where expressly stated, represents the original work of the author.

Acknowledgements

This research could not have been completed without the encouragement and guidance of my supervisor Dr C. Caple and other members of the academic and technical staff in the Department of Archaeology and other departments in the University of Durham. I expressly wish to thank Mr P. Clogg, Ms J. Jones, Mr D. Dungworth, Mr R. Coult, Mr R. Hardy, Dr S. Stallibrass, Dr T. V. Parry and Dr J. Cunningham for their assistance. I am indebted to Dr Richard Evershed and Dr Martin Richards for their work on lipid and DNA residues respectively. I should also like to thank Tim Schadla-Hall, Prof. Lawrence Barfield, Dr Colin Hazelgrove and Prof. Willy Child for kindly providing me with samples of bone. Finally, I would like to thank my wife Catriona for reading the manuscript and for all her patience and support. Financial support and facilities were provided by SBAC and SERC.

Introduction

The aim of this research is to identify those characteristics of excavated bones that most influence their chemical and mechanical behaviour once the bones have been removed from their burial environment, and particularly those aspects of their composition that affect the future integrity of the specimens and the quality of the evidence preserved within them. Furthermore, it is anticipated that this study will add to the understanding of processes occurring within bones whilst buried (diagenetic processes).

Living bone is composed of both organic and inorganic components, closely associated at a molecular level to form an extremely sophisticated composite material of great strength and adaptability. Organic and mineral fraction are present in the ratio of 25 percent organic to 75 percent inorganic by weight of dry bone. Of the organic fraction, approximately 90 percent by weight is made up by the structural protein collagen which also makes up the bulk of mammalian skin and tendon. The remaining 10 percent of the organic matter comprises non-structural noncollagenous proteins, mucosubstances and lipids (fatty materials). Intimately bonded to the collagen, which forms a template for the deposition of bone tissue, is a calcium phosphate salt which is generally accepted to conform approximately to the mineral hydroxyapatite ($Ca_{10}(PO_4)_6(OH)_2$). The hydroxyapatite is present in the form of minute crystals or crystallites that lie embedded within rope-like collagen fibres and cover their outer surfaces. As the bone matures, the original collagen template becomes increasingly mineralized by the addition of further crystallites within and between the collagen fibres, resulting in a tough and rigid structure. Throughout the life of the organism, however, this seemingly obdurate material is constantly remodelled to accommodate growth, facilitate the repair of injuries and to meet the demands of metabolic processes and increasing loads upon the skeleton. Once the organism has died, the materials making up bones are no longer constrained by the metabolic processes which, during life, carefully controlled the chemical composition of the bone tissue and its surrounding environment. Following biodegradation of the soft tissues, bones are exposed to a radically different environment in which the bone tissue may react chemically with a much wider range of elements and chemical species, the availability of which in turn depends upon factors such as local geology, water transport, pH, microbial activity, oxygen concentration and temperature. Despite the differences between the surroundings of bone in the living organism and those of the subsequent burial environment, dead bones can survive remarkably well even over geological time scales. This is largely due to the fact that the mineral component of living bone surrounds and shields the collagen from microbial degradation long enough to allow some bones to become buried in a protective blanket of sediments.

This research was originally conceived as part of a much broader programme of work related to the conservation problems presented by freshly excavated skeletal material. In this context the term

conservation refers to attempts to preserve the structural and chemical integrity of excavated material by the application of chemical consolidants or stabilisers and suitable storage environments. The vast majority of skeletal material excavated from archaeological sites is both robust and stable and suffers little serious deterioration during storage. However, it has been recognised for some time that some bone, antler and (to a lesser extent) teeth excavated from certain contexts can exhibit both chemical and dimensional instability subsequent to their removal from the burial environment. Many bone assemblages have survived well for decades, despite the low status that has in the past frequently been assigned to such collections (when contrasted with the importance attributed to pottery or metalwork from archaeological sites) and their consequent poor storage environment. Some prehistoric bones however, particularly those from wetland sites may shrink, crack and warp during drying or suffer considerable deterioration during long-term storage whereas other bones from similar conditions may remain perfectly stable. Since it is often difficult to distinguish stable bones from potentially unstable ones by cursory inspection, identification of those specimens likely to suffer deterioration on drying has usually been empirical. In practice, waterlogged bone has almost invariably been impregnated by a consolidant soon after excavation and whilst still damp. One of the most commonly applied consolidants has been poly-vinyl acetate (PVAc) either by prolonged immersion or vacuum impregnation (Clark 1954). In recent years PVAc has been to some extent been superseded by acrylic resins, either in the form of fine colloidal dispersals (Koob 1984) or dissolved in a suitable solvent such as acetone. One of the most widely used and espoused acrylic resins for conservation purposes is Paraloid B72, an ethyl-methacrylate/methyl-acrylate co-polymer. Despite the arguable improvements in the properties and reversibility of the materials applied to excavated skeletal materials in recent years, the decision to use them on any particular specimen continues to be made on a rather *ad hoc* basis. This situation is likely to persist in the absence of a clearer understanding of the gross physical and chemical changes that skeletal material undergoes during burial and unless a simple diagnostic test can be developed to assess the current and future stability of a given specimen. Also, in the light of recent developments in the retrieval of genetic, imunological and other biomolecular evidence from ancient bones, even from bones millions of years old, the routine use of fungicides, biocides and consolidants must be tempered with extreme caution. Although the treatment of freshly excavated bones with some sort of consolidant can have obvious advantages in the short term, there is a serious risk of compromising future chemical or immunological analysis. On the other hand, it could also be argued that some important collections may well not have survived to the present day without the application of consolidants.

Although there is an enormous corpus of research into the composition of ancient bones, particularly human or fossil hominid bone, the vast majority has focused on subtle variations in trace element concentrations with a view to dating individual bones or exploring the diet of past populations. Comparatively little work has examined those physical and chemical characteristics that contribute to the behaviour of bone as a material once it has undergone diagenetic alteration. Previous studies

that have examined the gross behaviour of archaeological bones are Ellam's experiments in the freeze-drying of waterlogged bones (Ellam 1985a, 1985b), work on the responses of bone and ivory to fluctuation in ambient relative humidity (by Bunn 1985; Lafontain & Wood 1982 respectively) and work on the tensile strengths of archaeological bones by Battaglia (Battaglia 1985).

In contrast to previous research, the scope of this work intended to examine the composition and properties of skeletal remains from a variety of depositional environments, using a number of different analytical techniques and approaches, to determine those factors which influenced the physical and chemical behaviour of individual specimens and which measurements could best be used to characterize their condition. Because of the structural and compositional differences between bone, antler, dentine and tooth enamel, this study was restricted to bone tissues alone. In addition, compact bone taken from the shafts of long bones was used in analysis wherever possible. A number of different techniques have been used in this investigation, some requiring sophisticated analytical equipment, others involving relatively simple procedures and facilities commonly found in the most basic laboratories in the hope that such techniques could be adapted to form the basis of a rapid and cheap assessment of the condition of bone assemblages. Because of the relatively small number of samples examined and since the specimens chosen for analysis were selected on the basis of apparent differences in their states of preservation (as opposed to a large number of similar samples) statistical analysis of the results has been kept to a minimum. Similarly, since the object of the research was to identify gross trends in the characteristics of the selected samples, there was concern that a sophisticated statistical treatment of the data may obscure these trends by highlighting possibly spurious correlations between factors that were, in reality, unconnected.

Building upon the work of previous researchers, this project employed several analytical techniques already widely used for the investigation of skeletal materials. These included microscopical examination of specimens (both in thin section and of the broken surfaces of small fragments), X-ray diffraction analysis and infrared spectroscopy. The chemical composition of specimens was determined using a combination of carbon, hydrogen and nitrogen analyses (where the elemental concentrations are calculated by combustion of the sample) to examine the organic component of the bones, together with X-ray fluorescence spectrometry to explore changes in the bones' mineral fraction and quantify the ingress of exogenous elements from the soil. In addition, the effects on bone of changes in atmospheric moisture content were explored by monitoring the weight of water absorbed by the bones' structure both in conditions in which the specimen was in equilibrium with its environment and in dynamic conditions.

The tensile strengths of fresh (unburied) bones and ancient (buried) bones were determined using a technique not previously used in the examination of skeletal materials. Use of the diametral compression or 'Brazilian' test to determine the tensile strength of bone permitted very small samples

to be examined. This had two major advantages, firstly the use of a small sample rather than using a single, large portion of the bone specimen meant that there was a reduced chance of the test piece failing at a point of weakness unrepresentative of the whole bone. Secondly, several samples could be tested from a single bone specimen, giving a better picture of the strength of the bone as a whole and highlighting spurious or potentially misleading results.

Because this research was intended to cover bones from a wide range of depositional environments and ages the term 'fossil', being derived from the Latin *fossilis* meaning dug up, has been used throughout, irrespective of the age or appearance of the specimen. This definition of fossil bone, as any bone that 'is dead, buried and dug up' has become increasingly adopted by researchers into bone diagenesis in recent years. Other terms; archaeological bone, permineralized-, sub-fossil- or fossil bone are frequently subjective in their use and depend to a great extent on the discipline of the person examining the specimen.

Because of the growth of interest in the biomolecular evidence preserved in fossils in general and bones in particular, it was decided to examine some specimens for surviving biomacromolecules. Since the study of such complex molecules is a highly specialized discipline and requires very specific techniques and equipment, this work was done in collaboration with other specialists. The techniques chosen were the extraction and amplification of genetic markers (DNA) and the extraction and analysis of lipids. In both cases, sample selection was done by the author and in the case of the lipid analysis, sample preparation was also done by the author. However, interpretation of the results was done by a relevant specialist in each case: Dr Richard Evershed of the Department of Biochemistry, University of Liverpool and Dr Martin Richards of the Institute of Molecular Medicine, John Radcliffe Hospital, Oxford.

Since much of the existing work on fossil bone has been published by specialists in the fields of anatomy and orthopaedics or by archaeometrists with backgrounds in chemistry and the physical sciences, many papers presume a considerable understanding of both the structure and chemistry of bone and the applications of sophisticated analytical techniques. In order to place this particular research in context and to provide a broad foundation for future investigations, Chapters one and two present an exhaustive review of the nature of bone and the interpretation of fossil bones respectively, from the earliest work to the most recent. The review of current analytical work on fossil bones presented in Chapter two also serves to highlight the importance of skeletal material as a source of evidence for many disciplines, ranging from medicine to ecology, and to stress the need to preserve as much of that potential as possible following discovery and excavation. Because many different analytical techniques were used in this study, the work has been presented in such a way that a brief description of the techniques, the experimental methods and the results for each analytical approach occupy a separate Chapter, with different sections being cross-referenced where necessary. To avoid

a lengthy and unwieldy chapter containing an interpretation of all the results, and so that each chapter could in effect 'stand alone', a brief discussion is given together with the results of the analyses in each of the relevant sections. The discussion and conclusions presented in Chapter 10 draw together the salient points of the previous chapters and set them in into a wider picture. As a result of this presentation it is inevitable that there will be a certain amount of repetition between different chapters. Similarly, because a multi-disciplinary approach has been used in this research, some of the analytical techniques or equipment used have been described in considerable detail as a means of introducing non-specialist readers to the concepts involved.

1. The Nature and Properties of Bone

The term bone may be used to describe a single member of those parts that together form the skeleton of vertebrate animals. It may also denote the hard, inflexible tissue of which the skeletal components are composed. Bone performs a multiplicity of functions in the bodies of living organisms. It supports the shape of the animal against the force of gravity, provides a rigid and protective envelope around vital organs (such as those in the cranium and thoracic cavity) and furnishes a system of inflexible levers that multiply the forces generated by muscle contraction, translating these into locomotion. The common perception of bone as an inert tissue is far from the truth, in fact it is immensely adaptable and may be considerably remodelled during the life of a single organism. For example, in an adult human the skeleton contains approximately 1.2kg of calcium of which 4g is available for rapid exchange with the extracellular fluid or plasma. The average daily turnover of calcium moving into and out of the bone tissues is 0.5g compared to an average daily dietary intake of 1g (Berne & Levy 1990, 516-517). The same basic form of the skeleton, derived from the earliest fishes, has been gradually but extensively modified to meet the very varied demands of amphibians, reptiles, mammals and birds in a multitude of forms. Organisms as disparate as the giant dinosaurs and smallest humming birds have shared a common structural material and similar skeletal architecture, thus demonstrating the remarkable versatility of bone.

At a cellular level, bone performs an equally crucial role in maintaining the balance of mineral salts in the blood and hence in the soft tissues of the body. This equilibrium or 'mineral homeostasis', particularly with respect to ions of calcium, sodium, magnesium and inorganic phosphate, is essential for the correct function of many of the body's cellular mechanisms (Vaughan 1975, 25-27). The role of the skeleton as a reservoir of calcium ions is especially important. The bones contain 99% of the human body's calcium, an element that is essential for the activity of some enzymes and plays a crucial role in the contraction of muscles, the transmission of nerve impulses and the clotting of blood (Junqueira *et al.* 1986). In the case of lactating females and in instances where there are special demands, such as the annual growth of antlers in deer, this reserve is crucial. The bones also act as a depository for the storage of unwanted or toxic metal ions poisonous to the body's soft tissues such as lead, strontium and uranium (Posner 1985a). Such elements are often described as 'bone seekers'.

Bone is the hardest tissue in the body after dentine and enamel, yet at the same time possesses remarkable toughness and durability. It is a highly specialized connective tissue that has become adapted to withstand the compressive forces arising from the force of gravity and the complex loads imposed by the demands of locomotion. Increased resistance to these loads is achieved by the intercellular deposition of inorganic mineral salts composed principally of calcium, phosphate and

carbonate. At the same time bone is able to resist tensile forces and has excellent resilience to impact and deformation due to the presence of long collagen (protein) fibres in close association with the inorganic phase.

Unlike the largely avascular cartilage, to which bone is related, bones are provided with an extensive network of blood vessels ensuring a constant supply of nutrients to the tissues which, in turn, facilitates the growth, repair and remodelling of skeletal members. The shapes of bones are modified by the gradual and continuous destruction of bone tissue and its subsequent replacement with new bone. Thus, bone is a dynamic tissue in a constant cycle of resorption and growth throughout the life of the animal. This plasticity of bone allows it to respond appropriately to the demands of changing forces as the animal grows in size and strength. For example, the long bones of foetal humans are near-circular in cross-section but acquire a more triangular section during early childhood due to the development of the muscles of the limbs and the asymmetric loads applied during walking. Similarly, the positions of the teeth in the jaw may be modified by lateral pressure applied by orthodontic devices (Junqueira *et al.* 1986, 158). By this mechanism of remodelling to accommodate additional loads, each bone, in effect, bears testament to the stresses borne in its recent past, so that the bones of bodybuilders and weight lifters become heavier and stronger as the musculature develops and loads increase. This picture of bone and the skeleton itself as a living and responsive tissue is in marked contrast to its popular conception as an inert framework, supporting animate flesh.

1.1 The Structure of Bone

At a macroscopic level, two types of bone structure may be distinguished when mature, healthy bones are examined:

> compact or *cortical* bone, which forms the tubular shaft of long bones and the external surfaces of others.

and

> spongy or *cancellous* bone, an interpenetrating network of fine buttresses or *trabeculae* that make up the ends of long bones and fills the core of flat, tabular bones such as those of the skull, sternum and ribs.

The arrangement of the trabeculae in the jointed ends of long bones closely follows the principle lines of stress, forming two sets of buttresses intersecting at angles close to a right angle. This arrangement, which is particularly striking in the case of the human femur (Figures 1.1-1.2) was first

noted by Ward and Meyer in the early 1800's and later elaborated on by Wolff (1892). The apparent 'crystallization of lines of force' is sometimes referred to as 'Wolff's law'. This pattern is not present at birth but develops as the loading on the leg increases with increased mobility. It is clear that there is a positive feedback mechanism by which areas of bone under tension or compression are reinforced by the addition of further material whereas bone that is not stressed is removed. The result of this mechanism is a structure from which all unnecessary or redundant weight has been removed and yet with the strength and flexibility to accommodate the complex stress patterns produced by running and jumping. In mature individuals, the spaces between the trebaculae in the ends of long bones are filled with *red marrow*, which is responsible for the production of blood cells. By contrast the hollow shafts of long bones contain *yellow marrow*, which is largely fat.

At a microscopic level, the structure of bone is examined in thin sections, the study of which is called *histology* from the Greek words *histos* and *logos* meaning 'tissue' and 'word' respectively (Drury & Wallington 1980, 1). The term histology refers to the study of all animal tissues, which are normally embedded in a soft substrate such as paraffin wax before being cut into fine slices using a *microtome*. These slices may then be stained and examined using light or transmission electron microscopy. Because bone is both much harder and more brittle than the body's soft tissues it is difficult to section with a microtome in the usual way. Specimens are either demineralized using mineral acids or a calcium chelating agent such as ethylenediamine-tetraacetic acid (EDTA) before sectioning in the same way as soft tissues or, alternatively, sawn sections of whole bone are ground and polished with abrasives to the required thickness (see 3.1.1).

In light microscopy, a wide range of structures is visible in thin sections of whole bone, even without staining. In mature compact bone the most striking of these features are the numerous circular structures. At the centre of these features lies a canal that encloses blood vessels, nerves and loose connective tissue and around which bone cells are arranged in concentric layers. This whole complex of concentric lamellae of bone surrounding a *Haversian canal* is called a *Haversian system* or *osteon*. Haversian systems represent secondary bone tissue that has been deposited during remodelling of primary bone. Primary bone tissue or woven bone is the first to form in bone growth and repair. This temporary structure is gradually replaced by resorption around blood vessels and subsequent deposition of secondary bone, leading to the characteristic form of osteons. Immature or woven bone often persists in the area of tendon insertions and ligaments although these themselves may become mineralized in old age. Primary bone tissue has an irregular arrangement of collagen fibres, a higher proportion of bone cells or *osteocytes* and a lower mineral content than the denser secondary bone. During growth then and throughout adult life, there is a continuous destruction and rebuilding of Haversian systems and this succession is often reflected in overlapping osteons. Primary bone can often still be distinguished in the outer and inner circumferential lamellae lying

close to the external and internal surfaces of bones (Figure 1.3). This has led some texts to describe the structure of bone as having an inner and outer layer separated by Haversian bone (Chaplin 1975).

1.2 Bone as a Tissue

Bone cells fall into three different types:

> *osteoblasts*, which synthesize the organic constituents of bone
>
> *osteocytes*, resting cells that are found in small cavities or *lacunae* within the bone
>
> *osteoclasts*, large cells with many nuclei that are responsible for the destruction and resorption of bone.

Osteoblast cells are responsible for the synthesis of *osteoid tissue* or the uncalcified proteinaceous precursor to bone. These comprise, Type 1 collagen (see 1.4), proteoglycans and glycoproteins. The osteoblasts are situated at the surfaces of bone tissues where they form a layer one cell thick. They are present in the *periosteum* and *endosteum*, the soft tissues forming the outer and inner surfaces of bones respectively, where they play a prominent role in bone growth and repair. Osteoblasts are also found in the epiphyseal plate of growing bones where they form an osseous matrix on the remnants of calcified hyaline cartilage. This hyaline cartilage separates the bone shaft or *diaphysis* from the articulating end of the bone or *epiphysis* and growth takes place by the addition of new cartilage which forms a model or template which is gradually translated into new bone. On reaching maturity the hyaline cartilage ceases to grow and calcification causes the *epiphyses* to fuse with the diaphysis preventing further elongation, although the bone may increase in thickness and strength by the deposition of new bone by the periosteum. Other key cells in the synthesis of bone tissues are *fibroblasts* which are also found in connective tissues. They are responsible for the synthesis of extra-cellular collagen and *ground substance*, a mucopolysaccharide-protein complex found in bone and the dermis of skin. Fibroblasts are found at the periosteal surface where new bone is being deposited.

Osteocytes are single osteoblasts that have become enclosed by the surrounding bone tissues. They occupy almond-shaped spaces called *lacunae* between adjacent lamellae and are regularly spaced around osteocytes and throughout lamellar bone. Osteocytes are not isolated however and communicate with neighbouring cells and ultimately with blood vessels via fine filaments or extensions known as *filopodial processes* passing through *canaliculi* in the surrounding bone tissues (Figure 1.4). These interconnecting processes permit the flow of ions, hormones and nutrients between osteocytes and the removal of metabolites or waste products. A chain of up to 15 successive osteocytes may be supported from any blood vessel.

Osteoclasts are comparatively much larger cells, containing up to 50 nuclei, that are responsible for the breakdown and resorption of bone tissue. Electron micrographs reveal that the surfaces of osteoclast cells actively resorbing bone have a corrugated or ruffled border where they are in contact with bone tissue. It is thought that these folds increase the active surface area and provide pockets where bone may be isolated and subjected to enzymatic attack. Some observers report calcium containing crystals and disintegrating collagen fibres in the spaces between these folds (Vaughan 1975, Figure 2.41; Ham & Leeson 1961, 292-296). Although the precise role of osteoclasts is not yet fully understood, it is known that they secrete acid, collagenase and other proteolytic enzymes and that they are responsible for the removal of the debris resulting from bone resorption.

1.3 Bone Chemistry

The hard mineralized tissue of bone is made up of both organic and inorganic components, generally understood to be collagen and calcium phosphate respectively. These mineralized tissues, often termed 'vertebrate hard tissues' have an extremely ancient origin and occur in various forms throughout the fossil record. Recent work on a group of fossil elements called *conodonts* has confirmed that these tooth-like structures represent the grasping mouth-parts of primitive marine animals resembling eels (Briggs 1992). These elements are extremely small, measuring between 0.2 mm and 2 mm in length, and composed of the calcium phosphate mineral carbonate fluorapatite. Investigations of the micro-structure of conodont elements have shown that they bear many features in common with the hard tissues (such as calcified cartilage, bones and teeth) of more advanced vertebrates (Sansom *et al.* 1992). These latest discoveries push back the origin of bony tissues and consequently our ultimate ancestors, to the Late Cambrian period, over 500 million years ago.

There is considerable variation in the figures quoted in the literature for the relative proportions of organic and mineral matter. Some authors state that inorganic matter accounts for approximately 50% of the dry weight of bone (Junqueira *et al.* 1986), whereas others quote values of 70% inorganic salts to 30% protein (Young 1975) and 60% to 40% (Posner 1985b). Gray's Anatomy (first published 1858) describes bone as consisting of an 'animal and an earthy part intimately combined together' and quotes the proportions as one third organic to two thirds inorganic. Of the earthy matter, he goes on to say that 'five sixths is calcium phosphate with the remainder consisting of calcium carbonate, calcium fluoride, calcium chloride and magnesium phosphate' (Gray 1992). After more than one hundred years there remains considerable disagreement over the composition of bone mineral and its relation to the organic component. Although there can be some natural variation in the composition of bone tissues, arising from differences between different species, age of the individual and part of skeleton sampled, some of the confusion over relative proportions of

organic and inorganic matter probably arises as a result of different extraction techniques and the high capacity of fresh bone for adsorbed water. Estimates of mineral content based on the ashing of bone are invariably too high because loss of adsorbed water and the thermal decomposition of carbonate is unwittingly included as 'organic' (see Table 1.2). Reliable figures for the composition of whole, air-dried, bovine cortical bone were given by Eastoe and Eastoe as early as 1954, and are set out in Table 1.1. Table 1.3 is taken from Vaughan (1975, 59) and shows the composition of bovine cortical bone derived from Eastoe & Eastoe and other sources. Here, water has been excluded from the figures quoted in Table 1.1 by drying the bone at 105°C. It also shows that non-collagenous organic material accounts for approximately 11 percent by weight.

Composition of dry bovine bone	wt.%
Inorganic matter (insoluble in hot water)	69.66
Inorganic matter (soluble in water)	1.25
Collagen	18.64
Mucopolysaccharide-protein complex	0.24
'Resistant protein'	1.02
Fat	0.00
Carbohydrate (sugars)	0.00
Water (lost below 105°C)	8.18
Total	98.99

Table 1.1 Composition of air-dried compact bone tissue (from Eastoe & Eastoe 1954).

Total inorganic content	wt.%
Unashed (from Table 1.1)	70.91
Ashed at 450°C	70.1
Ashed at 500°C	68.7
Ashed at 550°C	67.9

Table 1.2 Inorganic matter in bone as determined by ashing (from Eastoe & Eastoe 1954).

Composition of dry bovine cortical bone:	wt.%
Inorganic matter	77.23
Organic matter	22.77
Composition of organic matter:	
Collagen	89.15
'Resistant protein'	4.87
Mucosubstances	1.14
Sialoprotein	0.81-1.15
Glycoprotein	0.31-0.44
Lipids	0.42
Peptides	0.54
Total	97.24-97.71

Table 1.3 Composition of dry bovine cortical bone (from Vaughan 1975, 59).

1.4 Bone Collagen

Collagen is the most important and ubiquitous protein in the vertebrates, where it accounts for approximately one third of the total body protein and is the major structural constituent. It is found in bones, skin, tendon and in the connective tissues joining and supporting the internal organs. It occurs in smaller proportions in the invertebrates such as insects, spiders, coelenterates (*e.g.* sea anemones) and sponges and no animal *phylum* has been found that does not contain at least some collagen in its structure (Woodhead-Galloway 1980).

Of the total collagen in vertebrates, approximately 40% lies in the skin, 10-20% in skeletal tissues such as cartilage and bone (where it forms the organic scaffolding around which mineralization takes place) and a few percent in blood vessels. Tendon, the inextensible cord-like tissue that translates the contraction of muscles into movement of the skeleton, is almost entirely composed of collagen. *In vivo* collagen, such as that contained in bones and skin, always contains up to 50% water, a 'ground substance' of mucopolysaccharides and traces of various fats or lipids (Woodhead-Galloway 1980).

The collagen molecule is a protein composed of countless, unbranched sequences of approximately 20 different amino acids joined by peptide bonds. It has a characteristic 'signature' of amino acid composition with glycine accounting for one third of its residues, the other major constituent amino acids being proline, hydroxyproline and alanine. Hydroxyproline is not a naturally occurring free amino acid but is derived from proline after incorporation in the protein. Hydroxyproline is rarely found in other proteins but amounts to one in ten of the amino acids in collagen (Woodhead-Galloway 1980, 12). From the amino acid composition it is possible to estimate the molecular weight of collagen, which is close to 100,000. Direct experimental evidence, however, gives a much higher value of around 300,000. This apparent contradiction is resolved if each collagen molecule is composed of three amino acid chains bound together as a trimer.

Ramachandran and Kartha (1954) proposed a model for the structure of collagen, based on the evidence above. They proposed that each of the three amino acid chains is twisted into a left-hand helix (called the alpha helix) with three amino acids in each successive turn (Figure 1.5a). This picture corresponds well with every third amino acid being glycine. Three of these alpha chains are then twisted together in a right-handed helix with glycines in the centre, forming the tropocollagen macromolecule. The three chains are tightly held together by hydrogen bonds (Figure 1.5b). Differences in the sequence of amino acids in the alpha chains (the so-called primary structure of the protein) and the possibility of covalent cross-links between adjacent chains in the triple helix, leads to the existence of (at least) five kinds of collagen designated Type I to Type V. Bone collagen is Type I collagen and shows peculiar chemical and structural characteristics unique to mineralized

tissues. The triple helical arrangement described above is specific to Type I collagen and is responsible for its characteristic X-ray diffraction pattern (Glimcher 1976). At each end of the collagen molecule, non-helical peptides form sites of cross-links with adjacent molecules.

Although very large, approximately 300 nanometers long (1 nanometer = 1 nm = 10^{-9} m) and 1.5 nanometers in diameter, by the standards of proteins, the collagen molecule is still much smaller than the collagen fibres seen in bone, dentine and other tissues. In fact, collagen is a self-assembling molecule and solutions containing collagen molecules will naturally aggregate into short microfibrils (Woodhead-Galloway 1980, 20). In the extra-cellular matrix, collagen molecules polymerize and aggregate together in a highly organised manner to form fibrils which show the characteristic transverse striations with a repeat period of 64 nanometers (Figure 1.5c &1.7). Evidence from electron microscopy, X-ray diffraction studies and the manner in which collagen molecules may be grown from solution led Hodge and Petruscka (1963) to propose a theory in which collagen molecules are arranged axially and bonded by covalent cross-links, with each molecule staggered by one quarter of its length with respect to its neighbour. The staggered molecules are arranged in such a way that there is a discrete gap between the amino end of one triple helix and the carboxyl end of the next. The model proposed by Hodge and Petruscka has been modified in recent years (Glimcher 1976; Lees *et al.* 1984) to describe tropocollagen molecules aligning in a 'quasi-hexagonal packing scheme' similar to that illustrated in Figure 1.5d. Collagen fibrils form the basic structural unit in the construction of all bone structures where they aggregate into larger collagen fibres and fibre bundles that may be resolved by light microscopy. This tiered structure with successively coiled fibres, reminiscent of rope, is what gives tissues composed of collagen their extraordinary strength and flexibility. It is probably also responsible for the swelling collagenous material undergoes when hydrated, or soaked in ionic solutions, since water and other polar molecules are able to interpose between the fibres.

The gap regions between successive tropocollagen molecules, also called 'hole zones' are accepted to be the nucleation sites for the deposition of bone mineral (Glimcher *et al.* 1957). In bone and other skeletal tissues, the orientation of mineral deposits is closely related to the structure of the organic template or matrix, with crystals aligned with their long axes parallel to the collagen fibrils, a view in close accordance with the models proposed by Hodge and Petruscka and later workers. The close affinity between collagen and the calcium phosphate mineral, hydroxyapatite, is evident in the ability of collagen fibres to nucleate its crystallization *in vitro* at concentrations well below the solubility product for hydroxyapatite (Neuman & Neuman 1958). This model for the epitaxial growth of hydroxyapatite crystals on a collagen template in bones raises the question of why other collagenous connective tissues do not become calcified (except in some pathological conditions). Clearly some inhibitor or crystal poison must be present in these tissues and Fleisch (1964) was able to isolate pyrophosphate as a calcification inhibitor by blocking the seeding sites for crystal growth.

Adenosine triphosphate (ATP), the major fuel for cellular activity, is known to give rise to adenosine monophosphate (AMP) and pyrophosphate ions in the presence of apatites (Halstead 1974, 24). Alkaline phosphatase, which had long been identified in sites of active calcification, has been postulated as responsible for preventing ATP from inhibiting calcification but the role of alkaline phosphatase in mineralization remains enigmatic.

In the body, nucleation of apatite by collagen seems to be mediated by phosphoproteins synthesized within osteoblast cells and extruded into the extra-cellular matrix of mineralizing tissue. Here the phosphoproteins either bind with free calcium ions before being bound on a specific site on the collagen fibril (Glimcher 1984) or are the substrate on which apatite nucleates directly.

1.5 The Nature of Bone Apatites

Just as there have been contradictory reports on the relative proportions of organic and mineral components in bone, there has been possibly even greater confusion about the nature of bone mineral. Table 1.4 shows the composition of the mineral phase of bone, first published in 1894 by Gabriel and reprinted by Dallemagne and Richelle (1973).

Constituent (wt.%)	Human Femur	Cow Femur	Goose Femur
Ca as CaO	36.67	36.65	36.46
Mg as MgO	0.46	0.63	0.77
K as K_2O	0.27	0.15	0.16
Na as Na_2O	0.77	0.81	0.82
P as P_2O_5	15.99	16.35	16.67
CO_2	5.86	5.06	4.11
Cl	0.01	0.04	0.06
F (approx.)	0.23	0.30	?
H_2O	3.78	3.70	4.12
Total	64.04	63.69	63.17

Table 1.4 Composition of (deproteinized) bone mineral (after Dallemagne and Richelle 1973).

The total chemical composition of bone mineral is not in itself a problem, as is demonstrated by the similarity between the values in Table 1.4 and those quoted in a paper by Armstrong and Singer (1965) and reproduced in Table 1.5 (in order to facilitate comparison with Table 1.4, column 3 shows the equivalent percentages for bone mineral after adjustment to compensate for 27% organic matter in whole bone). Rather, the problem is in determining how the different ionic species are combined.

Constituent	wt.%	wt.% (mineral)
Ca	26.700	36.579
Mg	0.436	0.597
Na	0.731	1.002
K	0.055	0.075
Sr	0.035	0.048
P as PO_4	12.470	17.084
CO_2	3.480	4.768
Citric acid	0.863	1.182
Cl	0.077	0.106
F	0.072	0.099
Nitrogen	4.920	n.a.
Total	49.839	61.54

Table 1.5 Composition of dry, fat-free bovine cortical bone (after Armstrong & Singer 1965)

In the early years of this century, Gassman (1911) proposed that the atomic ratios of $Ca:PO_4:CO_3$ were constant in bone, irrespective of age, skeletal part or pathological conditions. This suggested that the three ionic groups were combined in a single molecular complex rather than a simple mechanical mixture of calcium phosphate and calcium carbonate, leading Gassmann to accept the formula for carbonate apatite, $Ca_{10}(PO_4)_6CO_3$, as the major component in bone mineral. This model was supported when De Jong used X-ray diffraction to establish that bone mineral gave a pattern similar to those of the apatite group of minerals (De Jong 1926). Shortly afterwards, Mehmel (1930) postulated that bone mineral was equivalent to a fluorapatite structure in which hydroxyl ions substituted for fluoride in the lattice to give 'hydroxyapatite' $Ca_{10}(PO_4)_6.(OH)_2$ (Eastoe 1960). With improvements in experimental procedures and an increased understanding of crystallography, Klement (1934) was able to demonstrate that the ratios of Ca. PO_4 and CO_3 were actually independent and that the model proposed by Gassmann was untenable. Assuming that the ions Na^+, K^+ and Mg^{2+} were not actually included in the bone mineral but rather existed as carbonates or bicarbonates in the extra-cellular fluids, Klement determined the ratios of $Ca_3(PO_4)_2:Ca(OH)_2:CaCO_3$ to be 3:0.99:0.4. He therefore described the formula for bone mineral as $3Ca_3(PO_4)_2.Ca(OH)_2 + 0.4CaCO_3$, the first part of which is identical to hydroxyapatite. The chemical independence between phosphate and carbonate suggested by the equation above is supported by the observation that, when bone mineral is treated with acids, carbonate is released preferentially to phosphate (Dallemagne & Richelle 1973). The basis of the model proposed by Klement was undermined by the later discovery of an arithmetical error on his part and the correct value of the ratios of $Ca_3(PO_4)_2:Ca(OH)_2:CaCO_3$ were recalculated to be 3:0.71:0.7, making hydroxyapatite a less likely candidate for the crystalline component in bone mineral (Dallemagne, 1942). Dallemagne and Richelle (op. cit., 28-30) have suggested a hydrated tricalcium phosphate generally referred to as 'α-tricalcium phosphate' in which some of the calcium ions are replaced by H_3O^+ or hydronium ions and having the formula $Ca_9(PO_4)_6.H_2(OH)_2$. According to this model, the

mineral component of bones and teeth are composed of a mixture of α-tricalcium phosphate and calcium carbonate.

Dallemagne originally considered the hydrated. α-tricalcium phosphate to be both chemically and mineralogically distinct from hydroxyapatite, despite the obvious similarities in their X-ray diffraction spectra. When heated above 700°C, α-tricalcium phosphate is transformed by the loss of water into β-tricalcium phosphate with the formula $Ca_3(PO_4)_2$ and known to mineralogists as whitlockite. Both hydroxyapatite and α-tricalcium phosphate belong to the hexagonal crystal system but whitlockite is trigonal and has a rhombohedral crystal structure (Bishop 1967, 208-238). On heating up to 900°C, hydroxyapatite shows an increase in crystal size but retains a hexagonal structure. The assumption that bone mineral consisted of α-tricalcium phosphate was, however, seriously undermined when burnt or ashed bone was examined - no rhombohedral structure was discovered (Dallemagne & Richelle 1973, 29). Although experiments with synthetic α-tricalcium phosphate heated in contact with calcium carbonate have demonstrated that calcium ions liberated by thermal decomposition can react with the hydrated tricalcium phosphate to produce hydroxyapatite. there are considerable problems with such a model, most damming being the instability of α-tricalcium phosphate in water where it spontaneously hydrolyses to give hydroxyapatite and free phosphate ions (Dallemagne & Richelle 1973). Blumenthal *et al.* (1975) investigated this reaction by studying the transformation of 'amorphous calcium phosphate' (ACP), taken to be α-tricalcium phosphate, into crystalline hydroxyapatite in solutions of horse and bovine serum at 25°C.

The brief historical overview above serves to underline the great difficulty in assigning a definite chemical or mineralogical classification to bone mineral. One of the reasons for this difficulty is the extremely small size of the mineral particles. In adult human bone. the crystals are between 25 and 35 nanometers long, have widths of the order of 2.5 to 5 nanometers (Posner 1987) and appear as needles or plates in transmission electron microscopes. With unit cell measurements for bone mineral of 9.38 Ångstrom in the *c* or long axis and 6.88 Ångstrom in the *a* or short axis (Hassan *et al.* 1977), there can be no more than a few hundred unit cells per crystal. The extreme small size of the individual bone crystals, or more properly 'crystallites', present an enormous active surface area, estimated at between 100 and 200 m^3g^{-1} (Posner 1985b; Newesely 1989). This large surface area to volume ratio, combined with the highly polarized nature or surface activity of the crystallites has led Neuman and others (Neuman & Neuman 1953, 1958; Posner. *op. cit.*) to conclude that surface chemistry effects dominate both the composition and behaviour of bone mineral. Neuman and Neuman concluded that the deviation of bone mineral stoichiometry from hydroxyapatite, and its lower calcium/phosphate ratio was attributable to the adsorption of HPO_4^{2-} groups on the surfaces of crystallites (Neuman & Neuman 1973, 11), a hypothesis supported by experiments with bone mineral and solutions containing radioactive calcium and phosphate ions (Dallemagne & Richelle 1973. 29).

In 1954, Posner *et al.* proposed that hydroxyapatite, hydrated tricalcium phosphate and another calcium phosphate mineral, octacalcium phosphate, formed a continuous series of apatites containing 8 to 10 calcium ions for every 6 phosphate groups (Posner *et al.* 1954). Their chemical formulae are listed below, together with their respective molar calcium/phosphate ratios:

$Ca_{10}(PO_4)_6.(OH)_2$	1.67
$Ca_9(PO_4)_6.H_2(OH)_2$	1.50
$Ca_8(PO_4)_6.(OH)_2.(H_3O)_4$	1.33

This continuous series of calcium deficient apatites they described by the expression:

$$Ca_{10-x}H_{2x}(PO_4)_6.(OH)_2$$

They explained the inability of X-ray diffraction to distinguish any differences in the crystal structure of all these proposed minerals by suggesting that defect sites were randomly distributed throughout the crystal with H^+ ions substituting for Ca^{2+} in the lattice. Since two H^+ ions cannot occupy the site vacated by one Ca^{2+}, it was further proposed that the hydrogen ions were present in the form of hydrogen bonds between the oxygens of adjacent phosphate groups or as acid phosphates:

$$Ca_9(PO_4H)_2(PO_4)_4(OH)_2$$

Although this theory had a certain elegance and simplicity, there was no chemical, structural or thermogravimetric evidence for the presence of hydrogen ions in bone apatite and it retained the concept of a mechanical mixture of calcium-deficient apatite and $CaCO_3$, a model that was rapidly losing favour.

Newesely has written extensively on the nature and behaviour of apatites, with particular reference to bone apatite. In one of his few English language publications (Newesely 1989) he gives an excellent overview of the inorganic phase of bone, which he considers as composed of crystalline, paracrystalline and amorphous phases. In common with earlier researchers, he attributes the departure of bone apatites from pure hydroxyapatite to the small size of the crystallites, the consequence of which is that many of their constituent ions lie at or near the surface. In addition, the surface activity of the crystallites leads to adsorption, ionic exchange and isomorphous exchange with ionic species present in body fluids bathing the extra-cellular bone tissues. Rules for substitution are based primarily on space considerations, symmetry factors and polarization behaviour and not solely on the charge distribution in the hydroxyapatite lattice. Ions substituting in the lattice generally have the same valency as the exchanged ions but differences in valency may be

overcome in coupled substitutions (simultaneous exchange at cationic and anionic sites) and ionic exchange, irrespective of charge differences, may take place so long as electrical neutrality is preserved (Newesely 1989). Ultimately, this leads to the inclusion of carbonate, citrate, fluoride, and traces of magnesium, strontium, barium and sodium in bone apatites. Traces of silica have also been found and there is a suggestion that this element plays a crucial role in normal skeletal development (Francillon-Vieillot *et al.* 1990). Compared to pure hydroxyapatite, bone apatite has a 40% deficiency in OH^-, a Ca/P molar ratio closer to 1.5 than 1.67, 5 weight percent or more CO_3^{2-}, 5-10% water (half of which is structural in the lattice), up to 10% HPO_4^{2-} (acid phosphate) and a few percent of Cl^-, F^-, Na^{2+} and Mg^{2+} (Newesely 1989).

If basic calcium phosphate is precipitated from a solution containing carbonate or hydrogen-carbonate, at room temperature, the product is an apatite that invariably contains carbonate up to a few percent (Posner 1985, 91). These conditions are close to those in the body and the resulting apatites are structurally similar to biological apatites. In fact, Posner states that carbonate is so readily incorporated into the hydroxyapatite structure that the preparation of carbonate-free hydroxyapatite requires stringent controls of both reagents and reaction conditions. Strictly carbonate-free solutions and a thorough purging of the laboratory apparatus with nitrogen are required if pure hydroxyapatite is to be precipitated (Posner 1985, 91). If no precautions are taken, the resulting hydroxyapatite incorporates approximately 1% weight percent of CO_3^{2-}. Biological apatites precipitated from body fluids contain approximately 4% CO_3^{2-}(Posner 1985). The substitution of CO_3^{2-} ions in PO_4^{2-} positions results in structural distortions in the atomic lattice of small crystallites, arising from the strain induced by introducing a planar CO_3^{2-} ion into a position vacated by a tetrahedral PO_4^{2-} ion. The resulting misalignment of lattice planes significantly contributes to the X-ray diffraction peak broadening observed in biological apatites.

The presence of the carbonate ion is crucial in determining the size and solubility of bone mineral crystallites. Carbonate has the effect of substantially reducing the crystallinity of apatites and large amounts of carbonate result in an essentially amorphous product. Incorporation of CO_3^{2-} in apatite also results in increased solubility due to this reduction in crystallite size and corresponding increase in surface area (Sillen and LeGeros 1991). Strain in the crystal lattice due to incorporation of species with different ionic radii also contributes to solubility. The large surface area and ready solubility of biological apatites have clear advantages in maintaining mineral homeostasis in the living organism.

Newesely describes the carbonate containing apatites as belonging to a continuous binary series, with hydroxyapatite and calcite as its end members. Both calcite and apatite occur as highly ordered crystalline solids but each is increasingly disordered by the addition of the other and the mid point is an amorphous solid. The main problem with the carbonate containing apatites is the question of whether carbonate forms an integral part of the crystallite lattice, is adsorbed onto the surface or

forms a separate phase altogether. In a crystal growing from solution, if a carbonate or phosphate ion reaches the surface it may be fixed or captured by a Ca site. Because the phosphate bond is stronger than that with carbonate, the growing crystal discriminates against carbonate. Also, since the carbonate ion cannot exchange sites with its neighbours by diffusion, any exchange must take place by dissolution and recrystallization (Newesely 1989, 238). A rapidly precipitated, high carbonate apatite is unstable with respect to one with a lower CO_3^{2-} level and will, under the right conditions, recrystallize (by dissolution and recrystallization) to one containing less carbonate. Carbonate may also substitute for hydroxyl ions in hydroxyapatite, although this is usually restricted to hydrothermal reactions in geological specimens. X-ray diffraction studies have shown that there is a significant reduction in the lattice parallel to the a axis when CO_3^{2-} replaces PO_4^{3-} and a decrease in the lattice parallel to the c (long) axis in the case of $Ca_{10}(PO_4)_6CO_3^{2-}$. It should be noted that the presence of fluoride has the opposite effect to that of carbonate, i.e. increased crystallinity, decreased surface area and decreased solubility. Partial substitution of Sr for Ca in synthetic apatites has been shown to result in an increase in solubility, an observation borne out by solubility determinations of Sr rich fossil bones (Sillen and Legeros 1991).

If both fluoride and carbonate are present in solutions saturated with respect to hydroxyapatite, then F^- ions preferentially replace OH^- in the lattice and carbonate substitutes for phosphate. Differences in electric charge are accommodated by coupled substitutions such as the substitution of $CO_3^{2-} + F^-$ for PO_4^{3-} and Na^+ for Ca^{2+}. Living bone and tooth apatites have low F^- values and fall into the category of the mineral *dahllite* (carbonate hydroxyapatite) whereas fossil bones frequently have acquired fluoride from the ground water and contain apatites belonging to the *francolithe* (carbonate fluorapatite) group (Newesely 1989, 239).

The more amorphous products of precipitation from solution, which Newesely calls the paracrystalline phase, arise from the rapid aggregation of free particles. The resulting structure is effectively random with stretched bonds and distorted bond angles. Ionic species are not ordered into a stable lattice but their positions are determined by accommodating the nearest available valency site. As a consequence, these structures are thermodynamically unstable and will recrystallize if the available energy exceeds that required for the reordering of ionic species. This mechanism, which could be compared to the annealing of a strained metal lattice, may be responsible for the increase in crystallinity of burnt bone or of very ancient bone. In these poorly crystallized apatites and carbonate apatites, the individual unit cells may be considered as having structures that deviate significantly from the ideal, however the summation of the ionic species leads to a composition comparable to that of the true apatites although usually with a lower calcium:phosphate ratio.

The calcium/phosphate ratio for this paracrystalline material is often considerably lower than that for stoichiometrically pure hydroxyapatite, between 1.3 and 1.6 compared to 1.67 (Newesely1989, 241).

This lower value may arise by any of several mechanisms: removal or deficit of calcium ions in the lattice, adsorption of phosphate ions or an admixture with other calcium phosphates such as octacalcium phosphate. Of these mechanisms, perhaps the surface adsorption of phosphate groups is the most attractive model. To lower the calcium/phosphate ratio appreciably there must be a high surface area, of 150-200 m^3g^{-1}, a value that agrees well with those claimed for bone apatites. As particle size increases, the contribution of adsorbed phosphates decreases correspondingly.

Most researchers are agreed that the initial phases of mineralization in bone involve an amorphous precursor to apatite (Termine & Posner 1967; Newesely 1989; Francillon-Vieillot *et al.* 1990). Studies of the line broadening (inversely related to crystal size and lattice perfection) of X-ray diffraction spectra (principally the (002) peak) for bone of different specific gravities indicate that there is a correlation between bone density and degree of crystallization. In general there is a trend towards larger or more ordered crystallites as mineralization progresses. However, evidence suggests that this progression is not linear and continuous but rather that there is a deposition of non-crystalline particles in the organic matrix, followed by the rapid development of temporary, first-generation crystals that are themselves supplemented and replaced by the slow growth of a second generation of crystals (Newesely, 243). Various mineral species have been proposed for this intermediate phase including octacalcium phosphate, $Ca_8(PO_4)_6.(OH)_2.(H_3O)_4$, brushite, $CaHPO_4.2H_2O$ and whitlockite, $Ca_3(PO_4)_2$ (Brown 1966; Roufosse *et al.* 1979; McConnell 1973).

It is assumed that the initial amorphous phase is deposited exclusively from ions held in solution in the surrounding serum and that this primary mineral is in the form of amorphous calcium phosphate (Termine & Posner 1967; Eanes *et al.* 1973). An initial but temporary crystalline precipitate, the paracrystalline phase, develops and this is gradually replaced by larger and more ordered crystallites with a composition close to that of hydroxyapatite. It is assumed that these larger crystallites grow at the expense of the amorphous phase and by epitaxial growth from solution. Subsequent mineralization proceeds by the precipitation of amorphous calcium phosphate and its progressive crystallization (Newesely 1989, 243). Evidence suggests that individual crystallites do not increase greatly in size with progressive mineralization, from a dimension in the long axis from 15 to 21.5 nanometers, and that the observed increase in the density of bone tissue is attributable to an increase in the number of crystallites.

1.6 The Relationship Between Bone Apatite and Collagen

It has already been stressed that collagen has the ability to nucleate the crystallization of hydroxyapatite at concentrations below saturation and there is an undeniably strong affinity between collagen fibres and apatites (Glimcher 1976). In fact, hydroxyapatite has a strong affinity for many proteins and related organic compounds and is frequently used as a chromatography material for proteins and enzymes. Neuman and Neuman (1973) described the chemisorption and concentration of amino acids, particularly aspartic acid, glutamic acid and glycine on the surface of hydroxyapatite, although hydroxyproline showed no adsorption phenomena. Their experiments attempted the production of polypeptides by condensation polymerization at low temperatures on apatite surfaces, which they considered to have been and important mechanism for the production of proteins as precursors to life in the primitive oceans. Neuman and Neuman attributed the surface activity of apatite crystals to structural grooves lying in their surfaces. These grooves were described as separated by a distance of 9.42 Ångstrom with reactive sites, the tetrahedral oxygen atoms of the phosphate groups, spaced every 3.44 Ångstrom along their length (Neuman & Neuman 1973, 12).

Skeletal biomineralization represents the opposite aspect of this affinity between proteins and apatites, the nucleation and aggregation of bone mineral crystallites in and around collagen fibrils. Vincent has suggested that collagen acts as a template by providing an array of charged ionic groups with the appropriate geometrical spacing to coincide with corresponding charged groups on the apatite crystallites (Vincent 1982). This would encourage epitaxial growth such as that proposed to explain the precipitation of hydroxyapatite from solutions containing collagen, even at solute concentrations below saturation (see section 1.4). The initial sites of apatite growth are the 'hole zones' corresponding to the gaps between successive tropocollagen molecules (see Figure 1.6) and this mineralization accentuates the 64 nanometer periodic striations seen in transmission electron microscopy (TEM) (Francillon-Vieillot *et al.*, 519). Apatite crystallites in and immediately surrounding the collagen fibrils are aligned with their long axis (the c axis) parallel to the fibrils. Subsequent nucleation of apatite crystallites appears to take place in the interfibril matrix and recent research using TEM has shown that crystallites originating in the gap zone grow in length until they penetrate the body of the collagen fibril. This observation explains why the characteristic banding of collagen fibrils is gradually lost as mineralization advances.(Traub *et al.* 1989; Weiner *et al* 1991; Wiener & Traub 1992). The lengths of the individual apatite crystallites can vary enormously, from 10nm to over 100nm. Estimates vary for the amount of bone mineral accommodated by the hole zone or intrafibril sites, from up to 50% of the total mineral load of bone (Hodge & Petruscka 1963; Glimcher & Krane 1968) to as little as 20% (Lees *et al.* 1984).

The intimate association of the bone apatite crystallites and bone collagen has implications for the optical properties of bone. Bone tissue is a birefringent material and its refractive index differs

depending upon the direction of the collagen fibres. Although collagen itself is birefringent the major part of the optical properties of bone are determined by the mineral component and demineralized bone suffers marked loss of birefringence. All members of the apatite group are optically active (negative) and the birefringence of apatites varies with substitutions in the OH, F and Cl species, the highest birefringence being exhibited by hydroxyapatite. Birefringence in the carbonate apatites is especially pronounced whereas birefringence is reduced in the fluorapatites. The cryptocrystalline variety of apatite, collophane, may appear isotropic or only weakly birefringent due to the aggregate polarization effects of the mass of sub-microscopic crystallites. When viewed in polarized light (with polarizer and analyser at 90°) thin sections of bone exhibit alternating dark and light bands corresponding to successive different lamellae. Haversian systems have a characteristic 'Maltese Cross' appearance. These dark and light bands arise as a consequence of changes in the alignment of collagen fibrils, and hence the c-axes of the crystallites, between successive lamellae.

1.7 The Non-collagenous Components

Collagen accounts for approximately 90% by weight of the organic constituents of fresh, dry bone. The remaining organic matter comprises non-collagenous proteins, phosphoproteins, lipids and several complex macromolecules falling into the category loosely known as mucosubstances. These mucosubstances, sometimes called mucopolysaccharides, are complex carbohydrate-containing macromolecules, more properly called proteoglycans. These contain between 10 and 50 characteristic carbohydrate chains, covalently bound to a protein backbone. In bone, the proteoglycans are intimately associated with the collagen fibrils where their attachment points are periodic and coincide with the hole regions of the tropocollagen molecules (Francillon-Vieillot *et al.* 1990, 517). The mineralization of bone tissue is accompanied by an appreciable decrease in the proteoglycan content, suggesting that they in some way regulate calcification by blocking or exposing the collagen hole zones to calcium and phosphate ions. Mucopolysaccharides with shorter carbohydrate molecules than those found in the proteoglycans are termed glycoproteins (Herring 1973).

Bone sialoproteins are found in growing bone tissues and consist of non-collagenous proteins, containing sialic acid, bound to short-chain oligosaccharides. Their function is, at present, unknown. The role of phosphoproteins has already been discussed in section 1.6. Osteonectin, the best characterized of the phosphoproteins, is known to bind both collagen and hydroxyapatite. It has been suggested that osteonectin is involved in the nucleation and growth of apatite in the hole region in collagen fibrils and accounts for 15% of the non-collagenous protein residues in bone (Termine *et al.* 1981). Osteocalcin contains specific amino acid residues that have a special affinity for calcium ions and has been implicated in the remodelling of primary bone tissue.

A wide range of lipids has been recognised in bone tissues, including cholesterol and phospholipids, amounting to approximately 5% of the total organic content (Shapiro 1973). These lipids contain both polar and non-polar varieties. Histochemical studies have shown that lipids accumulate in the areas of active mineralization and it is possible that the phospholipids play a key role in the calcium and phosphorus transport mechanism during the initial deposition of apatite (*op. cit.*, 137).

1.8 Bone as a Structural Material

Many early researchers viewed bone as a simple composite, similar to some modern structural materials such as reinforced concrete or fibreglass (Currey 1970; Halstead 1974). Such composite materials are considerably stronger than the sum of their component parts. For example, collagen has a tensile strength of 50 MN m^{-2} while that for hydroxyapatite is approximately of 100 MN m^{-2} (Vincent 1982, 147). Assuming that bone is composed of approximately 25% collagen and 75% hydroxyapatite the sum of its individual components would give a tensile strength of the order of 85 to 90 MN m^{-2}. In contrast, bone has a tensile strength of 130 MN m^{-2}. Bone is also unusual in that it has comparable strengths in tension and compression, quoted by Halstead as 105 MN m^{-2} and 172 MN m^{-2} respectively (Halstead 1974). Normally, materials that have a high Young's modulus (a measure of stiffness) are brittle and have a correspondingly low tensile strength. For example, porcelain is both hard and rigid with a compressive strength of 552 MN m^{-2} but a tensile strength of only 55 MN m^{-2}. A simple model would be to consider bone as a stiff, two-phase composite of inorganic or ceramic-like crystals in a continuous organic matrix. Calculations of the volume fractions of collagen and bone mineral from their relative breaking strengths, suggest that the mineral phase is probably the main load bearer in bone (Wainwright *et al.* 1976). However, these calculations rely on a number of critical assumptions, such as the presumption that there is a strong mechanical couple between the mineral and organic components that can effectively transfer stress from the collagen to the apatite and *vice versa* (Vincent, *op. cit.*, 147). Collagen is quite capable of transmitting stress (tendons are essentially inelastic cords for the transmission of forces from the muscles to the limb bones) and it is possible that it is the organic phase that is the main load-bearer. Studies of human scapulae using neutron diffraction have demonstrated that the c-axes of the bone apatite crystallites, and therefore the collagen fibrils, are aligned parallel to the principle lines of force applied by the attached muscle groups (Vincent, 148). Furthermore, Halstead states categorically that it is inconceivable that a brittle mineral such as apatite could resist a tensional stress in excess of 190 MN m^{-2}, whereas a simple calculation of the relative loads at the ultimate stress of bone in tension gives values of 1.5 MN m^{-2} for collagen and 206 MN m^{-2} for bone apatite (Halstead 1974, 112).

Vincent suggested that collagen may well act as the major load bearer and that the apatite crystallites act as filler particles, providing lateral restraint and limiting changes in cross-sectional area when bone material is under stress. This behaviour has been described as the 'strait-jacket' effect. Vincent extended his argument by stressing that both the collagen and apatite crystallites have their long axes aligned parallel to the directions of stress in bone (see also Wolff's law in section 1.1) and that therefore both are capable of bearing loads independent. However, since the exact relationship between collagen and bone apatite remains poorly understood, this argument should be viewed with extreme caution since there are many other factors that may account for this common alignment.

Studies by Currey (1988) and Piekarski (1973) have shown that there are two major factors that determine the strength and mechanical properties of bone; porosity and mineral content. The percentage porosity of adult compact or cortical bone can be very high for a structural material (around 20%) due to the presence of vascular channels, osteocyte lacunae and the fine network of canaliculi. The mineral load of bone tissues increases with the maturity of that tissue with compact laminar bone yielding 67% ash and Haversian or secondary bone yielding 63%. Piekarski measured both porosity and mineral content for foetal and adult bovine bone and for bone from the ear of a whale. He found that Young's modulus (E) increases with increasing mineral content and decreases with increasing porosity. When these values of E were corrected for zero porosity, Piekarski found that they corresponded best to a model for a composite material in which both the collagen and bone apatite work in parallel and bear equal strain (see Vincent 1982, 149).

In addition to porosity and mineral content as factors in the mechanical strength of bone, the rate or speed at which loads are applied is also a crucial factor. Bone, in common with many other biological materials, is a viscoelastic material, *i.e.* response to imposed loads is not instantaneous but involves a degree of slow or viscous deformation (Vincent 1982, 10-11). Thus a viscoelastic material will return to its original shape once a deforming force has been removed even though it may take some time to do so, in other words some of the energy of deformation is stored and released slowly as the material returns to its original shape. If bone is loaded at a speed higher than the rate at which it can accommodate the resulting deformation by viscous flow, then its mechanical properties change dramatically. For low strain rates, typically those encountered in everyday life, living bone is tough and resilient. However, at very high rates of deformation, such as those encountered in road traffic accidents, bone becomes very brittle and can shatter like glass. This constraint limits the speed at which racehorses can run by limiting the rate of impact between the leg and the ground. Fracture surfaces produced by slow strain rates are very rough and show evidence of the pulling out of osteons in a pattern similar to the fracture of glass reinforced plastics. By contrast the fracture surfaces produced under high strain rates are smooth and the propagation of cracks appears independent of microstructure (Vincent 1082, 157).

It is likely that the microstructure of bone contributes to its toughness by limiting the propagation of cracks. Cracks grow because there is an intense concentration of stress around the 'crack tip' where the radius of curvature of the fracture surface is vanishingly small. If the crack tip meets a void in the substrate with a relatively much larger radius of curvature, then this stress concentration is diffused and the crack may be prevented from spreading further. Cracks may also be prevented from propagating if they meet a weak interface at right angles. In this case the component of stress parallel to the direction of propagation has a maximum value just ahead of the crack tip. As the crack tip approaches a weak interface this stress concentration opens up a second crack at right angles to the original which deflects or stops the growth of the original. This mechanism, leading to the formation of 'T-shaped' crack-stoppers or the blunting of cracks at a weak interface, is known as the Cook-Gordon effect (Gordon 1983, 117-119). Planes of weakness are provided in lamellar bone by successive lamellae in which the collagen fibres are organised orthogonally in a structure reminiscent of plywood (Francillon-Vieillot *et al.* 1990, 502 & 510) and in Haversian bone by the concentric cylinders of bone tissue that also have a plywood-like structure. Lamellar bone frequently persists in the compact, outer portions of long bones where it represents periods of annual growth separated by 'lines of arrested growth' representing fine, lamellar, avascular bone tissue (Francillon-Vieillot *et al.* 1990, 510).

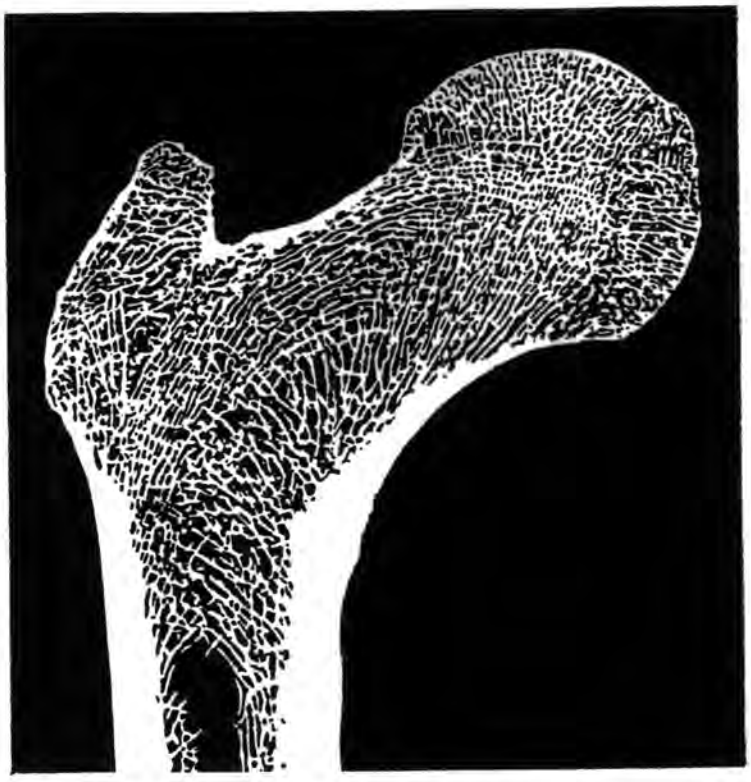

Figure 1.1 Cross-section of human femoral head showing trajectories of trabeculae

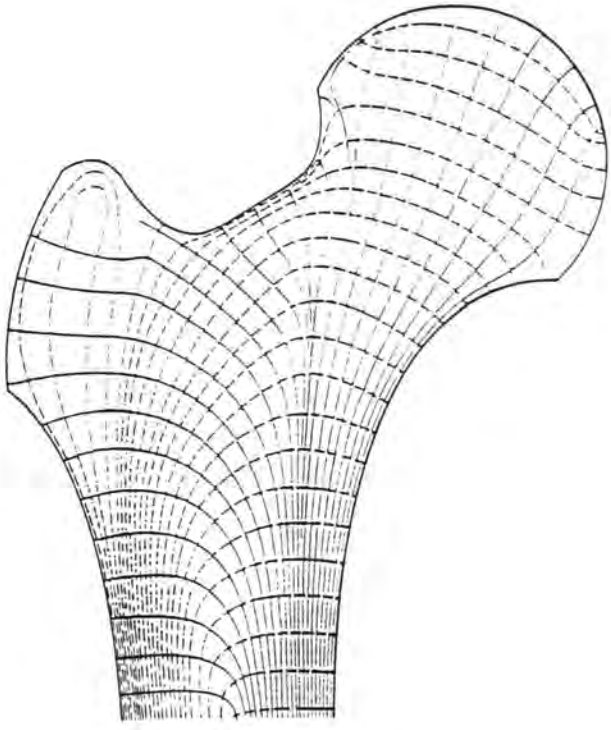

Figure 1.2 Principal lines of stress in human femur (after Pauwels 1980)

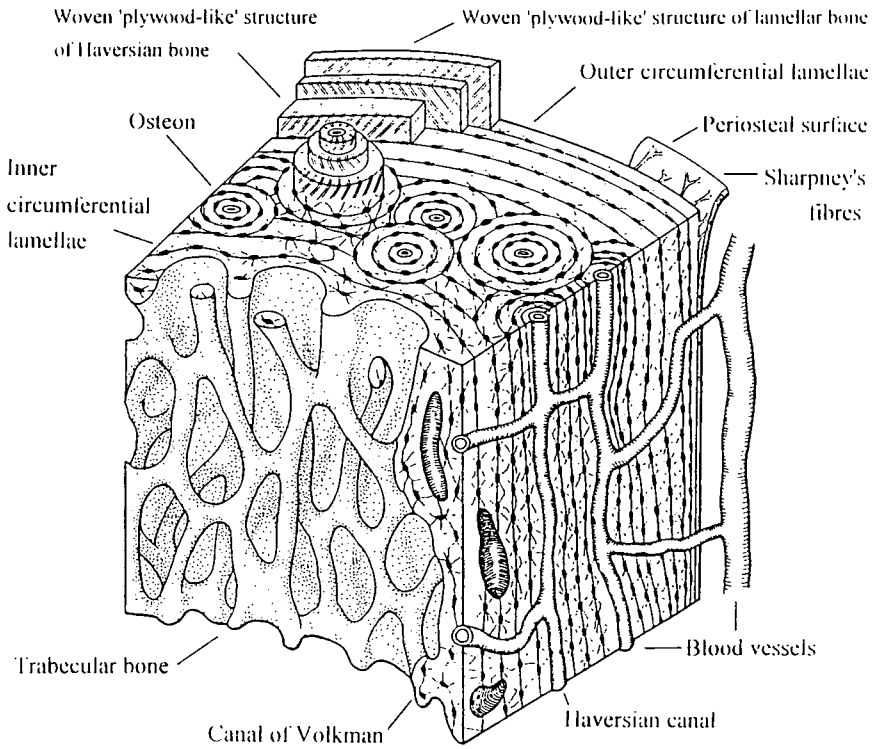

Figure 1.3 Simplified drawing of part of the mid-shaft of a long bone showing gross and microscopic structures

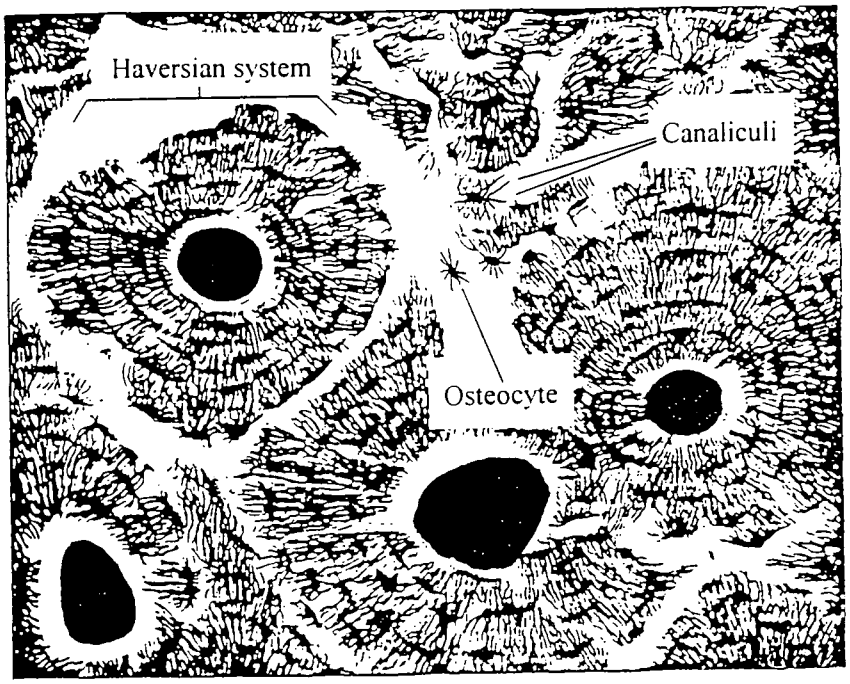

Figure 1.4 Exaggerated view of osteocytes and canaliculi in bone

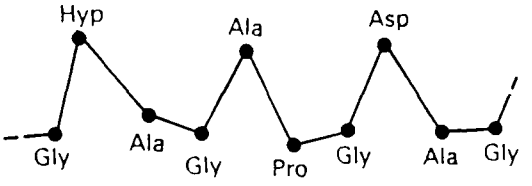

Figure 1.5a Primary structure of collagen
(after Woodhead-Galloway)

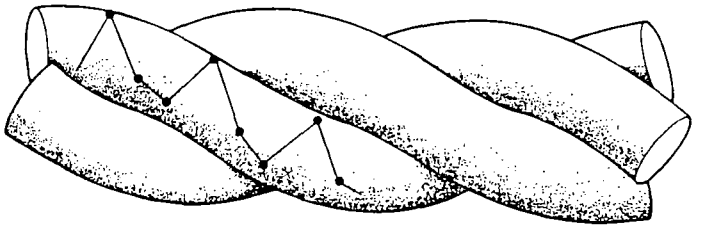

Figure 1.5b Collagen trimer forming left-handed triple helix

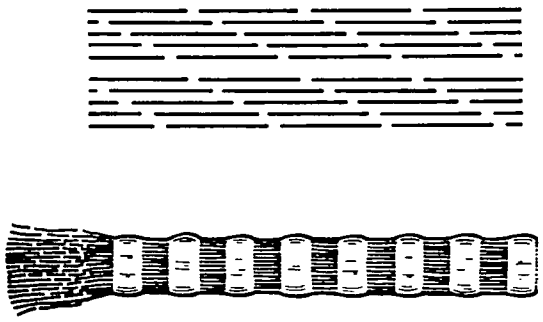

Figure 1.5c Aggregation of collagen molecules into fibrils with gap- and overlap zones

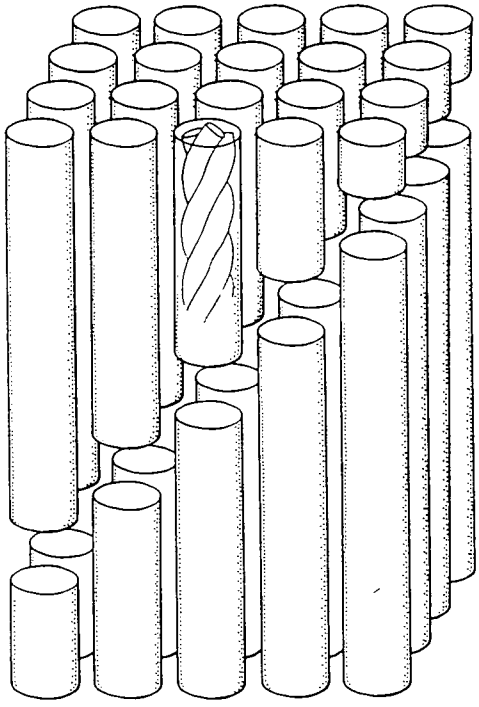

Figure 1.5d Quasi-hexagonal packing of collagen molecules in fibrils (after Glimcher 1984)

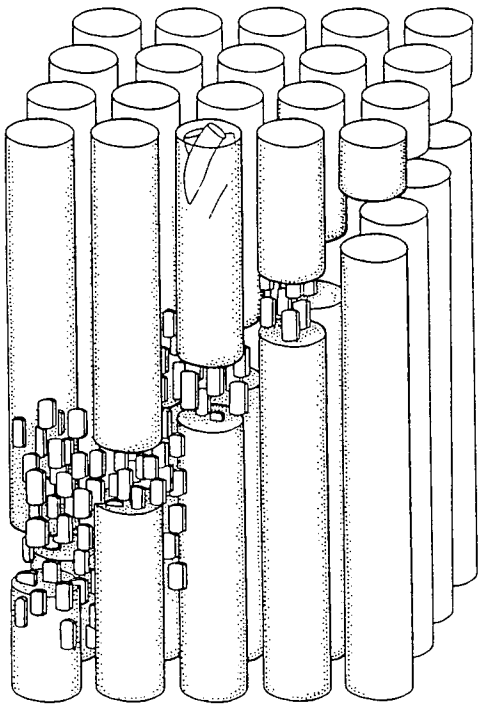

Figure 1.6 Drawing showing successive stages (right to left) in the mineralization of collagen fibrils (after Glimcher 1984)

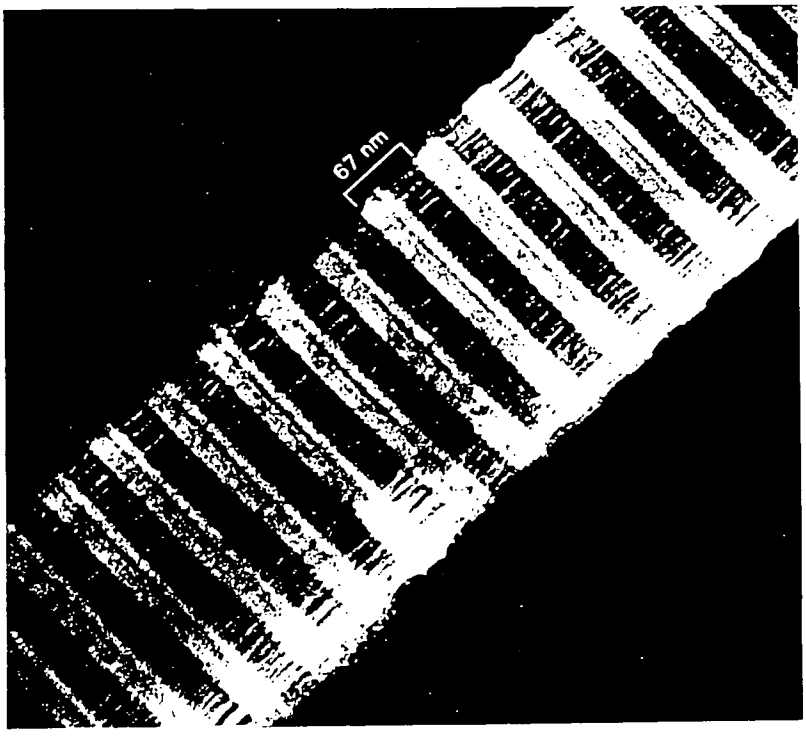

Figure 1.7 Transmission electron micrograph of collagen fibril (after Halstead)

2. A Review of Current Research into Fossil Bone

Much of the research into ancient bone has fallen into two major categories, one concerned with what an individual bone or assemblage of bones can tell us about past environments, cultures, economies and diet, the other attempting to understand how this picture may be distorted by burial processes. The term *taphonomy*, defined by Efremov in 1940, literally means 'the laws of burial' and concerns all aspects of the passage of organisms from the *biosphere* (the living world) to the *lithosphere* or Earth's crust (Olson 1980). Strategies for investigating taphonomic processes include:

field studies of human and animal behaviour (anthropology and ethology)

the identification and study of naturally deposited bone in the environment

the study of bone specimens recovered from specific environments

laboratory simulations of soil processes.

The study of taphonomy is important at all levels, from the macroscopic to the chemical or even biomolecular. Although much of the biological or cultural information associated with a bone is lost shortly after death, or during the period of time between its burial and eventual recovery, it is still possible to extract potentially valuable evidence from apparently unpromising assemblages. The primary goal of taphonomic studies is to work backwards from the surviving bone assemblages to the composition, structure and dynamics of the parent populations (human or animal) using variously: evidence recovered from the bones themselves, the nature of their contexts and an understanding of post-mortem processes (Olsen 1988). In most cases, the nature and quantity of evidence that survives depends upon the time interval between deposition and recovery. This 'entropy view' of formation processes of the archaeological record, expounded by Ascher (1968) saw 'time's arrow' reducing both the quantity and quality of evidence held within an archaeological site with progressively increasing time since deposition. This view presupposes that the survival of evidence is directly related to degradation which in turn is dependant upon time. However, survival is more often correlated to specific mechanisms of degradation and depositional environment than time, as evidenced by the spectacular preservation found in special environments such as those associated with Egyptian mummies, frozen tombs or bog finds.

Once skeletal remains have been recovered, they are the subjects of study by a wide range of specialists and researchers, each looking at a one or more aspects of the potential evidence held within a particular bone or assemblage. If the results recovered from one sample are to be meaningfully compared with those from another, then the changes wrought by taphonomic processes must be fully understood and taken into account except in those rare cases where the bone has survived effectively unchanged, i.e. 'time's arrow' has been stopped.

The geological term *diagenesis* is defined as the processes by which sediment is transformed into sedimentary rock under conditions of low temperature and pressure. Similarly, diagenesis and diagenetic alteration are used to describe the changes undergone by bone in the lithosphere (of which the archaeological record forms a part). These changes may involve: dissolution of bone tissue or its cementation by exogenic minerals, recrystallization of bone mineral or its replacement by other mineral species and, in the case of bones buried under a heavy overburden of sediments, considerable distortion and compaction. These processes are often crudely referred to as fossilization (Behrensmeyer & Hill 1980) even though the excavated bones may have an appearance far removed from that of the fossils of extinct species seen in museums. In spite of this disparity the description of excavated bones as fossils is quite useful since the term may be used to include all skeletal material that has at some time been buried.

From a historical perspective the study of skeletal remains, in common with most other material from archaeological contexts (for example, ceramics and metals), has shifted from an examination of gross morphology towards microscopic and chemical analyses as new technologies make sophisticated analytical techniques more readily available and measurement increasingly precise. Often, the sample required by modern analytical techniques is sufficiently small to allow analysis of even the most precious finds, such as those of fossil hominids. The extreme sensitivity of these modern techniques, however, introduces another problem to those handling or treating this material, which is the increased potential for contamination by foreign matter by careless handling or the ill-considered application of an inappropriate treatment.

The examination and analysis of ancient bone then, may be divided into three broad categories or levels, although each category may encompass a number of different disciplines and techniques. These categories are:

macroscopic examination: This level of examination involves the visual inspection of hand specimens with the aim of identifying species, skeletal element (e.g. proximal end of left humerus), sex, any gross pathological signs (such as disease or trauma) that may be preserved in the bone tissues and any post-mortem damage or working by man.

microscopic examination: This includes both the examination of complete hand specimens using a binocular microscope as an adjunct to macroscopic analysis and, more importantly, the examination of specially prepared samples using a wide range of imaging techniques. Microscopic examination of thin sections is used to study the structure of bone tissues at a cellular level to investigate its internal micro-architecture. Histological examination throws light on the development of bone as a living tissue, which itself is influenced by such factors as age, species and certain degenerative diseases. Such

examination is also crucial to a full understanding of the extent and nature of post-mortem deterioration, whether by biological agents or by physico-chemical alteration. Microscopic examination can involve viewing bone samples using a wide range of incident radiation. Thin sections are most often examined using visible light or plain polarized light, although ultra-violet (u.v.) light may also be used to highlight areas containing certain complex organic molecules such as humic and fulvic acids or antibiotics. Hand specimens or thin sections may also be subjected to X-radiography to investigate their internal structures and degree of mineralization. Increasingly, electron microscopy has been employed to examine the micro-architecture, histology and diagenetic alteration of excavated bone. Thin sections, embedded, and mounted fragments have all been investigated by scanning electron microscope (S.E.M.) which has proved to be a very powerful tool.

chemical analysis: The analysis of bone using a variety of chemical techniques has in the past been divided into two groups, attempting to date ancient bone (frequently human remains) and to understand the diets of past human populations. However, developments in molecular biology in recent years have ushered in a potential revolution in the study of human and animal remains. New techniques in the handling and analysis of trace amounts of organic molecules have been applied to archaeological material, leading to the establishment of a new and exciting branch of archaeological science; that of molecular archaeology. This new science may potentially revolutionise the study of archaeology as much as the introduction of radio-carbon dating in the early 1950's.

Current ways of examining skeletal remains, together with potential future developments are described in greater detail below. For each technique, possible post-excavation deterioration, contamination and interference will be outlined.

2.1 Macroscopic Examination

2.1.1 Archaeozoology

As suggested above, the earliest studies of ancient skeletal remains were confined to recording the gross morphological characteristics of excavated bones with the intent of determining the species, sex and age of the animal at death. In 1907, Hue compiled an atlas of animal bones, the *Musee Osteologique*, specifically as a guide for archaeologists (Cornwall 1974, 16). Much of this information can be determined from simple visual inspection of a complete or fragmentary bone accompanied by comparison to a suitable reference collection of modern material. In many cases, especially if only a relatively small fragment of the bone survives, identification rests on the

recognition of small excrescences, ridges and grooves or *foramina* on the surfaces of the specimen. These features are also frequently used as the reference points in the systematic measurement of the dimensions of bones. Age determination often relies upon the stage of development or ossification of the bones of the skull and the epiphyses of long bones (Cornwall 1974; Chaplin 1971). Clearly, it is essential that these external details and the articulating surfaces of joints are preserved with the bone if a secure identification is to be made. Conversely, it is equally important that if bones are broken by predators or the ends are eroded by wind or water action, these important indicators of taphonomic processes are retained and not confused with damage caused by careless handling or post-excavation deterioration. There has been considerable work on the consequences of taphonomic processes and their recognition in fossil and sub-fossil bone. In his major work on modern taphonomic processes in Africa, Brain studied the characteristic fracture and wear patterns attributable to human activity and natural agents such as predation by scavengers, trampling by large ungulates and the action of wind-blown sand and sun (Brain 1981). He illustrates and compares the spiral fractures on bovid limb bones produced by both human action and the jaws of hyenas (*op. cit.* 140). Myers *et al.* (1980) discuss the potential confusion that may arise between rudimentary bone tools and long bones that have been broken as a result of incidental trampling by ungulates, both of which exhibit comparable spiral fractures. Similar fractures are visible in some of the long bones of red deer from the Mesolithic site at Star Carr (Legge & Rowley-Conwy 1988). The distal articulations of some auroch metapodials from this site are abraded, leading to the suggestion that these bones may have been used as pounding tools (*op. cit.*, 45). Evidence of depredation of the cancellous or spongy epiphyses of bones by dogs and hyenas and the erosion of bone surfaces by smaller scavengers such as porcupine and rats can also be seen in examples from the archaeological record (Schrenk & Maguire 1988).

The external surfaces of animal bones may also bear cut marks and broken edges characteristic of butchering, allowing inferences to be made about how the carcass was divided up. The earliest study of evidence for processing of animal carcasses was undertaken by Martin in the early years of the 19th century. He photographed and illustrated classic examples of traces indicating skinning, evisceration, disarticulation and filleting, including the results of breaking and burning bones. Some distinction should be made between evidence of systematic butchering and other cut marks found on bones. 'To qualify as a butchering mark two criteria were applied: i) repetition in specimen after specimen at precisely the same location on the bone; ii) that there was some anatomically dictated reason why a particular mark should occur at any given spot' (Binford 1981). Studies of experimentally butchered animals and excavated remains have been augmented by ethnographic evidence such as the study of Eskimos (Binford, 97-105) and African Hottentots (Brain 1981, 15-18). A number of cow scapulae from Roman Colchester show butchering marks and characteristic punctures in some shoulder blades are suggestive that joints had been hung up, possibly for smoking (Luff 1984, Plate 6). Butchery techniques or offcuts often give clues to the secondary or industrial

importance of parts of some wild or domesticated animals. McGregor (1980) cites the presence of sawn-off articular ends of cattle metapodials in medieval archaeological contexts as evidence of comb making. Examples were found in Saxon Southampton and in 8th century deposits in Munster. Excavations in medieval urban contexts such as York have produced unfinished comb fragments, often composite artefacts with antler teeth riveted to bone backs. Excavations of medieval Sleswig unearthed large numbers of jaw-bones with neatly drilled holes indicating the specialist manufacture of spindle whorls or gaming counters (*op. cit.*, 65-66).

It is clear that a great deal can be learnt about past ecologies through an examination of the gross or external features of skeletal remains. To the archaeozoologist, data from a large assemblage of bones may allow a picture to be built up of the relationships between domestic and hunted animals and, to a lesser extent, the local fauna. On a broader scale, the study of assemblages from many sites of different dates gives clues to the introduction of new species and an insight into the development of urban ecologies.

2.1.2 Physical Anthropology

In human remains, the analysis of the shape, relative size and development of certain characteristics of individual bones or skeletons currently forms the basis of our understanding of human evolution. When physical anthropologists study ancient human remains, they address the questions: Where and how did early man originate? What did our ancestors look like? and how did the differences between different populations arise? In these studies osteometrics, or the precise measurement of bones, plays an important role. For example, the living statures of prehistoric and ancient peoples may be reconstructed by systematic measurement of the lengths of long bones (usually the femur) and the application of simple formulae. A number of such formulae have been worked out for different populations and races (Brothwell 1972, 100-106). It is worth noting, however, that some of the earliest work in this field was concerned to place white Europeans at the pinnacle of a perceived evolutionary tree

When large populations are studied, such as in the analysis of many individuals excavated from cemetery sites, it is possible to reconstruct something of that population's demography. Demographic studies are primarily concerned with the balance of age and sex within any population. Clearly, when dealing with extinct populations these are determined by an analysis of their physical remains and this branch of the science is often referred to as paleodemography. Palaeodemographic principles have been applied to human remains from several sites, usually of early medieval date or later (Brothwell 1968; Boddington 1987) although Hedges (1982) has published a palaeodemographic perspective on over 300 individuals from the Neolithic tomb of Isbester, South Ronaldsay, Orkney. This latter group represents an incomplete and mixed record of individuals

whose bodies had been defleshed elsewhere before being interred in a common tomb. Sufficient information on sex and age at death was recoverable to reconstruct, in part, a picture of life expectancy and infant mortality.

Sexing of human skeletons is achieved through the recognition of subtle differences in the size and shape of specific features on the bones of the skull and pelvis. However, these subtle differences between male and female skeletal development are not consistently expressed in all individuals or races and there is considerable overlap, making positive identification difficult in some cases (Brothwell, 1972, 51). Compounding these effects is the incompleteness of some ancient bones, particularly of fossil hominids. The study of ancient man is further complicated by the distortions that may occur due to the pressure of overlying sediments (Brain 1981, 134-137) or as a consequence of the loss of rigidity caused by demineralization in acidic environments. The latter is clearly demonstrated in the case of Lindow man and other bog bodies, such as those found in Scandinavian wetlands (Stead & Brothwell 1986; Andersen & Geertinger 1984; Bennike & Ebbesen, 1986a; Bennike *et al.* 1986b). In cases where human skeletal remains are incomplete or damaged, low power SEM examination of the internal architecture of cancellous bones such as the ribs and vertebrae has been demonstrated to be of considerable promise in the determination of age at death and sex, in addition to revealing evidence of pathological conditions (Wakely *et al.* 1989).

2.1.3 Palaeopathology

Human bone and, to a lesser extent, animal bone also contains potential evidence of trauma during the life of the organism and the manner in which it met its death. The examination of ancient bone for pathological signs is known as palaeopathology. Such studies are often restricted to human remains, partly because of the anthropocentric nature of much scholarship and partly because of far greater understanding of human diseases and the possible significance of these studies to modern epidemiology. Nevertheless, the application of palaeopathology to animal bones is of growing interest to archaeozoologists and palaeontologists (Brothwell 1969). Chaplin devotes several pages to bone pathology, covering abnormalities of development, injuries, diseases of the joints and the consequences of castration on development (Chaplin 1971 108-119). Characteristic broadening of the distal metapodials and proximal phalanges of some cattle has been cited as evidence of the individual's use as a draught animal. This condition is similar to spavin, principally a disease of the horse but also reported on draught cattle. For a fuller description of this and other animal diseases found in the archaeological record the extensive work by Baker and Brothwell (1980) should be consulted. Wear patterns on the teeth of Palaeolithic horses has been interpreted by some as evidence for the use of bridles to restrain the animal but the evidence is, at best, inconclusive and this interpretation remains controversial.

Skeletal remains occasionally preserve evidence of human diseases, for instance tuberculosis, which frequently causes severe disfigurement of the vertebrae. This condition, Pott's tuberculous osteomyelitis of the spine, may be recognised by collapse and fusion of two or more vertebrae, leading to curvature of the spine typical of 'hunchbacks' (Manchester 1986, 1987). Epidemiological studies of the occurrence of other human diseases affecting the skeleton, such as leprosy (Manchester 1968, 25-28) or syphilis and also congenital or genetic conditions, such as dwarfism or achondroplasia, in different populations can shed light on the influence of co-factors such as diet, environment and increasing urbanization (Brothwell 1972; Wells 1964; Zivanovic 1982). Cultural evidence may also be preserved in skeletal remains. Bones of individuals from certain cultures show signs of skull-flattening, trepanation or deliberate mutilation such as the filing or extraction of teeth for cosmetic purposes (Brothwell 1972, 120) or the foot-binding of women in the case of the Chinese.

Radiography is sometimes used as an adjunct to palaeopathology and is particularly useful in the detection of periods of dietary stress during the growth of long bones. Periods of starvation or illness during infancy or adolescence can cause lines of arrested growth which appear as transverse lines on the metaphesial parts of the bone shaft (Zivanovic 1982, 81). These features, variously known as Milkman's lines, Looser's zones or, more recently, Harris's lines arise because of a temporary halt in the growth of long bones during periods of poor nutrition, leading to stunted growth. A number of successive lines indicate repeated periods of malnutrition during infancy or adolescence. Radiography also reveals healed fractures and pathological alteration of bone (such as osteoporosis or arthritis) which may be invisible or ambiguous from a superficial examination.

Evidence of cause of death is particularly striking in the case of individuals killed by violence. Even when soft tissues have been lost it is still possible to determine the cause of death by an close examination of the bones. In rare cases, traces of the weapon remain lodged in bone tissues (Manjo 1975, Figure 2.1).

2.2 Microscopic Examination

Microscopic analysis of bone may be divided into two broad categories: the examination of thin sections or optically flat embedded specimens and the imaging of three-dimensional structures. Microscopic examination covers an extreme range of magnifications, ranging from the inspection of butchering marks on bone using a low-power binocular microscope, through intermediate levels to the use of transmission electron microscopes to view individual collagen fibres or apatite crystals in calcified tissue.

2.2.1 Palaeohistology

Histological examination of thin sections is most usually restricted to specimens removed from recent cadavers where bone and pathologically calcified tissues are investigated for diagnostic or research purposes. Because of the mineral content of bone, normal histological techniques must be modified unless the bone mineral is removed by decalcification of the specimen (Drury & Wallington 1980, 199). The term palaeohistology was coined in 1926 by Moodie and subsequently defined by Graf (1949):

> 'It would seem rather natural to apply the term palaeohistology to the examination of microscopic sections of human beings and the recognising of tissues and cells in such sections' (quoted from Garland 1987, 109).

A major work on the comparative histology of modern and fossil bone was published by Enlow and Brown between 1956 and 1958 (Enlow & Brown 1956, 1957, 1958). These publications give detailed instructions on the preparation and examination of thin sections together with a definitive classification of the major groups of structural patterns found in bone, covering both recent and fossil genera of fishes, mammals and birds. However, this work was primarily concerned with understanding the evolution of bone as a tissue, rather than its diagenetic alteration. Histological studies of juvenile and adult dinosaur bones have shown well developed vascularity and Haversian systems, providing evidence of high growth rate and metabolism of some dinosaurs and leading some researchers to conclude that they may have been warm-blooded. Similar studies of the bones of early mammal-like reptiles (dinocephalians) have also indicated that these too may have been endothermic (Ricqles 1972; Bakker 1975; Kemp 1982).

Initially, palaeohistological work was restricted to the biological ageing of exhumed human skeletons and as part of larger studies of palaeopathology (Wells 1967). More recently, quantitative techniques have been applied to the study of ancient human remains in thin section. Histomorphometry, the study of the density and distribution of osteons in histological sections, has the potential for revealing much more than merely the 'age at death' of an individual. Stout (1983) claims to have identified consistently higher cortical bone remodelling rates among a New World population whose staple diet was maize, compared to other ancient New World peoples. This higher turnover of bone material may reflect the fact that maize is deficient in calcium and high in phosphorus, a combination which could lead to reduced levels of calcium in blood serum and increases in parathyroid hormone- known to stimulate bone remodelling (Stout 1989). The same author reports fewer osteons in bones from individuals whose mobility is impaired by crippling illness or quadriplegia (Stout 1982).

In the past two decades histological techniques have been increasingly applied by many researchers investigating the diagenetic changes undergone by buried bone (Hackett 1981; Hanson & Buikstra

1987; Garland 1989). One of most striking features of the appearance of fossil bone in thin section is the obvious increase in porosity of bone tissues. The development of small, often interconnecting channels and voids in bone is frequently referred to as 'tunnelling' and has been attributed to the action of micro-organisms. Hackett calls this tunnelling 'microscopical focal destruction' and recognises four distinct forms of tunnels or foci (Hackett 1981, 250-258).

Wedl tunnels (named after the late 19th Century researcher) are characterized by meandering and often bifurcating channels. These channels are described as centrifugal Wedl tunnels since they extend from the outer cortex and centres of Haversian canals inwards, towards the body of the bone. Their diameters are uniformly 5-10um, rarely smaller, and their progress does not appear to be influenced by cement lines, either in Haversian or lamellate bone. Roux, working in the late 19th century, also identified these features in fossil bones and termed them bored channels or '*bohrkanale*'. The fine, brown filaments visible in these tunnels suggested the action of fungi in their formation.

Linear longitudinal tunnels are recognisable in longitudinal sections of fossil bones and have diameters similar to those of Wedl tunnels. In transverse sections they appear to be sub-round voids surrounding osteones. X-radiographs of thin sections (microradiographs) indicate alterations in the mineralization of the bone tissue, i.e. demineralization or leaching of the bone apatite and subsequent recrystallization. This remineralization is accompanied by loss of birefringence when viewed in polarized light. These tunnels appear to be confined within lamellae and their spread is inhibited by the cement lines in Haversian systems and between lamellae.

Budded tunnels bear a superficial resemblance to Wedl tunnels but are larger and tend to run longitudinally rather than radially. Where the tunnels divide, side branches (buds) form acute angles to the main channel and have irregular, globular terminals. Their presence is accompanied by marked remineralization and loss of birefringence. The walls of budded tunnels bear longitudinal striations. Microradiography suggests that there is substantial demineralization of bone around these tunnels and subsequent redeposition in the walls known as 'cuffing' (Hackett 1981, 247).

Lamellate foci are rounded or globular voids that often appear curved in transverse sections of bone since they are confined within the lamellae of osteones. These features grow much larger than other focal destructions and may have a maximum dimension up to 0.4 mm. They often appear close to, but not connected with, an Haversian canal. Lamellation of the osteons is visible in ordinary light, leading Hackett to postulate that this results from the attack and solution of the non-collagenous organic material, exposing the collagen fibres of the lamellae and partially dissolving the bone mineral. Birefringence in polarized light is substantially reduced in these areas. Extensive 'cuffing' or mineral redeposition can be seen around these foci as borders of dense, hypermineralized zones in

microradiographs (Hackett 1981, 159; Hanson & Buikstra 1987, 555-558). Several foci may surround a single osteon and these may coalesce to open large voids in the structure of the bone.

Linear longitudinal, budded and lamellate destruction are all thought to result from the action of bacteria as opposed to fungi which are implicated in the formation of Wedl tunnels. Colonisation of the bone by invading organisms begins at the periosteal and endosteal surfaces of the bone and inwards from the surfaces of the Haversian canals. Obviously, colonisation of the osteon tissue relies on access via the channels provided by blood vessels. However, Hackett maintains that he found no evidence for utilization of osteocyte canaliculi although these are often much more obvious in fossil bone due to staining or leaching. The tunnels and voids opened up by micro-organisms frequently contain mineral inclusions and other matter, particularly iron compounds that also stain the surrounding tissue. Garland recognises two types of inclusion in exhumed bone: biological and mineral (Garland 1987, 118). Biological inclusions comprise fungal cells, hyphae, bacteria and insect fragments. Mineral inclusions encompass soil particles and precipitated salts. He describes infiltrations as extraneous matter within the bone itself such as staining by metal salts or humic and fulvic acids.

The histology of modern and fossil bone has also been examined using scanning electron microscopy (SEM), both to investigate pathological conditions and to asses the changes wrought by diagenesis (Boyde *et al.* 1986; Bell 1990). Bell examined adult human femur, both modern and from archaeological contexts, which were embedded in poly(methyl-methacrylate). The embedded specimens were then polished optically flat and examined using backscatter electron imaging in a SEM. Backscattered electron (BSE) imaging utilises the detection of electrons from the primary beam which have rebounded from atoms in the specimen. Electrons striking atoms of high atomic number (Z) are scattered with a higher proportion of their initial energy and at greater angles than those striking relatively light atoms and are therefore more likely to leave the surface of the sample and enter the detector. BSE images of bone sections therefore provide density maps which in turn are related to their chemical composition. One of the conspicuous features seen in BSE images of embedded bone sections is the mosaic-like pattern caused by differences in density, effectively variations in the degree of mineralization of the bone tissue, between adjoining osteons. In this respect BSE images appear very similar to microradiographs of histological sections (compare Plates 3.3 and 3.4). Diagenetic change has been demonstrated to be clearly visible in BSE images of archaeological bones, superimposed upon normal histological structures. Bell also reports the importance of the osteonal canals to the initial stages and spread of diagenetic change. Interestingly, she reports that trebaculate or spongy bone lining the medullary cavity was relatively unaffected by agents responsible for diagenetic alteration whereas denser, cortical bone suffered more dramatic destruction (Bell 1990, 95).

Examination of the pathological archaeological bone seemed to indicate that the porous and weakened areas of pathologically altered tissue were not subject to extensive diagenesis, which once again affected the denser cortical bone. Focal destruction was found to be closely associated to osteonal canals but did not always centre on osteocyte lacunae. Demineralization and re-precipitation of denser bone was evident on all of the diagenetically altered bone that Bell examined. This re-precipitated material is generally accepted to be recrystallized hydroxyapatite that has previously been dissolved from areas of focal destruction. The greater density of this re-precipitated material is evident from its relative brightness in BSE images and its increased opacity to X-rays in microradiographs. Piepenbrink attributes this to 'increased crystallinity' (Piepenbrink 1989, 277) but it is more probably due to increased crystal size and reduced carbonate content. Scanning electron microscopy has proved particularly useful in the location and analysis of contaminant minerals in fossil bone. Piepenbrink has published photographs and identifications of several mineral species, including calcite, brushite and vivianite (an iron phosphate) he claims to have has found in fossil or interred human bone.

Electron microscopy has also been widely used to examine the external surfaces of bone for macroscopic and microscopic signs of post-mortem damage characteristic of taphonomic processes such as cut and chop marks, gnawing by rodents, compression fractures and abrasion. Schrenk and Maguire (1988) examined an assemblage of bone fragments from the Makapansgat Limeworks site in South Africa for examples of micro-damage to the bone surfaces. This early hominid site is recognised as one of the most important 'bone caves' in the African continent and contains an estimated two million animal bone fragments, many of which have been interpreted as tools. By comparing microscopic details of the surfaces of modern bones subject to hyena and porcupine damage with those of bones recovered from the 'bone cave' the authors were able to suggest that these scavengers were the principle collecting agents for the assemblage. Similar studies have been applied to fossil teeth of the earlyhominoid(*Gigantopithecus blacki*) found in China. Using electron microscopy, combined with qualitative X-ray microanalysis, Piperno and Ciochon (1990) were able to locate and identify phytoliths, microscopic silicate bodies present in plant tissues, that had become embedded in tooth enamel. From their identification of the plant species from which these phytoliths came the authors were able to tentatively suggest the likely diet of this extinct primate.

2.2.2 Microbiological Research

Marchiafava *et al.* (1974), Hackett (1981) and Piepenbrink (1986) all conducted experiments on the fungal attack on buried bone in an attempt to replicate tunnelling and other features associated with diagenesis. Marchiafava *et al.* used fresh human vertebrae (dissected from cadavers) which they buried in moist garden soil for 45 days at 20°C, then examined using transmission electron microscopy (TEM) and optical microscopy. They then compared the features seen in these vertebrae

with the characteristic diagenetic tunnelling found in a fragment of Neanderthal skull. Mould specimens which developed spontaneously around and within the vertebrae were cultivated on agar for identification and subsequent inoculation into both sterilized soil and bone autoclaved at 200°C for 20 minutes. The fungi colonizing the bone buried in garden soil were identified as members of the genera *Mucor*, *Candida* and *Cladosporum*. Of these, however, only *Mucor* was successfully cultivated in isolation on inoculated sterile bone buried in sterilized earth although the authors point out that the proliferation of this fungus is much reduced on sterile substrates when compared to its growth in un-sterilized soil. This observation may imply that bone matrix does not form the sole source of food for *Mucor* or that it relies in part upon other organisms to release nutrients from bone. Fungal hyphae filled the medullary cavity of these bones and were closely packed on the surfaces of the bone, producing characteristic notching or pitting visible in thin section (Marchiafava *et al.* 1974, 197). In other areas the bone had experienced considerable decalcification and here the fungi appeared to have accumulations of lipid in the hyphae. The fungi in the decalcified areas were always in an advanced stage of degeneration. Marchiafava *et al.* concluded that any material that enters the fungus does so by the fungal membrane in contact with the bone surface and that such material is already in aqueous solution. They state that 'there can be no doubt that enzymes and other substances able to attack bone are present inside and outside the fungus membrane and attack crystallites and organic matrix simultaneously' (Marchiafava *et al. 1974*, 207).

Hackett (1981) also experimented in the production of focal destruction in bone using samples of sterilized compact bone. These he had buried in controlled conditions in garden soil at room temperature for one year. On excavation and microscopic examination, at least two of these showed tunnelling and evidence of dissolution and re-precipitation of bone mineral. However, no Wedl tunnels were seen in any of these specimens. Of the six species of fungi isolated from these bones only one, of the species *Fusarium*, produced tunnelling when inoculated into sterilized bone, although the results of this experiment were inconclusive since the original bone from which the *Fusarium* specimen was isolated failed to show tunnelling after further burial nor did it succeed in producing tunnelling in subsequent experiments. Towards the end of his paper, Hackett suggested that the narrow Wedl tunnels found in exhumed and fossil bone may result from the activity of certain bacteria, deriving their nourishment from the debris left by fungi.

Piepenbrink (1986) also investigated what he termed 'biogenous dead bone decomposition, using a wide variety of analytical techniques, including histology, microradiography and microbiological incubation. His results concur closely with those of Garland, Hackett and Hanson & Buikstra. Moreover, by examining thin sections of inoculated bone in ultraviolet light, he was able to demonstrate the location of active fungi around osteon canals. Micro-organisms compete with other species mainly by the excretion of antibiotics, of which penicillin is an example. Many of these compounds contain fluorophores (fluorescing functional groups) or chromophores (strongly coloured

functional groups). Fluorescence microscopy of exhumed human bone inoculated with the fungus *Stachybotrys* revealed bright rings of yellow-green fluorescence caused by several unidentified fluorescing antibodies (Piepenbrink 1986, 421). Piepenbrink also investigated the stains, reported by many observers on exhumed bone and found red, black and violet-blue discolouration on the exposed bone surfaces. He identified fungi (isolated by incubation in sterilized soil) from these stained areas as *Stachybotrys cylindrospora*, *Doratomyces stemonitis*, and two others of the genera *Pythium* and *Rhysoctonia* and concluded that 'the observed erosion of cortical bone (was) a result of increased amounts of bone-decomposing metabolites in intensively colonized bone surfaces'. These fungi were found to rapidly colonise exhumed bone (covering an age range of 200-1300 years old) previously sterilized by exposure to X-ray radiation (10^6 rad). However, none of these fungi produced any tunnelling when inoculated into the sterile bone. In addition, no staining was produced by the end of the incubation period, nor was there any visible reduction in birefringence when examined histologically. Despite the absence of tunnelling, Piepenbrink reported considerable yellowish-green fluorescence in the area of fungal colonisation, particularly in those samples inoculated by *Stachybotrys*. In addition to the failure of the isolated fungi to produce tunnelling or any of the other features associated with diagenetic alteration of bone (such as loss of birefringence) uronic acid assay of the stained areas of exhumed bone failed to demonstrate conclusively any depletion in mucopolysaccharides forming the ground substance of bone (Piepenbrink 1986, 425).

Numerous researchers have stressed the role of the production of organic acid metabolites by micro-organisms in the dissolution of bone mineral (White & Hannus 1983, 321; Piepenbrink 1986) but none have addressed the problem of how the organic fraction of bone is metabolized by these organisms. Marchiafava *et al.* (1974) found that demineralization and collagen destruction were almost simultaneous. Child and Pollard (1990) have investigated the effects of collagenase producing microbes on bone collagen. Collagenases may be defined as those enzymes that can catalyse the hydrolysis of un-denatured collagen, *i.e.* collagen as it is found in the body and unaltered by chemical or thermal degradation. Those micro-organisms that can excrete a enzyme capable of hydrolysing collagen will clearly have an advantage over other organisms in environments where this protein represents a readily available source of food. However, in order for these collagenases to engage and hydrolyse native collagen it must first be released from its intimate association with the inorganic bone mineral (Child, pers. com.). Several species of fungi and bacteria have been recognised that can produce collagenases, including micro-organisms found in the mouth (*Bacteriodes gingivalis* and *Candida albicans*) and gut (*Clostridium histolyticum*) of living humans and those present in the soil (*Clostridium histolyticum* and *Streptomycetes sp.*). These organisms could readily colonise skeletal remains once the corpse has been interred or discarded bone has entered the soil.

By incubating samples of mouth and skin swabs and samples of faeces in both aerated and anaerobic environments, Child and Pollard were able to isolate 144 micro-organisms able to utilize collagen as their sole source of nitrogen and 41 bacteria able to use D-aspartic acid (Child & Pollard 1990, 621). D-aspartic acid is used to estimate age at death of individuals or to date archaeological bone by amino acid racemization (see 2.3.3) and as such an understanding of any potential diagenetic alteration it may undergo is of crucial importance to the interpretation of dates based on this technique.

Grupe and Piepenbrink (1989) inoculated fresh, irradiation sterilized pig bone with fungi of the species *Clostridium* and *Penicillium* and placed on culture media enriched with salts containing either strontium, barium, magnesium or zinc. After storage in the dark at 4°C for 6 months, the bone samples were removed, thoroughly cleaned (using mechanical and chemical techniques) and analysed using atomic absorption spectrophotometry. Elemental concentrations remained high in the samples from enriched media, strongly suggesting that microbial activity in buried bones is implicated in the contamination of bone tissue during diagenesis. However, they reported that no tunnelling could be detected on any of the samples examined. The same authors, together with Schoeninger (Grupe *et al.* 1989) also demonstrated that fungal activity during burial could also influence the ratio of carbon 12 and carbon 13, with clear consequences for palaeodietary studies (see below).

2.3 Chemical Analysis

Until very recently, the chemical analysis of fossil bone has been restricted to two fields of interest; dating techniques and the study of palaeodiet. However, with recent advances in molecular biology, immuno-assay and DNA profiling there is now the potential for a new and radical approach to the study of ancient peoples. Dating techniques, palaeodietary studies and some of the more recent developments in molecular archaeology are described below.

2.3.1 Radiometric Dating

Radiocarbon dating is probably the best established science-based dating technique in archaeology, producing absolute or chronometric dates from ancient organic (carbon containing) matter. Absolute dates are those that may be expressed in calendar years (usually with a quoted error or level of confidence) rather than placed in a floating sequence or succession as in relative dates. Since its introduction in the 1950's, techniques of radiocarbon dating have improved enormously, both in accuracy and the ability to date progressively smaller samples. Radiocarbon and other radiometric dating methods are used to date organic objects that have become separated from their original context or where there are no cultural associations to give a relative date. Examples of this are

provided by the confirmation in 1959 that the Piltdown find was indeed a modern hoax by the radiocarbon dating of the jaw to a few centuries in age (de Vries & Oakley 1959) and the recent demonstration of the Turin shroud to be of medieval date (Damon *et al.* 1989) rather than dating to the first century A.D. An excellent, if somewhat ambiguous, example of the dating of an isolated find by the radiocarbon method is the dating of a 'bog body' from Lindow Moss (in Cheshire, N. W. England) and the surrounding peat in which it was found. Dates for the body range from AD 410 to AD 560 (calibrated) although samples analysed by different laboratories give un-calibrated dates spanning almost a thousand years. The surrounding peat has been more confidently dated to 400 to 200 BC (Otlet *et al.* 1986).

Radiocarbon dating relies on the detection and quantification of the ratios of the unstable isotope carbon-14 and the stable carbon-12. Since the half-life of carbon-14 is a measurable physical constant the age of any carbon containing compound can be calculated from this ratio, if the relative proportions at formation can be calculated by other means. The underlying principles of radiometric dating techniques and the practical problems of radiocarbon dating in particular are discussed by Aitken (1990). Sampling and sample preparation have always been a problem in radiocarbon dating. Although the amount of sample required has fallen dramatically, from 6 grams of carbon in the 1950's (Brothwell & Higgs 1969, 36) to 5-100mg in the 1990's (Aitken 1990, 78), the carbonaceous material must be purified to remove extraneous and contaminant carbon. In bone specimens where there is a measurable collagen content, purified collagen is used as the source of carbon. In specimens where no intact collagen survives attempts have been made to obtain dates from bone mineral carbonate (Hassan *et al.* 1977). However, the carbonate fraction in bone mineral is unreliable due to the likely presence of secondary carbonates washed in from the soil, although numerous papers have been published on its detection and removal (Haynes 1968; Hassan *et al.* 1977; Hassan & Ortner 1977; El-Kammar *et al.* 1989; Lee-Thorpe *et al.* 1991). Humic acids derived from the soil may be removed from bone specimens by washing in alkali. Contamination by other, exogenous, proteinaceous matter may be assessed by checking the amino acid signature against that for fresh bone collagen. If accelerator dating is to be used contamination may be kept to a minimum by using only the hydroxyproline fraction of the amino acid content since this amino acid is almost unique to bone (Aitken 1990; van Klinken 1989). The ratio of carbon isotopes is determined either by measuring the beta activity of the sample or by directly counting the atoms themselves using accelerator mass spectrometry. The maximum age of bones that can be confidantly dated by radiocarbon is approximately 50 thousand years (Aitken 1990).

Calcium-41 is a radioisotope that is potentially ideally suited to the dating of bone since calcium comprises a major component of living bone. It is formed in the top meter or so of soil due to the action of cosmic ray neutrons on the stable isotope calcium-40 and from there enters the food chain. During the life of an animal its bones continue to be irradiated causing the further transformation of

calcium-40 into calcium-41. This process is only halted if the bones become shielded by more than a meter of overburden post-mortem, after which the concentration of calcium-41 decreases due to radioactive decay. In practice, therefore, only bone found in caves and rock shelters is appropriate for this dating technique. The radioactive half-life of calcium-41 (approximately 100,000 years) is particularly suited to the dating of fossil man but as yet this technique has been little used compared to other radiometric techniques such as uranium series dating. This is partly due to the difficulty of estimating the initial isotopic ratio at deposition (time zero). Because calcium-41 is formed locally in the soil and does not enter a large reservoir as carbon dioxide does in the atmosphere, the initial $^{41}Ca/^{40}Ca$ ratio may vary with geographical location as well as over time. Nevertheless, recent studies have investigated the potential of this dating method to archaeology (Henning *et al.* 1987; Middleton *et al.* 1989). The ratio of calcium-41 to calcium-40 is expected to be extremely small, possibly as little as 10^{-14}. Further, it is not known what effect, if any, the migration of calcium into or out of the bone during burial may have on the detection limits or accuracy (Aitken 1990).

2.3.2 Uranium Series Dating

Fossil bones with an age range between 5 thousand and 350 thousand years may be dated with some success by measuring the relative proportions of the decay products of the radioactive uranium isotopes uranium-235 and uranium-238. For dating purposes, only the long-lived daughter products are used, uranium-234 and thorium-230 in the case of uranium 238 decay, since short-lived isotopes will have decayed to undetectable levels. As with radiocarbon dating, the detection of these daughter products relies on either measurement of sample radioactivity, in this case gamma emission, or by mass spectrometry.

This technique may be applied to calcite encrusted or impregnated bones from cave deposits or bone breccias containing calcite (Schwartz 1980). This is possible because although uranium often occurs as a trace contaminant in calcite crystals deposited from solution, thorium is not normally present because of its low solubility in water. Precipitation of calcite crystals therefore effectively sets the atomic clock to zero and thorium accumulates solely through the decay of uranium. The low solubility of thorium salts has the added advantage of minimising potential alteration of the thorium content, either by leaching or further precipitation as a consequence of diagenesis. Clearly however, movement of the more soluble, uranium ions may lead to either enhancement or depletion, leading to false measurements of the thorium to uranium ratio. Microscopic examination of samples combined with additional measurements of the uranium-234 to uranium-238 ratio may used to check for potential contamination and dates derived from the decay of uranium-235 to protractinium-231 may also be used to check the validity of thorium/uranium dating (Chen & Yuan 1988). Recent research by Tracey Elliott at the University of Durham (Department of Anthropology) has attempted to model the uptake of uranium in bone during diagenesis by immersing modern sheep bones in solutions

containing uranium salts in different concentrations and at various pHs (Elliot & Grime 1993). Recent research by others (Rae *et al.* 1989; van der Plicht *et al.* 1989) suggests that uranium series dating may, in fact, be of limited value in the dating of bones, including those from apparently ideal burial conditions such as caves where, even there, considerable leaching of uranium by ground water may take place. However, uranium series has been used with some success in the dating of fossil cave bear bones from Italy and Austria (Leitner-Wild & Steffan 1993). In this case the dates obtained have demonstrated good self-consistence in the concordance of the dates obtained by the uranium-thorium method and the uranium-protactinium method. Both sets of results also agreed well with radiocarbon dates for the samples.

2.3.3 Amino Acid Dating

Amino acids are the monomers from which the long chain protein molecules that make up living tissues, including bone collagen are formed. The chiral nature (left or right-handedness) of the four bonds on the alpha carbon atom of each amino acid makes these molecules optically active, *i.e.* solutions containing these molecules can rotate the plane of polarized light. There are two such *optical isomers* of most amino acids, designated L and D according to the sense in which polarized light is rotated, with the exception of glycine which contains only two carbon atoms and therefore exhibits bilateral symmetry. All naturally occurring amino acids are synthesised as the L isomer but after incorporation into living tissues, these are slowly transformed into the D form by a process called *racemization*, until an equilibrium is reached with equal proportions of the L and D forms. The end point of this equalization constitutes a racemic mixture. The racemization of L amino acids over time takes the form of an exponential relationship, but unlike radioactive decay can be influenced by several environmental factors such as temperature, the availability of water and pH. In common with the exponential decay of radioactive isotopes, the process of racemization is also commonly expressed in terms of a half-life (Bada 1982). The racemization of aspartic acid, which constitutes approximately 4.5% of the total amino acid composition for human bone (Woodhead-Galloway 1980.11), is most frequently used for dating of bones and teeth (Bada 1985).

Of the factors influencing racemization, by far the most important is temperature (Hare 1988). A one degree increase in temperature can cause an increase of 25% in the rate of racemization of aspartic acid. For example, aspartic acid has a racemization half-life (at pH 7.6) of 430 thousand years at 0°C and 3 thousand years at 25°C (Aitken 1990, 205). This can present problems if the thermal history of the bone is unknown, *i.e.* was the bone been cremated or cooked before deposition? If the age of the bone is known some information of its thermal history may be learnt from the L/D ratio of its amino acids. From the extent of aspartic acid racemization, Bada *et al.* (1989) were able to determine that the body of the German Emperor, Lothar I (died 1137) was boiled for 6 hours to remove soft tissues prior to transport to his final resting place. Diagenesis also alters

the rate of availability of peptide chains and hence also the rate of racemization, in addition to introducing non-collagenous proteins in the form of foreign micro-organisms (Elster *et al.* 1991). Clearly the introduction of exogenous amino acids can dramatically alter the relative proportions of the two isomers of isolated amino acids. Research undertaken by Child and Pollard has identified several bacteria able to utilize D-aspartic acid as a food source (Child & Pollard 1990, 621). Possible diagenetic alteration of the L/D aspartic acid ratio by the action of such micro-organisms is of crucial importance to the interpretation of dates based on this technique.

Measurement relies on the separation of individual amino acids from purified and hydrolysed collagen, using gas or liquid chromatography, or high performance liquid chromatography. Sample sizes required range from 1-10 grams. The age range for this technique is between 50 thousand and 100 thousand years. The reliability of this technique is not determined by the accuracy of the measurement but by the ability to make a suitable calibration and an assessment of the past environment of the sample. For example, initial dates obtained for the fossil bones of palaeoindians, found on the west coast of North America based on amino acid racemization were estimated at between 40,000 and 50,000 years ago. These dates relied upon calibration based on the age of one skeleton from Laguna Beach, California, which was itself dated by the β-decay counting radiocarbon technique. Subsequent re-analysis of the Laguna Beach specimen using accelerator mass spectrometry radiocarbon dating of the amino acid extract reduced its calculated age by approximately 12,000 years (Bada *et al.* 1984).

Since the amino acid content of bones and teeth undergo racemization during the life of the organism, the ratio of isomers has sometimes been used to estimate the age at death of individuals for whom the date of death is known. Using the relative resistance of teeth to diagenetic alteration (when compared to bone) Gillard *et al.* (1990) compared the percent D-aspartic acid in first premolars with age at death in both a modern human population and in individuals of known age and date of death from excavations at Christchurch, in Spitalfields, London. They concluded that the technique could be used to estimate age at death in an unidentified individual but that the method was no more accurate than other techniques in current use.

2.3.4 Electron Spin Resonance Dating

Electron spin resonance (ESR) relies on an evaluation of the dose of radiation received by a sample due to the radioactive decay of unstable isotopes within that sample or in its immediate burial environment. Subatomic particles, produced by radioactive decay, interact with any crystalline materials present within the sample causing imperfections or defects in the crystal structure. Energy trapped or stored in the lattice in this way may be released (as electromagnetic

radiation) if the sample is subject to energy above a certain threshold. Measurement of the energy released therefore has the potential for measurement of the total received dose. In ESR this measurement relies on the detection and quantization of lattice defects using controlled electric and magnetic fields (see Aitken 1990, 187-201). It has been applied to tooth enamel which has a high crystallinity compared to that of bone and is remarkably compact, thereby reducing contamination resulting from diagenetic change. ESR dating of bone is complicated by its poor crystallinity and its susceptibility to diagenesis. The presence of iron salts, for instance, has the effect of *quenching* or attenuating the ESR signal and iron is a frequent contaminant in buried bone. Despite these problems, ESR has been used with some success for the dating of early hominid bones (Ikeya & Miki 1980; Yokoyama *et al.* 1983; Zymela *et al.* 1988; Sales *et al.* 1989; Schwartz & Grün 1989; Grün & Stringer 1991).

2.3.5 Palaeodietary Research

The ratios of certain isotopes, particularly those of carbon and nitrogen, within living tissues is dependant upon those present in the diet of the organism and this in turn is reflected in the isotopic ratios preserved in the hard tissues after death. Analysis of the stable isotopes of carbon and nitrogen in prehistoric human bone may, in principle, be used to reconstruct past diets and ancient food chains (Parkington 1991). Most studies have been done on the stable carbon isotopes, carbon-12 and carbon-13 but more recently nitrogen isotopes have also been investigated (Ambrose 1986, 1990; Ambrose & DeNiro 1986, 1989; Hare & Estep 1983; Katzenberg 1989).

2.3.6 Carbon Isotope Analysis

The basis for carbon isotope analysis is that the ratio of the stable isotopes, carbon-12 and carbon-13 in living tissues depends upon the pathway by which the carbon enters the food chain. Carbon enters the terrestrial food chain primarily as a result of photosynthesis from atmospheric CO_2 which has an effectively constant ratio of ^{13}C to ^{12}C of around 1:99 (*i.e.* 1% ^{13}C). A degree of isotopic fractionation takes place during the chemical reactions involved in the conversion of carbon dioxide and water into vegetable matter. Subtle variations in the ^{13}C to ^{12}C ratio arise because two distinct photosynthetic pathways exist, generally known as the C_3 and C_4 cycles. For marine plants the picture is further complicated since they derive their carbon from dissolved bicarbonates rather than atmospheric carbon dioxide.

Carbon isotope ratios are expressed:

$$\delta^{13}C = \left(\frac{^{13}C/^{12}C\text{sample}}{^{13}C/^{12}C\text{standard}} - 1\right) \times 1000$$

A negative value of $\delta^{13}C$ indicates a sample that is depleted in ^{13}C relative to the standard (Chisholm 1989, 12).

Plants, in turn, may be consumed by animals with the result that carbon isotopes are incorporated into meat and bone tissues, a process that involves further isotopic fractionation. There is an additional fractionation step if the animal tissues of herbivores are devoured by carnivores. As a consequence, the ratio for herbivores is different to that for carnivores and may be seen as sensitive to the proportion of meat in the diet. For example, a herbivore feeding only on corn with a $\delta^{13}C$ value of -12.5‰ will have a bone collagen value of around -7‰ to -6‰ and the flesh with a value -11‰ to -10‰. A carnivore feeding on this flesh will have a bone collagen value of around -6‰ to -5‰ (Schoeninger 1989, 40).

Collagen is extracted by demineralization of the bone to separate it from any possible contaminants containing carbon, such as carbonates. The purity of the collagen can then be checked by amino acid analysis. The purified collagen or isolated (hydrolysed) amino acids can then be burnt to carbon dioxide and the isotopic composition determined by mass spectrometry (Hare *et al* 1991). The use of individual amino acids for stable isotope analysis has the advantage that a single amino acid can, in principle at least, be traced through the food chain (Hare *et al* 1991, 286). It also isolates collagen from any other lipids, carbohydrates and non-collagenous proteins in the bone sample.

2.3.7 Nitrogen Isotope Analysis

The ratio of the stable isotopes of nitrogen, nitrogen-14 and nitrogen-15, in animal tissues reflects their ratio in the diet of the organism and therefore may also be used to investigate past food webs (Ambrose 1991). Again, the ratios of these isotopes in bones depends upon the pathway of nitrogen compounds (proteins) through the food chain. There are three potential pathways:

nitrogen fixing plants and those animals that feed on them

terrestrial food chains not involving nitrogen fixation

marine food chains not involving nitrogen fixation.

In principle therefore, it should be possible to distinguish between populations that relied primarily on seafood diets and those consuming vegetables, grain and terrestrial animals, by an analysis of their bones. However, climatic and physiological effects on nitrogen isotope variations in food webs must be taken into account when interpreting the nitrogen isotope ratios in human bones. For example, East African forest-dwelling herbivores have low $^{15}N/^{14}N$ ratios whereas savannah-dwelling species that conserve water by excreting concentrated urine have high values. These

environmental adaptations pose serious problems in the interpretation of nitrogen isotope analysis in the study of ancient diets but may also represent a new tool for the investigation of past climates (Ambrose 1991, 294).

The combination of carbon and nitrogen isotope analyses of human bone provides the most successful tool for the investigation of ancient diet. By plotting the $\delta^{13}C$ values for prehistoric human bone, corn and marine foods against those for $\delta^{15}N$, Ericson *et al.* (1989) were able to isolate groups of individuals with different dietary inputs (i.e. different proportions of protein derived from plants, terrestrial meat and seafoods) within a prehistoric population in Peru. Ericson *et al.* also plotted the carbon isotope ratios derived from bone collagen (gelatin) and bone apatite. The distribution of values on this graph allowed the contribution to diet by corn to be estimated and demonstrated that meat also formed an essential part of the people's diet. This technique has also been applied to the fossil remains of Cretaceous dinosaurs, comparing the carbon and nitrogen isotope values for carnivorous, omnivorous and herbivorous terrestrial dinosaurs and aquatic dinosaurs and other vertebrates (Macko & Engel 1991).

2.3.8 Trace Element Analysis

Several studies have been made on the trace elements in human bone, usually with a view to addressing one of two questions: can trace elements be used as dietary discriminants? (Lambert *et al.* 1979, 1982, 1983) and to what extent has diagenesis altered the original chemical composition? (Lambert *et al.* 1984; El-Kammar *et al.* 1989; Badone & Farquhar 1982; Buikstra *et al.* 1989; Grupe & Piepenbrink 1989; Pate *et al.* 1989; Price *et al.* 1985; Price 1989a, 1989b, 1989c). An comprehensive review of trace element analyses is given by Buikstra in *The Chemistry of Prehistoric Human Bone* (Price 1989a).

Of the trace elements in human bone, perhaps the most frequently examined is strontium. This element is chemically very similar to calcium and readily substitutes for it in bone mineral. In most studies, a high level of strontium is taken to be an indication of a largely vegetarian diet. Since strontium is a bone seeker, carnivores devouring principally flesh and leaving the bone would be expected to have bones relatively deficient in strontium. Very often, female skeletons contain demonstrably more strontium than males in the same population although it is not clear whether this is an indication of lower status, and consequently less access to meat, or reflects a physiological difference (Sillen & Kavanaugh 1982; Vourinen *et al.* 1990).

The zinc content of bones is also thought to reflect the contribution of animal sources to the diet. A high zinc content would be consistent with a diet rich in meat. Shellfish and seafood in particular

are rich sources of strontium. For obvious reasons the strontium and zinc levels are usually considered together when reconstructing past diet (Lambert *et al.* 1979).

High intakes of zinc can also cause a deficiency in copper (Casey & Robinson 1984). Both copper and barium are potentially important elements in the analysis of ancient diet. Traces of copper ingested as foodstuffs such as crustaceans, shellfish and offal is readily absorbed by the body and enters the skeleton (Lambert *et al.* 1984). Barium is a Group II element as are calcium and strontium. Its larger ionic radius may possibly cause it to be discriminated against by meat eaters to a greater extent than strontium, making it a more sensitive indicator of diet (Lambert *et al.* 1979, 132). In modern material, fur seals with a diet of fish have bones containing up to twice the barium found in the bones of vegetarian deer (Wessen *et al.* 1978). However the effects of diagenesis on barium is, as yet poorly understood. A diet rich in nuts may be expected to introduce enhanced levels of manganese, strontium, vanadium, copper and zinc (Buikstra 1989, 164).

A wide range of analytical techniques have been applied to investigating the chemical nature of bone. The accuracy of these analyses have increased dramatically in recent years with the development of improved extraction techniques and instruments of increased sensitivity. Techniques fall into two categories, those involving the digestion or dissolution of the sample in acid or other solvent and those relying on direct analysis of elemental concentration *in situ*. In general, although those methods that require an aqueous solution for analysis present problems of complete dissolution of the sample and the danger of contamination during preparation (Marlow & Winter 1991), they are by far the most sensitive with detection limits in the parts per million or even parts per trillion range. Other techniques involving analysis of a mounted whole sample often have reduced sensitivity but allow variation of composition with position to be mapped.

Those techniques that require the sample to be completely digested into an aqueous solution include, atomic emission spectroscopy (Antoine *et al.* 1988,), atomic absorption spectrophotometry (Lambert *et al.* 1985, 1991) and more recently, extremely accurate results have been obtained from inductively coupled plasma/atomic emission spectroscopy (Price 1989; Fischer *et al.* 1981) and inductively coupled plasma/mass spectrometry (Marlow & Winter 1991.).

Other techniques that do not require the sample to be in aqueous solution usually involve irradiating the specimen with ionizing radiation with the aim of stimulating fluorescence or nuclear reactions. Neutron activation analysis was first used to determine the concentrations of major trace elements in human bone of Hellenistic date from Greece (Edward *et al.* 1984) and Native American remains from North America (Badone *et al.* 1982). X-ray analysis using an electron microprobe has been used extensively, to detect both contamination and trace elements in archaeological bone (El-Kammar 1989). A similar technique using a beam of protons to stimulate the emission of X-rays

(Elliott & Grime 1993) or gamma rays has been used more recently to detect trace and heavy metals with extreme accuracy (Vuorinen 1990).

Element distribution maps for naturally occurring radioisotopes of uranium and thorium have been produced using the technique of auto radiography, where sections of bone are placed in intimate contact with a photographic plate or a solid state nuclear track detector. This technique was used to investigate a radioactive fossil fish found in Scotland (Bowie & Atkin 1956). The technique has also been extensively used in the experimental investigation of radioactive poisoning (Schubert, 1955) and to investigate the early mineralization of developing bone using radioactively labelled calcium salts (Jowsey 1973). This work was built upon by Williams and Potts (1988) by combining the use of naturally occurring radioisotopes with neutron induced beta auto radiography to quantitatively map the distribution of uranium, calcium, phosphorus, scandium and cobalt.

With the exception of those analyses directed at measuring the infiltration of radioactive elements for dating purposes, the majority of the investigations described above have been concerned with separating an endogenous chemical signal from exogenous, diagenetic contamination. The problem of diagenetic contamination is compounded by the low concentrations of dietary discriminants in living bone tissues and the relatively poor understanding of how diagenetic processes affect the chemistry of both organic and inorganic components of bone. These problems are discussed further in the interpretation of the analytical data presented in this study (see Chapter 10).

2.4 Other Analyses

Powder X-ray diffraction (XRD) has been used in the past both as a means of determining the effects of diagenesis and to assist in the identification of intrusive minerals. Its first use was to assess the contamination of fossil bone specimens prior to radiocarbon dating of the biologically derived carbonate component (Hassan and Ortner 1977; Hassan *et al.* 1977). Researchers claim to have identified a number of intrusive minerals and types of modified bone mineral. In addition, most XRD studies have demonstrated a sharpening of the peaks of diffractographs (i.e. reduced peak broadening) with increasing age of archaeological bone corresponding to increased crystallinity (Schoeninger *et al.* 1989; Tuross *et al.* 1989). It is not yet clear whether this increasing crystallinity is due to the recrystallization of amorphous calcium phosphate or an increase in crystallite size. XRD spectra of bone also show characteristic modifications when the specimen has been cooked or heated. These transformations occur between 550-600 degrees, at 650 and at 700 degrees Celsius. Several studies have been conducted on prehistoric bones from the Mousterian and Acheullian period in France (Perinet 1964, 1969, 1972).

Hassan *et al.* (1977) supplemented their mineralogical studies of modern and fossil bone with

analyses of the IR spectra of the samples. Their results demonstrate a sharpening of the IR absorbency bands with increasing age which correlates well with the sharpening of diffraction peaks in XRD studies. Weiner and Bar-Yosef (1990) used what they described as the crystallinity index or splitting factor of their samples, derived from the double absorption bands of the phosphate bond, as an indicator of diagenetic change. They also used infra-red spectrophotometry to examine the acid-insoluble (collagenous) fractions of fossil bones. Lee-Thorpe *et al.* (1991) used infra-red spectrophotometry to monitor the removal of diagenetic or intrusive calcium carbonate from fossil bone samples prior to isotopic analysis. This work also demonstrated the transformation of bone apatite to the acid phosphate, brushite during prolonged pre-treatment with acetic acid.

2.5 Biomolecular Palaeontology

The recent explosion in the applications of molecular biology has spawned a wide range of applications to the study of ancient organisms. With this expansion have come new disciplines and new names, ranging from molecular palaeontology (Ambler & Daniel 1991) to amino acid cosmogeochemistry (Bada 1991). The term molecular archaeology may be applied to the study of a range of organic macromolecules that may be preserved in fossils, archaeological deposits and other sediments and especially in bone.

The detection of blood group activity in exhumed bone was first discussed by Glemser in 1963 (Brothwell & Higgs 1963). Only the ABO antigens can usually be detected in ancient bone and antigens for Rh factor and other systems are only preserved in exceptional conditions. It is also suspected that certain micro-organisms can introduce errors and false identifications. Some species of the bacterium *Clostridium* are able to remove sugars from blood group substances while the differences between the major blood group systems lie in subtle differences in sugar residues in their mucopolysaccharides (Watkins *et al.* 1962; Watkins 1966). Haemoglobin has been detected in Roman and medieval human skeletal remains using enzyme linked immunosorbent assay (ELISA) (Ascenzi *et al.* 1985; Smith and Wilson 1990). Lipids and other organic residues have been extracted from bog body tissue and other archaeological material and identified using gas chromatography and combined gas chromatography/mass spectrometry (Connolly *et al.* 1986; Evershed 1990a; Evershed 1990b; Evershed *et al.* 1990c; Charters *et al.* 1991; Oudemans *et al.* 1991). These techniques could be readily and profitably extended to cover more general human and animal remains.

Attempts to recover and analyse protein residues from the tissues of extinct animals such as mammoth and thylocene enjoyed some success in the 1960's and 1970's but the potential for retrieving genetic information from ancient tissue seemed poor. In 1984 however, a short length of DNA (the complex protein carrying the genetic code of an individual organism) was successfully

isolated and cloned from a museum specimen of the skin of a quagga, a recently extinct African member of the zebra family (Higuchi *et al.* 1984). Shortly afterwards, Paabo succeeded in isolating and cloning DNA from a 2400 year old Egyptian mummy, producing a strand of DNA 3400 base pairs long (Paabo 1985). The major breakthrough came in 1985 with the development of the polymerase chain reaction (PCR), a technique for precisely amplifying tiny amounts of DNA (Mullis 1990). Operating in repeated cycles of splitting and enzymatically copying short strands of DNA this technique amplifies isolated molecules exponentially, generating sufficient material to sequenced. The technique of PCR, commonly called genetic fingerprinting, has been successfully applied to recently buried remains in the line of forensic investigations (Hagelberg *et al.* 1991) and also to archaeological material (Paabo et al. 1988; 1989). Most recently, DNA fingerprinting has been applied to skeletal remains suggested to be those of the Romanovs, the last Tzar of Russia and his family, executed by the Bolsheviks in 1918 (*Daily Telegraph*, September 14, 1992).

Hagelberg *et al.* were the first to amplify DNA from human bone (Hagelberg *et al.* 1989) and have subsequently examined excavated bones ranging in ages up to 750 years, succeeding in obtaining PCR amplifications of mitochondrial DNA. They were also able to correlate, to some extent, the preservation of DNA with the general preservation of the bone itself using SEM examination of polished, transverse sections (Hagelberg *et al.* 1991). However, the exact relation between DNA preservation, protein content, depth of burial and soil pH are as yet poorly understood. The actual sites and mechanisms of preservation of DNA in buried bone are also unclear. Several factors can interfere with the action of DNA polymerase when attempting to amplify ancient DNA samples. The most important factor is degradation and damage during burial, resulting in the breaking-up of the target DNA into short lengths. Other factors may include complex organic molecules from the soil. Amplification of samples of modern DNA has been demonstrated to be slightly inhibited by the addition of ancient, degraded DNA (Hagelberg *et al.* 1991, 402).

The extreme sensitivity of the PCR technique exaggerates the potential for contamination, a single strand of DNA derived from either the excavator or geneticist may be amplified along with the target molecule. Also, up to 95% of the DNA isolated from ancient bone is bacterial in origin (Richards pers. com.). Hagelberg *et al.* by amplifying only porcine DNA from a pig bone recovered from the shipwreck, *Mary Rose* were able to demonstrate that the problem of contamination during handling could be overcome (Hagelberg & Clegg 1991). However, this bone is not representative of the vast majority of archaeological bone nor were the circumstances of its recovery representative of those prevalent on archaeological excavations (Richards *et al.* 1993). It should also be noted that at around 400 years old this bone is comparatively recent in archaeological terms. There have been recent attempts to investigate the genetic affiliations of different human populations by an examination of the mitochondrial DNA of living peoples and that recovered from fossil bones (Horai *et al.* 1987, 1989, 1991). Palaeoanthropologists at the University of New Mexico are currently

working on the PCR amplification of ancient DNA from a 50,000 year old Neanderthal vertebra found in Iraq (Ross 1992), potentially the oldest human genetic material examined to date.

Despite the spectacular outward preservation of soft tissues in bog bodies, DNA would not be expected to survive because of the generally acidic conditions encountered in anoxic, waterlogged environments. DNA appears to degrade most readily in aqueous environments. In fact no DNA was detected in the body of Lindow Man (Hughes, 1986), although it should be noted that samples of tissue were examined using elaborate cloning techniques rather than PCR which is capable of amplifying tiny amounts of DNA. However, excavations at the site of a pool at Windover in Florida have yielded the bones of 177 individual humans, including the remains of brain tissue, dating back 7,000-8,000 years. Here the surrounding limestone has effectively buffered the stagnant waters, preventing excessive suppression of the pH. PCR amplification of material from this brain tissue has identified segments of the genetic code responsible for the regulation of the immune system (Ross 1992, 75). Several workers in the U.S., including Noreen Tuross are establishing a database of ancient DNA from pre-European populations in the Americas and hope to study the effects of Old World diseases such as smallpox on Native American peoples. Tuross is also examining bones for traces of antibodies resulting from severe infections with venereal syphilis, endemic syphilis and yaws, successfully isolating immunoglobins of the IgG class in two geographically isolated New World skeletal populations. This and similar work should resolve the question of whether or not syphilis was brought to Europe from the Americas by Columbus's men. In addition to shedding light on both genetic disorders and infectious diseases in ancient populations, the study of remnant DNA, particularly mitochondrial DNA may support or refute the controversial theory, based on the DNA evidence from modern individuals, that all living populations may be traced through the maternal line to a single female living in Africa around 150,000-200,000 years ago; the 'mitochondrial Eve' hypothesis.

The survival of amino acids in fossilized bones and mineralized tissues has been recognised for many years. More recently, immunologically active macromolecules have been found in brachiopod shells and bones of geological age (Collins *et al.* 1991; Muyzer *et al.* 1992). Remarkably, even quite labile (chemically mobile) organic materials such as polysaccharides, which would be expected to become solubilized, can survive in the fossil record over millions of years. However, unlike DNA, proteins and polysaccharides cannot be amplified in any way analogous to the PCR reaction and the majority of studies of fossil macromolecules have been restricted to amino acid or sugar analyses of hydrolysed samples. Such studies have in the past demonstrated that amino acids from dinosaur bones are different from those obtained from the surrounding rock matrix, indicating that they are probably derived from the bone tissues themselves. Furthermore, the relative proportions of the different amino acids are consistent with the primary structures being distinct from collagen, the major protein in bone.

The use of antibodies to identify specific biomolecules provides a powerful tool in the investigation of biomarkers in bone and other mineralized tissues, although the problem of separating the desired material from the complex mixture of its decomposition products remains to be fully overcome (Child & Pollard 1992). Species specific proteins have been identified in bones from extinct mammals, *e.g.* albumin has been detected in a 13,000 year-old mastodon from Taima-taima, Venezuela (Tuross 1989) and antisera to material extracted from a 10,000 year-old mastodon produced a positive response with modern elephant serum and elephant collagen (Lowenstein & Scheuenstuhl 1991). The bone protein osteocalcin has also been detected in the bones of fossil vertebrates, including dinosaurs, using two different immunological assays (Muyzer *et al.* 1992). Osteocalcin forms 1-2% of all bone protein and, in life, circulates in the plasma where it is implicated as an inhibitor of mineralization (Berne & Levi 1990). Muyzer *et al.* used both dot-immunobinding assay (DIBA) and radioimmunoassay (RIA) techniques to detect osteocalcin in modern and ancient bone specimens. Their results are summarized in Table 2.1.

Sample	Animal	Age (Ma)	DIBA	RIA ($ng.ml^{-1}$)
R1	Cow	0	very strong	>25
R2	Horse	0	very strong	>25
R3	Alligator	0	very strong	>25
R4	Chicken	0	very strong	>25
F12.T9	Deer	1	strong	n.d.
F13.T10	Bovid	1	strong	n.d.
F14.T8	Bovid	1	strong	n.d.
F18.56	Horse	3.5	weak	n.d.
F30.52	Turtle	15	weak	>20
F32.17	Titanothere	30	n.d.	0
F33.12	Ceratopsian	75?	moderate	52
F33.46	Ceratopsian	75?	weak	28
F34.CV	Sauropod	150	weak	92
F38.2	Hadrosaur	75.5	moderate	45
F38.51	Hadrosaur	75.5	weak	>80
F39.24	Ceratopsian	73.25	n.d.	1.6

Table 2.1 Osteocalcin in bones (after Muyzer *et al.* 1992)

In some of the dinosaur bones (F33.12, F33.46, F34.CV and F38.2) the ratios of glutamic acid to γ-carboxy glutamic acid gives clear evidence that there is preferential preservation of osteocalcin over other proteins, probably because osteocalcin binds even more strongly to the mineral phase than does collagen (Muyzer *et al.* 1992, 873). Berne and Levi also stress that osteocalcin has a high affinity for calcium and uncrystallised hydroxyapatite (Berne & Levi 1990, 519). Muyzer *et al.* concluded that osteocalcin survived in bone by virtue of its close association with bone mineral crystallites, either being tightly bound onto their surfaces or actually incarcerated within individual crystallites.

3. Microscopical Analysis of Fossil Bone

The presence of the substantial amount of hard, mineral deposit in bone distinguishes it from other tissues in the body and constrains the use of a microtome for the preparation of thin sections. Traditionally, several methods have been employed to overcome these problems but no single sample preparation technique can adequately preserve or illustrate every aspect of this complex tissue (Ham & Leeson 1961, 280-281). In the pathology laboratory, the most common approach is to examine decalcified bone in which specimens for study are demineralized prior to embedding in molten paraffin wax and slicing into thin sections using a microtome, as with soft tissues. Before decalcification, bone must first be 'fixed' in order to arrest the normal processes of post-mortem decomposition and preserve the soft tissues in a condition as near as possible to that found during life (Drury & Wallington 1980, 41). Common fixatives include several different recipes based on aqueous solutions of formaldehyde, alcoholic solutions of acetic acid or various concoctions containing mercuric or chromic salts.

Bone mineral, or hydroxyapatite, may be stripped from bone tissue either by the use of mineral acids (such as 5-10% nitric acid in water or water/ethanol), organic acids (such as 10% formic acid or trichloroacetic acid) or by the use of chelating agents such as EDTA; ethylenediamene-tetra-acetic acid (Drury & Wallington *op. cit.*, 200-204). After decalcification and section cutting, the specimens may be mounted on glass slides and stained to enhance certain histological structures in the same way as other biological tissues examined by light microscopy.

As an alternative to decalcification and microtoming, samples of fully mineralized bone may be cut into thin slices and subsequently ground down to the required thickness between two glass sheets whose surfaces have been 'sharpened' using an abrasive powder. These 'ground sections' are frequently prepared when examining pathological specimens that exhibit imperfect calcification as a result of disease or malnutrition such as osteomalacia or rickets (respectively). The distribution of mineral salts in these ground sections may then be studied by microradiographic techniques (Drury & Wallington 1980, 208). Microradiographs (sometimes more correctly referred to as photomicroradiographs) are high resolution X-rays of thin sections of bone which may then be viewed at high magnification. In microradiographs, areas of bone that exhibit relatively high levels of bone apatite appear lighter due to increased absorption of X-rays. Microradiography has the advantage therefore of readily distinguishing osteons with different degrees of mineralization, which in turn are related to their maturity.

In this research the microscopic examination of bone specimens set out to accomplish three major goals:

identification of features found in healthy bone tissues

recognition of characteristic changes in these features caused by diagenetic processes

investigation of how these diagenetic changes relate to the original structure of the bone

and further, if possible, to relate these diagenetic changes to the burial environment and identify the agents responsible for the changes.

3.1 Experimental Methods and Materials

Some aspects of the microscopy of bone tissues were introduced in Chapter 2 when discussing bone histology and previous related work on palaeopathology and diagenesis. This earlier work formed the foundation upon which the many of the procedures described below were based. In addition, some techniques more usually employed in the metallographic analysis of metal artefacts were also employed or adapted to the study of bone.

3.1.1 Sample Preparation

All specimens were examined in an undecalcified state to allow simultaneous assessment of both mineral and organic components. Specimens were prepared as embedded samples and ground and polished to give an optically flat surface. In many cases thin sections were subsequently prepared from these embedded specimens to permit examination by both transmitted and reflected light microscopy. The embedded specimens could only be examined using reflected light.

Prior to embedding and mounting, all specimens were fixed in Carnoy's fluid, a non-aqueous solution composed of:

ethanol	60%
trichloromethane	30%
ethanoic acid	10%

Drury & Wallington (1980, 52) suggest that specimens with a thickness not exceeding 3mm are fixed for a period of 30 to 90 minutes. Since many of the samples to be examined were considerably larger than this they were fixed for at least 24 hours in sealed glass jars containing Carnoy's fluid. Samples were then dehydrated by prolonged soaking in progressively higher concentrations of

ethanol and water (70, 90 and 100 percent respectively). Finally, the samples were transferred to a vacuum desiccator to prevent any adsorption of atmospheric water vapour.

After fixing and dehydration, all samples were vacuum embedded in a low viscosity cold mounting epoxy resin specifically designed for the mounting of metallographic specimens (Epofix Resin HQ). When this resin had fully cured (approximately 24 hours at room temperature) the mounts were hand-ground and polished on a rotating metallographic polishing machine to give an optically flat surface. Grinding was achieved with silicon carbide papers using water as a lubricant (see comments below) and final polishing was carried out using a nap cloth disc lubricated by industrial methylated spirits and impregnated with 4 micron diamond paste. Diamond paste was chosen so that the specimens would not be contaminated by the use of polishing media containing alumina or iron oxide. These embedded and polished specimens could be viewed in reflected light without further preparation.

For transmitted light microscopy, thin sections were cut from the polished mounts. Since both the undecalcified bone and the embedding resin were too hard to be cut using a conventional microtome, an alternative approach was developed. The embedded specimens were cemented to degreased glass microscope slides using a cyanoacrylate adhesive and with the polished surface brought into close contact with the slide. Experience proved that best results were obtained if the mounts were held in place using light finger pressure for a few seconds, rather than clamped, whilst the adhesive cured. After a few minutes to permit curing of the adhesive a section, of 1 to 2mm thickness immediately adjacent to the glass slide, could be cut from the embedded sample using a fine, jeweller's saw. The sawn face of each section was then polished as before by attaching a rubber sucker to the reverse of each slide and presenting them face down to the polishing wheel. Thin sections of predetermined and constant thickness were achieved by wrapping two or more turns of cellophane adhesive tape around each end of the microscope slide. 'Sellotape' clear adhesive tape has a thickness of 50 microns allowing thin sections of approximately 50, 100 or 150μm to be prepared according to the opacity of the bone. In addition, the tape served to prevent uneven or wedge-shaped grinding of the sections and also reduced the danger of a thin section being inadvertently ground away completely. After final polishing, the tape was removed and the whole slide washed in ethanol to remove diamond paste, residual adhesive and to dehydrate the specimen once more. For those specimens with a high organic content, volume expansion of the thin section resulting from the absorption of water during grinding frequently caused cockling and detachment from the glass slide. It was therefore essential to prevent air-drying of the thin sections after they had become wetted during grinding, since this almost always caused shrinkage and cracking or detachment from the slide.

3.1.2 Optical Microscopy

Thin sections were examined using a Leitz, binocular microscope at magnifications of 100, 200, 500 and 1000 times, employing both transmitted and reflected light. These samples were also examined in plane polarized light, using crossed polarizers to explore changes in birefringence brought about by diagenetic processes. It was possible to examine the embedded specimens in reflected light and this also proved a very useful technique, especially in the case of diagenetically altered bone when viewed through crossed polarizers.

In addition to visible light microscopy, ultraviolet light (u.v.) fluorescence microscopy and cathodoluminescent microscopy were also explored as potential techniques. Although some possible blue fluorescence was seen in certain features of archaeological bone when using u.v. light, it proved impossible to distinguish this fluorescence from reflected u.v. due to increased reflectivity in areas of the sample. Since no other coloured fluorescence could be distinguished in any of the specimens examined the results were considered to be inconclusive and the technique was not persued further.

When attempting cathodoluminescent microscopy, a technique frequently used in the examination of petrological sections, localised heating caused by the incident electron beam resulted in burning and blistering of the resin. This in turn lead to considerable damage, both to the bone specimens and the resin mounts and, as a consequence, the technique was similarly not pursued.

3.1.3 Scanning Electron Microscopy

Electron microscopy was used to provide both three-dimensional pictures of broken fragments and two-dimensional images of bone that had been embedded and polished to show their cross sections. Small fragments were broken off recent and archaeological bone to give clean, freshly broken surfaces. These fragments were mounted on aluminium stubs and gold coated by vacuum deposition to render the surfaces electrically conducting in preparation for examination in the electron microscope. A conducting surface is essential to prevent the build up of electric charge on the sample since this charging can lead to severe distortion or disruption of the resulting image. Since the gold coating of samples can compromise microanalysis by swamping the radiation from lighter elements in the specimen, the polished cross-sections were vacuum coated with carbon to permit semi-quantitative analysis and the distribution of selected elements to be mapped. Electron microscopy and elemental dot mapping have also been used by Lambert *et al.* (1991).

Two different electron microscopes were used in the study. The fracture surfaces of small specimens were examined at the Physics Department of the University of Durham, using a Cambridge Series 600 scanning electron microscope equipped with a Link 860 series 2, energy dispersive (EDAX)

microanalyser. The polished cross-sections and selected smaller fragments were examined using a Cameca Semprobe scanning electron microscope equipped with both an energy dispersive and a wavelength dispersive microanalyzer. The microscope forms the basis of the Science and Engineering research Council, Science Based Archaeology, SEM facility based at the Oxford Laboratory for Art and Archaeology. Using the Cameca it was possible to image the specimens using backscattered electrons whilst simultaneously mapping the distributions of two pre-selected elements. In this 'dot mapping' the Kα X-ray emission lines were used.

Backscattered electron microscopy utilises the detection of those electrons from the primary (scanning) beam that have been scattered through a wide angle by interacting with an atom in the surface of the specimen. Since the rebound angle and the energy of the backscattered electrons (BSE) effectively increase with the mass of the atoms in the surface, backscattered electrons carry information about the composition of the specimen being imaged. In effect, the higher the average atomic number of the area under the primary electron beam, the greater the number of backscattered electrons detected and the brighter the image of that area. The use of backscattered electrons, therefore, provided an effective way of comparing the mineral content of different areas in the same image. Regions with denser, more mineralized, tissue or with greater contamination by heavy elements appear brighter in BSE images.

Microanalysis of specimens imaged by scanning electron microscopy is possible because the primary beam of fast electrons used to illuminate the specimen also ionises atoms within the specimen's surface, thus stimulating the emission of X-rays. The X-ray photons generated have energies (or wavelengths) characteristic of the atom from which they originate (see section 4.1.4). Elemental dot maps of the surface of a specimen may be built up if detection of a characteristic X-ray energy for a particular element is co-ordinated with the scanning of the primary electron beam. Similarly, if the electron beam is held stationary, or scanned over a small area, then a X-ray spectrum containing the characteristic lines (fingerprint) of those atoms within the surface under the beam may be collected.

3.1.4 Results

Optical microscopy of thin sections proved to be a relatively rapid, inexpensive and flexible technique for the examination of diagenetically altered bone. Many of the structures and features that characterize fossil and archaeological bone are visible at modest magnifications and when combined with the use of polarized light, optical microscopy is capable of distinguishing even subtle differences between normal bone tissue and that which has undergone diagenetic changes. Plate 3.1 shows a cross-section of bone collected from the surface of a pebble beach in Cyprus. This specimen, though undoubtedly of relatively recent origin was water worn but nevertheless illustrates many of the features of fresh bone tissue. This transverse section shows compact or cortical bone containing

several Haversian systems or osteons, recognisable by the concentric arrangement of osteocyte lacunae around a central channel or Haversian canal that, in life, would have contained blood vessels and nerves (see Figure 1.3). The dark linear feature at the centre top is a drying crack that developed in the specimen prior to collection.

When viewed in polarized light with polarizer and analyser at 90 degrees, this specimen shows very distinctive birefringence (Plate 3.2). Successive concentric layers or 'Haversian lamellae' are visible in each osteon, many of which exhibit the 'Maltese Cross' pattern characteristic of Haversian bone. The Haversian systems are superimposed on a background of interstitial lamellar bone running roughly from top left to bottom right of the field of view. The presence of such perfect birefringence in this bone section testifies that there has been little post-mortem alteration of the bone tissue other than loss of osteocytes and other soft tissues. The birefringence of bone tissue arises from the intimate association between, and preferential alignment of, the collagen fibres and apatite crystallites in bone. The plywood-like structures of lamellar and Haversian bone lead to the alternate transmission and extinction of polarized light in adjacent lamellae which in turn gives rise to the patterns visible in Plate 3.2 (Giraud-Guille 1988).

Haversian systems and lamellar bone may also be identified in backscatter SEM pictures of compact bone (Plate 3.3). This resin embedded, transverse section of bone of Pleistocene age also illustrates that osteons are frequently less well mineralized than the surrounding lamellar bone and as a consequence appears darker in BSE images. For comparison, Plate 3.4 shows a microradiograph of Haversian bone in which highly mineralized areas appear light and poorly mineralized areas darker. The variation in mineralization between individual osteons reflect differences in the age or maturity of the bone in different Haversian systems as described in Section 2.2.1. The bright features visible in Plate 3.3 are dense areas of exogenous mineral filling the voids of the Haversian canals. The cracks result from shrinkage associated with grinding and polishing of the specimen. At still higher magnifications it is possible to identify the fine canals or canaliculi that interconnect adjacent osteocyte lacunae and supply blood and nutrients to bone cells during life (Plates 3.5 and 3.6).

If the area close to the surface of the bone illustrated in Plates 3.1 and 3.2 is examined, then it is possible to distinguish the early stages of the most common diagenetic change that overtakes bone lying on or in the soil (Plate 3.7). A network of fine channels can be seen to penetrate the bone up to a depth of 1 to 2 millimetres from the surface. These channels result from the 'tunnelling' described in the section on palaeohistology (Section 2.2.1). By the meandering nature of the tunnels visible in Plate 3.7 and the fact that they cross into adjacent lamellae, they may be identified as 'Wedl tunnels'. The tunnels have diameters that are much larger than those of the canaliculi and are made immediately visible due to the dark staining of their walls. In addition, Hackett (1981, 247) claimed that there was 'no evidence .... that tunnels were in any way influenced by the osteocyte spaces and

their canaliculi'. This view appears to be supported by the image in Plate 3.8, in which tunnels conforming to the type Hackett identifies as 'linear longitudinal' and with a typical diameter of 20 μm penetrate both Haversian and lamellar bone seemingly with little relation to the osteocyte lacunae. It should be noted that the centres of focal destruction seen in Plate 3.8 are clustered around and run parallel to the osteones, *i.e.* the long axis of the bone. Most authors agree that tunnelling is produced by the action of soil micro-organisms, most probably fungi and it would seem reasonable that the extensive networks of Haversian canals, canals of Volkman and canaliculi present the most immediate access for soil organisms to the bone tissue. Plate 3.9 would seem to reinforce this interpretation by showing tunnels clustered around, and possibly radiating out from what is probably a canal of Volkman penetrating lamellar bone. When viewed in polarized light the bone immediately adjacent to the tunnels has clearly lost its birefringent properties and appears pale 'milky' brown and opaque (Plate 3.10). Plate 3.11 shows a transverse section of bone in which several osteones have been similarly affected. However, the bone section illustrated in Plates 3.12 and 3.13 demonstrates that bone tissues can be affected even in the absence of visible tunnelling. Plate 3.14 shows that part of an osteon may be affected whilst other parts are completely unaffected. This loss of birefringence in fossil or exhumed bone is frequently reported by other researchers (Piepenbrink 1986; Hackett 1981; Garland 1987, 1989).

Extensive tunnelling by micro-organisms ultimately results in complete disruption of the bone structure, although curiously the outer surfaces of the bone (where it has been in direct contact with the soil) are often considerably better preserved (Plates 3.15 and 3.16). This disruption is accompanied by complete loss of birefringence, although isolated pockets of unaffected bone may survive in even the most degraded bones (Plates 3.17 and 3.18). Differential preservation of bone histology on a very local scale has also been noted by other researchers. Hanson and Buikstra, using microradiographic techniques, examined a large number of exhumed human skeletons with dates ranging from 180AD to 1200AD from the Lower Illinois Valley (Hanson & Buikstra 1987). Their aim was to assess the diagenetic alteration of the bones' chemistry by an examination of its histology, with particular reference to palaeodietary research. In addition to isolated focal destruction of bone tissue they identified specimens in which the whole cortex of the bones had been almost completely destroyed by the action of micro-organisms but in which the periosteal surface was preserved intact. They also found bones which exhibited partial intracortical destruction where the action of micro-organisms was confined to a band between intact periosteal surfaces and relatively unaffected Haversian bone in the interior. Hanson and Buikstra suggest that Haversian bone is mechanically weaker and less mineralized than interstitial and lamellar bone and that the initial spread of micro-organisms may be dependant upon the 'intrinsic protein-mineral bond' (Hanson & Buikstra 1987, 559). They further noted that initially, micro-organisms appear to favour the less mineralized tissues but once they have become established, create a local environment in which attack of the more mineralized tissues becomes possible. Schoeninger *et al.* similarly suggest that diagenesis does not

begin at the surface of bones and travel inwards in a simple manner but is strongly influenced by the distribution of Haversian canals and interstitial spaces (Schoeninger *et al.* 1989, 283). These provide longitudinal pathways in the bone and give rise to a much more complex interaction between individual bones and their burial environment. However, other evidence suggests that differential preservation of the periosteal surface may result from physico-chemical mechanisms rather than the spread of micro-organisms. Work on the dissolution of dental enamel exposed to acidic solutions has shown that the surface in contact with the acid is resistant to demineralization to a depth of approximately 0.5mm whereas the interior suffers considerable dissolution of hydroxyapatite (Anderson & Elliot 1993). This differential demineralization occurs over a matter of days and does not appear to involve the action of micro-organisms or the influence of metal ions. Hanson and Buikstra (1987, 555) also refer to 'diffuse' demineralization, in which mineral is leached from bone tissues without any apparent destruction of histological features and without tunnelling. This type of demineralization is clearly visible in microradiographs and is accompanied by pronounced 'cuffing' or hypermineralization of the borders of the Haversian canals.

In addition to tunnelling and the loss of birefringence described above, buried bone is also infiltrated by metal ions from the soil, leading to staining and darkening of the bone tissues close to the outer surfaces (Plate 3.19). This staining appears to be independent of the mechanisms that cause loss of birefringence since heavily stained bone still preserves the 'Maltese Cross' pattern in polarized light (Plate 3.20). The presence of iron salts in the stained border shown in the thin section 3.19 is demonstrated in Plate 3.21 a BSE image of medieval bone and Plate 3.22 which shows a distribution map for iron in the same section. Copper may also be taken up by bone. Plates 3.23 and 3.24 show a sheep metacarpal that was collected from the surface of an abandoned copper mine at Limni, in Cyprus. Green staining is visible at the boundary between unaffected bone in the interior and bone that has suffered loss of birefringence. Plate 3.25 shows a BSE image and copper distribution map for the same bone, clearly demonstrating the concentration of copper salts at the zone of biological activity. Lambert *et al.* (1991) also observed that higher concentrations of iron, aluminium and manganese were found on the surfaces of exhumed bones and in cracks or voids. Using SEM and elemental dot mapping they concluded that 'the vast majority of elemental incursion by Fe, Al and Mn is within 0.5mm of the surface'

When bones from alkaline burial environments are examined microscopically, there is a striking absence of staining. This is consistent with the relative insolubility of most metal salts at high pH's. Plates 3.26 and 3.27 show human bone of early medieval date, excavated from the site of a Byzantine basilica in western Cyprus. Certain areas of the bone appear white and show normal histology whereas others have become darkened and show some evidence of attack by micro-organisms. When viewed through crossed polars it is clear that birefringence has also been preserved in areas of good histological preservation but is again absent in those areas that appear 'milky' brown. Viewing thin

sections in polarized light dramatically highlights the mineral deposits that have precipitated in the voids and fissures present in this section. These massive deposits are also clearly visible in BSE images of sections from the same bone sample (Plate 3.28). The white areas in the BSE image represent regions of high density compared to the surrounding bone which has a considerably lower mineral content due to the presence of substantial quantities (by volume) of collagen. Dot maps for Fe Kα, P Kα and Ca Kα (Plates 3.28 and 3.29) confirm both the absence of iron salts in this bone and that the mineral deposits are calcium carbonate rather than a phosphate mineral. Subsequent X-ray diffraction and infrared studies confirmed the mineral in this specimen as calcite (Figures 5.11 and 6.15).

Bones recovered from waterlogged archaeological environments often exhibit very good preservation on excavation, although some of these bones may suffer deterioration once exposed to the air. Plate 3.30 shows a transverse section of a horse metatarsal excavated from waterlogged clay deposits excavated within the Roman fort at Ribchester, Lancashire. Although stained, this bone exhibits exceptional preservation of histology and when viewed in polarized light, demonstrates classic birefringence (Plate 3.31). The presence of blue (possibly Fe^{2+}) and rusty brown (Fe^{3+}) material in the Haversian canals indicates that iron salts have infiltrated the structure. This specimen, which is hard and slightly greasy to handle, also preserves what may be interpreted as soft tissues further into the centre of the bone. Plate 3.32 shows, at high magnification, an osteon which has clearly undergone negligible biological attack. Lying within the Haversian canal are several sub-round objects that appear thinner or perforated at the centre. Human red blood cells (*erythrocytes*) have a mean diameter of 7μm (Berne & Levi 1990) whereas the objects visible in Plate 3.32 have diameters of the order of 3-4μm. Although it seems unlikely that soft tissues would survive prolonged burial, the features visible in Plate 3.32 are the right order of size to be the shrunken remains of red blood cell. Furthermore, one researcher (Wilby 1992) is reported to have identified fossil blood cells preserved in a 100 million year old fish, in which soft tissues have been replaced by calcium phosphate crystallites; a process he terms the 'Medusa effect'. Electron microscopy studies of bone from a specimen of *Tyrannosaurus rex* have also provided convincing evidence for the survival of blood cells over geological time (Morrell 1993).

The circular features visible in Plate 3.32 should not be confused with another type of structure that frequently occurs in taphonomic bone. These structures were seen lying within the pore spaces of the bone recovered from a sea beach in Cyprus (Plate 3.33) and later identified in a number of different specimens from the Vale of Pickering. These circular structures, each composed of numerous, small, tightly packed grains appear very bright in reflected light (Plate 3.34). Similar structures were quickly recognised in SEM images of other bones from waterlogged contexts and identified as framboidal pyrite (Plates 3.35 to 3.37). X-ray spectra taken using the wavelength dispersive microanalyzer identified iron and sulphur in individual grains but no oxygen, confirming that they

were composed of an iron sulphide, probably iron pyrites. The presence of this lustrous mineral accounts for the high reflectivity of the pyrite framboids when viewed in reflective light. Framboidal pyrite has previously been reported in bones (Day & Molleson 1973; Parker & Toots 1974; Ellam 1985a; Garland 1987, 123) and other porous materials such as wood (Watson 1981, 1984) and pottery (Green 1992) recovered from waterlogged, anoxic and stagnant environments such as those associated with shipwrecks and deep, terrestrial sediments.

Other features are also found in association with framboidal pyrite in bones from waterlogged environments. Plate 3.38 shows a number of pyrite framboids (in the lower half of the picture) together with a smaller circular feature (top left) and some denser, fragmentary material (centre). Elemental dot maps for S Kα, P Kα and Ca Kα (Plates 3.38 and 3.39) suggest that both phosphorus and sulphur are present in the pyrite framboids, although calcium is absent. By contrast, the smaller and less dense framboid in the top left of the field of view contains both calcium and phosphorus but little sulphur. Pyrite framboids are commonly associated with the presence of sulphate reducing bacteria which generate high concentrations of sulphide ions as a by-product of their metabolism. Although resembling a pyrite framboid, the small circular feature in Plate 3.38 contains no sulphide and probably represents a colony of sulphate reducing bacteria in the course of utilising organic matter from the bone matrix but before the sulphide ion concentration has risen to the levels necessary for the formation of framboids. The chemistry of sulphate reducing bacteria and framboidal pyrite is discussed further in Chapter 10. The high concentrations of calcium and sulphur in the centre of the field of view suggest the presence of a calcium sulphate, possibly gypsum. The presence of a calcium sulphate mineral is better demonstrated in Plates 3.40 and 3.41. These views show a severely degraded, waterlogged bone containing lenticular crystals (here seen in cross-section) that are high in calcium and sulphur but once again containing little phosphorus.

Clusters of lenticular crystals could also be readily identified in SEM pictures of broken fragments of bones from waterlogged conditions. Plate 3.42 shows a crystal habit for gypsum commonly referred to as 'desert rose' and traces of gypsum in this bone were detectable using X-ray diffractometry. Other crystal habits for gypsum can also be identified filling the pore spaces of bones from waterlogged conditions (Plates 3.43 and 3.44). The crystals shown in Plate 3.45 had grown to a sufficient size that it was possible to carefully dissect individual crystals from the bone and obtain definite identifications using X-ray fluorescence and X-ray diffraction techniques (Figures 3.7 and 5.10).

Over geological time, the original amorphous or poorly crystalline pyrite framboids are transformed to massive and more crystalline iron pyrite by reaction with excess free sulphur (Love 1965). This massive pyrite can be seen in the Pleistocene bone shown in Plates 3.46 and 3.47. Spot microanalyses (Figures 3.1 & 3.2 and Tables 3.1 & 3.2) confirm that the bright material lining the

pore is iron sulphide whilst the less dense material is either iron oxide or a complex mineral containing oxides of iron and calcium.

Element	Relative K	Wt %
Na	0.0081	2.52
Mg	0.0048	1.00
Al	0.0048	0.78
Si	0.0074	0.97
P	0.0219	2.58
S	0.3812	42.98
K	0.0011	0.13
Ca	0.0397	4.35
Ti	0.0020	0.22
Mn	0.0007	0.07
Fe	0.3260	35.83
O		8.57
Total		100.00

Table 3.1 Microprobe analysis of sulphide within canal

Element	Relative K	Wt %
Na	0.0040	1.82
Mg	0.0053	1.45
Al	0.0052	1.06
Si	0.0030	0.46
P	0.0020	0.27
S	0.0038	0.44
K	0.0007	0.07
Ca	0.1054	10.27
Ti	0.0000	0.00
Mn	0.0608	6.64
Fe	0.5105	54.41
O		23.11
Total		100.00

Table 3.2 Microprobe analysis of iron oxide within canal

Plate 3.48 shows relatively much more recent bone, from a Mesolithic site in the Vale of Pickering. Elemental dot mapping over the area covered by the image (Plates 3.49 and 3.50) revealed that one of the pores contained a high concentration of iron and sulphur whereas the majority of the pores contained comparatively low concentrations of iron and no sulphur. Further examination of this specimen revealed the area shown in Plate 3.51 which contains both framboidal pyrite and massive deposits of a mineral containing iron, phosphorus and oxygen (Figures 3.3 & 3.4 and Tables 3.3 & 3.4). This mineral is almost certainly the hydrated iron phosphate, vivianite, $Fe_3(PO_4)_2.8H_2O$ which frequently occurs as bright blue, chalky deposits on and in some bones from waterlogged conditions. For example, Plate 3.52 shows a detail of the Roman horse metatarsal illustrated in Plate 3.30 and clearly shows a blue mineral filling a Haversian canal which may well represent vivianite although it was not possible to obtain a definite identification by analysis. Vivianite has been identified as

associated with buried bones for many years. In 1870 the Illustrated London News reported 'Great quantities of vivianitized bones....were found' during excavations (*Illust. Lond. News*, 1 Jan 1870) and Piepenbrink also identified vivianite on medieval human vertebrae by XRD analysis (Piepenbrink 1989, Figure 5).

Element	Relative K	Wt %
Na	0.0033	1.04
Mg	0.0000	0.01
Al	0.0031	0.50
Si	0.0073	0.95
P	0.0470	5.51
S	0.3552	40.64
K	0.0012	0.14
Ca	0.0364	3.99
Ti	0.0009	0.10
Mn	0.0011	0.13
Fe	0.3306	36.31
O		10.69
Total		100.00

Table 3.3 Microanalysis of pyrite framboids

Element	Relative K	Wt %
Na	0.0018	0.62
Mg	0.0043	0.95
Al	0.0040	0.69
Si	0.0056	0.78
P	0.1531	19.49
S	0.0000	0.00
K	0.0001	0.05
Ca	0.0025	0.26
Ti	0.0000	0.00
Mn	0.0016	0.18
Fe	0.3501	38.37
O		38.62
Total		100.00

Table 3.4 Microanalysis of vivianite deposits

In addition to mineral species derived from ions in the soil solution, considerable evidence could be found for the redeposition of dissolved bone apatites. Plates 3.53, 3.54 and 3.55 show hexagonal crystals deposited within voids in bones from the Mesolithic deposits in the Vale of Pickering. These crystals may well represent redeposited hydroxyapatite crystals but no microanalysis was possible on these structures. However, Plate 3.56 shows a transverse section of bone from the Vale of Pickering in which the brighter, denser material lining the Haversian canals and other voids was examined using microanalysis. This was found to have a composition identical to that of the surrounding bone (Figures 3.5 and 3.6 and Tables 3.5 & 3.6). This observation agrees well with the hypermineralization or cuffing around tunnelling and focal destruction reported by other researchers

(Piepenbrink 1986, 424 and Figure 6; Hackett 1981, 247-248 and Figure 4c). The redeposition of hydroxyapatite probably arises from the dissolution of bone mineral at low pH's created by the secretion of organic acids by micro-organisms in areas of active focal destruction. Hydroxyapatite will then be carried in solution within the structure of the bone until a rise in the local pH or an evaporation front causes its crystallization. Without the tight constraints of metabolic activity or with a reduced carbonate content, these redeposited hydroxyapatite crystals are free to grow to much larger dimensions than the original bone apatite crystallites; the crystals visible in Plate 3.53 to 3.55 have dimensions of approximately 20μm compared to 40nm in living bone tissues.

Element	Relative K	Wt %
Na	0.000	0.01
Mg	0.000	0.00
Al	0.0011	0.15
Si	0.0051	0.60
P	0.1532	17.58
S	0.0037	0.45
K	0.0002	0.02
Ca	0.3794	40.18
Ti	0.0000	0.00
Mn	0.0019	0.23
Fe	0.0082	0.96
O		39.84
Total		100.00

Table 3.5 Microanalysis of mineral in canal

Element	Relative K	Wt %
Na	0.0000	0.01
Mg	0.0000	0.00
Al	0.0000	0.00
Si	0.0047	0.55
P	0.1632	18.66
S	0.0053	0.64
K	0.0000	0.00
Ca	0.3670	38.97
Ti	0.0000	0.00
Mn	0.0003	0.04
Fe	0.0055	0.64
O		40.48
Total		100.00

Table 3.6 Microanalysis of bone immediately adjacent to canal

Crystals of a different nature are visible in Plate 3.57. In these images fine needle-like mineral deposits can be seen covering the surface of bone from the Vale of Pickering. In size and morphology these are very similar to crystals grown from a solution containing calcium and phosphate ions and various concentrations of fluoride in the ppm range. Both size and shape of the resulting crystals appear to be determined by the F^- concentration (Iijima *et al.* 1992). The crystals

described above were grown from solutions at pH 6.5 and a temperature of 37°C to mimic *in vivo* conditions. It appears likely that both the size and morphology of redeposited hydroxyapatite crystals will be sensitive to factors such as pH, temperature and the presence of trace ions, and that these factors determine the nature of hydroxyapatites found in fossil bones.

The increases in crystallinity seen in archaeological and taphonomic bone can be attributed to the contribution made by these redeposited hydroxyapatite crystals. Even small quantities of comparatively large (approximately 50 to 100 times larger than bone apatite crystallites) and more ordered crystals will substantially increase the average crystal size and result in the sharper, more defined X-ray diffraction spectra seen in archaeological and fossil bones (Tuross *et al.* 1989).

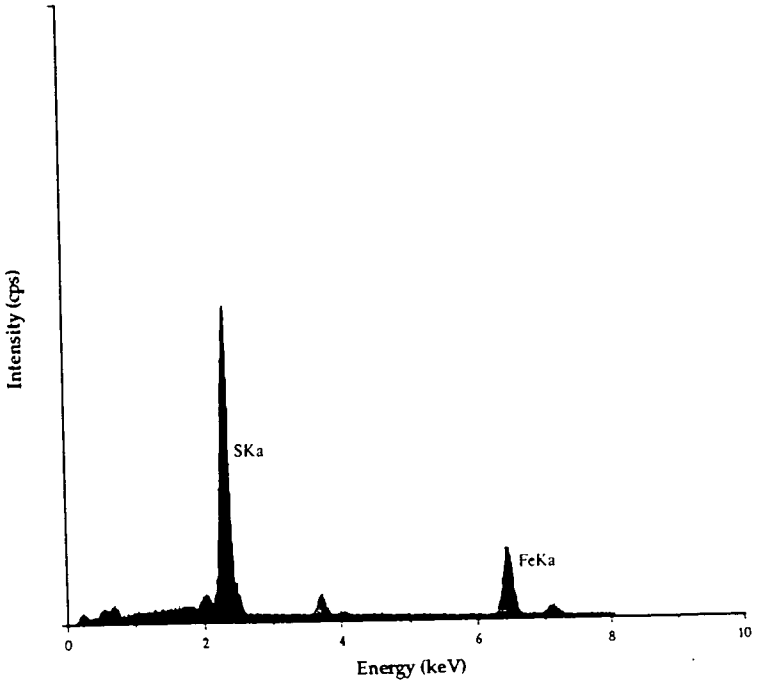

Figure 3.1 SEM microanalysis of iron sulphide in canal (Plate 3.46)

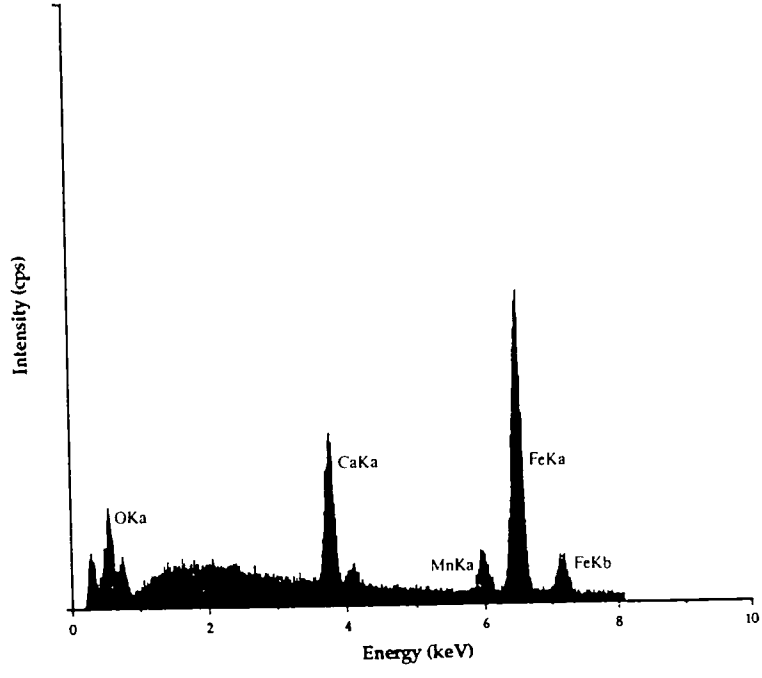

Figure 3.2 SEM microanalysis of iron oxide in canal (Plate 3.46)

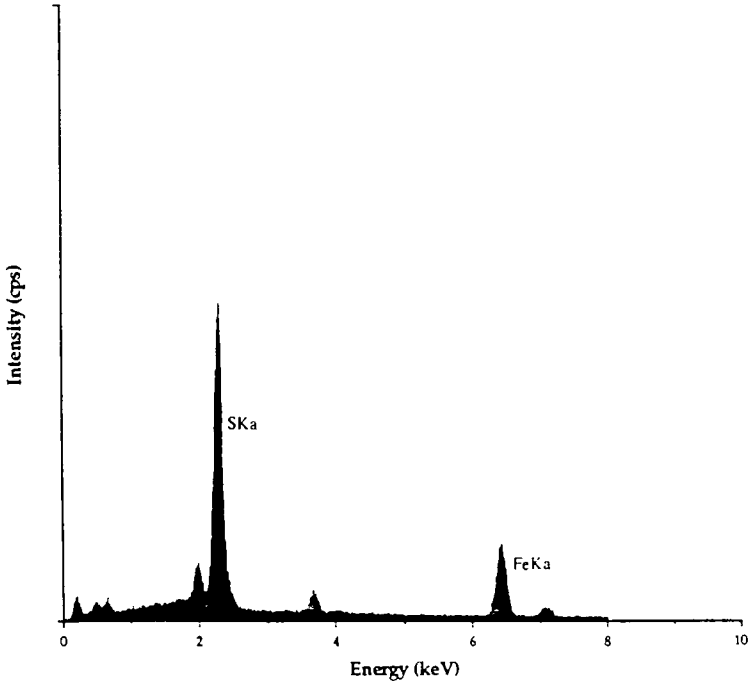

Figure 3.3 SEM microanalysis of pyrite framboid in Plate 3.51

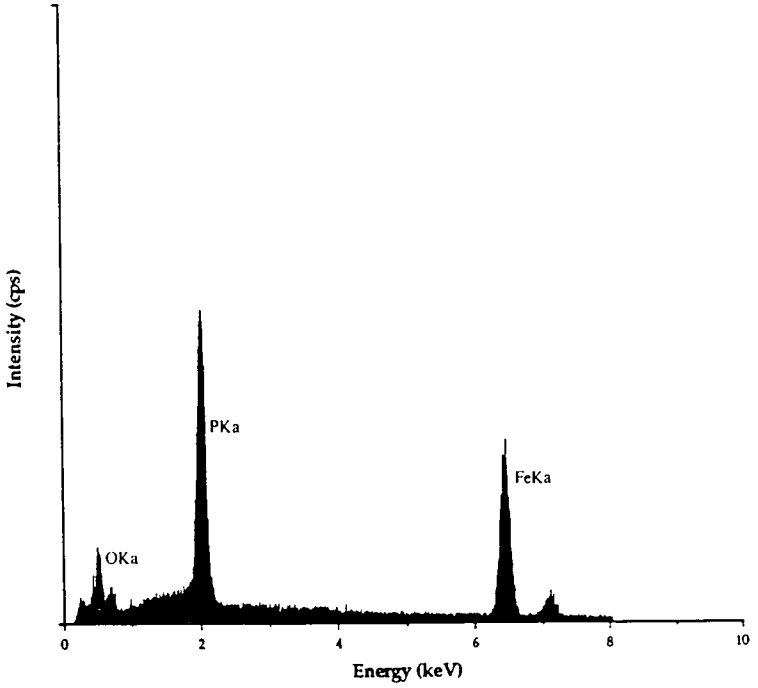

Figure 3.4 SEM microanalysis of vivianite (?) in Plate 3.51

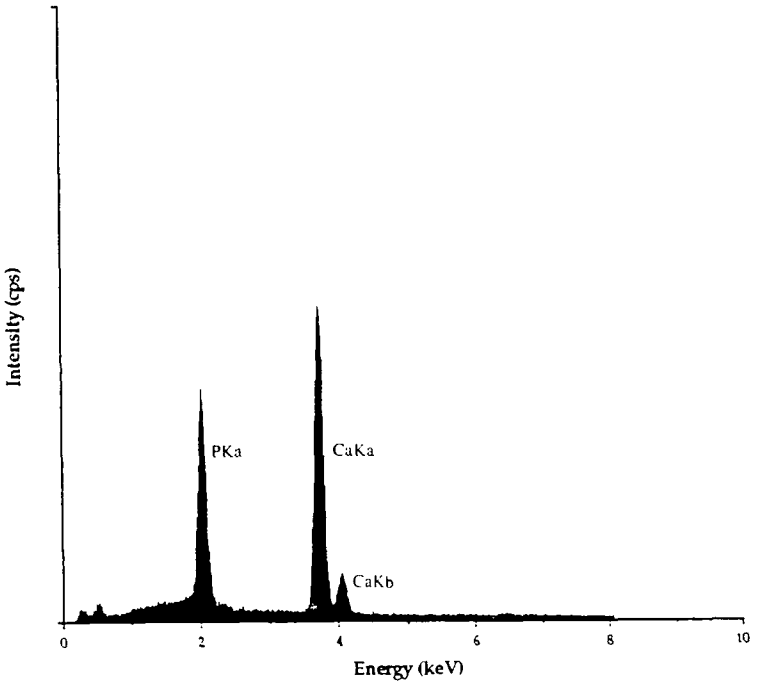

Figure 3.5 SEM microanalysis mineral filling elongated feature in Plate 3.56

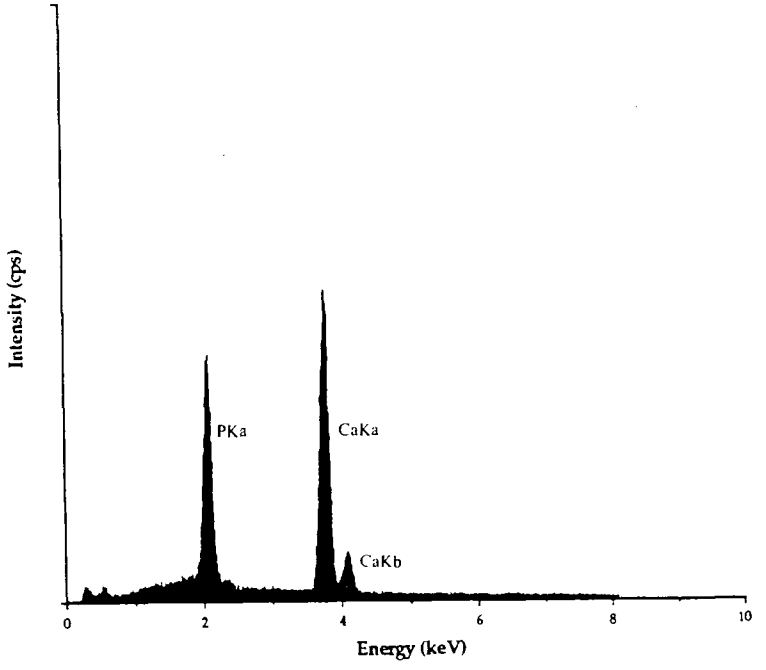

Figure 3.6 SEM microanalysis of bone surrounding the elongated feature in Plate 3.56

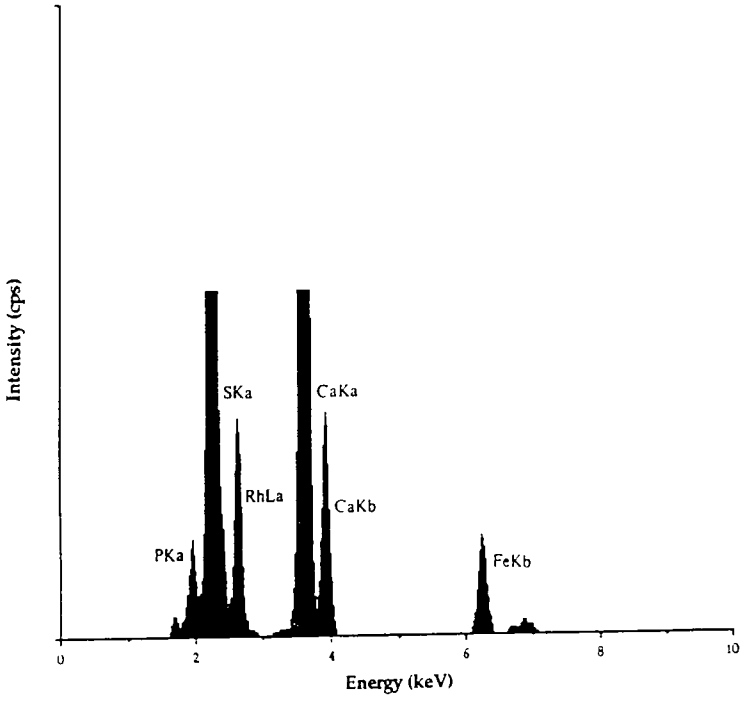

Figure 3.7 XRF analysis of gypsum crystals dissected from Sample 22

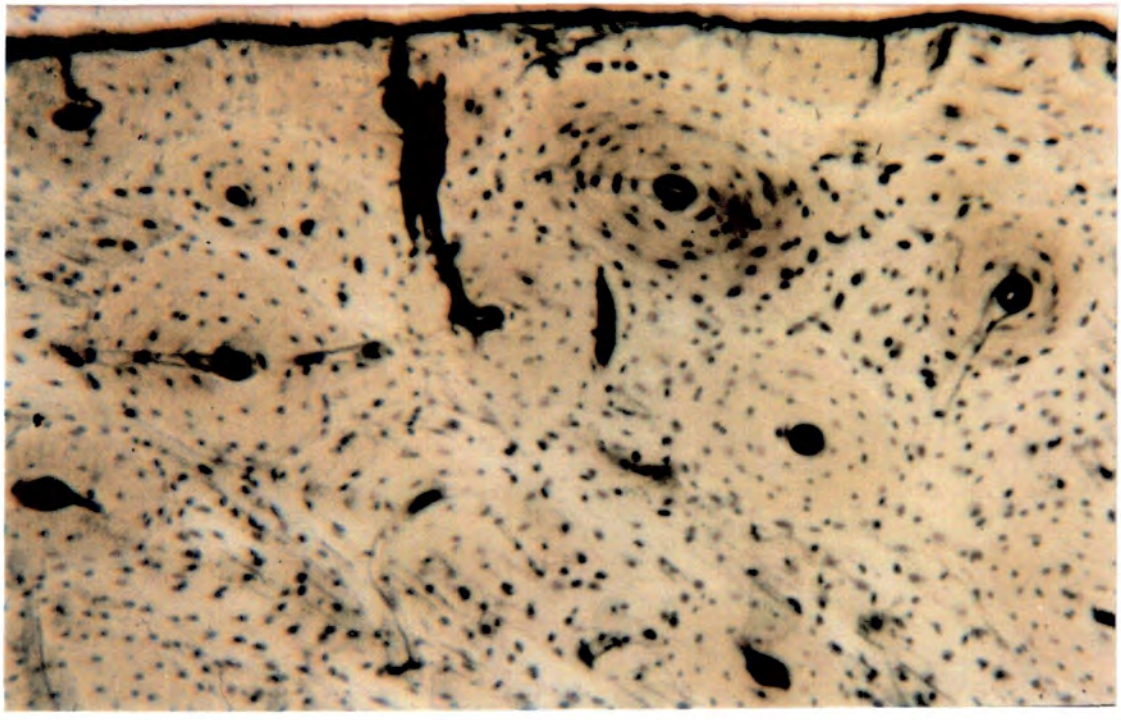

Plate 3.1 Thin section of bone collected from Polis beach
(field width 0.6mm)

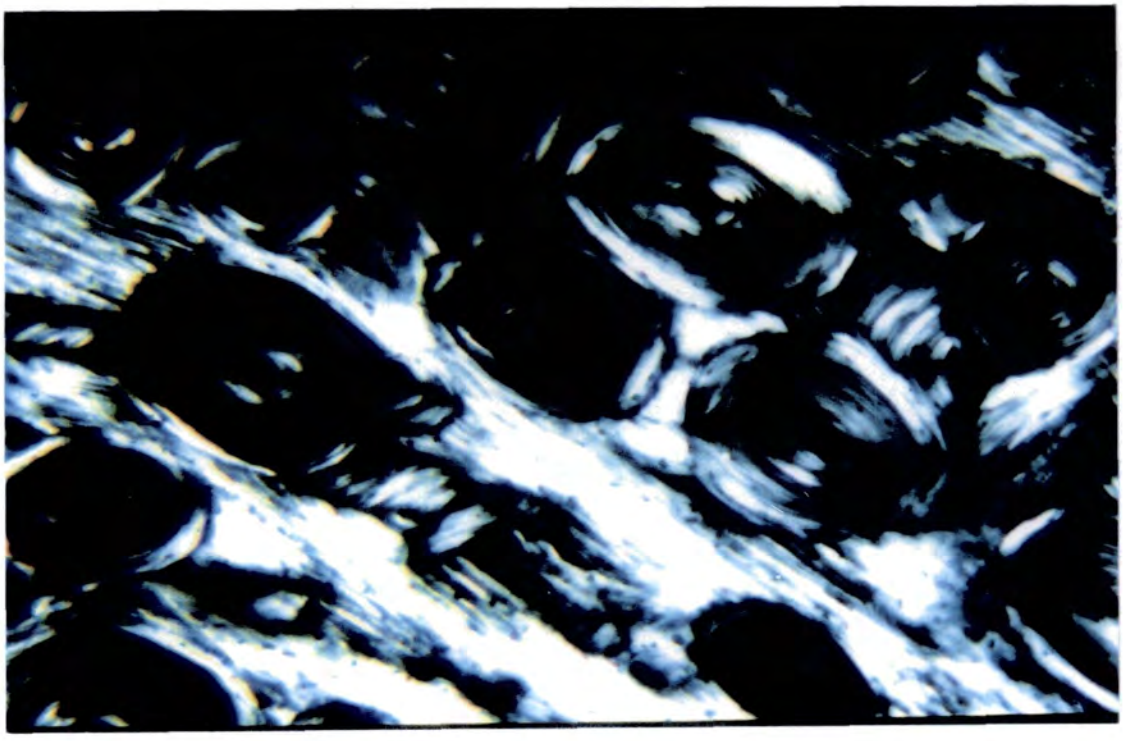

Plate 3.2 Bone from Polis beach viewed through crossed polars
(field width 0.6mm)

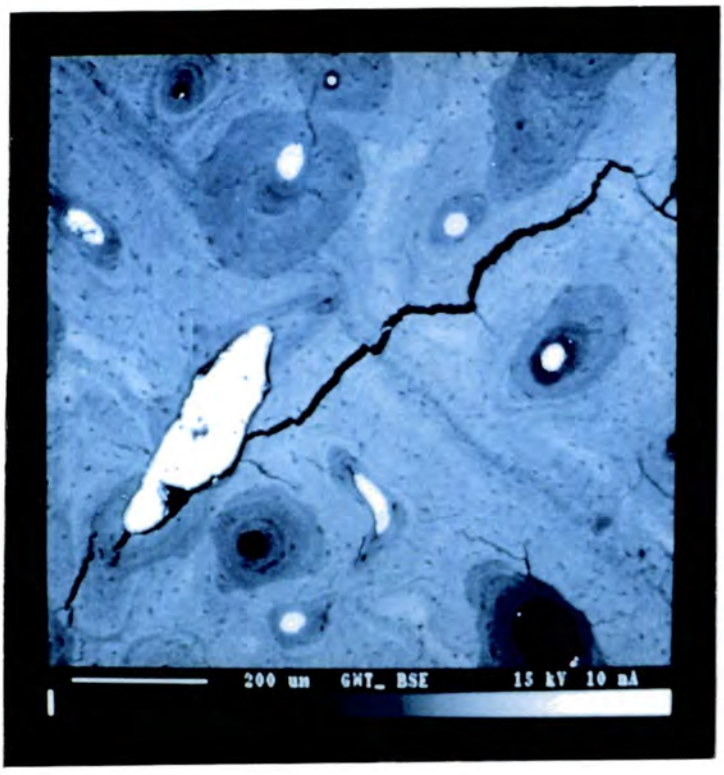

Plate 3.3 Haversian and lamellar bone in SEM backscatter mode

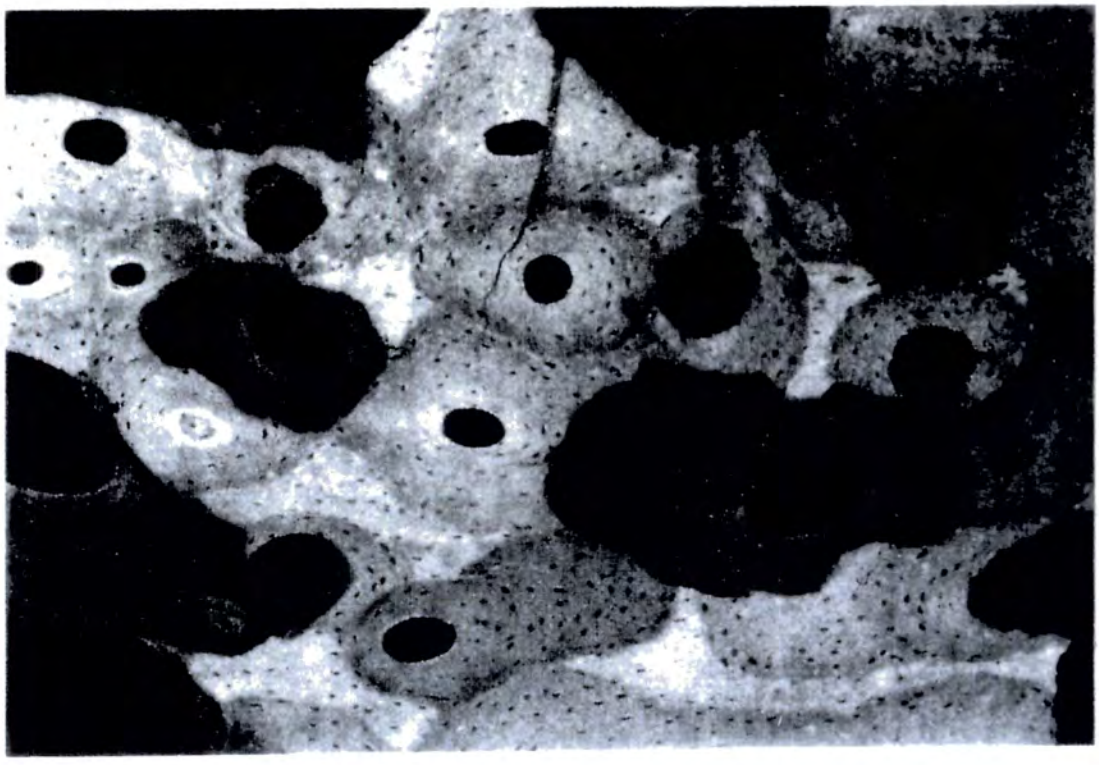

Plate 3.4 Photomicroradiograph of Haversian bone
(courtesy of Dr N. Garland and Manchester University Press)

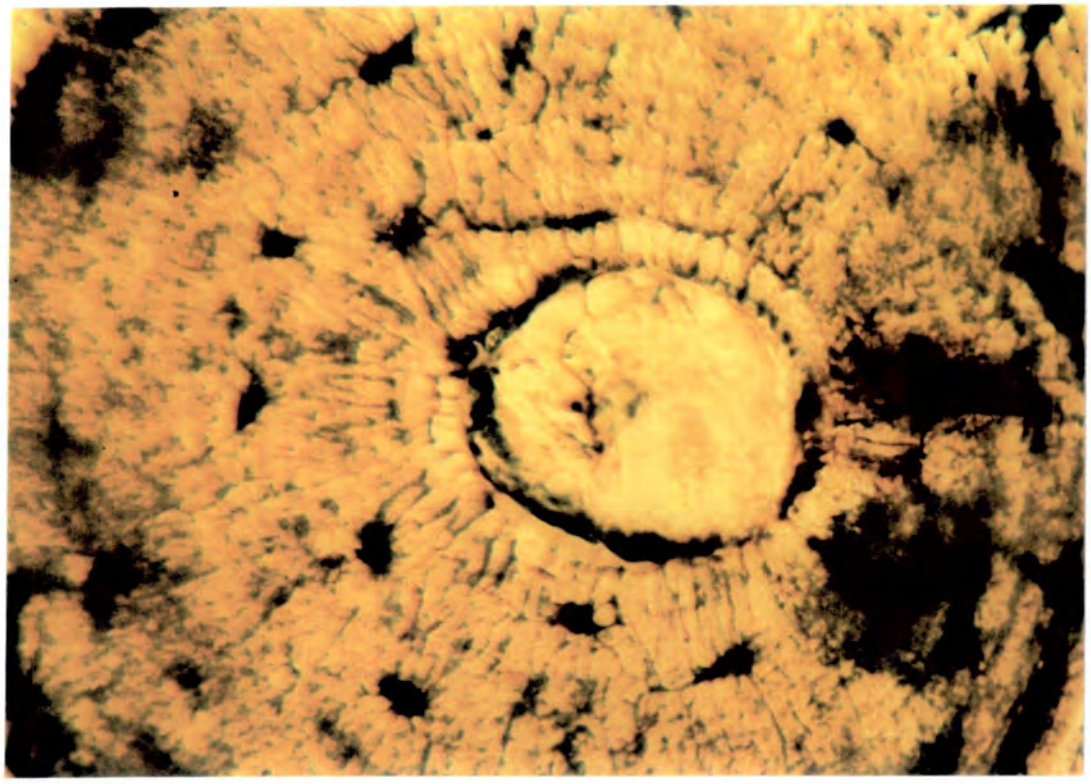

Plate 3.5 View of Haversian system showing osteocyte lacunae and canaliculi (field width 120μm)

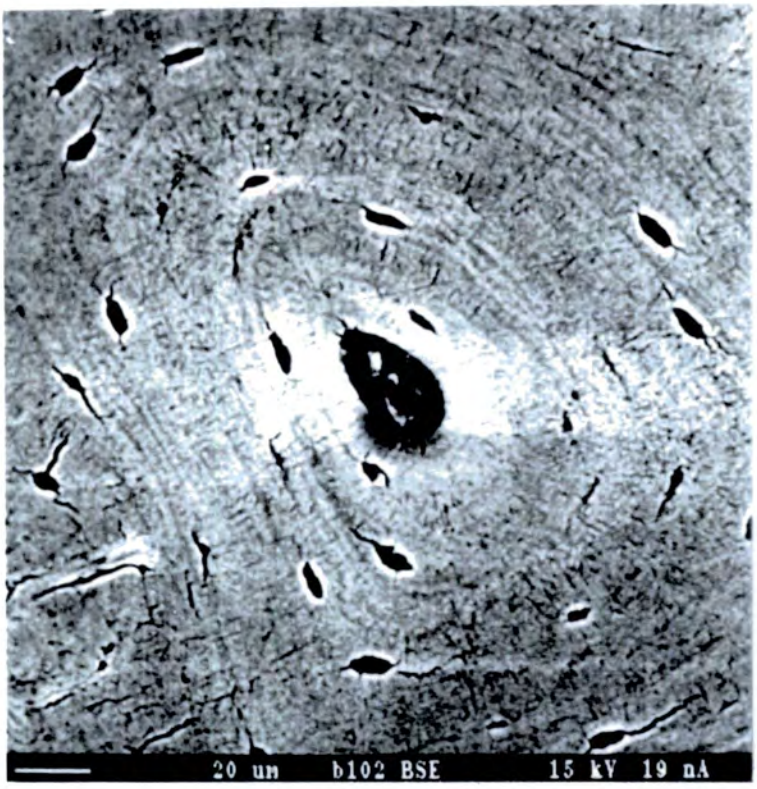

Plate 3.6 SEM backscatter image of Haversian system

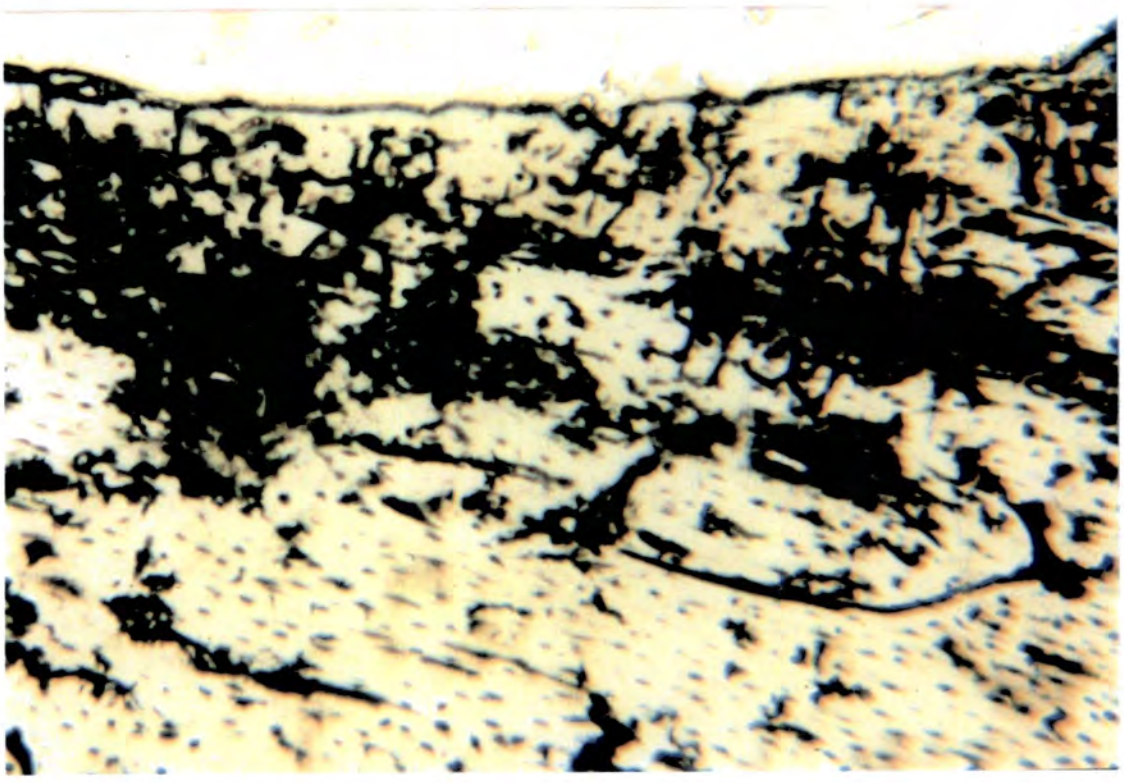

Plate 3.7 Section of bone found on Polis beach showing diagenetic tunnelling (field width 0.6mm)

Plate 3.8 SEM backscatter image of linear longitudinal tunnels penetrating both lamellar and Haversian bone

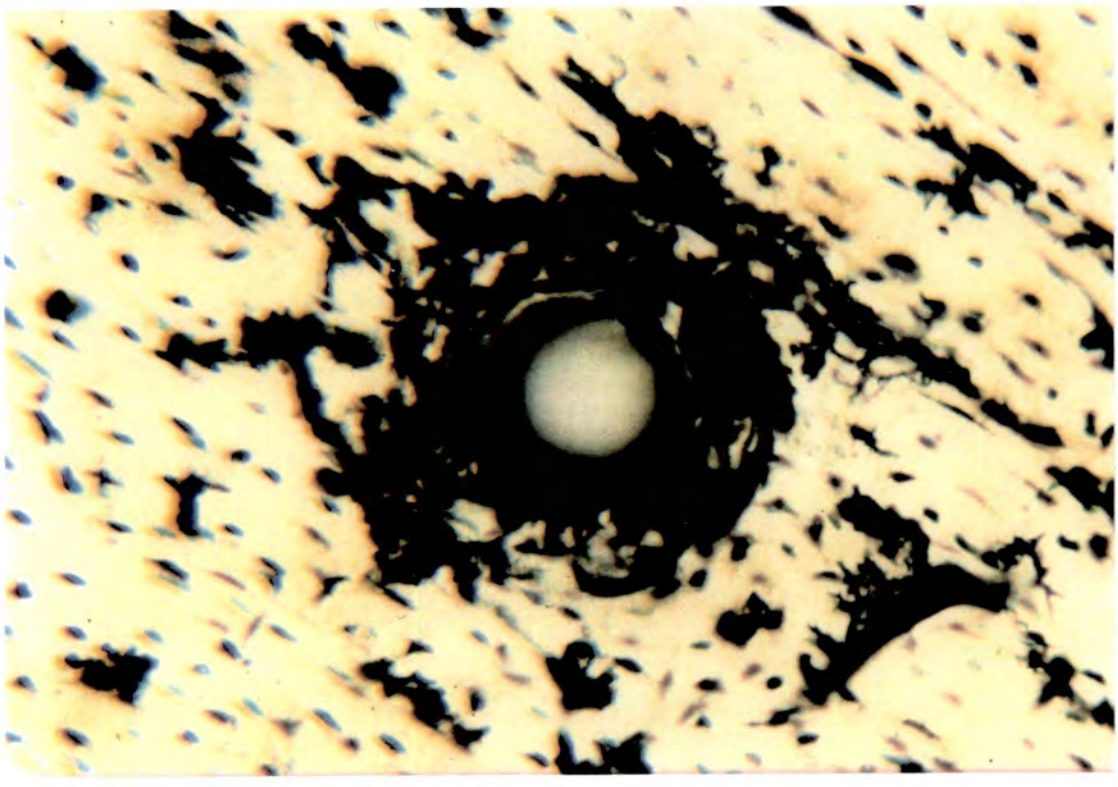

Plate 3.9 Tunnelling around canal in bone from Polis beach
(field width 0.3mm)

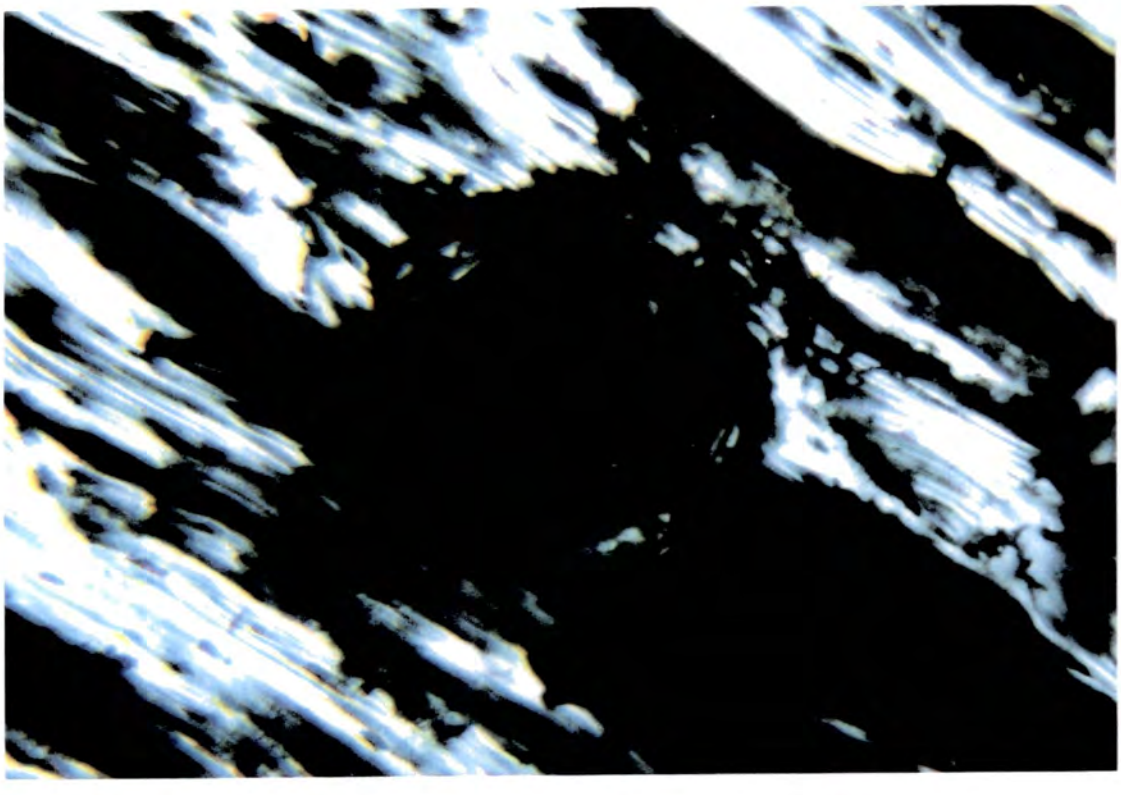

Plate 3.10 Same features viewed through crossed polars
(field width 0.3mm)

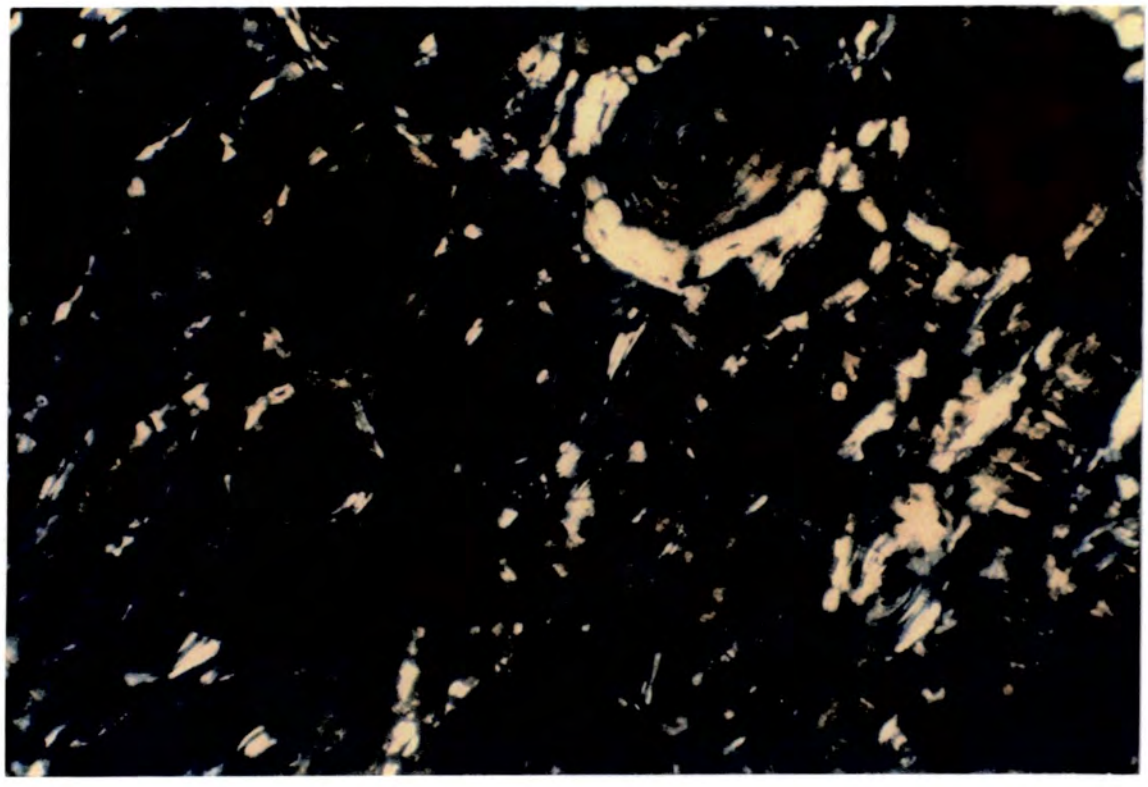

Plate 3.11 Area of bone from Polis beach showing loss of transparency and birefringence (crossed polars; field with 0.3mm)

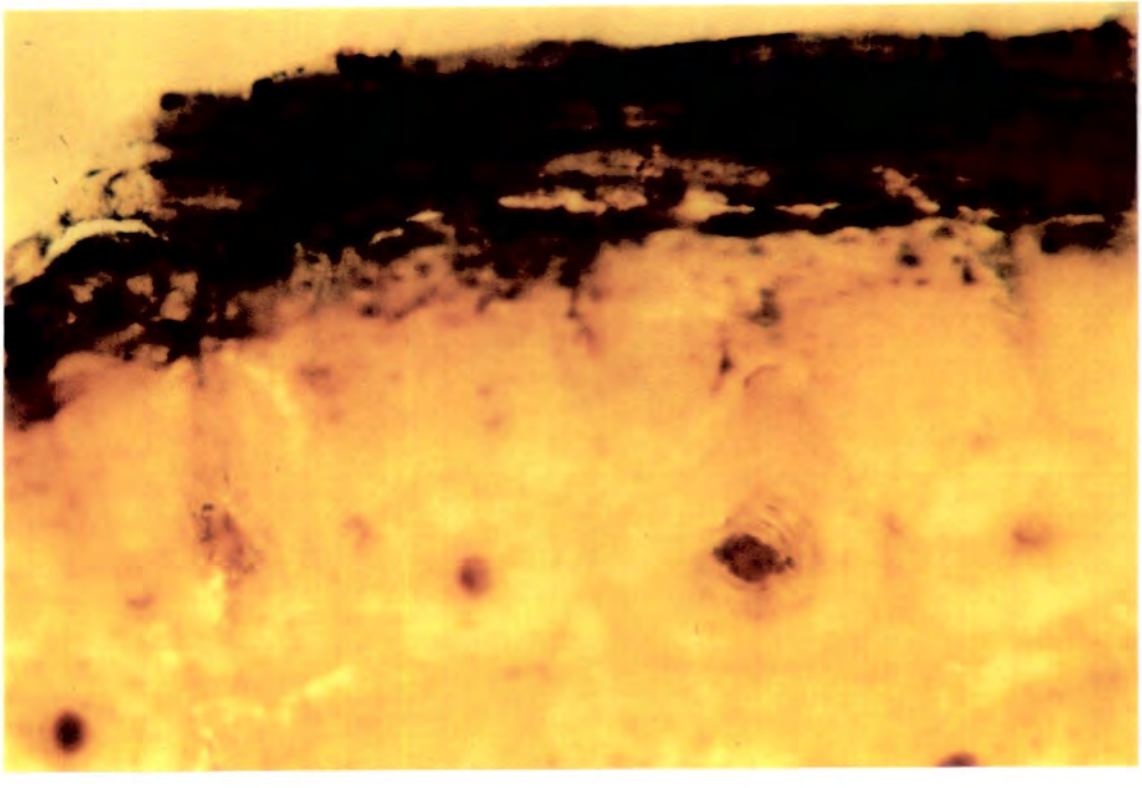

Plate 3.12 View showing loss of transparency in cortical bone and staining of the surface lamellae (field width 0.6mm)

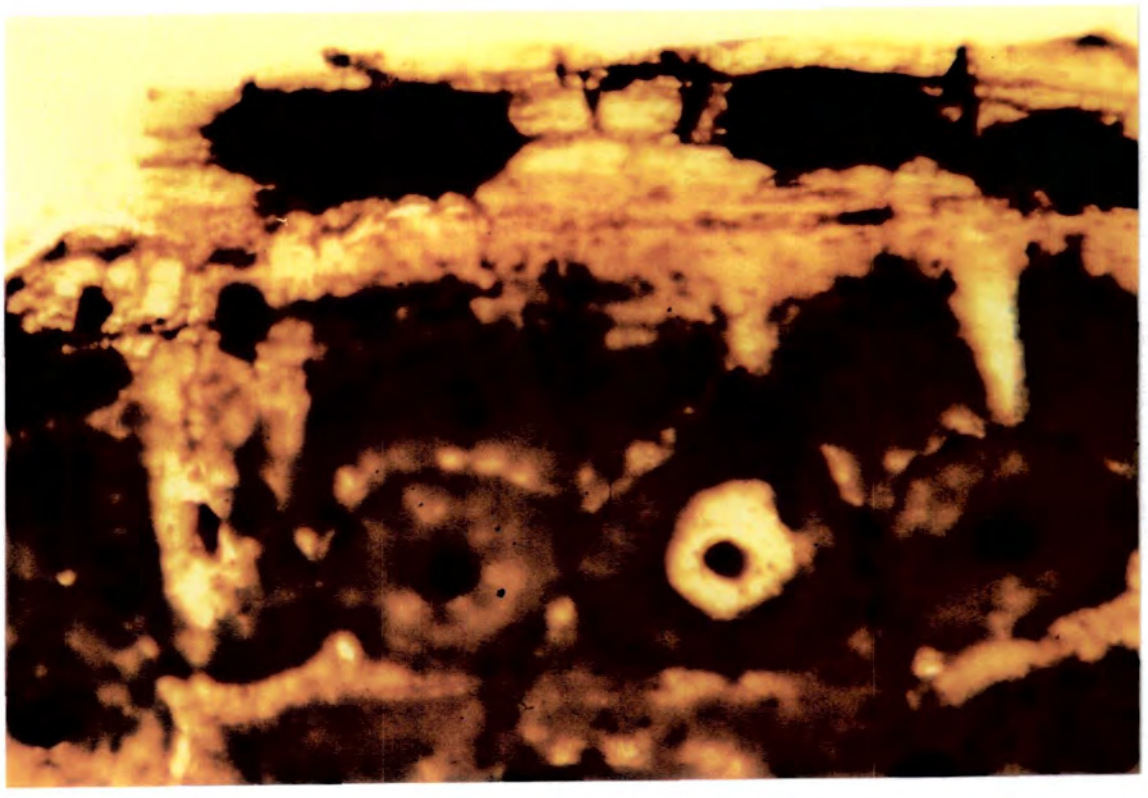

Plate 3.13 View of area seen in Plate 3.12 seen through crossed polars, note loss of birefringence in Haversian bone (field width 0.6mm)

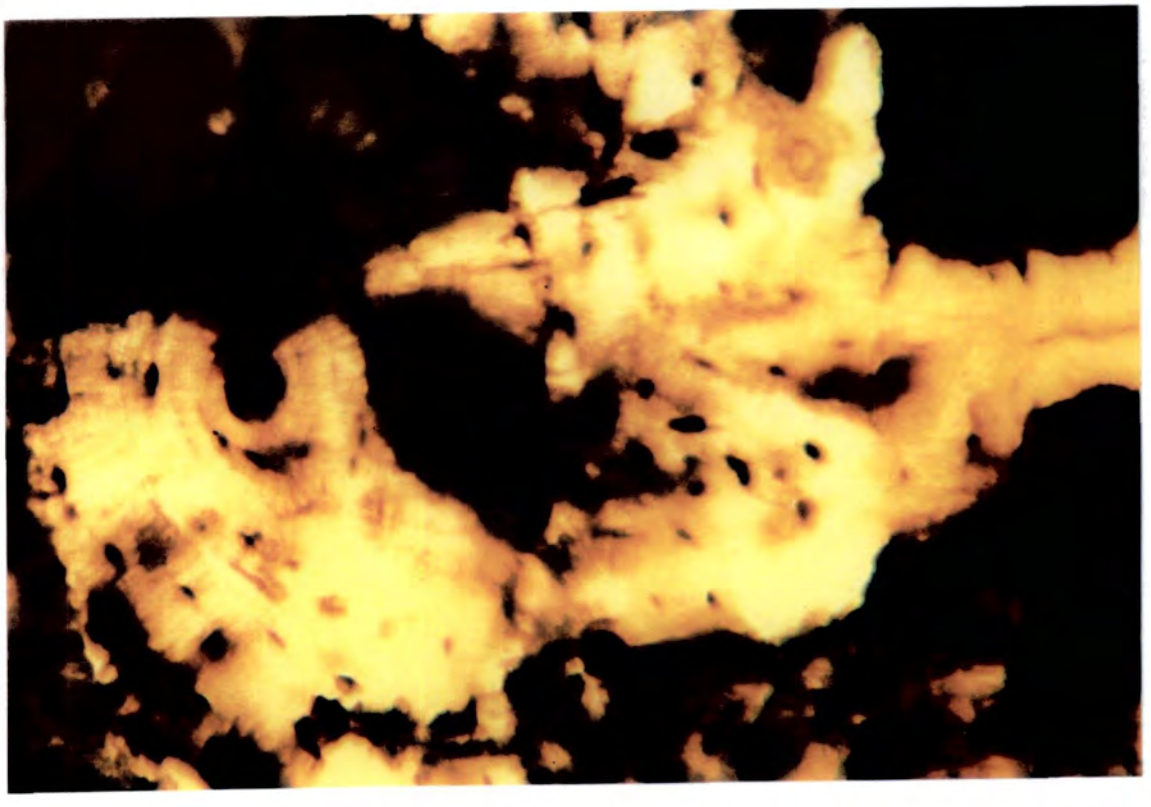

Plate 3.14 Area of bone specimen seen in Plates 3.12 & 3.13 demonstrating apparently random distribution of diagenetic alteration. Yellow-brown staining from the soil can be seen spreading from the crack or tunnel on the right hand side of image (field width 0.3mm)

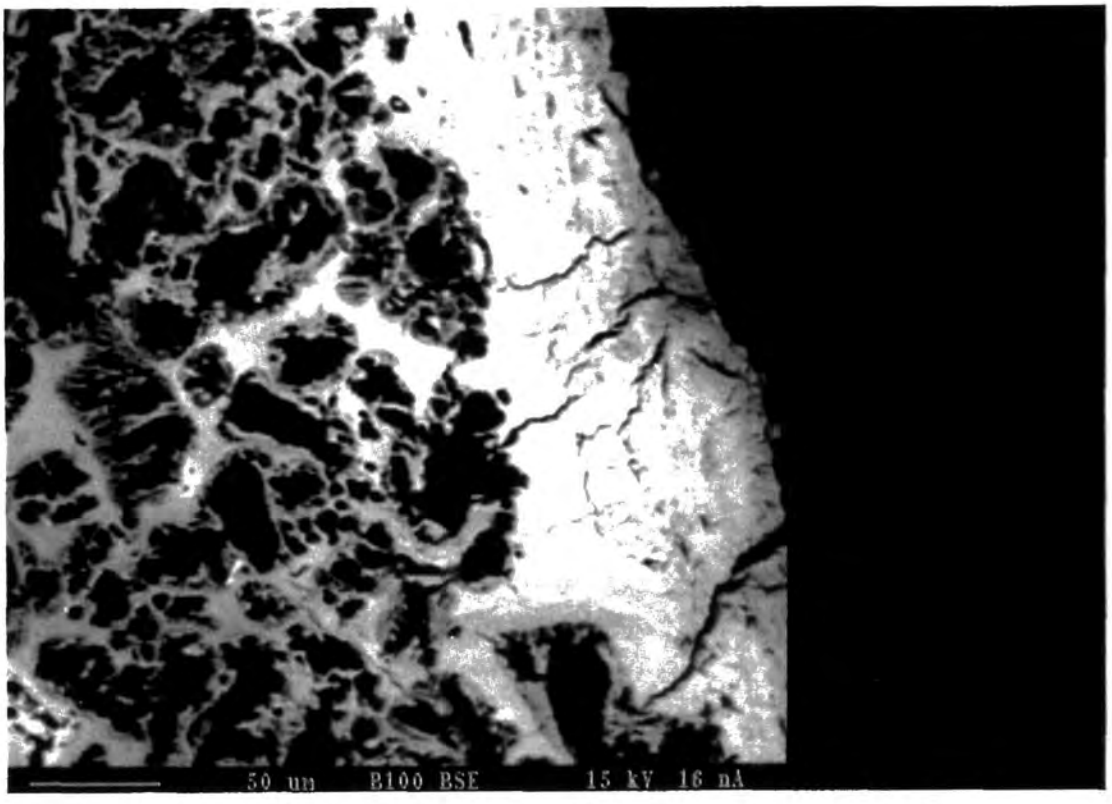

Plate 3.15 SEM backscatter image of bone showing severe microfocal destruction of interior contrasting with absence of tunnelling at surface

Plate 3.16 SEM backscatter image of bone showing almost total destruction of interior contrasted to apparently unaffected bone at surface (note the single, isolated, unaffected osteon)

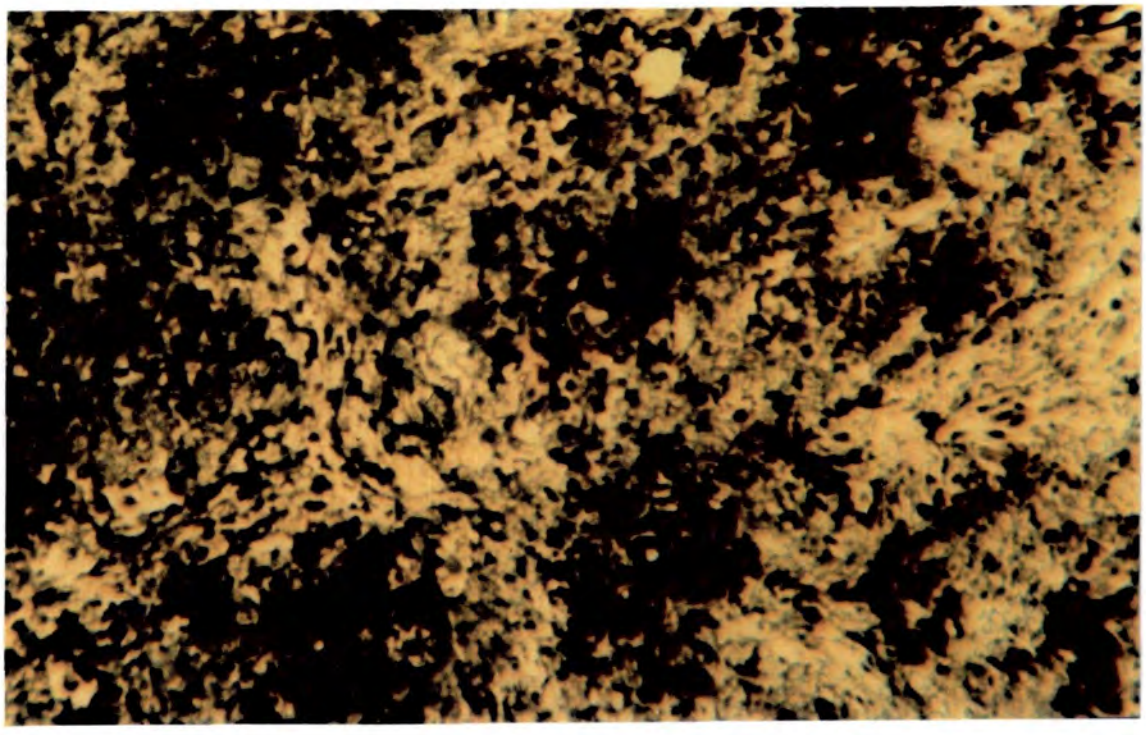

Plate 3.17 View of bone from the Neolithic site of Runnymede showing complete destruction of histological structures (field width 0.6mm)

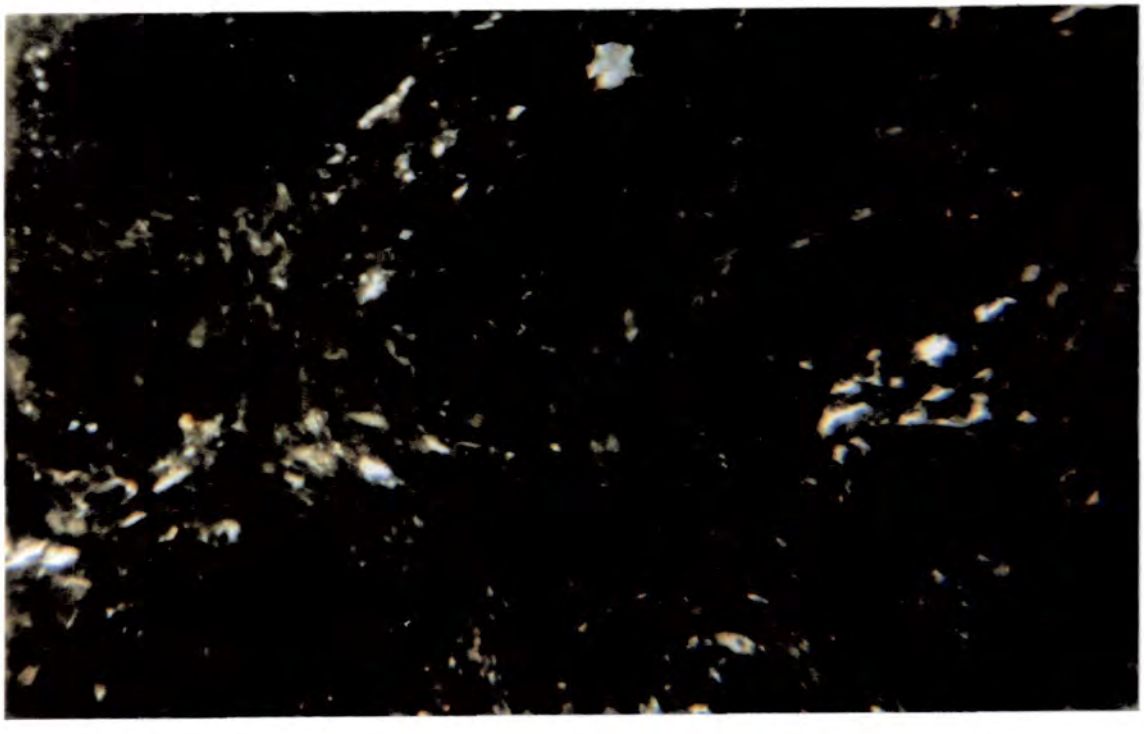

Plate 3.18 Area seen in Plate 3.17 viewed through crossed polars. A few small, isolated areas maintain some birefringence, demonstrating survival of collagen

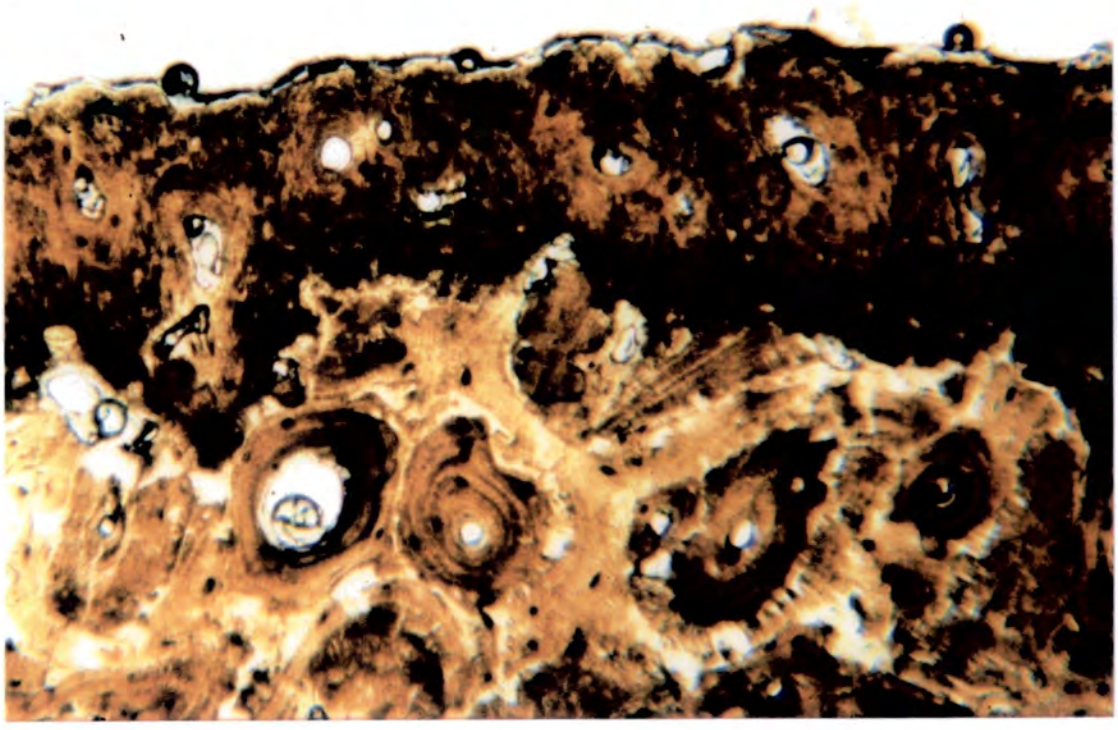

Plate 3.19 View of bone from an aerated soil (Dryslwyn) showing staining of periosteal surface and successive lamellae of Haversian systems (field width 0.6mm)

Plate 3.20 Area of bone in Plate 3.19 viewed through crossed polars. Note preservation of birefringence(field width 0.6mm)

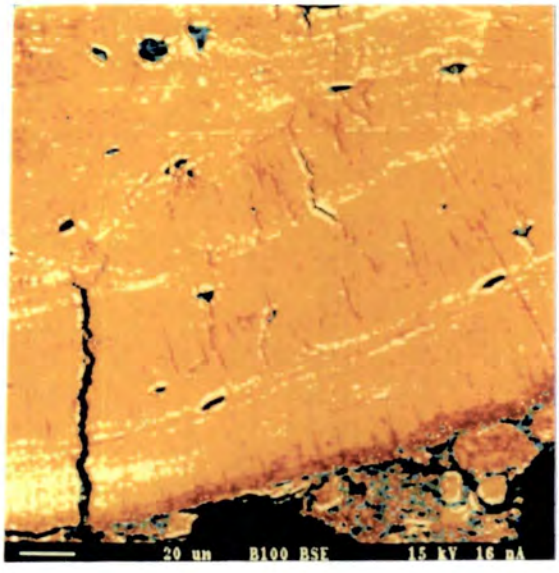

Plate 3.21 SEM backscatter image of bone from an aerated soil (Stanwick)

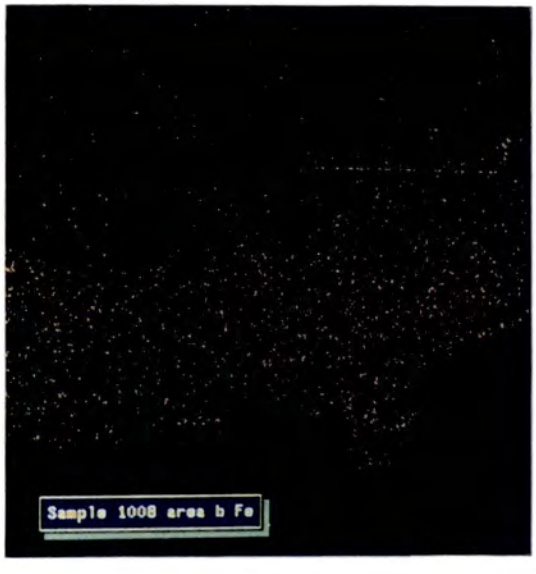

Plate 3.22 SEM FeKα dot map for over area shown in Plate 3.21. Note penetration of iron salts from the surface to the interior

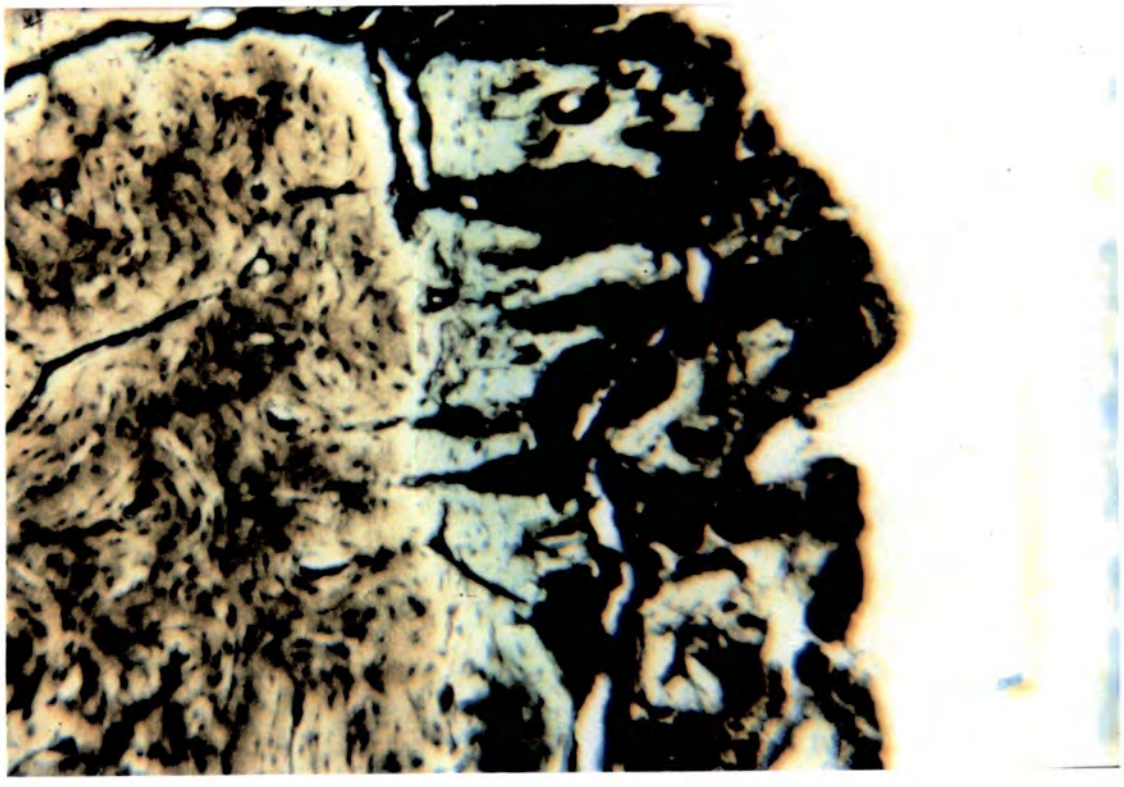

Plate 3.23 View of bone collected at Limni copper mine, Cyprus showing concentration of copper salts (field width 0.6mm)

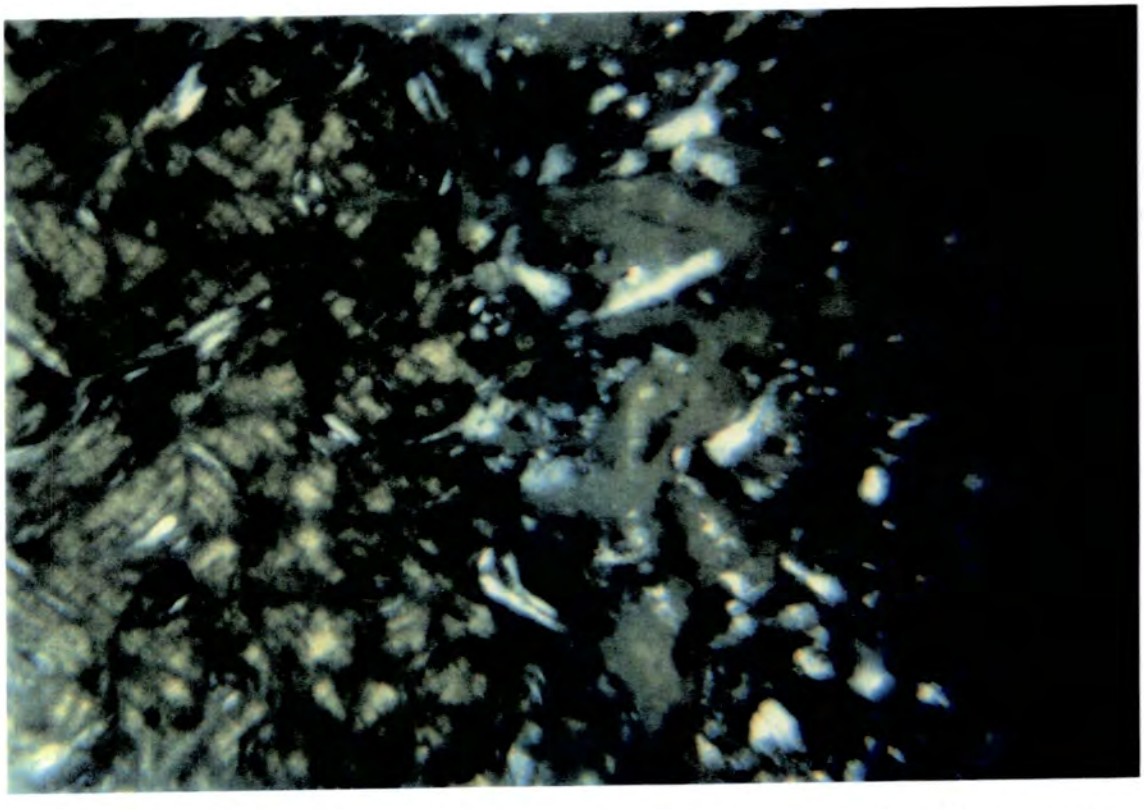

Plate 3.24 Area of bone in plate 3.23 viewed through crossed polars, showing loss of transparency and birefringence. Also note concentration of copper salts in region of active diagenetic degradation.

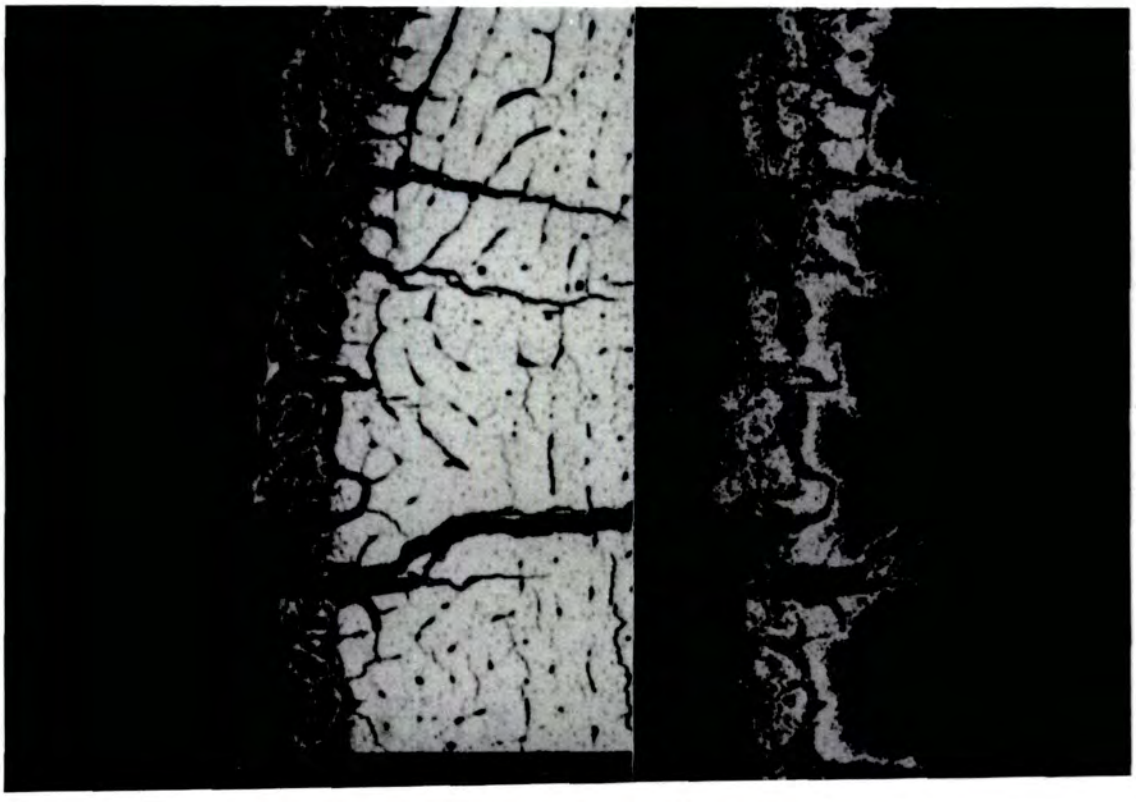

Plate 3.25 SEM backscatter image and CuKα dot map for another section of the bone from Limni copper mine

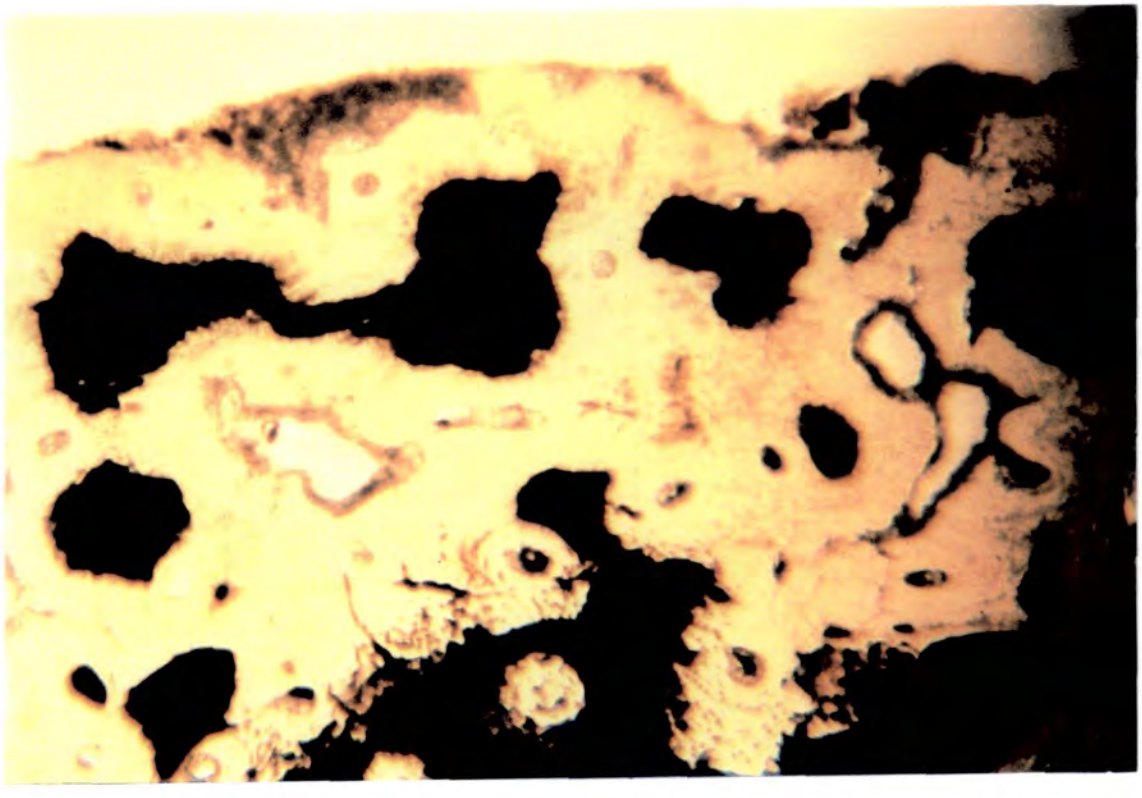

Plate 3.26 View of human bone from an alkaline soil (Polis Basilica) demonstrating differential preservation of histological structures (field width 0.6mm)

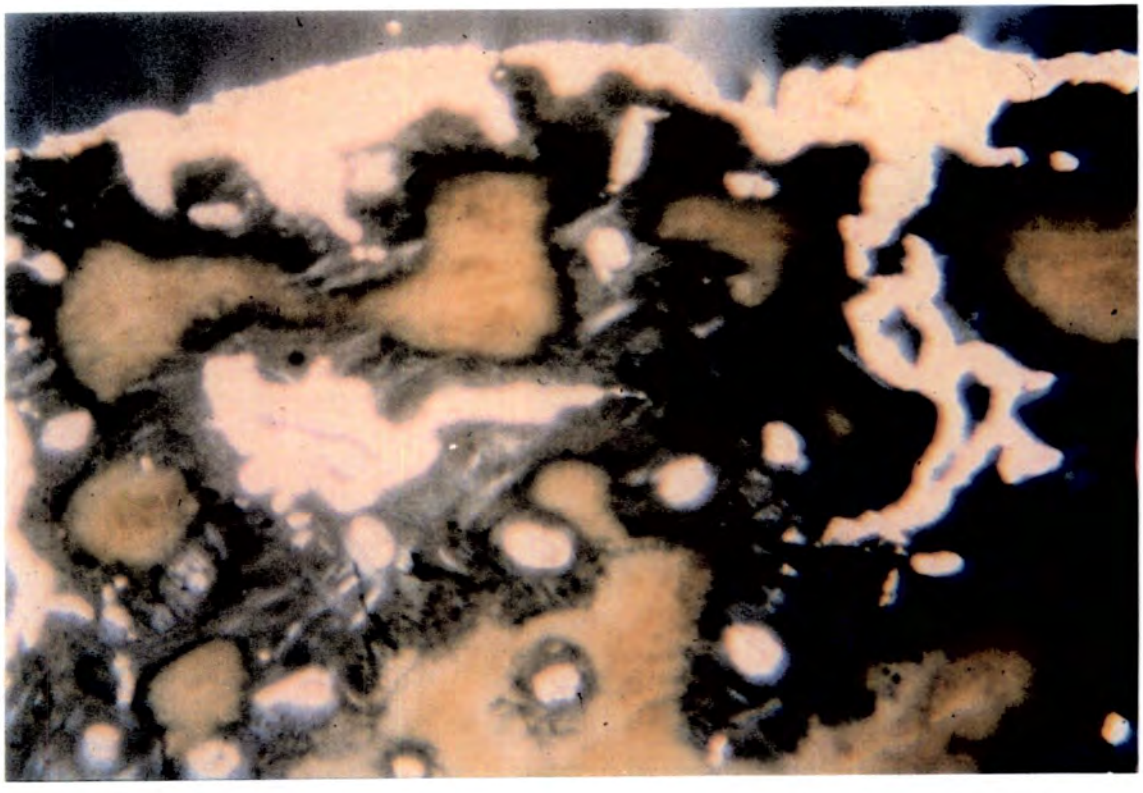

Plate 3.27 Area seen in Plate 3.26 viewed through crossed polars. Note the preservation of birefringence around osteons and presence of crystalline calcite

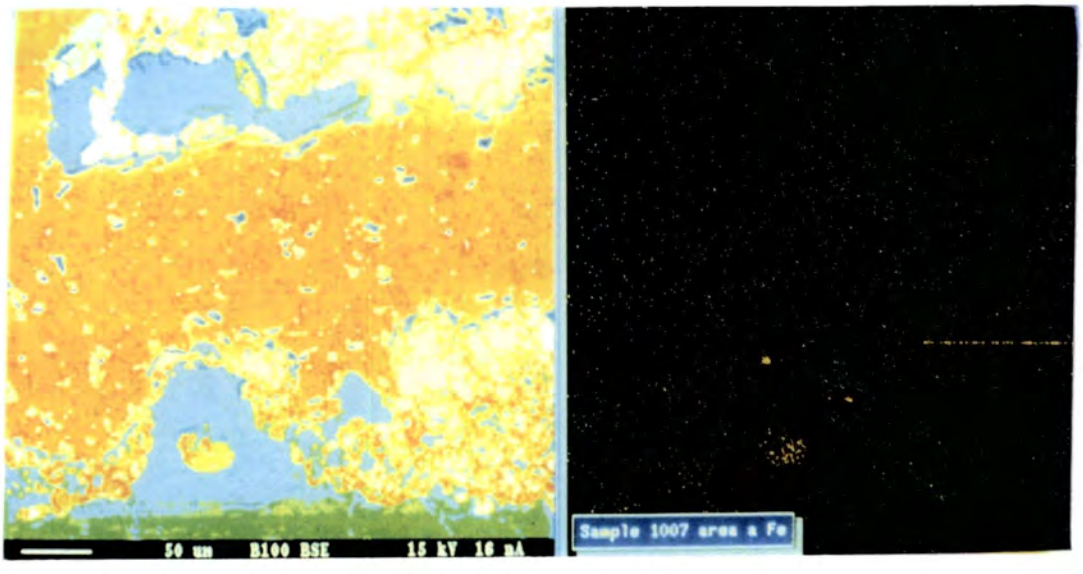

Plate 3.28 SEM backscatter image of bone seen in Plates 3.26 & 3.27, together with FeKα dot map. Note high density of mineral filling voids and low levels of iron salts

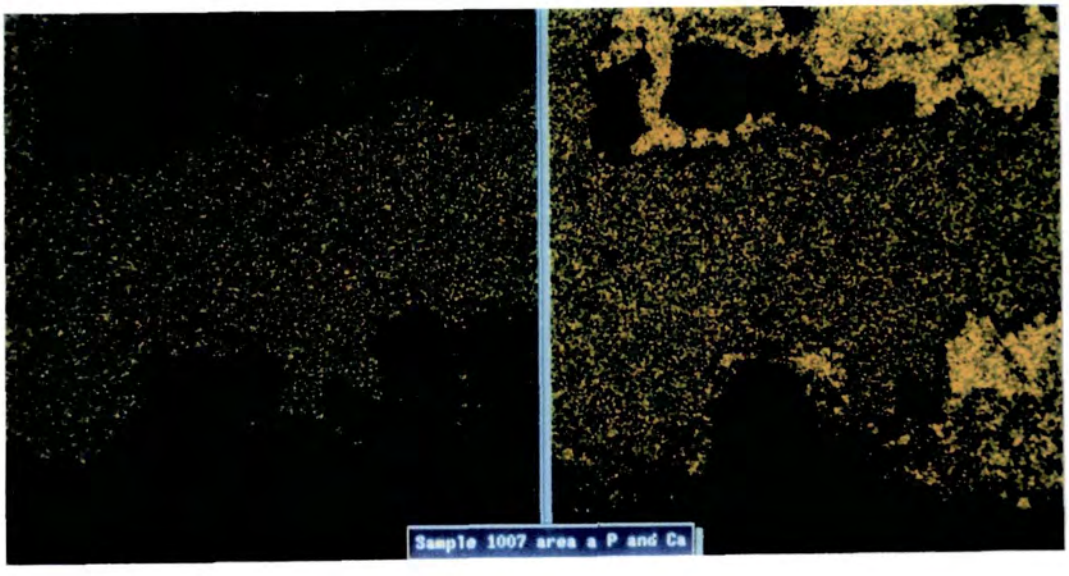

Plate3.29 PKα and CaKα dot maps for area seen in Plate3.28. Note high levels of calcium and low levels of phosphorus in mineral (calcite) filling voids

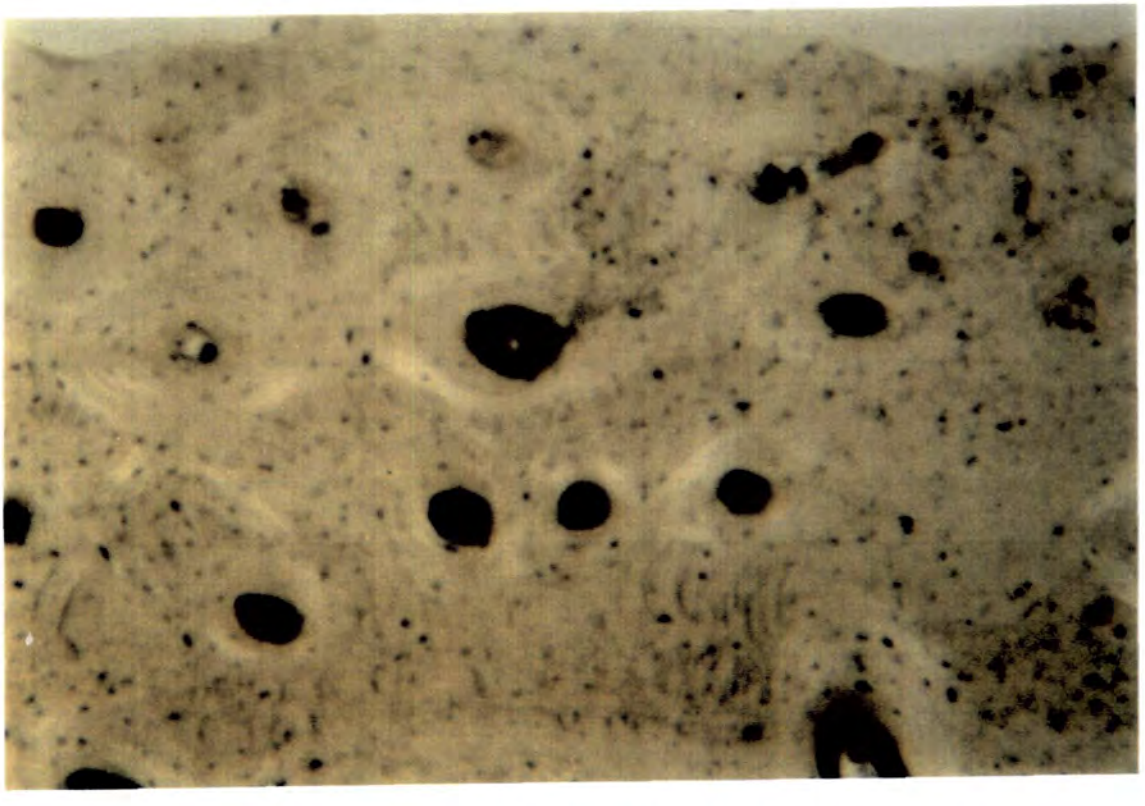

Plate 3.30 Section of horse metatarsal from Roman Ribchester demonstrating excellent histological preservation (field width 0.6mm)

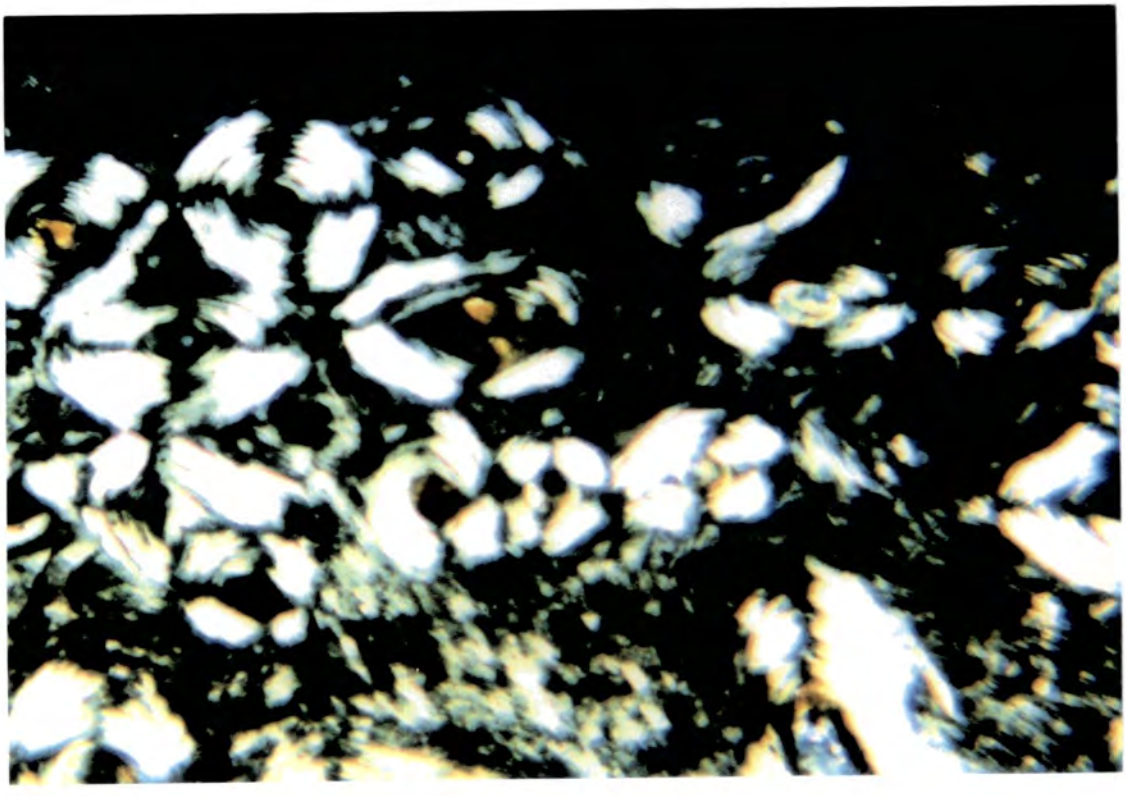

Plate 3.31 Area covered by Plate 3.30 viewed through crossed polars showing good preservation of birefringence

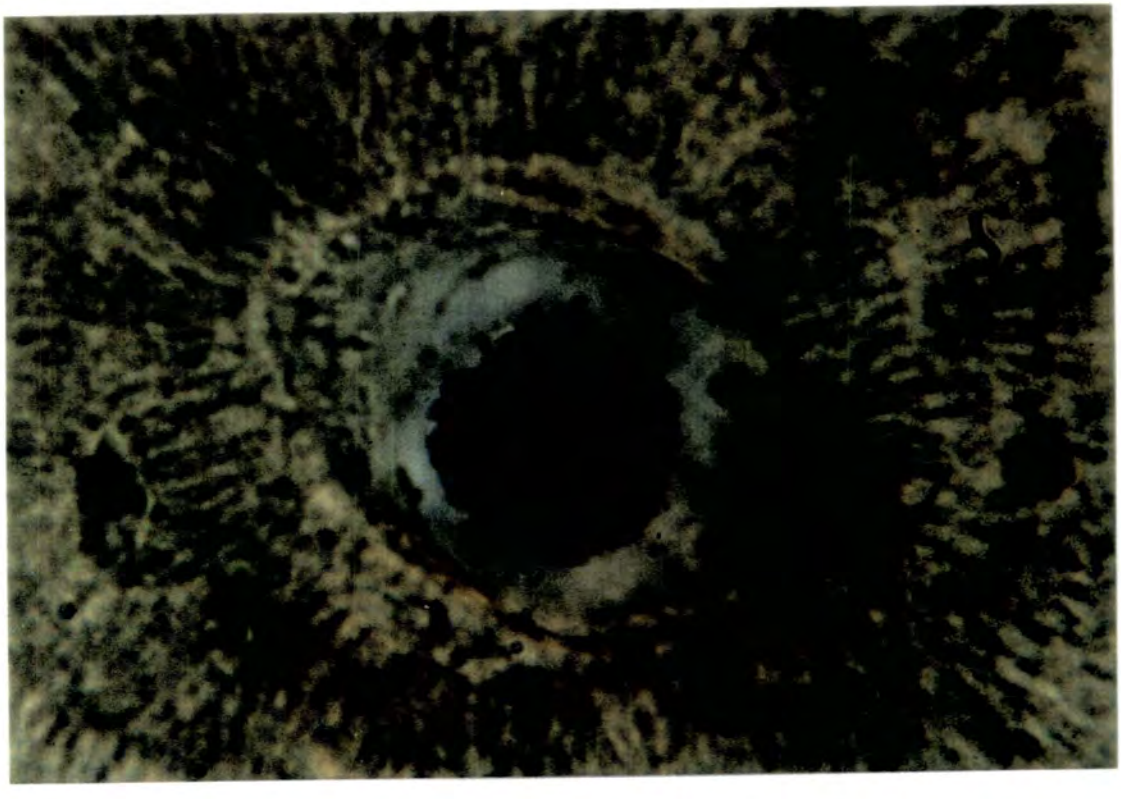

Plate 3.32 High magnification view of canal in Roman horse metatarsal showing possible survival of red blood cells. Diameter of circular features 3-4μm (field width 60μm)

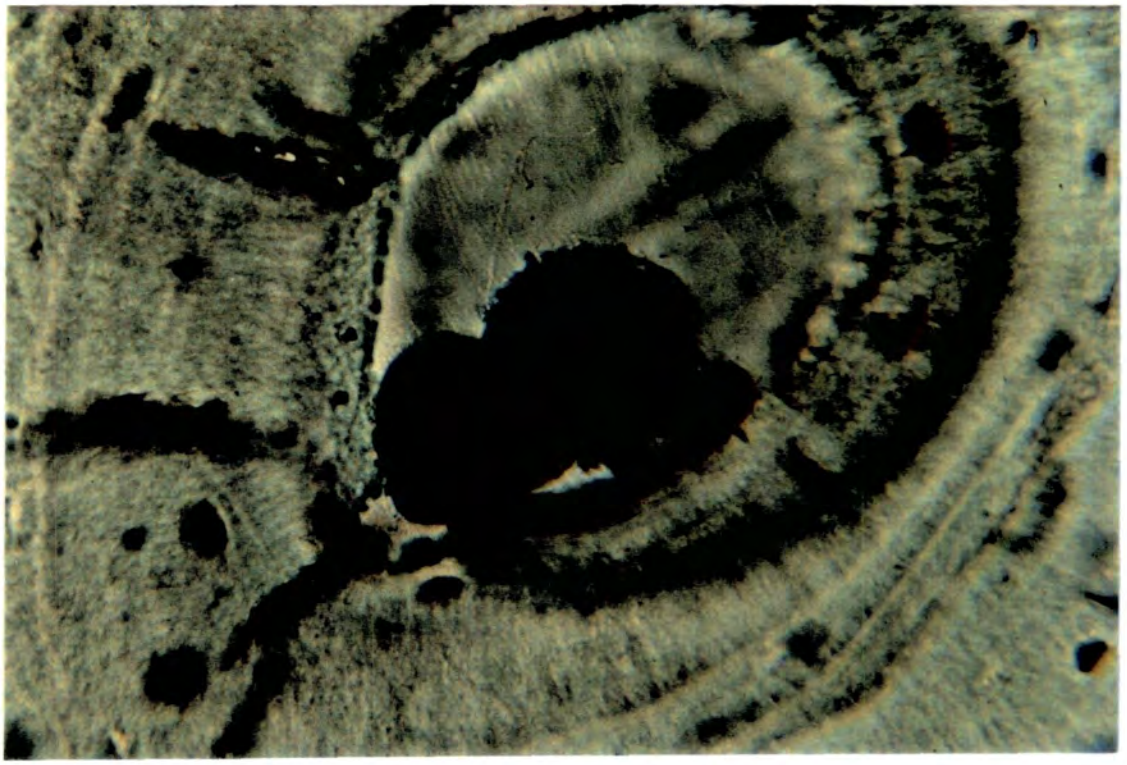

Plate 3.33 Framboidal pyrite lying within canal of bone from Polis beach (field width 60μm)

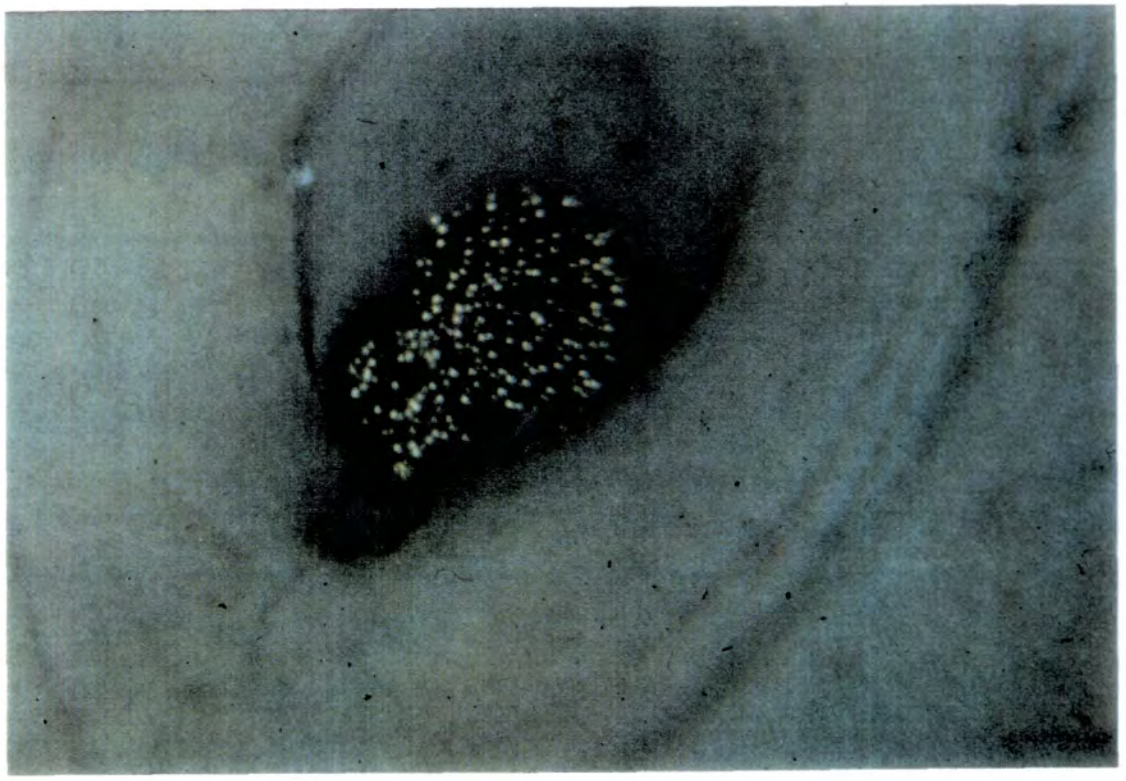

Plate 3.34 Framboidal pyrite seen in Plate 3.33 viewed in reflected light.
Note high reflectivity of pyrite grains

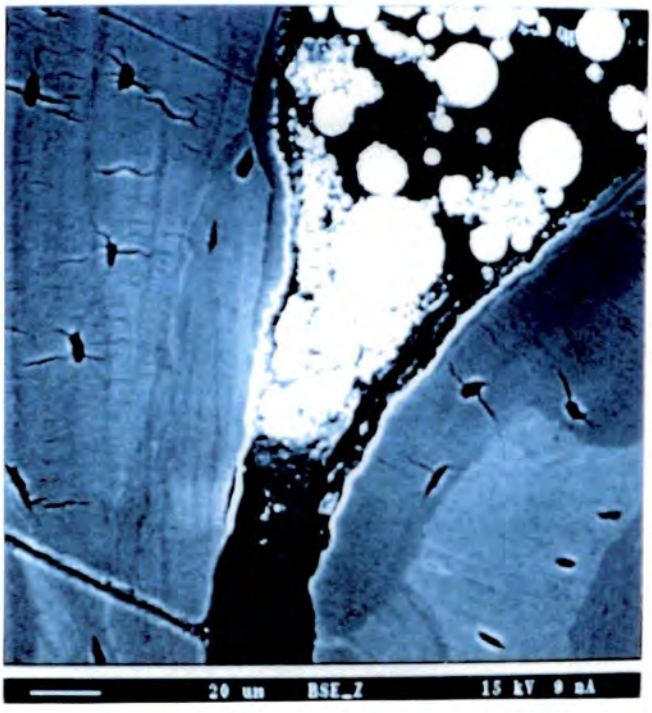

Plate 3.35 SEM backscatter image of several pyrite framboids in bone from the Vale of Pickering (Mesolithic)

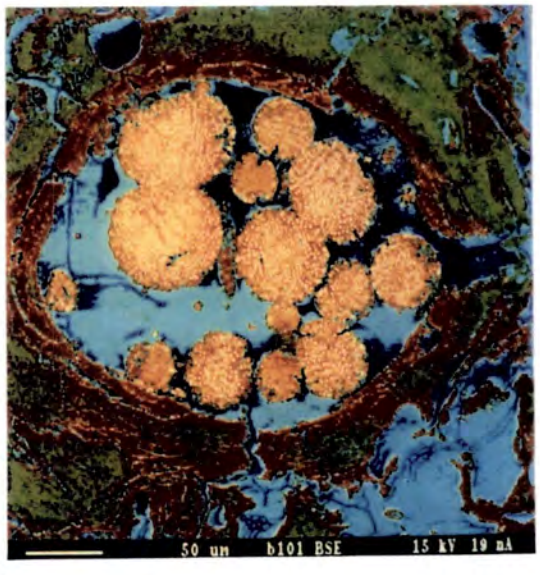

Plate 3.36 Well developed pyrite framboids in heavily degraded bone from the Vale of Pickering

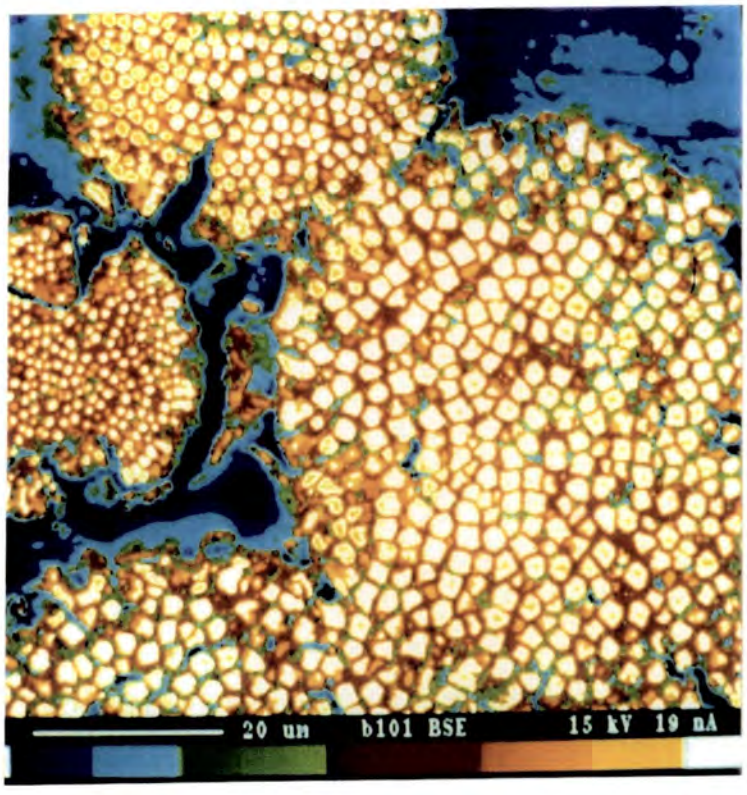

Plate 3.37 High magnification image of framboids in bone from the Vale of Pickering demonstrating polygonal structure of individual grains

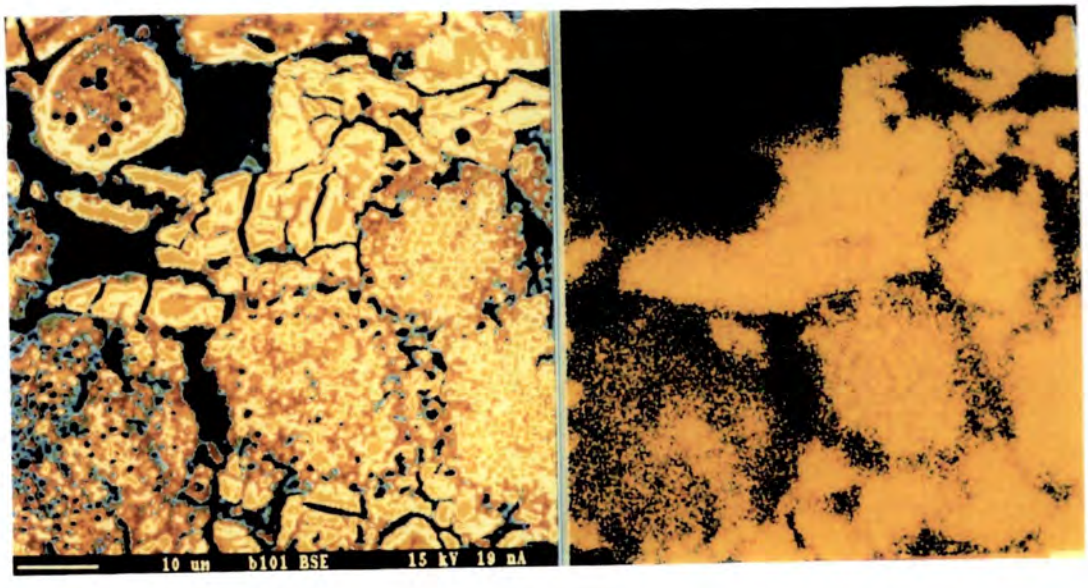

Plate 3.38 SEM backscatter image of framboidal pyrite and gypsum deposits in bone from the Vale of Pickering, together with SKa dot map of same area

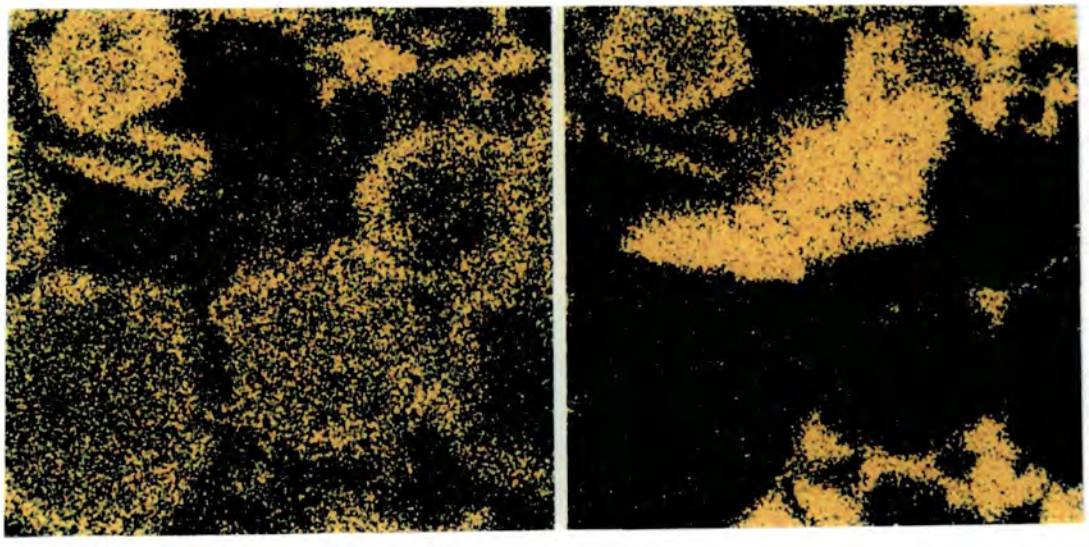

Plate 3.39 PKα and CaKα dot maps of area covered by Plate 3.38

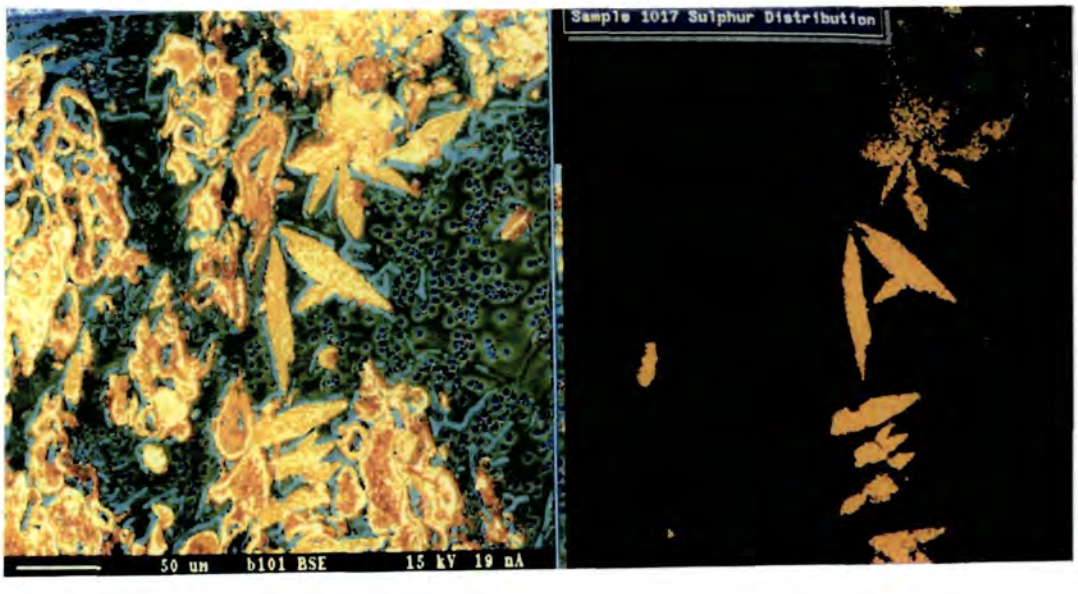

Plate 3.40 SEM backscatter image of badly degraded bone from the Vale of Pickering, together with SKα dot map of same area

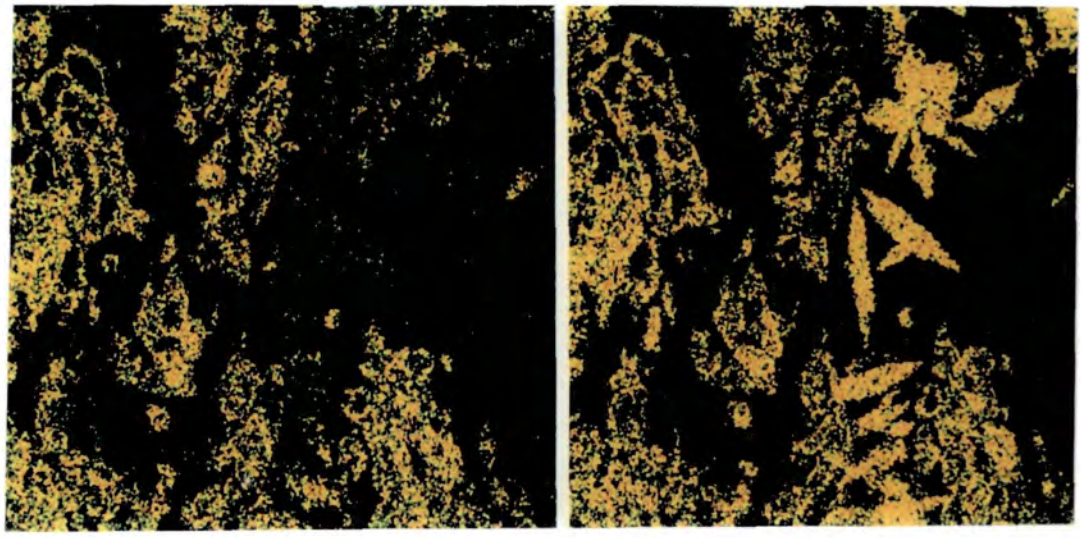

Plate 3.41 PKα and CaKα dot maps of area covered by Plate 3.40 demonstrating lenticular crystals are calcium sulphate

Plate 3.42 SEM view of gypsum crystals and fungal hyphae in pore structure of bone from the Vale of Pickering (x200)

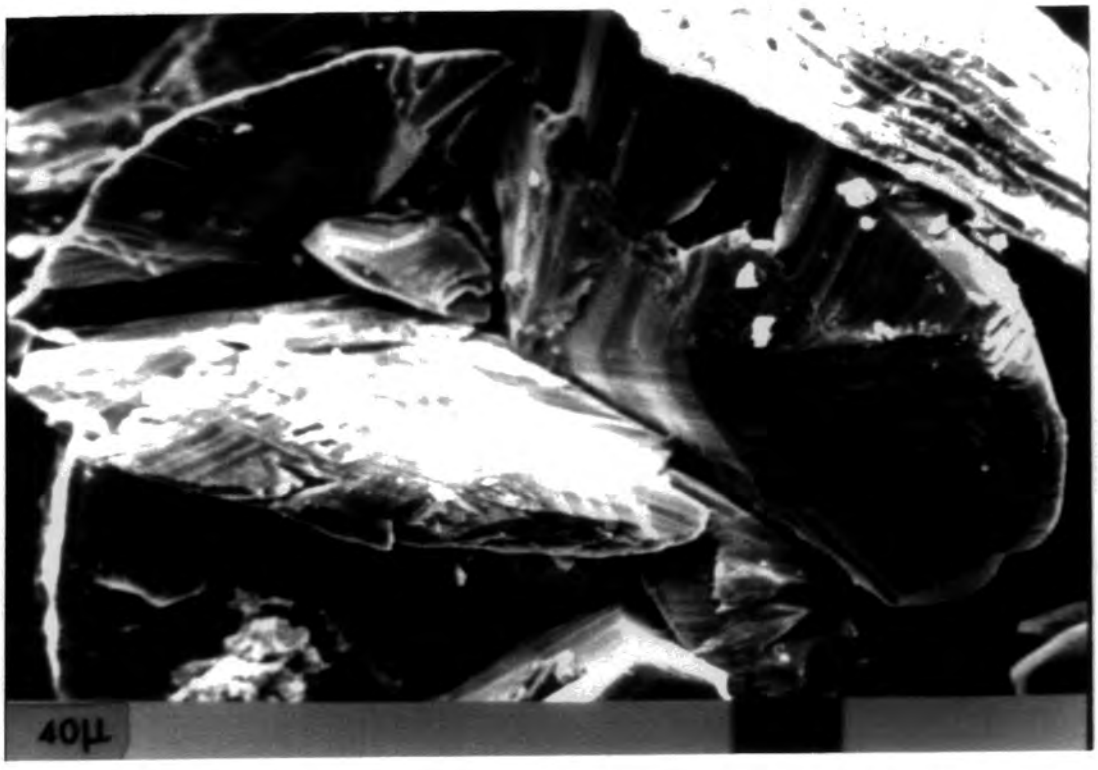

Plate 3.43 High magnification SEM image of gypsum crystals in degraded bone

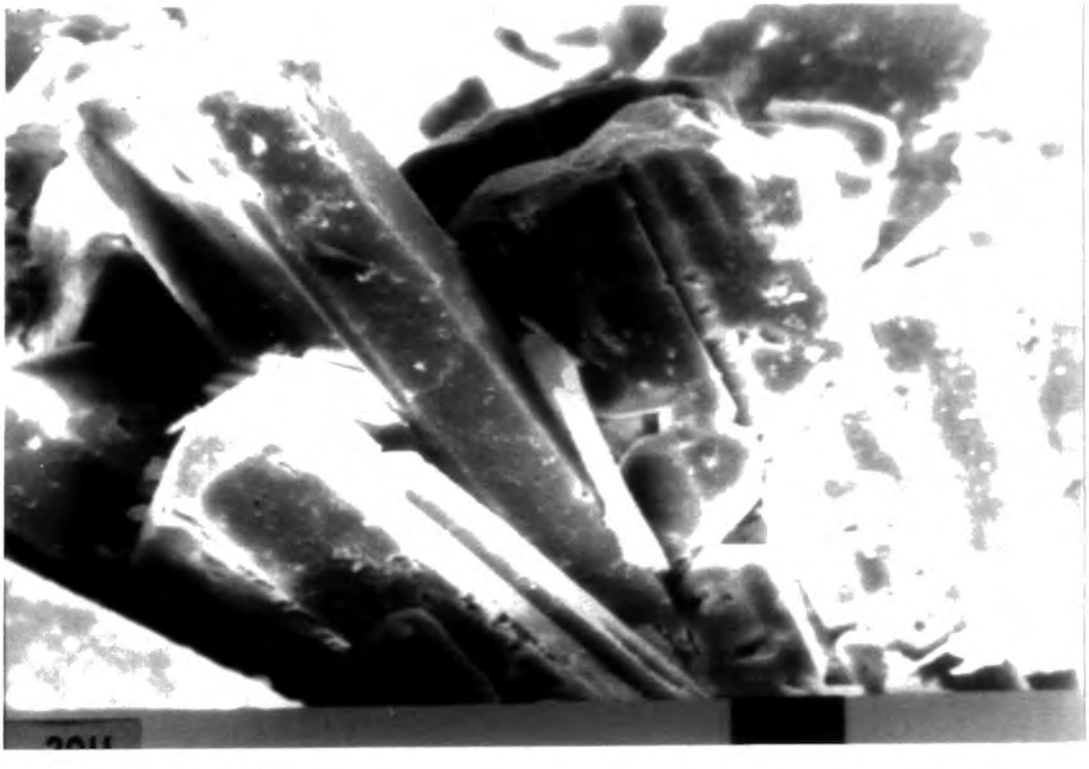

Plate 3.44 SEM image of gypsum crystals, illustrating another crystal habit. Found growing on the internal surface of exfoliating bone

Plate 3.45 Massive gypsum crystals found within the pores of a badly degraded bone from the Vale of Pickering. These crystals were discovered many weeks after careful drying of the specimen

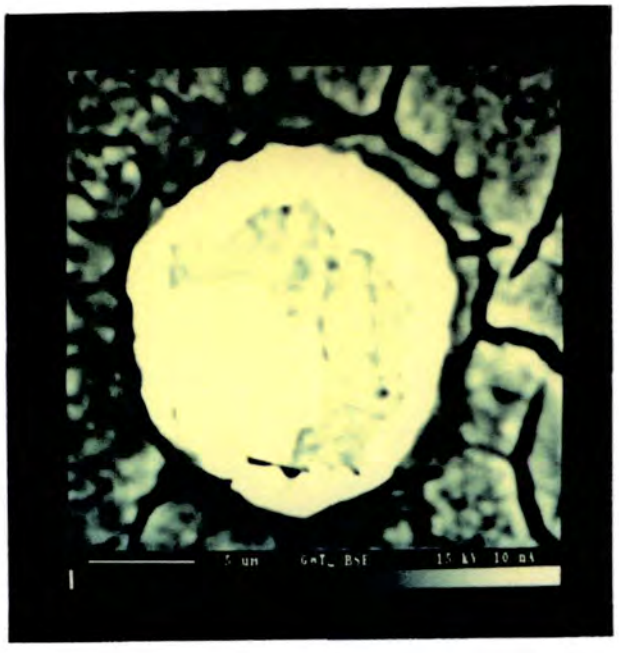

Plate 3.46 SEM image of massive pyrite lining canal of bone from the Cromerian Freshwater Beds

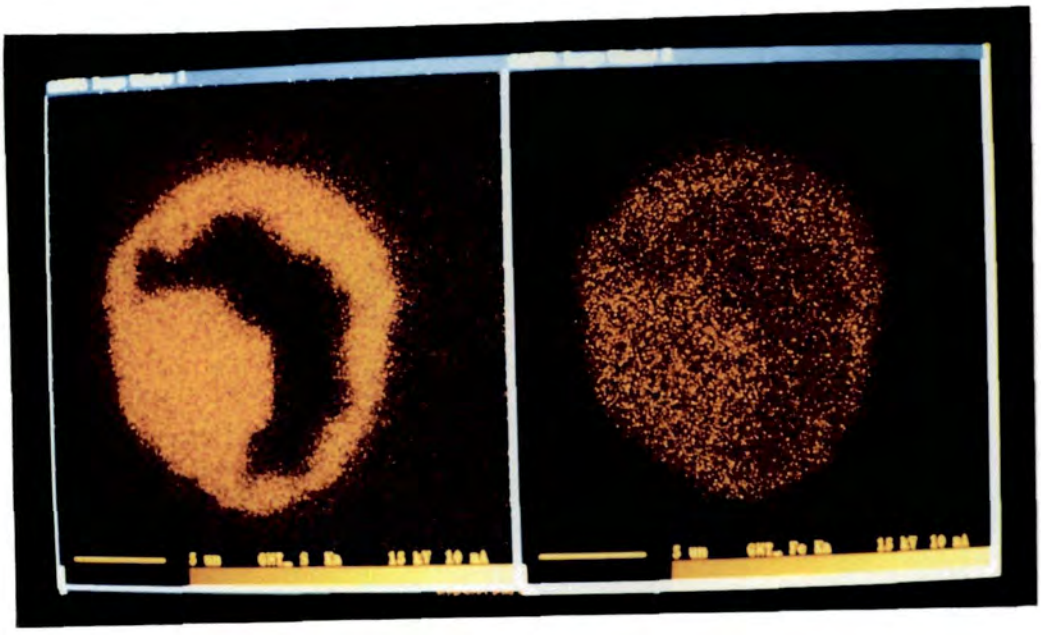

Plate 3.47 SKα and FeKα dot maps of area covered by Plate 3.46

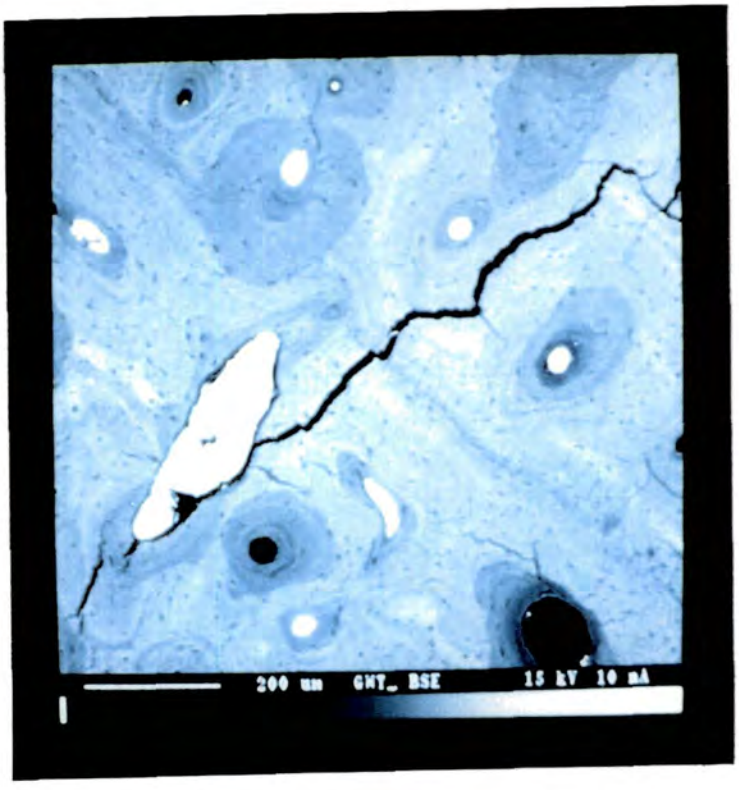

Plate 3.48 SEM backscatter image of bone from the Vale of Pickering showing infilling of pore structure with diagenetic minerals

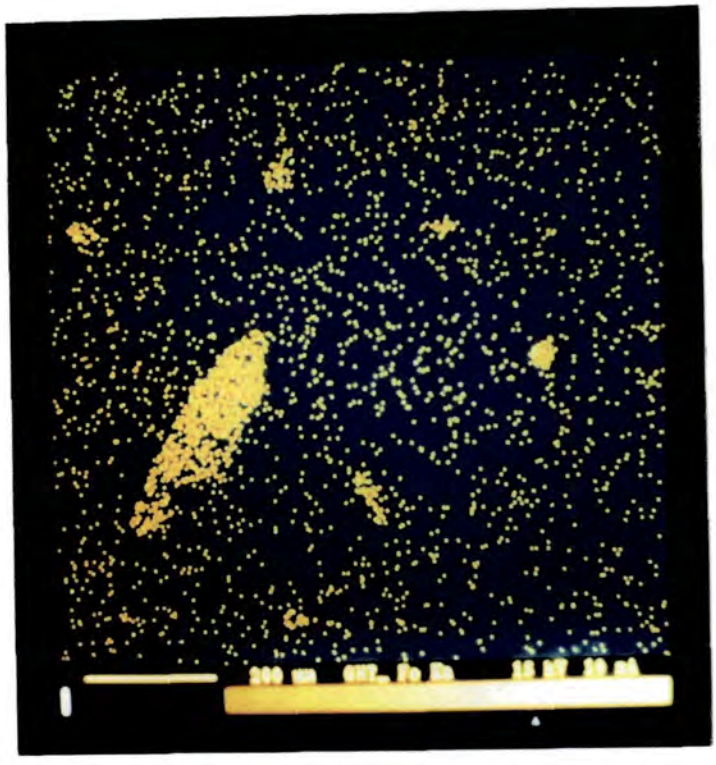

Plate 3.49 FeKa dot map of area covered by Plate 3.48

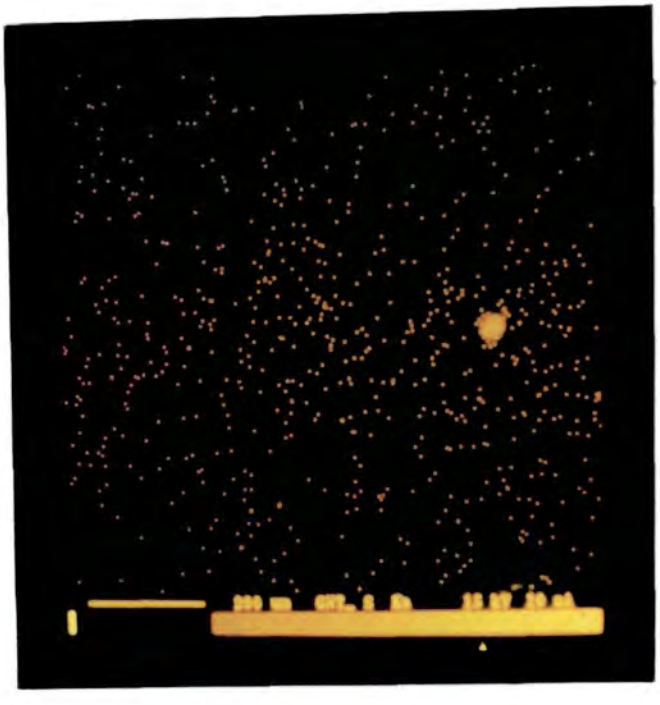

Plate 3.50 SKa dot map of area covered by Plates 3.48 and 3.49. Note presence of iron sulphide in small canal on right hand side of image

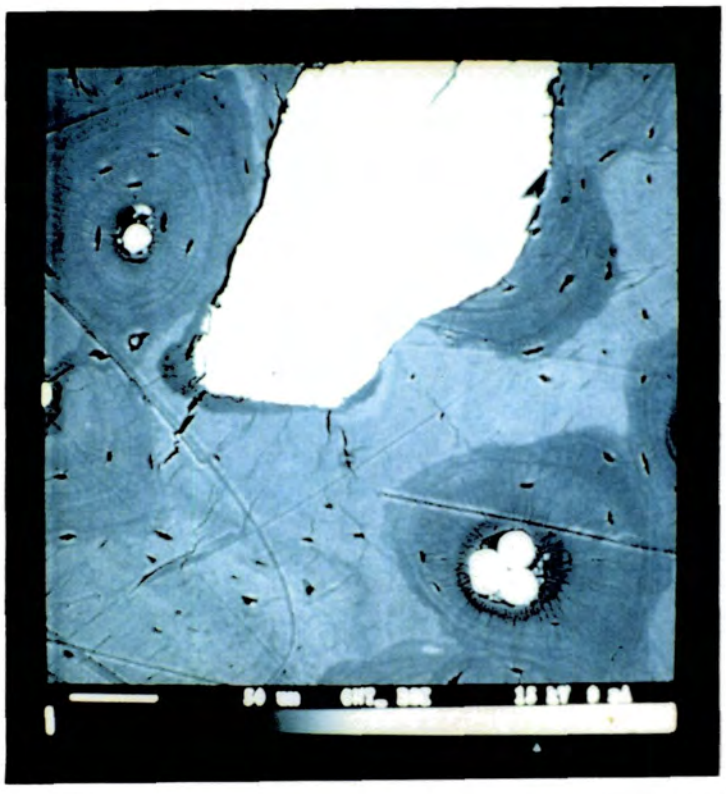

Plate 3.51 Another area of bone seen in Plates 3.48 to 3.50 showing close association of framboidal pyrite and vivianite deposits

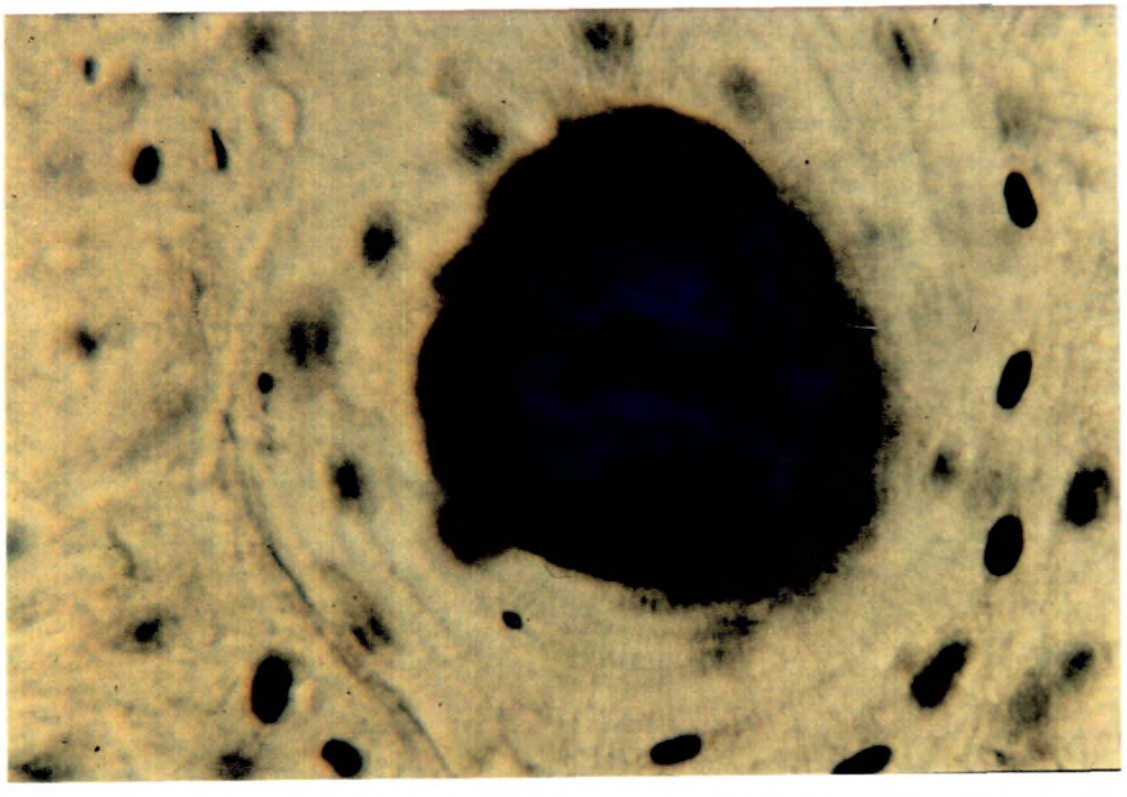

Plate 3.52 High magnification image of canal in Roman horse metatarsal showing bright blue deposits, possibly vivianite (field width 60μm)

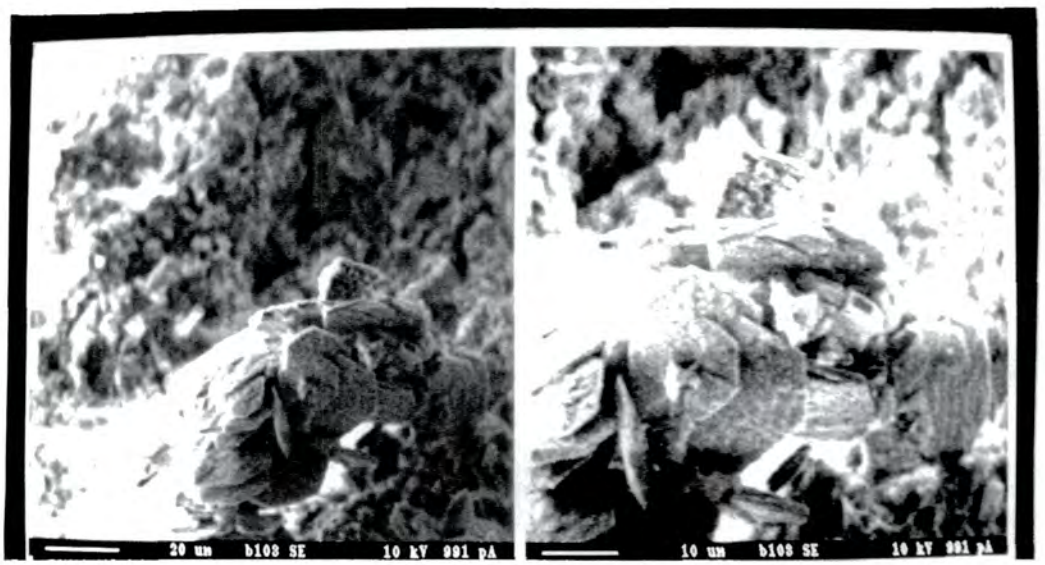

Plate 3.53 SEM image of redeposited hexagonal crystals (possible hydroxyapatite) in bone from the Vale of Pickering

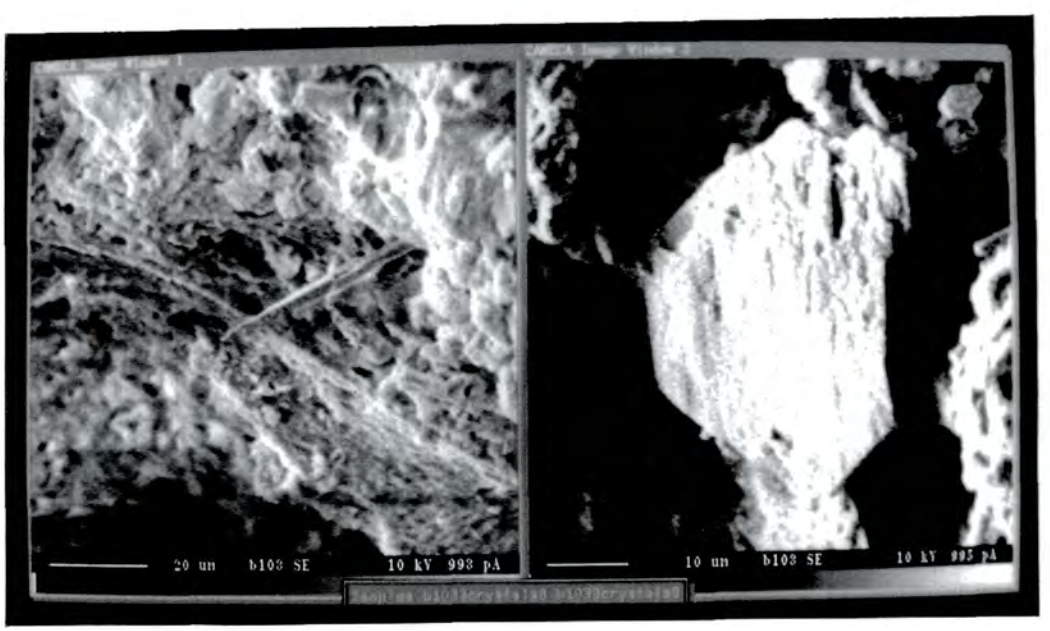

Plate 3.54 SEM image of hexagonal and needle-like crystals in bone from the Vale of Pickering

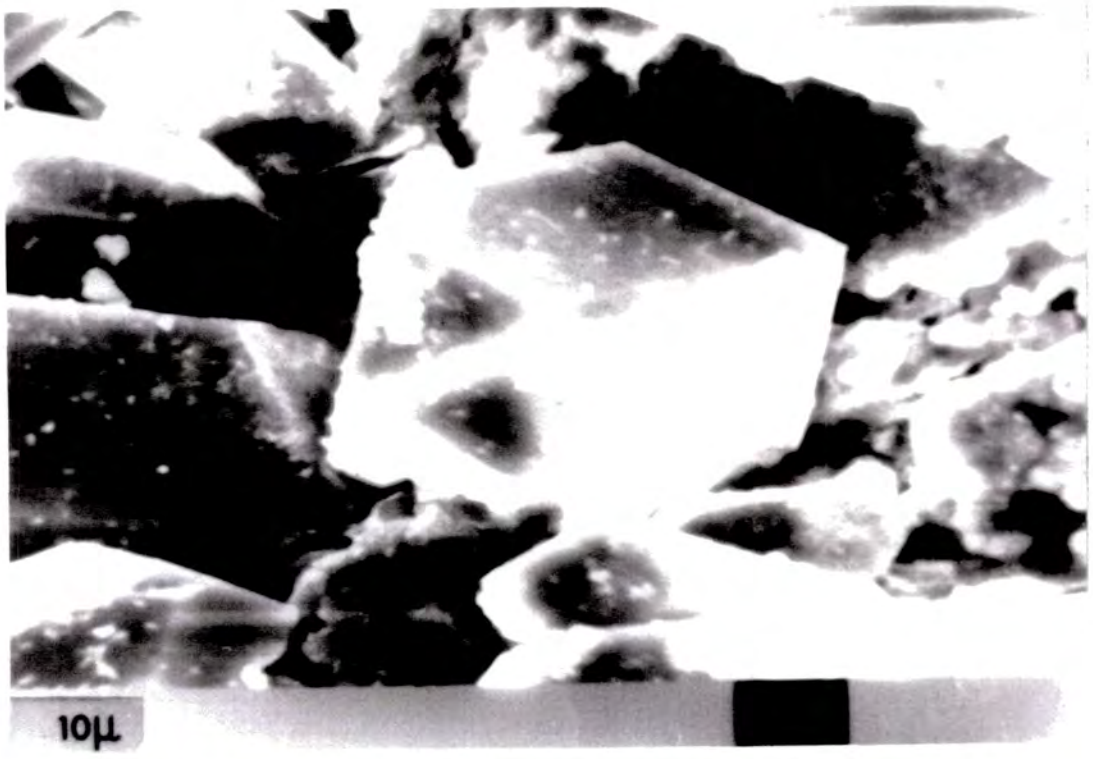

Plate 3.55 High magnification view of well-formed hexagonal crystal in bone from the Vale of Pickering
This crystal is approximately 45μm across

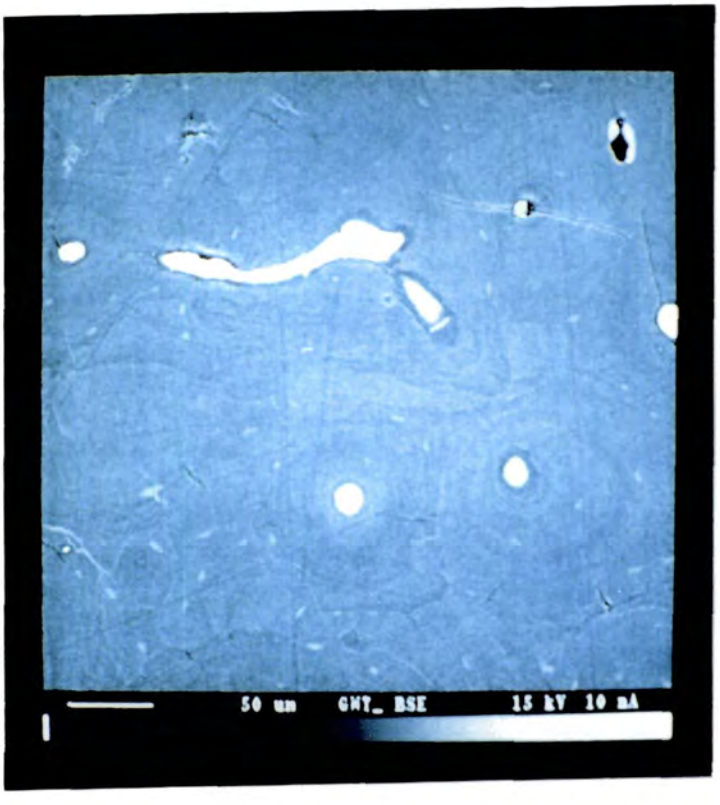

Plate 3.56 SEM backscatter image of bone from the Vale of Pickering. The elongated feature is filled with a denser material with the same calcium:phosphorus ratio as the surrounding bone

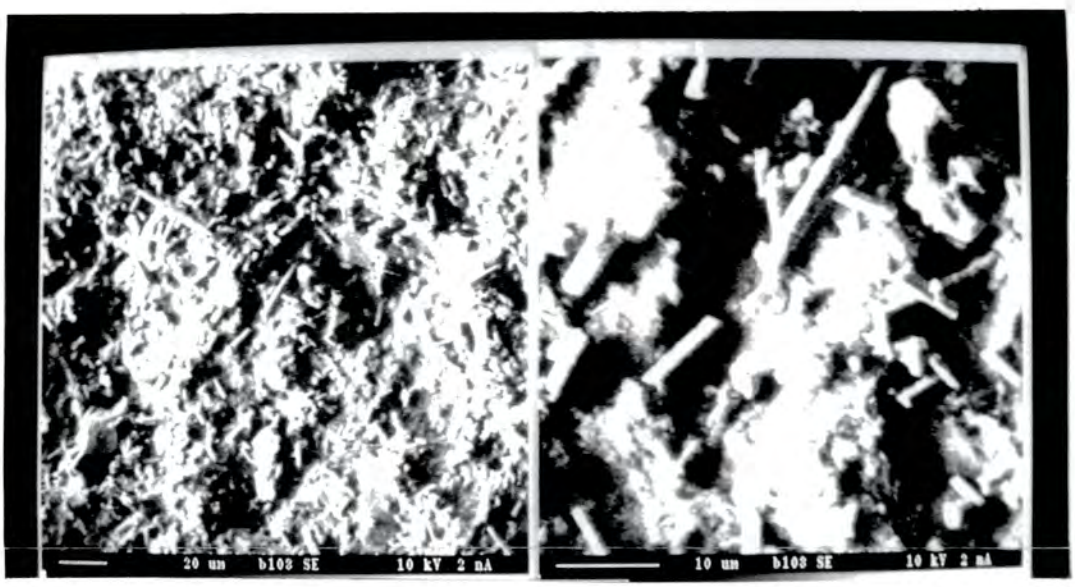

Plate 3.57 SEM image of needle-like crystals in bone from the Vale of Pickering

4. The Chemical Analysis of Fossil Bone

Many researchers have investigated the chemical composition of fossil or archaeological bone and a wide variety of different analytical techniques have been employed. Several of these techniques and the goals of the researchers were discussed in section 2.3. In the majority of these investigations, analysis has concentrated on very narrow aspects of the composition of fossil bone, such as the determination of strontium content or the ratios of certain isotopes in an attempt to understand past diets (see section 2.3.5). By contrast, the work described below aimed to provide an analysis of bones excavated from a wide range of environments and examining several elements, including both the organic and inorganic components. The analysis set out to address a number of specific questions:

> does a relationship exist between the proportion of surviving collagen and diagenetic alteration of the bone mineral?
>
> does the survival of collagen influence the uptake of iron salts and other metal ions from the soil?
>
> to what extent does the collagen alter during diagenesis?
>
> does the calcium:phosphate ratio change as a result of diagenesis?
>
> can any of these factors be used as a measure of diagenetic change?

4.1 Experimental Methods and Materials

Although many specimens were examined during this investigation, the main body of research was restricted to thirty-two samples of fossil (excavated) and unburied bone. These samples were selected from a range of archaeological, geological and other contexts and were chosen on the basis of obvious differences in their perceived states of preservation. The provenances and ages of the bone samples are shown in Table 4.1.

Samples with the prefix SW were excavated from the Iron Age site of Stanwick in North Yorkshire. Those with the prefix VP were excavated from within or below waterlogged peat deposits in the Vale of Pickering. Samples 3 and 4 come from rescue excavations within Durham Cathedral. Samples 8, 9 and 11 were collected in Cyprus and represent bone that has been exposed to high annual temperatures, plus alkaline and saline soil conditions. Those specimens suffixed (u/s) represent unstratified finds or bones picked up from the ground surface.

In addition to bone that had been exposed to post-mortem environmental influences (whether over a geological timescale or for only a handful of years) were bone specimens from freshly killed animals, obtained either from butchers or slaughterhouses. Sheep metatarsals and cow femurs were found to be the most suitable, readily available skeletal elements for examination.

Sample	Provenance	Period	Munsell
1	SW84 II.1120	Iron Age	2.5Y7/2
2	SW84 II.1120	Iron Age	2.5Y8/2
3	Cathedral	Medieval	5Y8/1
4	Cathedral	Medieval	White
5.1*	SW85 2200.70 (surface)	Iron Age	2.5Y6/2
5.2*	SW85 2200.70 (interior)	Iron Age	10YR8/3
6.1*	RO 255.0035 (surface)	Roman	10YR8/2
6.2*	RO 255.0035 (interior)	Roman	
7	Runnymede (u/s)	Neolithic	7.5YR5/2
8	Asproyia (u/s)	Unknown	White
9	Polis Basilica (u/s)	Byzantine	10YR8/1
10	Modern sheep	Modern	White
11	Polis seashore (u/s)	Recent	White
12*	RB89 9583.670	Roman	10YR7/2
13*	RB89 9582.684	Roman	10YR7/3
14*	VP86T 946.0039	Mesolithic	10YR4/3
15*	VP86BM 2168.504	Mesolithic	10YR5/2
16*	VP86Q 1714.0033	Mesolithic	10YR4/2
17*	VP86AE 2711.1016	Mesolithic	10YR6/4
18*	VP86AC 2568.5099	Mesolithic	10YR5/4
19*	VP86Q 1742.0039	Mesolithic	10YR6/3
20*	VP86Q 1767.0039	Mesolithic	10YR7/1
21*	VP86Q 1767.0039	Mesolithic	10YR6/3
22*	VP86 1715	Mesolithic	10YR5/3
23*	VP86 (u/s)	Mesolithic	10YR6/2
24*	Cromerian F'water Beds	Pleistocene	2.5Y6/2
25	Staines/Ashford (u/s)	Pleistocene	2.5Y8/2
26	Staines/Ashford (u/s)	Pleistocene	7.5YR7/4
27	Great Orme Mines (u/s)	Bronze Age	10YR8/1
28	Great Orme Mines (u/s)	Bronze Age	7.5YRN8
29	Rivoli I XIII VIII	Neolithic	5Y8/1
30	HIR79B 1.1725	Saxon	10YR8/2
31	SW85 2200.70	Iron Age	2.5Y8/2
32	SW85 2200	Iron Age	

Table 4.1 Provenances of the samples subjected to chemical analysis (samples marked with an asterix derive from "waterlogged" deposits)

Four separate, but related, analytical techniques were used to investigate the chemical composition of the samples:

total protein content

carbon, hydrogen and nitrogen analysis

total carbonate assay

X-ray fluorescence spectrometry.

These techniques are described in detail in the following sections.

4.1.1 Total Protein Content

Because of the chemical and structural changes that take place when bone mineral is heated (discussed in sections 1.3 and 1.5) and the resulting weight losses, ashing of bone was not considered a suitable method for determining collagen content. The data summarized in Table 1.2, taken from Eastoe and Eastoe (1954) demonstrate that ashing is, at best, a subjective measure of the organic content of bone and at worst completely unreliable. Previous studies (Shipman *et al.* 1984) have demonstrated that fresh bone heated to 525°C or below loses all of its organic matter, yet suffers no marked change in its crystal structure. Protein is gradually burnt out and lost as CO_2 and at low temperatures burning is accompanied by brown, black or grey discoloration produced by the condensation of soot particles on the exposed surfaces of the bone. At higher temperatures, complete combustion of all available organic matter is demonstrated by the bone ash having a white or pale grey colour. At still higher temperatures, of 645°C and above, there is a dramatic change in the X-ray diffraction spectra of bones (Shipman *et al. op.cit.*) and the broad, poorly defined diffraction peaks are replaced by strong, sharp lines indicating a clear structural change.

Thermogravimetric analysis of dentine has demonstrated that when heated slowly there are three temperature regions where rapid mass loss occurs; at approximately 110°C, 300°C and 700°C (Liboff & Shamos 1953). The results of experiments by Liboff and Shamos are summarized in Table 4.2.

Peak temp. °C	Up to temp. °C	% wt. loss	Postulated exudate
140	224	3.6 +/- 0.05	water
330	508	21.5 +/- 0.6	protein & water
530	720	26.4 +/- 0.4	carbonate
815	1000	31.9 +/- 0.7	$Ca_3(PO_4)_2$?

Table 4.2 Themogravimetric analysis of dentin heated in vacuum (after Liboff & Shamos 1953)

Liboff and Shamos postulated that the weight loss between 815°C and 100°C corresponds to the transformation of hydroxyapatite to β-tricalcium phosphate ($Ca_3(PO4)_2$).

Figure 4.1 shows thermogravimetric analyses for fresh collagen, fresh bovine bone and synthetic hydroxyapatite. Here, weight loss at a particular temperature is expressed as a percentage of the original weight. A few milligrams of each sample were heated in a platinum crucible, in air, at a rate of 20°C per minute. As anticipated, the sample of collagen was almost completely consumed, whereas the mineral sample lost less than ten percent in weight. The bone specimen lost a total of 36% of its initial weight. All samples had equilibrated to ambient humidity prior

to the experiments. Figures 4.2 to 4.4 show the time differentials of the weight losses plotted against temperature for the three samples. All three samples show clear peaks between 35°C and 100°C corresponding to loss of loosely bound water. The plot for collagen (Figure 4.2) shows a broad peak between 300°C and 400°C which probably represents thermal denaturing of the protein and corresponding loss of bound water. This is followed by a much broader, and possibly more complex, peak representing combustion of collagen in oxygen. Figure 4.3 shows the differential plot for bone and conforms very closely to the results obtained by Liboff and Shamos (Liboff and Shamos 1953, Figure 13). Denaturation and combustion of the collagen component takes place between 300°C and 550°C with loss of carbonate between 550°C and 750°C. The peak around 800°C probably represents the transformation of hydroxyapatite into β-tricalcium phosphate. Figure 4.4 shows the differential plot for synthetic hydroxyapatite, which may contain up to one percent carbonate, has a large peak at 550°C and a smaller peak at approximately 900°C. This latter peak has not been accounted for.

Many studies of the mineral fraction of bone, for example X-ray diffraction or determination of solubility profiles, require the removal of the organic matter from whole, fresh bone prior to analysis (Hassan *et al.* 1977; Sillen & LeGeros 1991). In these studies the collagenous fraction has been removed chemically using either ethylenediamine ($H_2NCH_2CH_2HN_2$) or sodium hypochlorite (NaClO) in aqueous solutions. Since these reactions take place in an aqueous solution and require prolonged washing there is the potential for loss of some of the more soluble inorganic matter (Termine *et al.* 1973). This possibility is exacerbated in the case of sodium hypochlorite treatment by the high temperature (approx. 117°C) at which this reaction is conducted. In the light of these problems it was decided that neither of these techniques were suitable for the determination of the collagen content of fossil bone.

Termine *et al.* (1973) describe a technique for the deproteinisation of bone, under almost anhydrous conditions and at only slightly elevated temperatures. This method employs hydrazine ($NH_2.NH_2.H_2O$), a free flowing liquid and strong reducing agent, which breaks the peptide bonds binding amino acids in proteins, a process known as hydrazinolysis. This effectively breaks the long chain collagen molecules into short segments which are then solubilized in the supernatent hydrazine. The inorganic component is effectively unchanged except for slight dehydration of loosely bound water. Furthermore, hydrazine is miscible with alcohols and the deproteinized bone may be readily rinsed of excess reagent without washing in water.

A third, alternative, method of determining the total organic content of different bone samples seemed equally promising. Enzymatic digestion of proteins is frequently used when isolating amino acids as an alternative to acid hydrolysis and it was thought that the potential for collagenase extraction of collagen from bone should be investigated. A simple experiment was

devised to compare the results of bone collagen content as determined by ashing, hydrazinolysis and enzyme digestion. These results were then compared with the carbon, hydrogen and nitrogen contents as determined by simple chemical analysis.

Samples taken from 15 specimens were broken up into small fragments, then sieved and washed to remove particles less than 1mm. Part of each sample was hand-ground in a glass pestle and mortar for separate carbon, hydrogen and nitrogen analysis, the rest was divided into three approximately equal portions for ashing, hydrazine extraction and enzyme digestion. All samples were dried in an oven at 105°C for 12 hours, cooled in a vacuum desiccator and weighed on an electronic balance (Mettler P161).

Those samples to be ashed were transferred to porcelain crucibles, covered by loosely fitting porcelain lids and heated in a muffle furnace at 550°C for 24 hours. Samples were allowed to cool to room temperature in the furnace.

Samples to undergo hydrazine treatment were sealed in polystyrene Sterilin tubes with10 ml of hydrazine hydrate and heated to 70°C for 100 hours. This regime is a slight modification of the method for the deproteinization of bone first described by Termine *et al.* in 1973. After hydrazine extraction, the samples were rinsed twice in 10ml ethanol for a period of 12 hours each.

The third group was placed in sterilin tubes with 30ml of a solution containing $50mgl^{-1}$ collagenase (from *Clostridium histolyticum*) buffered to pH 7.5 and heated to 35°C in a water bath for 50 hours. A sample of bovine tendon collagen was subjected to the same regime to asses the progress of enzyme digestion. The samples were then rinsed 3 times in 25ml of distilled water for 12 hours.

After treatment, all samples were again oven dried at 105°C and re-weighed. The loss in protein content of each sample was calculated as the change in weight expressed as a percentage of the original dried weight according to the formula:

$$\text{protein loss} = \frac{(\text{original weight} - \text{weight after treatment}) \times 100}{\text{original weight}}$$

4.1.2 Carbon, Hydrogen and Nitrogen Analysis

Specimens to be analysed were hand-ground to a fine powder in a pestle and mortar to homogenate the sample, then dried at 105°C. Nitrogen, hydrogen and total carbon content were determined using a Carlo Erba Strumentazione Elemental Analyser. In this analysis, weighed

samples are crimped into small, tin capsules and passed into a combustion chamber where any organic components are burnt to carbon dioxide, water vapour and nitrogen oxides in a stream of oxygen. These gasses are carried in a stream of helium over heated copper (I) oxide where excess oxygen is removed and nitrogen oxides are reduced to nitrogen gas. The CO_2, H_2O and N_2 are then carried into a separation column where they are separated before passing to a thermal conductivity detector (TCD). Simultaneous analysis of blanks provides a comparison, allowing the masses of the respective gasses to be calculated from the areas under the respective peaks on a graphical trace generated by the TCD.

In addition to recent and archaeological bone specimens, samples of synthetic hydroxyapatite, calcium carbonate and fresh bovine tendon collagen were also analysed for comparison. Powdered samples of the bone subjected to hydrazinolysis were also analysed for carbon, hydrogen and nitrogen to determine the efficiency of this technique in removing all the protein.

4.1.3 Total Carbonate Assay.

Where sufficient sample was available (samples 1 to 15), an attempt was made to determine the total carbonate content by simple titrometric analysis. Samples were hand-ground whenever possible but in the case of tough specimens such as fresh bone, shavings or filings were collected and used. Samples were dried thoroughly at 105°C and weighed to the nearest milligram (mg).

Stock solutions of 1 molar NaOH and 1 molar (approx.) HCl were prepared and titrated against one another to determine the molarity of the acid. The weighed bone samples were then transferred to conical flasks and 100ml of the acid added. It was found necessary to add a large excess of acid (far above that required to decompose the small quantities of carbonate present) in order to ensure complete dissolution of the bone mineral. The flasks were then stoppered, shaken, and allowed to stand overnight. Ten millilitre aliquots of the resultant supernatent were back titrated against 0.1 molar NaOH using 25-30 drops of bromomethyl blue indicator and a magnetic stirrer. It was necessary to add a considerable quantity of indicator because of the deep brown colouration of many of the solutions and because the precipitation of finely divided hydroxyapatite with increasing pH caused the solutions to become milky in appearance. The end point of each was approached with particular caution since bone has a capacity for self-buffering with the result that neutralization is accompanied by a gradual change in the indicator rather than an abrupt change in colour. The amount of carbonate present in each sample was calculated from the difference in the molar volumes of acid and alkali used, *i.e.* the quantity of acid exhausted in the total decomposition of carbonate or bicarbonate ion to carbon dioxide.

4.1.4 X-ray Fluorescence Spectrometry

X-ray fluorescence (XRF) spectrometry was used both in the qualitative identification of mineral species or contaminant metal ions and for the quantitative analysis of major and minor elements. Analysis was undertaken on a Link Systems XR200 energy dispersive X-ray fluorescence spectrometer, fitted with a rhodium tube. Detection was limited to elements of atomic number greater than 10 by the presence of a beryllium window between the sample vacuum chamber and the detector. For the analysis of bone specimens, tube voltage was set at 20kV, tube current was fixed at 100mA and a 4mm beam collimator was used. Count time was pre-set at 100 seconds although actual counting time was somewhat longer due to 'dead time' or counting time lost while the pulse processor is processing a signal from the detector.

In the case of qualitative analysis, small fragments dissected from larger bone samples were mounted on fine nylon cross-hairs using cellulose nitrate adhesive and positioned in the X-ray beam. However, because of the irreproducible way in which the spectra were collected, no quantitative analysis was attempted on these specimens. Bone samples for quantitative analysis were hand-ground to a fine powder in a ceramic pestle and mortar, then sieved through a 130μm mesh. The resulting powders were pressed into 12.5mm diameter pellets using purpose-built, stainless steel dies and a hand press. It was found that dry powder could be pressed into hard coherent pellets without the necessity for a binding agent. In those cases where little sample was available, it proved possible to press a serviceable pellet from as little as 0.15g of bone powder. When the resulting pellet was especially thin and liable to break, a suitably sized circle of masking tape was applied to the reverse to add extra mechanical support. Once the bone samples had been pressed into pellets the colour (of the homogenized sample) was classified for future reference using Munsell soil colour charts (see Table 4.1). Discs were positioned in the spectrometer using a perspex holder.

4.1.5 Principles of X-ray Fluorescence Spectrometry

This equipment employs an energy dispersive detection system in which the total energy of each X-ray photon entering the solid state detector is measured. An electronic signal generated in the detector is passed via a cable to the 'pulse processor' for amplification and measurement. The signal is then registered as a 'count' (representing the detection of a single X-ray photon) and assigned to the appropriate channel (corresponding to a particular X-ray energy) in the spectrum. This spectrum takes the form of a histogram in which the successive addition of counts accumulate to form a bell-shaped peak characteristic of a particular electronic transition (Figure 4.5).

During analysis, a collimated beam of X-rays (the primary radiation) is directed upon the surface of the sample where they interact with the outer electrons of its constituent atoms. As incident X-rays are scattered by atoms in the sample, electrons are ejected or promoted to higher energy states. The excited atoms return to a more stable configuration by promoted electrons falling to lower energy states with the accompanying emission of X-rays (secondary radiation), a phenomenon known as fluorescence. The energies (or wavelengths) of these fluorescent X-rays have precise values that are characteristic of the element involved (see Figure 4.5) and together form a spectrum from which that element may be identified.

The interaction of X-rays with a specimen involves a number of factors, principally absorption, scattering and the photoelectric effect. Absorption of X-rays, expressed as attenuation of the primary beam, is dependant upon the density of the sample, its thickness and the mass absorption coefficient of the sample. Absorption varies exponentially with all three factors so that for dense, strongly absorbing samples, the beam intensity effectively falls to zero in a very short distance.

The scattering of X-ray may be either elastic or inelastic. In elastic scattering there is no exchange of energy between the X-ray photon and the target atom's electrons and this type of interaction is called coherent or Rayleigh scattering. In the case of inelastic or Compton scattering, there is an interaction between the incident photon and the electrons of the target atom. The X-ray gives up some of its energy to an electron in one of the atom's orbitals and consequently emerges with a lower energy. The degree of scattering depends upon the number of loosely bound outer electrons in the specimen and hence on the atomic number of the atoms present. The photoelectric effect refers to the ejection of an electron from an atom by the incident X-ray photon. This ejection can occur for any electrons in an orbital with energy lower than that of the incoming X-ray and subsequent radiation arising from electron transitions within the atom may fall within a broad range of energies.

4.1.6 XRF Calibration

Although it is possible to determine the composition of an unknown sample from its XRF spectrum using empirical calculations, it is more usual to compare the unknown spectrum with the spectra of similar materials of known composition. It is essential that standards are prepared and presented to the beam in the same way as the unknown specimens and that the conditions under which the spectra are recorded are identical in each case. Best results are obtained if the composition of the calibration standard is close to that of the unknown. The spectrometer is calibrated so that the sensitivity of the system may be determined in terms of a relationship

between the intensity of a particular spectral line and the concentration in weight percent of that element. Since the intensity of the fluorescent radiation depends upon the number of incident X-ray photons it is essential that instrumental parameters (that is, tube voltage, tube current, count time and beam geometry) remain constant for both standard and unknown specimens.

If it is known which elements are present in the specimens under analysis, accurate results are best obtained if a calibration curve is prepared for each of the elements in question. Calibration curves are prepared using several calibration standards of known composition and containing the complete range of compositions of all the elements expected in the unknowns. At least three standards must be used in the preparation of calibration curves and between four and six is desirable. Calibration curves are generated by plotting peak intensity in counts per second against known concentration. The calibration software may then used to fit a straight line or a quadratic function to the data points after making suitable corrections for inter-element or matrix effects.

Calibration curves for calcium, phosphorus and sulphur were prepared using pellets pressed from pure samples and mechanical mixtures of the commercially available inorganic compounds listed below:

$Ca_{10}(PO_4)_6(OH)_2$

$CaHPO_4.2H_2O$

$CaHPO_4$

$CaCO_3$

$CaSO_4.2H_2O$.

Plots of intensity vs concentration for calcium, phosphorus and sulphur taken from spectra of the mechanical mixtures are shown in Figures 4.6 to 4.8. The graphs of intensity vs concentration for both phosphorus and sulphur conform closely to a straight line passing close to the origin. However, the considerable scatter in the points on the graph for calcium rule out the possibility of using simple mechanical mixtures in the preparation of calibration curves for bone. By contrast the three pure calcium phosphates gave a very good fit for both calcium and phosphorus (Figures 4.9 and 4.10). However, when a sample of bone of known composition (International Atomic Energy Agency bovine bone standard, H5) was included in the data, it proved impossible to distinguish a linear relationship between elemental concentration and peak intensity. It became clear that simple inorganic compounds of calcium and phosphorus were not comparable to biological apatites in bone, possibly because of complex inter-element effects or as a result of diffraction from the bone mineral crystallites.

Since all quantitative XRF analysis was conducted on pressed pellets, the possibility of diffraction effects resulting from preferential orientation of the bone apatite crystallites was a real possibility. Bone is a viscoelastic material and is capable of slow, plastic flow under load. Since the bone apatite crystallites are aligned with their c axes parallel to the long axes of the collagen fibres, compression of bone powder was likely to result in the crystallites becoming oriented with their a axes normal to the face of the pressed pellet (*i.e.* their short axes parallel to the line of compression). Enhancement of the calcium concentration in the calibration studies suggested that there was an interaction between the stimulated calcium radiation and the lattice of the crystallites.

It is possible to calculate the wavelength of X-ray photons from the energy of the electron transition (and hence the energy of the photon emitted) using the formula:

$$\lambda = \frac{12.3 \times 10^{-10}}{\sqrt{\varepsilon}}$$

where λ is the wavelength (in meters)and ε is the energy of the photon in electron Volts (Maron & Prutton 1972, 93-94). Taking the energy of the CaKα line to be 3.69 eV, the wavelength of the fluorescent calcium radiation was calculated to be 6.41x 10^{-10}m or 6.41Å. Using this value, tables of the d spacing for hydroxyapatite and the Bragg equation:

$$n\lambda = 2d \sin\theta$$

the potential diffraction angles for CaKα radiation could be calculated. For this wavelength, diffraction occurs at 58°, 61°, 60° and 58° from the 100, 211, 112 and 300 planes respectively (refer to Chapter 5 for a discussion of the principles of X-ray diffraction). Although the X-ray detector of the Link spectrometer lies at an angle of only 50° to the plane of the sample, the proximity of the detector window and the source-sample-detector geometry is such that fluorescent radiation that would normally be absorbed into the body of the pellet could be diffracted out of the sample towards the window of the detector. It is likely that this mechanism accounted for the enhancement in the detection of calcium in bone samples (including H5) compared to synthetic or mineral samples.

As a result of clear differences between bone and synthetic calcium phosphates, it was necessary to calibrate the spectrometer using H5 as a similar standard and analyse the unknowns using the software's 'Fundamental Parameters' model. In this type of analysis, peaks in the spectrum of an unknown are compared with profiles derived from spectra of single element standards stored on file. When using a similar standard, the ratios of peak intensity to concentration (the RST

values) are adjusted so that the calculated concentrations match closely the known composition of the standard. The quoted composition of the IAEA standard H5 is reproduced in Table 4.3.

Ca (wt. %)	P (wt. %)	Na (ppm)	Mg (ppm)	K (ppm)	Cl (ppm)
21.2	10.2	5000	3550	680	550
Sr (ppm)	Zn (ppm)	Ba (ppm)	Fe (ppm)	Br (ppm)	Pb (ppm)
96	89	79	79	3.5	3.1

Table 4.3 Quoted composition of IAEA bovine bone standard H5

Since the sulphur content of H5 is not quoted by the International Atomic Energy Agency. this was determined by independent chemical analysis and found to be less than 0.08% by weight. In the absence of a more accurate measurement. this figure was entered as the assumed sulphur content when calibrating the XRF spectrometer.

An analytical 'method' was created in which a suite of thirteen elements were analysed for. using the Fundamental Parameters model with carbon hydrogen and nitrogen as unanalysed elements and oxygen being determined by difference. The carbon. hydrogen and nitrogen contents. determined by separate chemical analysis (see section 4.1.2), of each sample were entered as unanalysed elements when prompted by the XRF software.

4.2 Results

The results of the ashing, hydrazinolysis and enzyme digestion experiments are shown in Tables 4.4, 4.5 and 4.6 respectively. In all of the following tables those samples derived from contexts considered to be 'waterlogged' are denoted by an asterisk.

Sample	Initial wt (g)	Treated wt (g)	Wt loss (g)	Protein (%)
1	1.882	1.415	0.467	24.81
2	2.312	2.047	0.265	11.46
3	1.830	1.355	0.475	25.96
4	2.109	1.579	0.530	25.13
5.1*	0.305	0.254	0.051	16.72
5.2*	0.576	0.473	0.103	17.88
6.1*	1.896	1.380	0.516	27.22
6.2*	not analysed	not analysed	not analysed	not analysed
7	2.522	2.254	0.268	10.63
8	2.042	1.685	0.357	17.48
9	2.125	2.060	0.065	30.58
10	0.521	0.357	0.164	31.48
11	1.455	1.127	0.328	22.54
12*	1.746	1.295	0.451	25.83
13*	1.627	1.193	0.434	26.67
14*	0.472	0.409	0.063	13.35
15*	1.120	0.890	0.230	20.54

Table 4.4 Results of ashing experiments: samples 1-15

(In the case of samples 5.1, 5.2, 6.1 and 6.2 the limited amount of sample available meant that some analytical techniques had to be omitted)

Sample	Initial wt (g)	Treated wt (g)	Wt loss (g)	Protein (%)
1	2.369	1.882	0.487	20.56
2	1.857	1.743	0.114	06.14
3	1.746	1.743	0.369	21.13
4	1.235	0.966	0.269	21.78
5.1*	not analysed	not analysed	not analysed	not analysed
5.2*	0.767	0.686	0.081	10.56
6.1*	1.952	1.501	0.451	23.10
6.2*	0.575	0.521	0.054	09.39
7	2.519	2.373	0.146	05.80
8	2.620	2.216	0.404	15.42
9	1.465	1.462	0.003	00.20
10	1.707	1.314	0.393	23.02
11	1.452	1.063	0.389	26.79
12*	1.566	1.225	0.341	21.78
13*	1.149	0.890	0.259	22.54
14*	0.510	0.459	0.051	10.00
15*	1.279	1.085	0.194	15.17

Table 4.5 Results of hydrazinolysis: samples 1-15

Sample	Initial wt (g)	Treated wt (g)	Wt loss (g)	Protein (%)
1	2.377	2.330	0.047	1.98
2	1.400	1.390	0.010	0.71
3	1.636	1.619	0.017	1.04
4	1.571	1.561	0.010	0.64
5.1*	0.508	0.502	0.006	1.18
5.2*	0.579	0.573	0.006	1.04
6.1*	1.742	1.718	0.024	1.38
6.2*	not analysed	not analysed	not analysed	not analysed
7	2.160	2.150	0.010	0.46
8	2.855	2.810	0.045	1.58
9	1.300	1.294	0.006	0.46
10	2.329	2.167	0.035	1.50
11	2.236	2.167	0.069	3.09
12*	1.391	1.356	0.035	2.52
13*	1.184	1.176	0.008	0.68
14*	0.528	0.516	0.012	2.27
15*	1.322	1.305	0.017	1.29

Table 4.6 Results of enzyme digestion: samples 1-15

The results of these three experiments are plotted in Figure 4.11. Although the weight losses after ashing are consistently higher, in the majority of samples there is a clear correspondence between the results obtained by ashing and those obtained by hydrazinolysis. Sample 9 lost a considerable amount of weight when ashed (over 30%) compared with very little after hydrazinolysis (only 0.2%). This specimen was excavated from a visibly alkaline soil which contained considerable carbonate deposits (in the form of calcium carbonate). Since bone collagen is susceptible to alkaline hydrolysis these results are consistent with almost total loss of organic matter and the infilling of pore spaces with calcium carbonate during burial. These carbonate deposits would undergo partial or complete thermal decomposition on ashing, accompanied by considerable loss of weight in the sample.

The use of the enzyme collagenase had demonstrably little, if any, success. The highest value for weight loss (3.09%) was recorded for sample number 11. The bulk of this weight loss can almost certainly be accounted for by loss of sodium chloride to the warm aqueous solution during the experiment since specimen 11 was collected from the inter tidal-zone of a sea beach. Other specimens with relatively high weight losses (over 2%) include specimens 12 and 14, both of which derive from acid waterlogged conditions where there may have been leaching of biological apatite from the bone tissue. It is now understood that in order for collagenases to successfully cleave the peptide bonds in collagen, the collagen molecule must be exposed and accessible to the enzyme (Angela Child, pers. comm.), in other words collagen that remains tightly bound to bone mineral cannot be engaged by collagenases since the enzyme is too large to enter between adjacent bone apatite crystallites. As a consequence, areas of bone that have

become demineralized may be expected to be more susceptible to enzymatic attack than those areas where the collagen remains bound to, and protected by, hydroxyapatite.

To determine whether the additional weight loss in the ashed bone was due to loss of lightly bound or adsorbed water (rather than structural water), the ashed samples were soaked in water under vacuum overnight in an attempt to rehydrate the surface of the bone mineral. The samples were again oven dried and reweighed. The weight of each sample was essentially unchanged by this immersion, leading to the conclusion that any water lost during ashing was lost irreversibly.

The efficiency of the hydrazine treatment in removing protein from fresh and archaeological bone was demonstrated by the carbon, hydrogen and nitrogen analysis of the treated samples (Table 4.7). In all but one case (specimen 6.2) the nitrogen content was below 1 percent and in most cases was below 0.5 percent. Some, if not all, of the nitrogen detected in the samples may well have derived from residual hydrazine (H_2-N_2-H_2). It was concluded that hydrazine treatment of bone was the simplest and most reliable method for the total extraction of protein, since ashing removed both bound water and adsorbed carbonate. By contrast, enzyme digestion using collagenase was considered completely ineffectual.

Sample	Carbon (%)	Hydrogen (%)	Nitrogen (%)
1	2.84	0.80	0.48
2	2.88	0.58	0.39
3	3.20	0.75	0.52
4	2.80	0.70	0.35
5.2*	2.58	0.62	0.28
6.1*	2.64	0.93	0.79
6.2*	1.78	0.85	3.51
7	2.89	0.60	0.25
8	2.41	0.55	0.35
9	2.95	0.43	0.11
10	2.74	0.73	0.41
11	2.70	0.74	0.39
12*	2.53	0.78	0.40
13*	2.31	0.79	0.28
14*	3.32	0.76	0.49
15*	6.21	0.99	0.86

Table 4.7 C, H & N analysis after hydrazinolysis: samples 1-15

Even after hydrazine extraction, the bone samples still retain a residual carbon content as is shown by the results in Table 4.7. Although it is possible that this carbon, resistant to hydrazinolysis, could be attributed to non-proteinaceous organic matter such as cellulose (present in the form of fine roots or fungal hyphae) it is much more probable that this represents endogenous matter in the form of lipids and bone mineral carbonate. If the residual carbon was

attributable solely to carbonate ion in bone apatite, then a simple calculation from the carbon contents in Table 4.7 would give a CO_3^{2-} concentration for fresh bone (sample 10) of over 13%. This figure is far higher than the accepted value of approximately 4 percent carbonate for biological apatites (see section 1.5). However, recent work has indicated that whole bone and archaeological bones can contain considerable quantities of lipids (Evershed *et al.* in prep.) . Although some researchers have observed that the lipids in ancient bone are poorly preserved (Liden *et al.* in prep.) other evidence suggests that some lipids are tightly bound to, or encapsulated in, the bone mineral. Up to 4.7% by weight of lipids may be extracted from fresh, whole bovine bone and a further 0.1 % can be extracted following demineralization of the bone tissue (Shapiro 1973).

The carbon, hydrogen and nitrogen contents before deproteinization of samples 1 to 15 are shown in Figure 4.12. There is a close correspondence between these graphs and the corresponding graph of weight loss after hydrazinolysis (except for sample 9 which contains diagenetic calcium carbonate).

Having determined the efficacy of hydrazinolysis and the usefulness of carbon, hydrogen and nitrogen analysis, a further 17 specimens of archaeological bone were selected for examination. The protein contents of samples 17 to 32 as determined by hydrazinolysis are shown in Table 4.8.

Sample	Initial wt (g)	Treated wt (g)	Wt loss (g)	Protein (%)
16*	1.575	1.545	0.030	01.90
17*	1.659	1.349	0.310	18.69
18*	1.129	1.036	0.093	08.24
19*	0.742	0.701	0.041	05.53
20*	0.489	0.441	0.048	09.82
21*	0.338	0.280	0.058	17.16
22*	0.455	0.430	0.025	05.49
23*	0.798	0.760	0.028	04.76
24*	1.299	1.240	0.059	04.54
25	1.100	1.094	0.006	00.55
26	1.175	1.169	0.006	00.51
27	1.932	1.559	0.373	19.31
28	1.573	1.304	0.269	17.10
29	0.993	0.841	0.152	15.31
30	1.443	1.250	0.193	13.37
31	1.701	1.614	0.087	05.11
32	1.373	1.327	0.046	03.35

Table 4.8 Results of hydrazinolysis: samples 16-32

The results of carbon, hydrogen and nitrogen analysis for all specimens (1 to 36) are shown in Table 4.9. To determine what, if any, relationships existed between these elements, simple

graphs were plotted of hydrogen vs carbon and nitrogen vs carbon. These graphs are shown in Figure 4.13 and Figure 4.14 respectively.

Sample	Carbon (%)	Hydrogen (%)	Nitrogen (%)
1	12.07	2.05	3.73
2	5.28	1.00	0.92
3	12.80	2.14	3.87
4	12.56	2.08	3.90
5.1*	5.89	1.16	1.28
5.2*	3.84	0.77	0.40
6.1*	12.88	2.23	3.97
7	4.95	0.97	0.96
8	8.76	1.48	2.66
9	4.07	0.53	0.10
10	20.94	3.40	6.50
11	11.79	2.10	4.15
12*	8.40	1.74	3.17
13*	12.10	2.23	4.77
14*	7.11	1.24	2.29
15*	9.74	1.55	1.85
16*	4.33	0.78	0.15
17*	11.20	1.53	2.21
18*	8.85	1.21	0.99
19*	3.89	1.00	0.14
20*	4.31	1.46	0.18
21*	4.62	1.48	0.22
22*	4.37	1.03	0.17
23*	4.18	0.91	0.11
24*	4.90	0.79	0.76
25	4.20	0.73	0.24
26	3.92	0.75	0.13
27	11.66	1.92	3.62
28	10.77	1.78	3.55
29	9.74	1.64	2.60
30	7.57	1.29	1.61
31	5.28	1.15	1.23
32	3.66	0.86	0.62
H'apatite	0.77	0.47	0.03
Calcite	12.00	0.02	0.09
Collagen	51.89	7.77	15.18
H5	21.04	3.38	5.77

Table 4.9 C. H & N analyses: samples 1-32

The figures quoted in Table 4.9 give no indication of the accuracy of the determinations of carbon, hydrogen and nitrogen contents of the samples. Performance of the equipment was monitored by the regular analysis of standards of known composition. Since each unknown was analysed only once, determination of the accuracy of results was more problematic. However, using this facility, measurements of total carbon content are generally accepted to be within 0.01% and values for nitrogen to be within 0.03%. Levels of accuracy for hydrogen contents are

more problematic, partly because of the low weight percent of hydrogen present in each sample and partly because of errors introduced by the considerable quantities of adsorbed water in each sample. Although all samples were dried overnight at 105°C before being sealed in glass vials, bone has the capacity to absorb a considerable proportion of its weight in water if allowed to stand in air at room temperature (see Chapter 7). A simple plot of hydrogen vs nitrogen for the samples analysed gave very good correspondence to a straight line, suggesting that there was little random error in the hydrogen determinations. However, systematic errors could still be present if the amount of adsorbed water was directly related to the amount of protein (nitrogen) present in the sample.

Cursory inspection of Figure 4.13 suggests that there is a linear relationship between the carbon and hydrogen contents of archaeological bones. Similarly, an approximately linear relationship is also suggested between the nitrogen and carbon contents of archaeological bone (Figure 4.14). In this case, however, the graph does not pass through the origin but intercepts the carbon axis at a value of between 2% and 3%. Again, this suggests that there is an excess of carbon even when all of the protein (nitrogen) has been removed from the bone by diagenetic processes. If the data from Table 4.9 is separated into two sets, representing samples from aerated and waterlogged contexts, then two different patterns emerge (Figure 4.15 and Figure 4.16 respectively). Here, straight line graphs have been fitted using root mean squares. The carbon and nitrogen data for aerated soils is very consistent ($R^2=0.983$) and has an intercept close to the origin with <0.2% excess hydrogen, possibly related to hydroxy groups or bound water. The slope of the graph indicates that these elements occur in a consistent ratio of approximately six to one by weight. This is equivalent to a molar ratio of two hydrogen atoms per carbon atom and is in excellent agreement with any long chain organic molecule of the form $R\text{-}(CH_2)_n\text{-}R'$ where R and R' may be any functional group such as the amino ($-NH_2$) group or the carboxyl (-COOH) group. This is consistent with a long chain polypeptide such as collagen. The carbon and nitrogen data shown in Figure 4.16 (corresponding to 'waterlogged' samples) shows considerable scatter and demonstrates that in these environments the results of diagenetic change are more complicated than is the case in aerated soils. The intercept at 0% carbon also indicates that these samples may contain relatively more inorganic hydrogen, potentially as a result of the greater mobility of contaminating minerals at low pH's or because mineral species containing hydrogen are more likely to form in acidic aqueous environments. If a quadratic curve ($R^2=0.984$) is applied to the carbon and nitrogen data for aerated soils, then the curve has an intercept corresponding to 3.2% excess carbon at the end point of protein loss (Figure 4.17). This result corresponds closely with the levels of carbon remaining in the deproteinized samples (Table 4.7). Once again there is considerably more scatter in the data for samples from waterlogged contexts (Figure 4.18).

The forms of the graphs in Figures 4.13 to 4.18 suggest that there is a progressive loss of protein from bone during burial and that the collagen is degraded in such a way as the C:N and C:H ratios are relatively unchanged. The progressive loss of nitrogen from archaeological or fossil bone has been known for many years, leading to early attempts to use nitrogen content as a means of obtaining relative dates for bones from the same site (Garlick 1971, 503-510; Brothwell 1972, 5). Since amino acids are readily soluble in water, degraded collagen should be rapidly lost from the bone. Furthermore, protein loss will be accelerated in the presence of micro-organisms. To investigate whether the organic matter surviving in buried bones retained the same elemental ratios of undegraded collagen the carbon, hydrogen and nitrogen contents of samples 1 to 32 have been normalized to 100 percent in Table 4.10.

Sample	Carbon (%)	Hydrogen (%)	Nitrogen (%)
1	67.62	11.48	20.90
2	73.33	13.89	12.78
3	68.05	11.38	20.57
4	67.74	11.22	21.04
5.1*	70.70	13.93	15.37
5.2*	76.65	15.37	7.98
6.1*	67.50	11.69	20.81
7	71.95	14.10	13.95
8	67.91	11.47	20.62
9	86.60	11.28	2.12
10	67.90	11.02	21.08
11	65.36	11.64	23.00
12*	63.11	13.07	23.82
13*	63.35	11.68	24.97
14*	66.83	11.65	21.52
15*	74.12	11.80	14.08
16*	82.32	14.83	2.85
17*	74.97	10.24	14.79
18*	80.09	10.95	8.96
19*	77.34	19.88	2.78
20*	72.43	24.54	3.03
21*	73.10	23.42	3.48
22*	78.46	18.49	3.05
23*	80.38	17.50	2.12
24*	75.97	12.25	11.78
25	81.24	14.12	4.64
26	81.66	15.63	2.71
27	67.79	11.16	21.05
28	66.89	11.06	22.05
29	69.67	11.73	18.60
30	72.30	12.32	15.38
31	68.93	15.01	16.06
32	71.21	16.73	12.06
Collagen	69.34	10.38	20.28
H5	69.69	11.20	19.11

Table 4.10 Normalized C, H & N values for samples 1-32

To establish the relationships between these three elements, their normalized values are plotted on a triangular or ternary diagram in Figure 4.19. Many of the points cluster around the composition for pure collagen (C~70%, H~11%, N~19) indicating that the collagen that remains in the bone is probably chemically unaltered although some collagen fibres may be broken up into shorter fibrils or even individual collagen molecules. The ternary diagram shares some features with Figure 4.14. There is a trend away from the composition of pure collagen towards increasing carbon content, although here the intercept on the hydrogen axis suggests that there may be as much as 10 percent excess hydrogen even when all protein has been removed from the bone during diagenesis. Again, this may represent 'organic' hydrogen in the form of non-proteinaceous matter or 'inorganic' hydrogen in the form of mineral bicarbonate (HCO_3^{-1}). The considerable scatter in those specimens from 'waterlogged' environments shown in Figures 4.14 and 4.16 is also evident in Figure 4.19. The carbonate contents calculated from the titrations for samples 1-15 are given in Table 4.11. Table 4.11 also shows the residual carbon for the same samples after deproteinization with hydrazine solution.

Sample	CO_3^{2-}(%)	C(%)
1	8.27	2.84
2	8.45	2.88
3	9.49	3.20
4	9.98	2.80
5.1*	7.59	unanalysed
5.2*	7.59	2.58
6.1*	unanalysed	2.64
6.2*	6.19	1.78
7	10.97	2.89
8	9.63	2.41
9	17.38	2.95
10	7.27	2.74
11	8.31	2.70
12*	5.98	2.53
13*	7.54	2.31
14*	6.68	3.32
15*	8.00	6.21

Table 4.11 Results of carbonate titration

The average carbonate ion content of the samples as determined by titration was 8.71% (st.dev.=2.69). This compares to an average value of 11.55% (st.dev.=3.74) CO_3^{2-} calculated from the residual carbon assuming that all the residual carbon represented bone apatite carbonate. Despite the problems associated with titration, it is clear that bone mineral carbonate cannot account for all of the carbon that remains in bone after diagenesis or hydrazinolysis. Sample 9 gave a titrated carbonate content of 17.38%, a value considerably higher than the average. Microscopic analysis of sample 9 showed that diagenetic calcite was present in some of

average. Microscopic analysis of sample 9 showed that diagenetic calcite was present in some of the pores and voids and it would be expected that this would be reflected in the results of the titrations.

Table 4.12 Results of XRF analysis

Sample	Ca (%)	P (%)	Fe (ppm)	Mn (ppm)	S (ppm)	Zn (ppm)	Ba (ppm)	Sr (ppm)
1	28.67±0.09	13.17±0.07	6432±125	1472±092	416±42	189±51	176±50	187±73
2	36.61±0.12	16.84±0.08	1816±088	290±076	308±46	143±61	221±62	206±84
3	27.22±0.09	12.35±0.07	1517±070	d.	345±41	d.	223±49	d.
4	26.92±0.09	12.30±0.07	659±059	342±063	401±40	167±46	230±48	d.
5.1*	32.93±0.11	15.75±0.08	8822±157	4226±142	744±52	2228±95	264±61	d.
5.2*	38.03±0.12	17.52±0.09	1344±083	288±079	527±52	2269±98	174±63	d.
6*	25.92±0.09	13.19±0.07	33280±260	7335±164	1063±51	161±74	418±57	161±74
7	36.59±0.12	15.78±0.08	10164±185	13089±232	601±50	122±56	280±68	183±87
8	33.61±0.11	15.31±0.08	729±063	n.d.	250±43	184±50	d.	d.
9	38.66±0.12	15.26±0.08	2500±098	d.	570±51	d.	148±62	183±84
10	25.64±0.08	12.30±0.07	1293±064	n.d.	320±37	127±45	198±45	120±
11	26.97±0.09	12.65±0.07	1126±065	632±069	950±53	d.	148±47	333±71
12*	28.88±0.10	14.24±0.08	26359±237	2629±121	565±47	175±55	228±57	195±75
13*	25.69±0.09	12.92±0.07	30767±243	2142±107	562±44	111±47	169±53	d.
14*	32.13±0.11	15.31±0.08	33274±276	1068±101	2067±68	434±65	356±64	191±83
15*	29.67±0.10	13.06±0.07	19517±207	444±80	1004±51	120±48	975±74	312±79
16*	35.27±0.11	16.65±0.09	17455±215	1505±111	2234±72	154±58	263±66	196±86
17*	28.71±0.09	12.93±0.07	16324±188	955±83	866±49	d.	690±66	177±77
18*	30.11±0.10	13.32±0.08	27401±247	2262±155	674±47	d.	880±72	321±83
19*	24.37±0.09	15.25±0.08	14902±173	343±069	2645±72	267±52	245±53	138±68
20*	6.65±0.04	11.05±0.07	62978±258	269±051	8920±106	2614±76	321±38	d.
21*	15.27±0.07	12.47±0.07	21896±177	637±065	5350±87	1423±63	249±45	103±
22*	32.32±0.11	16.36±0.09	31575±275	1308±106	4588±92	133±56	303±66	222±78
23*	27.48±0.10	15.18±0.09	35918±273	573±084	4121±87	3836±112	485±62	d.
24*	32.65±0.10	14.18±0.08	12576±177	1257±098	2441±70	135±50	253±56	266±82
25	37.30±0.12	16.49±0.09	8833±161	566±091	626±50	966±76	291±64	d.
26	32.70±0.11	14.51±0.08	20570±222	1252±102	551±47	470±64	403±64	300±84
27	29.56±0.09	12.85±0.07	911±066	1090±082	785±47	d.	159±51	d.
28	30.90±0.10	13.41±0.07	761±061	188±065	317±40	d.	268±53	d.
29	28.05±0.09	12.83±0.07	3365±096	727±075	248±37	230±50	327±55	d.
30	30.33±0.10	14.46±0.08	3269±099	194±066	460±43	429±57	280±60	190±76
31	35.26±0.11	16.58±0.08	9661±164	1127±097	242±44	129±56	212±60	269±86
32	38.18±0.12	17.83±0.09	894±073	307±079	320±47	212±58	257±66	171±80
H5	20.82±0.07	9.96±0.06	107±035	n.d.	770±41	108±38	112±38	d.

Sample	Pb (ppm)	Cl (ppm)	Na (ppm)	K (ppm)	Mg (ppm)	C (%)	H (%)	N (%)
1	n.d.	289±	d.	286±	d.	12.07±0.01	2.05	3.73±0.03
2	n.d.	281±	d.	358±	n.d.	5.28±0.01	1.00	0.92±0.03
3	599±	230±	d.	615±	5191±	12.08±0.01	2.14	3.87±0.03
4	d.	455±	d.	592±	3992±	12.56±0.01	2.08	3.90±0.03
5.1*	d.	592±	d.	d.	5504±	5.89±0.01	1.16	1.28±0.03
5.2*	d.	488±	d.	d.	7634±	3.84±0.01	0.77	0.40±0.03
6*	d.	148±	d.	d.	d.	12.88±0.01	2.23	3.97±0.03
7	d.	154±	d.	d.	n.d.	4.95±0.01	0.97	0.96±0.03
8	d.	311±	d.	d.	d.	8.76±0.01	1.48	2.66±0.03
9	d.	1441±	d.	589±	d.	4.07±0.01	0.53	0.10±0.03
10	n.d.	276±	d.	372±	3156±	20.94±0.01	3.40	6.50±0.03
11	d.	2806±	5853±	484±	5134±	11.79±0.01	2.10	4.15±0.03
12*	n.d.	216±	n.d.	479±	n.d.	8.40±0.01	1.74	3.17±0.03
13*	n.d.	347±	d.	533±	d.	12.10±0.01	2.23	1.85±0.03
14*	n.d.	278±	d.	d.	d.	7.11±0.01	1.24	2.29±0.03
15*	n.d.	299±	d.	n.d.	n.d.	9.74±0.01	1.55	1.85±0.03
16*	n.d.	189±	d.	d.	d.	4.33±0.01	0.78	0.15±0.03
17*	d.	d.	d.	d.	n.d.	11.20±0.01	1.53	2.21±0.03
18*	d.	239±	d.	d.	d.	8.85±0.01	1.21	0.99±0.03
19*	n.d.	n.d.	n.d.	d.	n.d.	3.89±0.01	1.00	0.14±0.03
20*	n.d.	d.	n.d.	d.	n.d.	4.31±0.01	1.46	0.18±0.03
21*	n.d.	d.	n.d.	d.	n.d.	4.62±0.01	1.48	0.22±0.03
22*	d.	214±	n.d.	d.	n.d.	4.37±0.01	1.03	0.17±0.03
23*	d.	245±	n.d.	376±	n.d.	4.18±0.01	0.91	0.11±0.03
24*	d.	474±	d.	d.	d.	4.90±0.01	0.79	0.76±0.03
25	d.	296±	d.	d.	d.	4.20±0.01	0.73	0.24±0.03
26	d.	145±	d.	595±	n.d.	3.92±0.01	0.75	0.13±0.03
27	d.	167±	d.	d.	3480±	11.66±0.01	1.92	3.62±0.03
28	355±	199±	d.	367±	2659±	10.77±0.01	1.78	3.55±0.03
29	d.	d.	n.d.	1134±	n.d.	9.74±0.01	1.64	2.60±0.03
30	n.d.	247±	d.	1099±	d.	7.57±0.01	1.29	1.61±0.03
31	d.	253±	d.	d.	d.	5.28±0.01	1.15	1.23±0.03
32	n.d.	235±	d.	d.	d.	3.66±0.01	0.86	0.62±0.03
H5	n.d.	n.d.	n.d.	n.d.	n.d.	51.89±0.01	7.77	15.18±0.03

The results of X-ray fluorescence analysis are shown in Table 4.12 where concentration of major elements are expressed in weight percent and minor elements in parts per million. Carbon, hydrogen and nitrogen contents (as determined by combustion) for each sample are also included. Certain elements, particularly lead and the lighter elements sodium, potassium and chlorine were not detected in levels greater than twice the relative error and therefore could not be quoted with any confidence. In such cases, the element was considered to be detected only and 'd' appears in the relevant column. Where 'n.d.' appears in a column it denotes that the element could not be detected above background.

On closer inspection of the data in Table 4.12 several clear trends emerge. Of the 16 samples with high iron contents (above 1 percent) all but two (sample 7 and sample 26) derived from those deposits recognised as waterlogged. Although these samples with considerable iron contents also have higher levels of manganese, there is not a simple relationship between the amounts of these elements in each sample, which might be expected if their availability in the soil solution was determined solely by soil pH for instance. In fact, some samples with especially high concentrations of manganese contain relatively little iron (*e.g.* sample 7 and sample 27). Although the presence of both framboidal pyrite and gypsum in bones from waterlogged deposits has been demonstrated by microscopy (see section 3.1.4) the evidence from XRF analysis strongly suggests that the majority of iron is present in a form other than sulphur compounds, most probably as oxides or oxyhydroxides. Nevertheless, some bones from waterlogged burial environments do have considerably higher sulphur contents than bones found in neutral or alkali soils. For example, samples 14, 16, 19, 21, 22, 23 and 24 have sulphur contents in excess of 0.2% compared to levels around 0.03% found in fresh bone and bones from neutral burial soils.

The results shown in Table 4.12 also demonstrate that the elements frequently used as dietary indicators, strontium and zinc are widely variable, possibly suggesting that some diagenetic change has taken place, but no clear patterns emerge to suggest what factors might determine or influence that change. In this respect the analyses for sample 5 in which the bone surface in contact with the soil solution and the interior were examined separately are particularly interesting. Here the zinc contents are almost identical, 2228ppm at the surface compared to 2269ppm in the interior, despite wide differences in the concentrations of other elements. Strontium was not detected in either surface or interior. The outer surface, which was dark brown in colour, had iron and manganese contents of 0.8822% and 4226ppm respectively compared to 0.1344% and 288ppm for the pale cream interior. The calcium and phosphorus contents of the outer surface were approximately nine tenths of the corresponding contents for the interior. Conversely, the carbon and hydrogen contents of the interior were only two thirds those of the outer surface. The nitrogen content of the interior was reduced to only about a third

of that of the surface. These analyses are consistent with considerable loss of bone mineral from the surfaces in contact with the soil and corresponding influx of soluble iron and manganese species, a picture consistent with a local lowering of pH. In the interior of the bone the situation appears to have been reversed with loss of collagen rather than the dissolution of bone apatites and limited mobility of metal ions suggesting alkaline conditions.

To explore possible diagenetic changes in the bone mineral of the samples, the calcium/phosphate ratio was examined. Figure 4.20 shows a plot of phosphorus vs calcium for samples 1 to 32. Here the samples have been separated into specimens from waterlogged, aerobic (neutral) soils, alkaline soils and 'fresh' or unburied bone. Many of the samples analysed lie on, or close to a straight line passing through the origin and corresponding to a calcium to phosphorus weight ratio of the theoretical composition of hydroxyapatite with a molar ratio of 10 to 6 or 1.67. All but 5 of the 32 points lie between lines representing Ca:P molar ratios of 1.5 and 1.8. Four of these specimens have an excess of phosphorus over what would be expected for hydroxyapatite or bone apatite and come from 'waterlogged' soils. Microscopy and other analyses (see Chapters 3, 5 and 6) have demonstrated that bones from waterlogged deposits frequently contain of the iron phosphate mineral vivianite, either in massive deposits or within the pore structure. Such deposits would significantly influence the calcium:phosphorus ratios of affected bones. The point with an apparent excess of calcium represents sample 9, a specimen from soil containing considerable calcareous deposits and one demonstrated to contain diagenetic calcite.

Returning to the specimens from aerobic, neutral soils, these all lie close to a line drawn between the compositions of fresh bovine bone and the theoretical composition of hydroxyapatite. Bone apatite , in common with other hydroxyapatites deposited from biological fluids, contains approximately 4% by weight of carbonate substituted in the place of phosphate ions and should therefore have a lower Ca:P ratio than pure hydroxyapatite. Although the titration experiments on the 32 samples were unsatisfactory it is widely accepted that bone mineral carbonate survives in bone after much of the collagen has been lost and many attempts have been made to obtain radiocarbon dates and dietary information from this source of endogenous carbon. The shaded area on Figure 4.20 encloses the triangle formed by the compositions of H5 (20.2% Ca, 10.2% P), stoicheometric hydroxyapatite (39.9% Ca, 18.5% P) and hydroxyapatite with 4% carbonate (39.9% Ca, 17.2% P). The scatter of many of the analysed samples within this triangle is consistent with a simple model of diagenesis in which bone collagen is lost by hydrolysis with little or no change in the composition of the bone mineral. As the protein is gradually lost the weight percent of the remaining mineral must increase without any appreciable change in the Ca:P ratio. In effect, bone behaves as a two component system during diagenesis.

In order to investigate reproducibility of XRF analysis and to check whether the scatter in the Ca:P ratios of the ancient bone was real, rather than the result of experimental error, a further six samples of deproteinized modern bone and another sample of the calibration standard H5 were analysed using the same experimental conditions. Four of these were also analysed for Ca and P using atomic absorption spectroscopy and colourimetry to reveal any variability in their compositions. The results of these analyses are shown in Tables 4.13 to 4.15. The results are plotted in Figure 4.21. It can be seen that the six samples of deproteinized bone analysed by XRF all cluster close to the theoretical composition of hydroxyapatite although with a slightly higher phosphorus content. This high phosphorus content, which is considerably higher than that predicted for a carbonate containing apatite can be accounted for if the lipids that remain tightly bound to the bone mineral crystallites after hydrazinolysis represent phospholipids. Similarly, the analysis for H5 lies on the line representing a molar ratio of 1.67, albeit with an apparently higher organic content than washed and oven dried fresh bone.

By comparison, the results obtained by standard wet chemical analysis of the deproteinized bone are far from the predicted composition and that obtained by XRF analysis. In fact it is well known that the determination of calcium by atomic absorption spectroscopy is compromised by complexation with phosphorus and measures have to be taken to ensure that calcium is not precipitated from solution before atomisation of the sample solution into the flame of the spectrometer. However, even if the discrepancies in the results of atomic absorption analysis are attributable to a reduced calcium concentration caused by precipitation from the sample solution, this would not affect the measurement of the phosphorus content which was determined by colourimetry.

Sample	Calcium (%)	Phosphorus (%)
A1-4	28.21	15.32
B1	25.85	15.54
B2	26.21	15.38
B6	24.86	15.98

Table 4.13 Wet chemical analysis of deproteinized bone

Sample	Carbon (%)	Hydrogen (%)	Nitrogen (%)
A1-4	1.69	0.72	0.21
B1	2.06	0.69	0.09
B2	2.08	0.72	0.13
B6	1.78	0.69	0.02

Table 4.14 Carbon, hydrogen and nitrogen analysis of deproteinized bone

Sample	Calcium (%)	Phosphorus (%)
A1-4a	40.39	19.12
A1-4b	40.27	19.20
B1a	39.32	18.75
B1b	39.79	18.99
B2	39.36	18.69
B6a	40.13	19.01
B6b	40.12	18.78
H5	22.36	10.08
H5	21.58	10.37

Table 4.15 XRF analysis of deproteinized bone and standard H5

In order to compare the robustness of XRF analysis as compared to other analytical techniques. the data from several different authors was examined. Figure 4.22 shows the results of data collected using XRF analysis (Pate *et al.* 1989) and neutron activation analysis (Williams & Potts 1988; El-Kammar *et al.* 1989). These analyses show a distribution of compositions very similar to those illustrated in Figure 4.20 above. When some other results where atomic absorption spectrometry and colourimetry were used to analyse archaeological or fossil bone are examined in the same way there appears to be considerably more scatter in the compositions of different samples (Figure 4.23). Vuorinen *et al.* used particle induced X-ray emission (PIXE) and particle induced gamma-ray emission (PIGE) to analyse the lead and other elemental contents of 8th century B. C. infant bones from Italy (Vuorinen *et al.* 1990). Their determination of calcium and phosphorus vales are plotted in Figure 4.24. These results show excellent internal consistancy and mirror the results of XRF analysis above.

Although it is impossible to comment upon the accuracy of any analyses undertaken by other researchers it is possible that analytical techniques that have a strong reliance on theoretical considerations, which include X-ray fluorescence analysis and neutron activation analysis, are much more robust than other methods which rely strongly on total dissolution of the specimen and calibration by stock solutions.

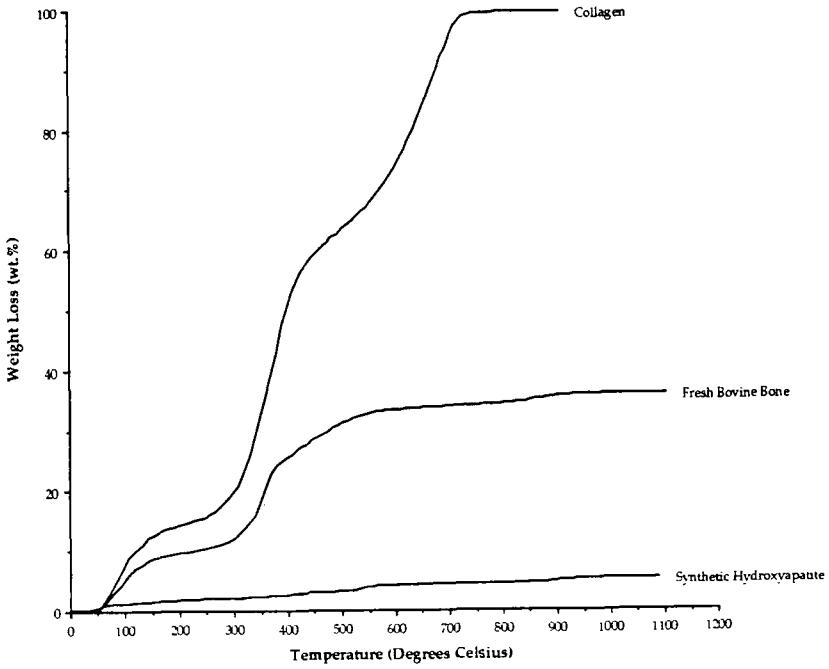

Figure 4.1 Thermogravimetric analysis for fresh collagen, fresh bovine bone and synthetic hydroxyapatite

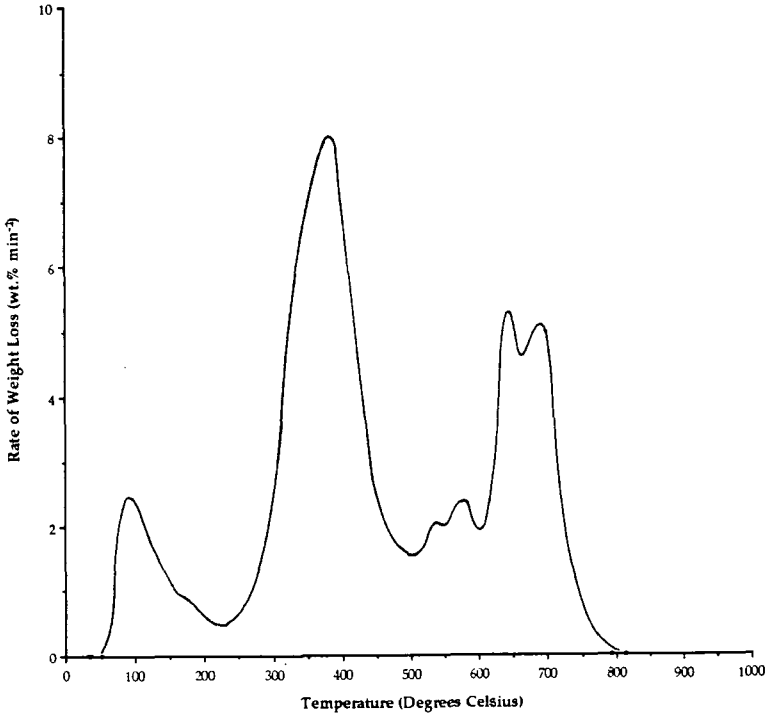

Figure 4.2 Differential thermal gravimetry for collagen

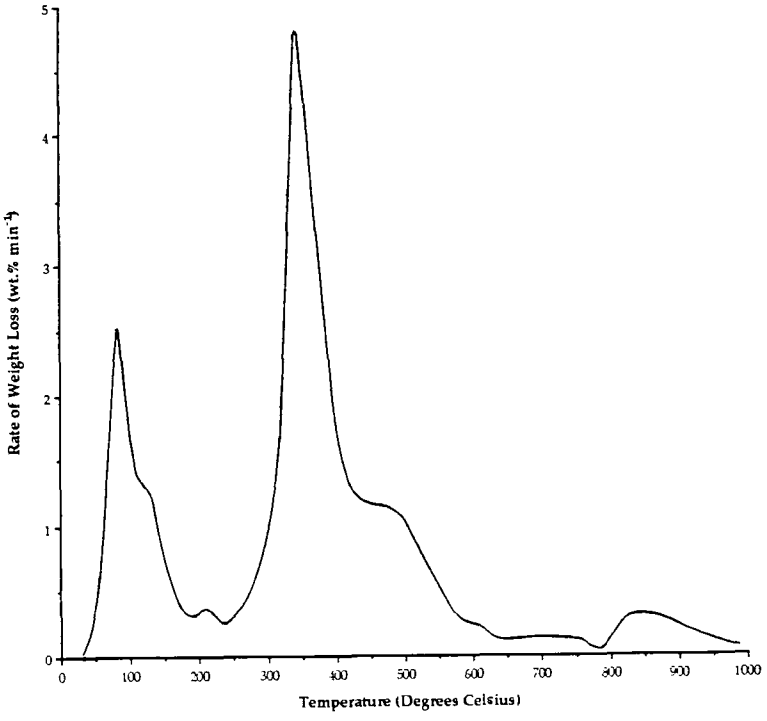

Figure 4.3 Differential thermal gravimetry for fresh bovine bone

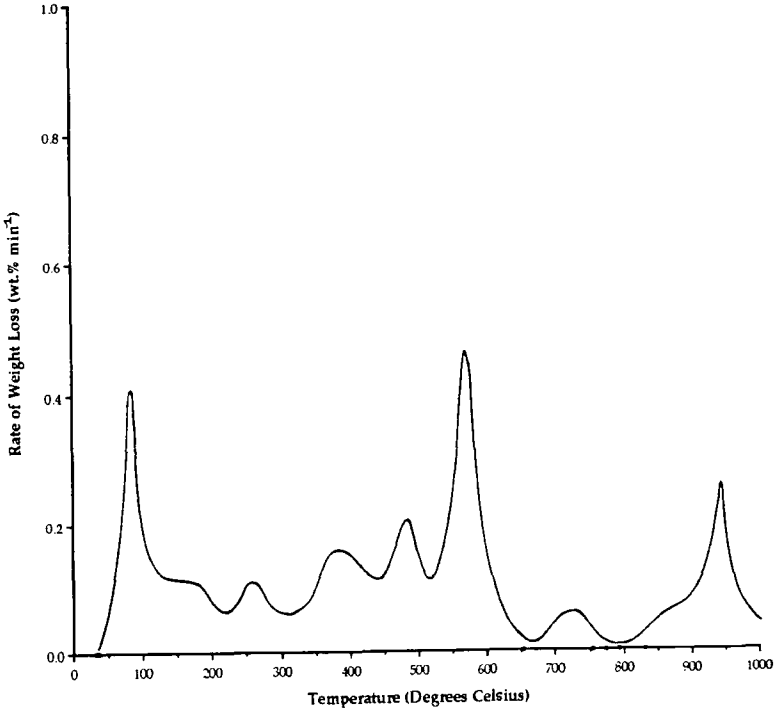

Figure 4.4 Differential thermal gravimetry for synthetic hydroxyapatite

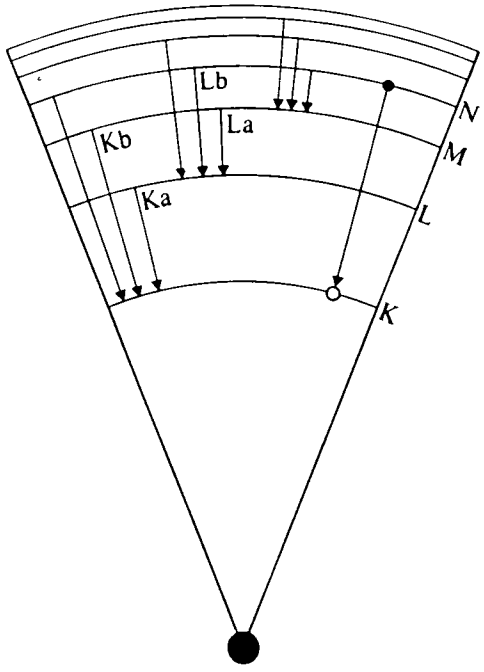

Figure 4.5a Electronic transitions in a typical atom, showing origin of Kα, Kβ, Lα radiation *etc*.

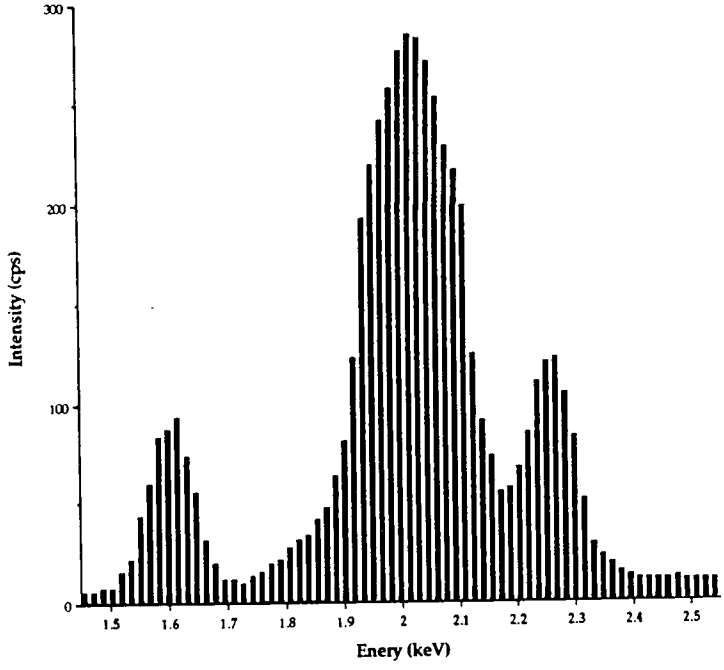

Figure 4.5b Part of typical XRF specrum

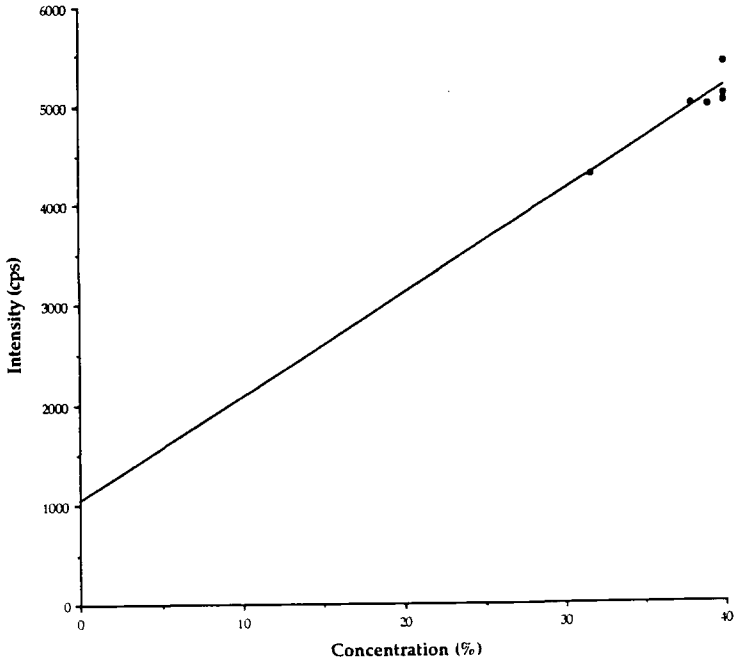

Figure 4.6 Plot of intensity vs concentration for calcium (mechanical mixtures of synthetic compounds)

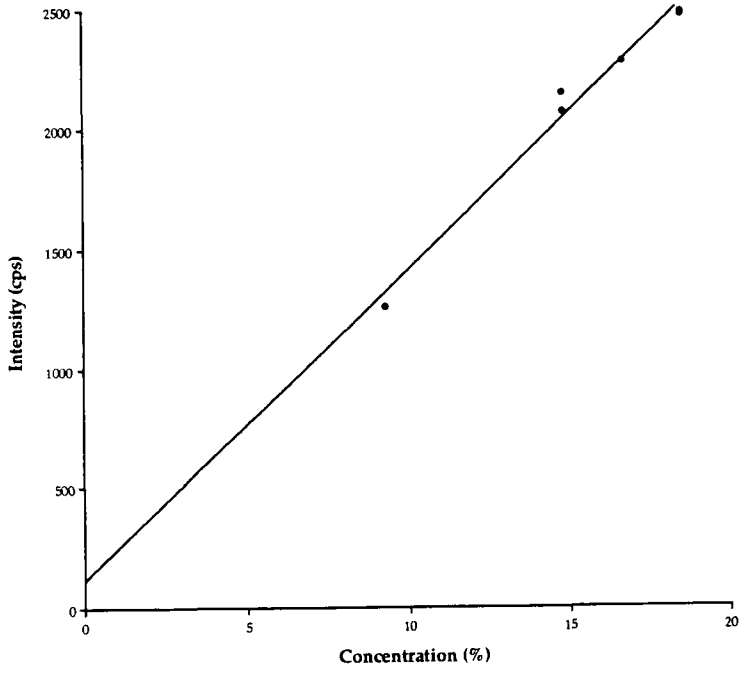

Figure 4.7 Plot of intensity vs concentration for phosphorus (mechanical mixtures ofsynthetic compounds)

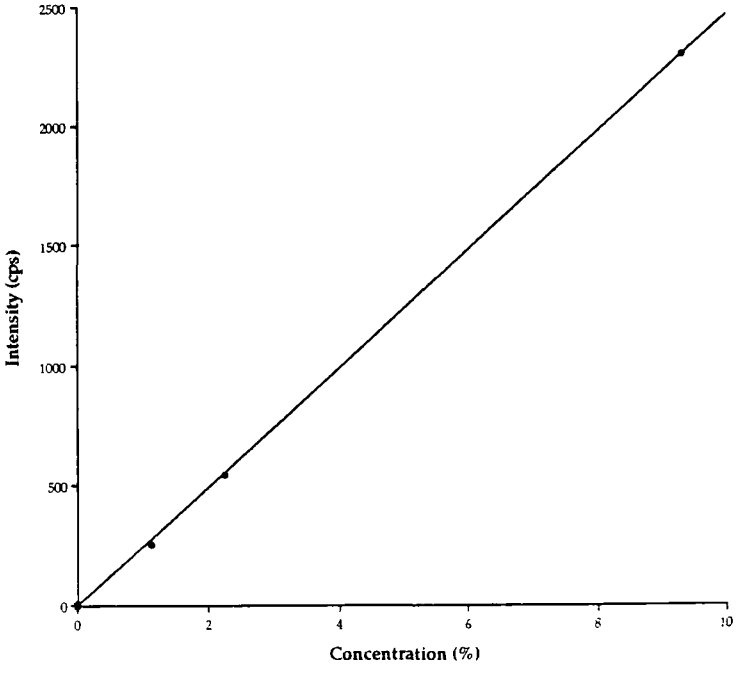

Figure 4.8 Plot of intensity vs concentration for sulphur (mechanical mixtures of synthetic compounds)

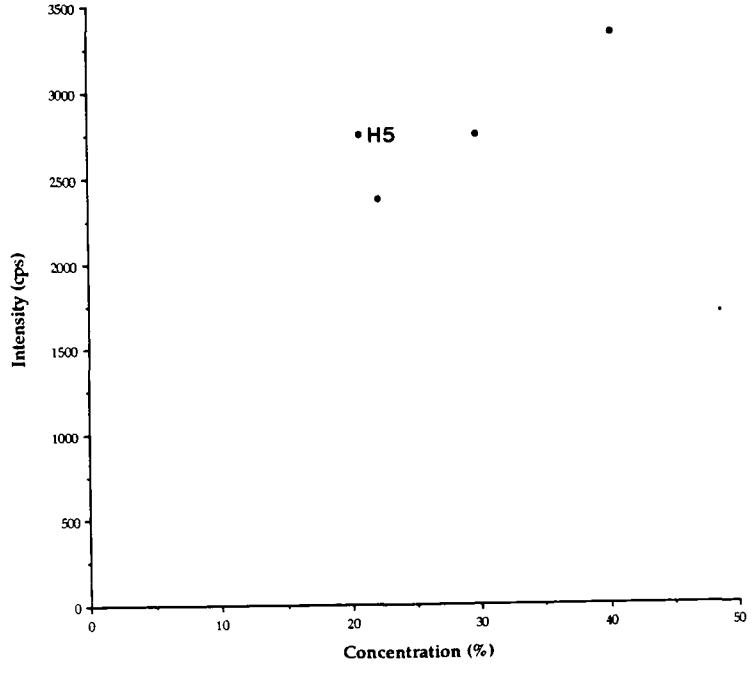

Figure 4.9 Plot of intensity vs concentration for calcium (pure calcium phosphates and H5)

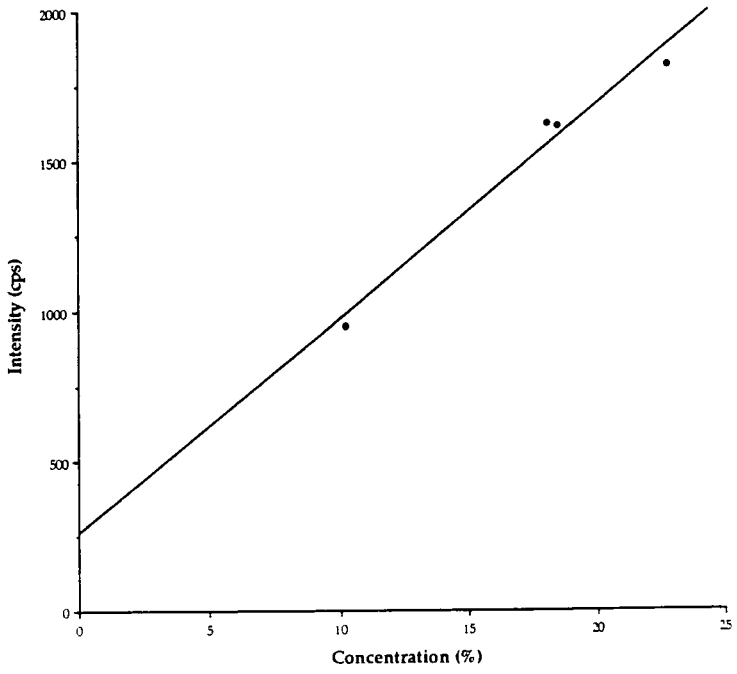

Figure 4.10 Plot of intensity vs concentration for phosphorus (pure calcium phosphates and H5)

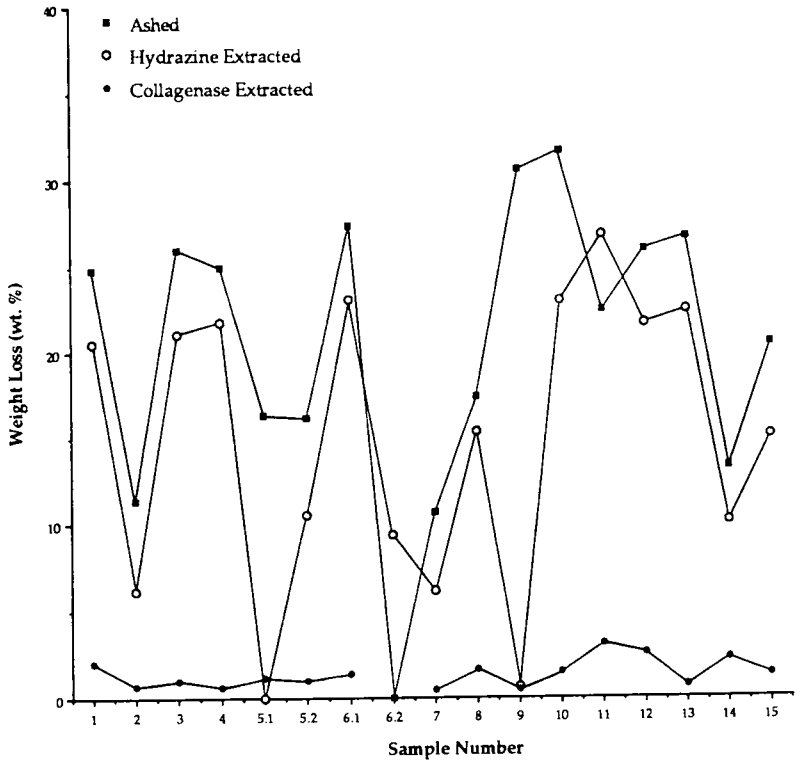

Figure 4.11 Results of protein removal experiments

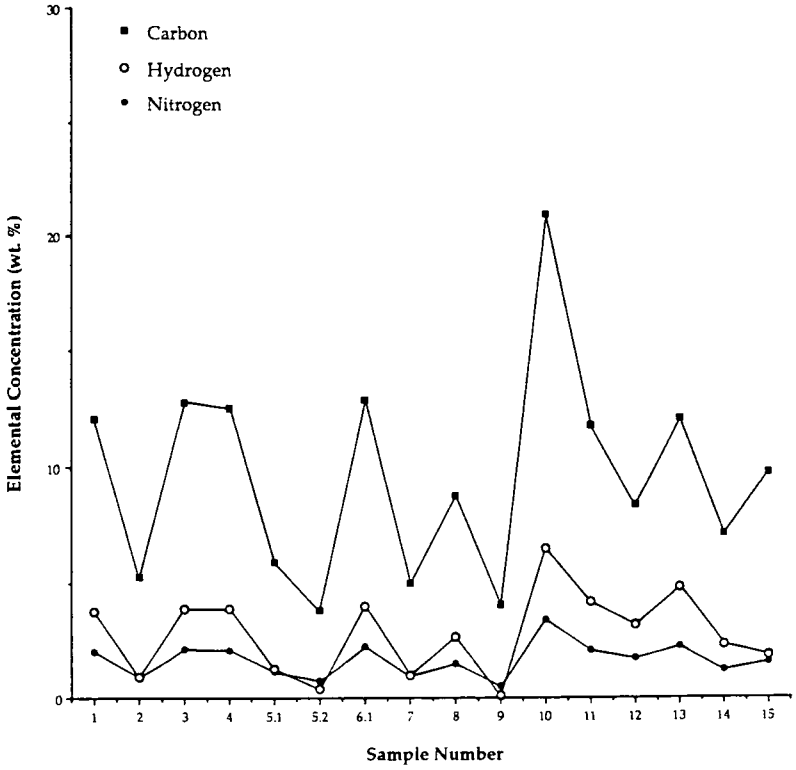

Figure 4.12 Carbon, hydrogen and nitrogen contents of samples 1-15 before protein removal

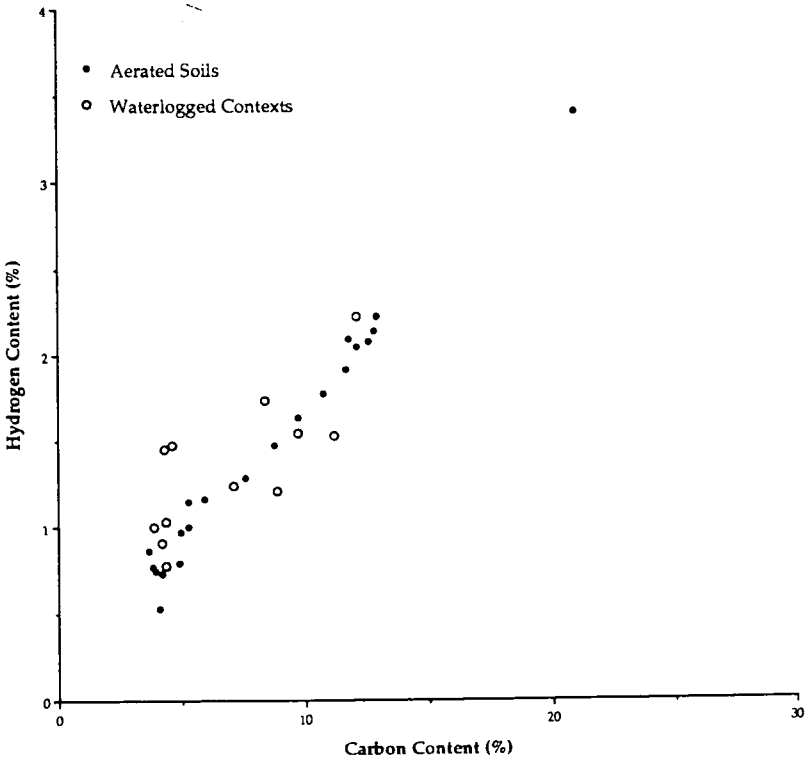

Figure 4.13 Plot of hydrogen vs carbon for samples 1-32 (before protein removal)

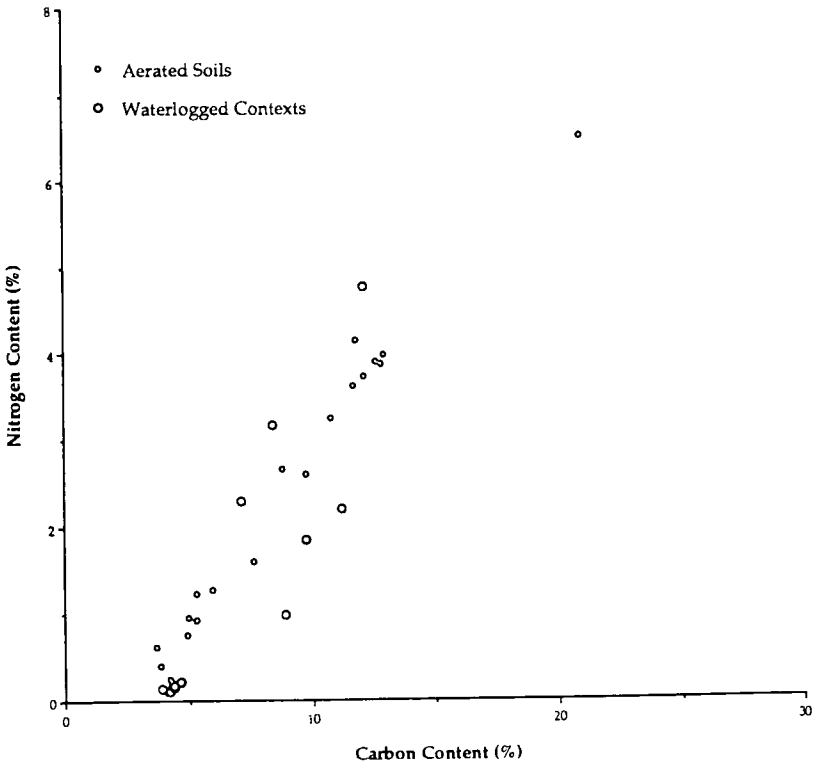

Figure 4.14 Plot of nitrogen vs carbon for samples 1-32 (before protein removal)

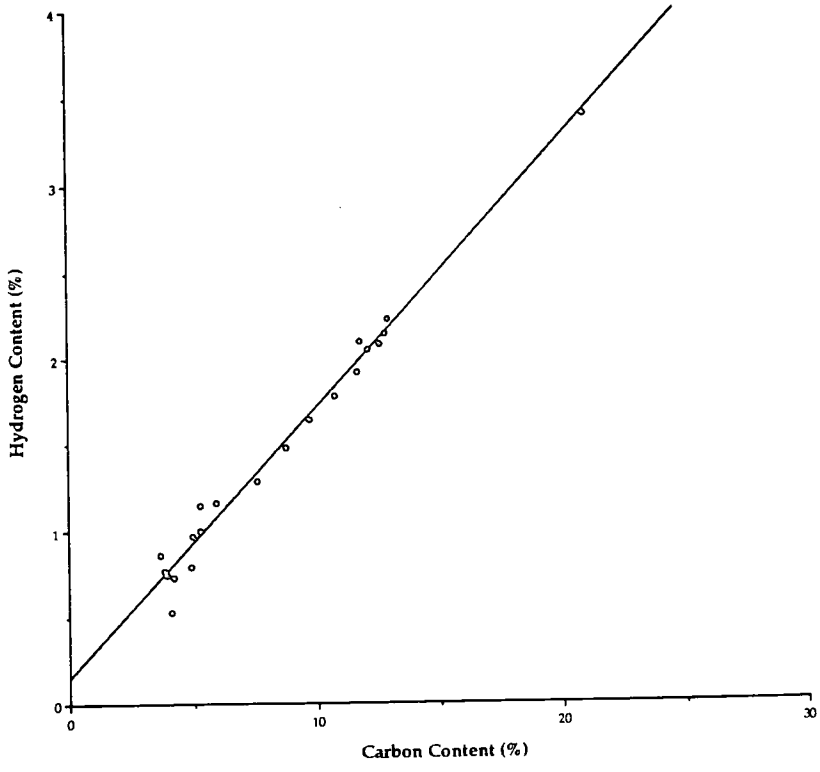

Figure 4.15 Plot of hydrogen vs carbon for samples from aerated soils

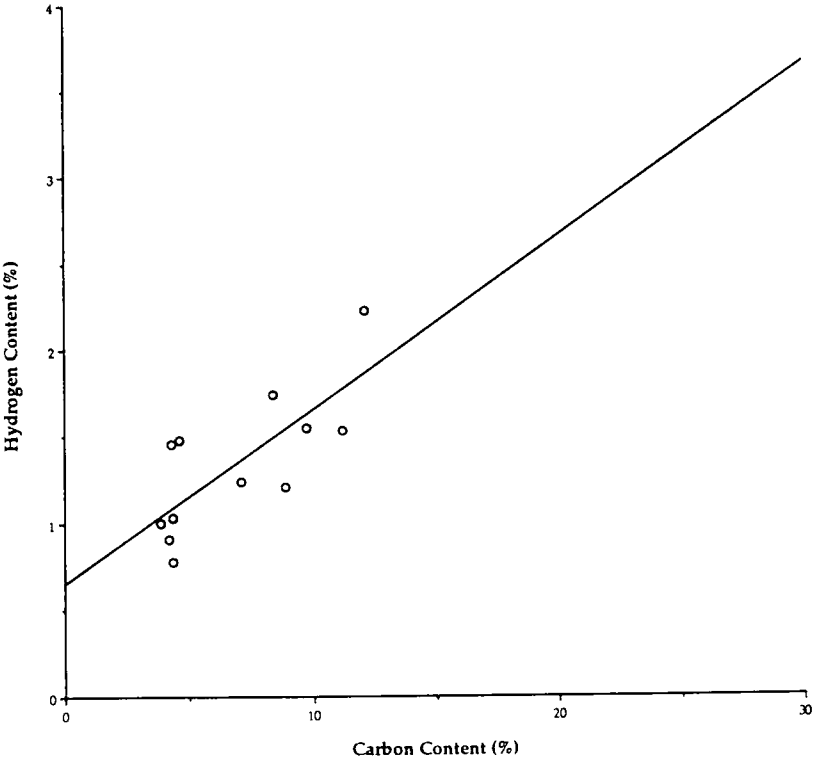

Figure 4.16 Plot of hydrogen vs carbon for samples from waterlogged contexts

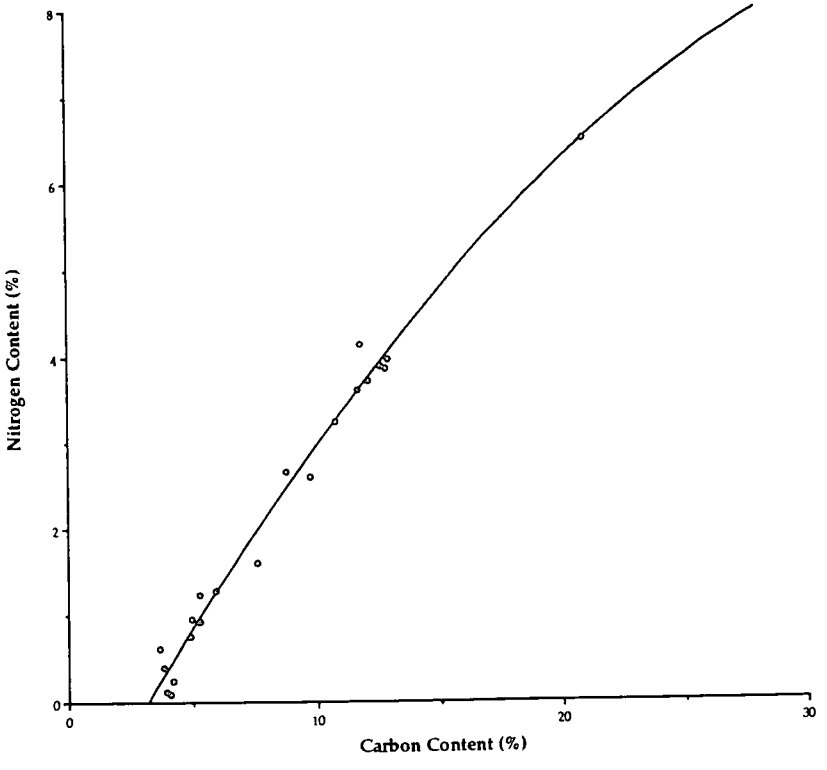

Figure 4.17 Plot of nitrogen vs carbon for samples from aerated soils

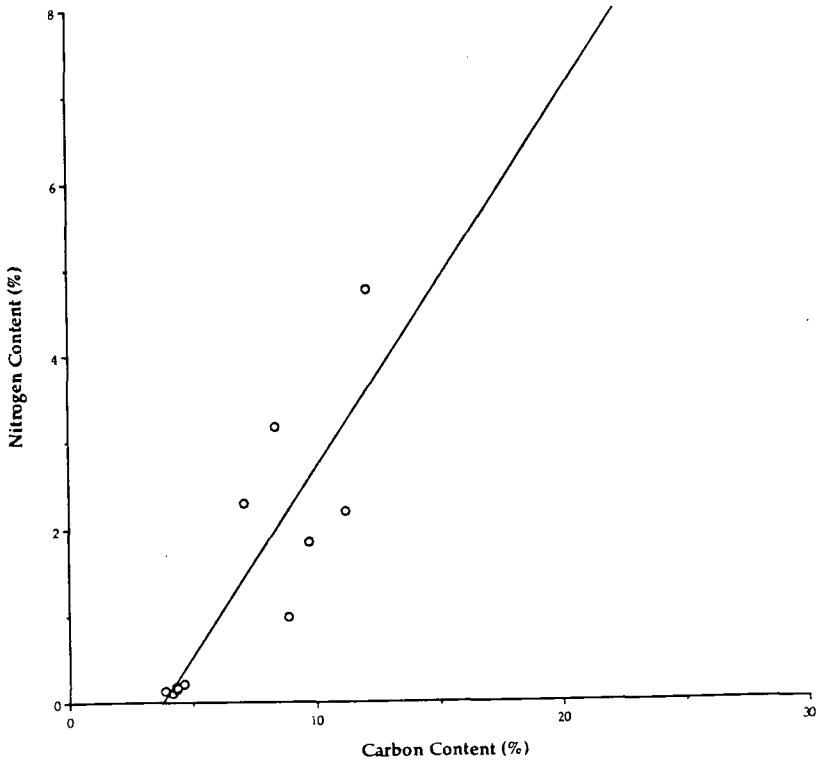

Figure 4.18 Plot of nirogen vs carbon for samples from waterlogged contexts

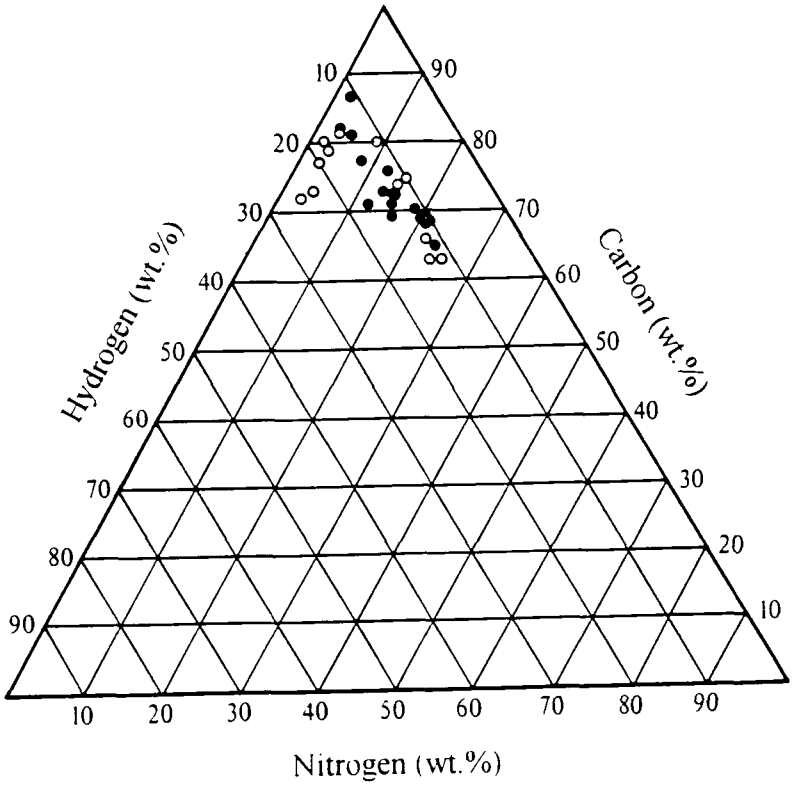

Figure 4.19 Ternary diagram of carbon, hydrogen and nitrogen contents of samples 1-32 (normalised to 100%)

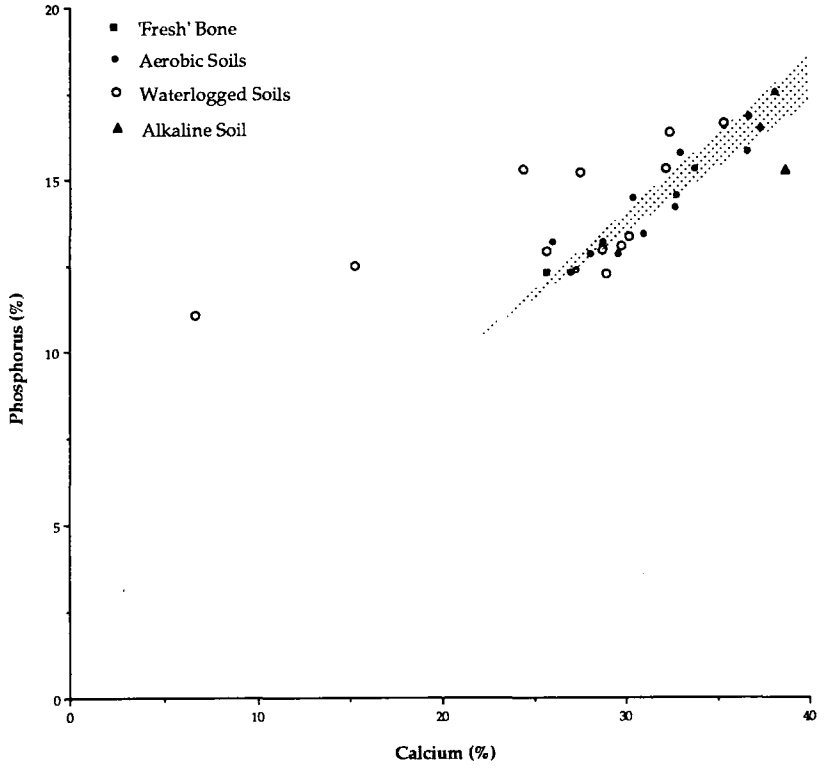

Figure 4.20 Plot of phosphorus vs calcium for samples 1-32

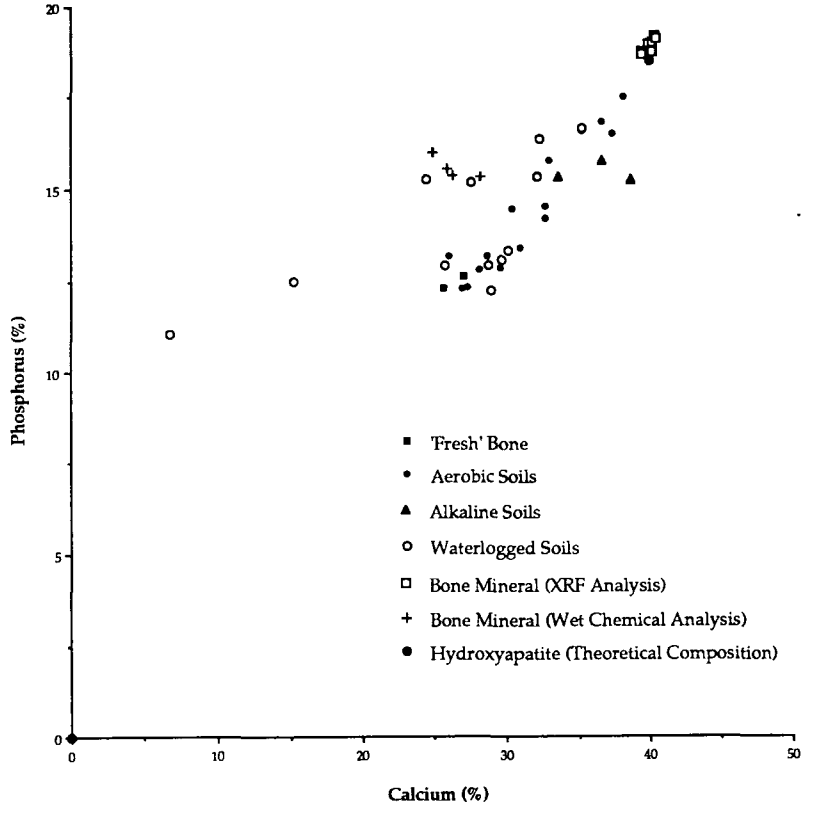

Figure 4.21 Plot of phosphorus vs calcium for samples 1-32, together with results for deproteinised bone mineral by XRF and wet chemical analysis

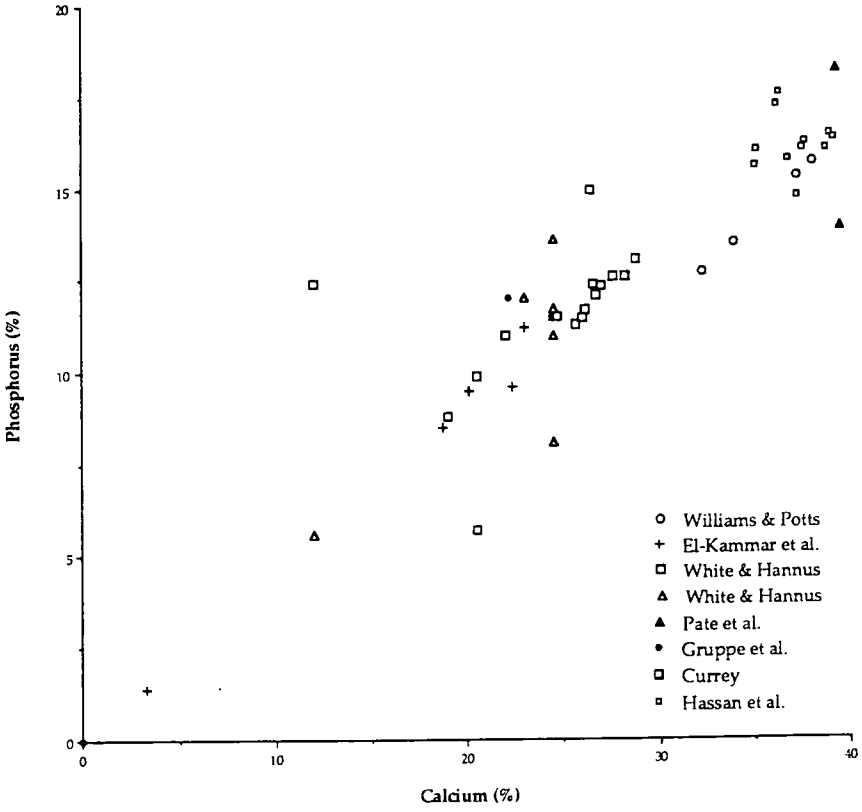

Figure 4.22 Plot of phosphorus vs calcium for data from several authors (Williams & Potts 1988; El-Kammar *et al.* 1989; White & Hannus 1983; Pate *et al.*1989; Gruppe *et al.* 1989; Currey 1970; Hassan *et al.* 1977)

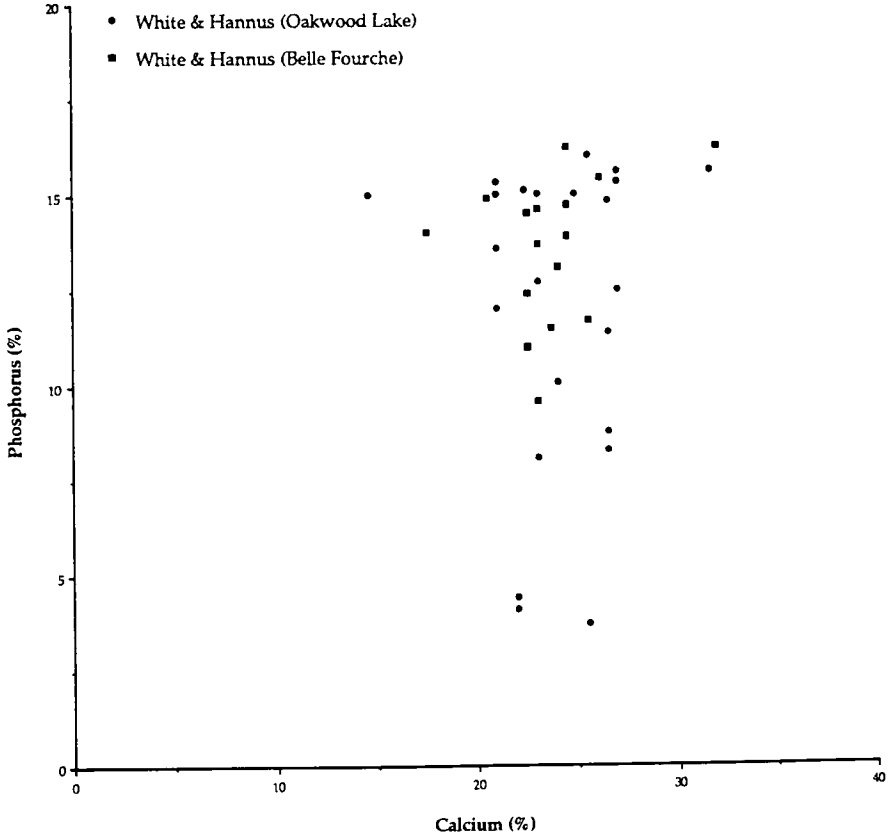

Figure 4.23 Plot of phosphorus vs calcium for samples analysed by wet chemical means; AAS and colourimetry (White & Hannus 1983)

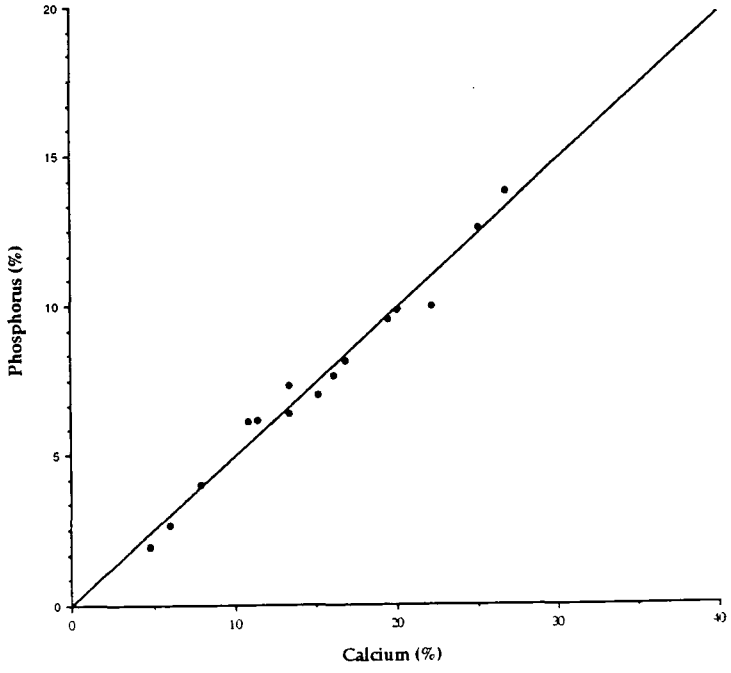

Figure 4.24 Plot of phosphorus vs calcium for samples analysed by Vourinen *et al.* (1990)

5. X-Ray Diffraction Studies of Fossil Bone

A number of studies has investigated the diagenetic changes to the inorganic component of fossil bones using X-ray diffraction and several mineral species have been reported, either as contaminants from the soil or arising from chemical transformation of the original bone apatite. These minerals include obvious contaminants such a quartz, feldspar, iron and manganese oxides and halite (El-Kammar *et. al.*, op. 1989) and others such as brushite, vivianite, whitlockite, gypsum and calcite which result from the interaction of bone apatite with the burial environment (Hassan and Ortner, 1977; Piepenbrink, 1986 and 1989; Newesely, 1989). X-ray diffraction spectra have also been used to quantify changes in the crystallinity of fossil bones by careful analysis of the shape and intensity of the diffraction peaks.

The X-ray diffraction studies discussed below set out to address a number of different questions:

what can the diffraction spectra of bone tell us about its composition?

how do the diffraction spectra of archaeological and fossil bones differ and what do these differences tell us about diagenetic change in the bone mineral?

what other minerals species are found in archaeological and fossil bones?

5.1 Principles of X-ray Diffraction

X-ray diffraction is one of the principle techniques used to investigate the structure of crystals and crystalline solids. A crystalline substance is one in which the constituent structural units are arranged in a definite geometrical configuration characteristic of that solid. According to this principle any crystal or fragment of a crystal is composed of successive repeats of a simple building block termed the *unit cell*. The shapes of the unit cells and hence the macroscopic forms of crystals are governed by three fundamental laws (Maron & Prutton 1965).

The first of these, the law of constancy of interfacial angle states that for any given crystalline substance, the planes forming the external faces of the crystal intersect at a definite and constant angle, *i.e.* the angle of intersection of any two corresponding faces is always the same for any crystal of the same substance.

The second law states that for any crystal, a set of three axes (*a*, *b*, *c*) may be drawn, usually with at least one axis parallel to a crystal edge and with their origin at the centre of the crystal. These are defined as the crystallographic axes. The crystal faces either intercept or are parallel to one or more of these crystallographic axes. It is also possible to select a reference plane (again, often parallel to a crystal face) which intersects each of the three axes at an arbitrary unit length. These unit lengths can then be used to define the orientation in space of any other plane by specifying the intercept on

each axis as either an integer multiple or a fraction of these unit lengths. In the case of a plane being parallel to one axis then the intersect on that axis is at infinity.

One way of expressing these intercepts is as the ratios of these intercepts with respect to those of the reference plane. A more convenient notation, and one now in common use is that of the Miller indices. The Miller indices of any plane are the normalized reciprocals of these intercepts and are usually expressed as small integers or zero (i.e. the plane is parallel to that axis). For example, the Miller notation (110) of a crystal plane indicates that it intercepts the *a* and *b* axes at unit length and is parallel to the *c* axis. The law of rational indices states that the relationship of any crystal face to the crystallographic axes may be expressed as three small numbers (four in the case of hexagonal and trigonal crystal systems).

The third law of crystallography states that all crystals of the same substance exhibit the same elements of symmetry with respect to their planes of symmetry, lines of symmetry and centre of symmetry. Because of this symmetry each plane will have a corresponding plane intersecting one or more of the *a*, *b* or *c* axes on the opposite side of the origin. Here the intercept will be negative and this is denoted in the Miller index by a minus sign above the number.

When a collimated (or parallel) beam of X-rays is incident on a crystal it interacts with the regular planes of atoms that make up crystalline solids and is reflected or 'diffracted'. The reflected waves may interfere either constructively or destructively depending upon the separation between successive atomic planes, the angle of incidence of the X-ray beam and its wavelength (see Figure 5.1). This dependence is described by the Bragg equation:

$$n\lambda = 2d.\sin\theta$$

where λ is the wavelength of the incident X-rays, 'd' is the separation between two planes of atoms in the crystal lattice and θ is the angle subtended between the X-ray beam and the plane of the atoms. For diffraction to occur (*i.e.* constructive interference) n must be a whole number (refer to Figure 5.1).

For any one crystal there are numerous lattice planes where the atoms are aligned and each can be described by its Miller indices. Thus if a finely powdered sample of the crystal is placed in the beam then the X-rays encounter a multitude of randomly oriented crystals, each of which will diffract the beam if its orientation is such as to satisfy the Bragg equation. Several distinct cones of diffracted beams are produced and can be projected onto a photographic film to produce a 'powder photograph'. Alternatively, the angles subtended by these cones can be determined by moving a suitable X-ray detector in an arc around the sample.

5.1.1 X-ray Diffractometry

In a typical diffractometer X-rays are generated by bombarding a metal target anode with high energy electrons. The spectrum of X-rays emitted consists of both a continuous spectrum of broad band radiation superimposed on a line spectrum, containing lines with wavelengths characteristic of the anode metal. For most X-ray sources, the most intense of these lines are the Kα and Kβ. This radiation is monochromated by passing it through a thin metal foil to filter out much of the unwanted background, including the Kβ line, leaving an intense source of X-rays with a very small range of wavelengths.

The X-rays are collimated by passing them through a thin slit to produce a fine beam which is then directed onto the sample which is rotated by a motor drive at a constant speed. When crystal planes in the sample achieve an appropriate angle they are diffracted in accordance with Bragg's law. The diffracted beam passes through a receiving slit and collimator before falling onto an electronic detector. The signal produced by the detector is amplified and passes to an electronic recorder.

5.1.2 X-ray Diffractometry of Powdered Samples

For the X-rays to be incident on a sufficient number of crystallographic planes to produce a satisfactory diffracted beam at any one angle, the sample must be ground to a fine powder. In large mineral and rock samples the original grain size must be reduced to a mean particle diameter of 5-10μm (Hardy & Tucker, 1988). Care must be taken not to reduce the particle to too small a size or damage the crystallite by strain since both cause diffraction line broadening (see Hardy & Tucker, Figure 7.15). Samples may be ground by hand or in a mechanical ball mill. Having ground the sample to powder it must be presented to the X-ray beam in such a way that its thickness is kept to a minimum. The simplest method of achieving this is to smear a suspension of the sample in a fast drying solvent onto a glass slide. This slide is then mounted into the diffractometer.

Since the intensity of any peak in the diffractogram of a sample is proportional to its concentration it is possible to make measurements of the relative proportions of minerals in a mixed sample by direct measurements of the peak heights or areas. This quantitative, XRD analysis can be improved by the use of internal standards and by careful calibration with known mixtures. In general, however, XRD is a qualitative technique, best suited to the identification of mineral species. Nevertheless, for poorly crystalline specimens it is possible to make qualitative judgements about the degree of crystallinity of different samples if instrument parameters are kept constant.

5.2.Materials and Methods

A wide range of bone specimens was examined, covering fresh animal bone, relatively recently discarded bone and excavated, archaeological bone of different ages. Fresh sheep and cow bone (metapodials and femur respectively) were examined both untreated and after various chemical treatments to determine factors affecting the crystallinity of bone mineral. Archaeological bone specimens were selected for XRD analysis either because of the nature of their preservation or because mineral species other than apatite could be seen with the naked eye or were suggested by the results of X-ray fluorescence. In some cases, where the macroscopic appearance suggested differential preservation (samples 5 and 6 in which the outer surfaces clearly had a higher organic content than the interiors), more than one sample of the same bone was examined.

Archaeological and fossil bones with a low organic content were hand ground in a ceramic pestle and mortar. In the case of modern bone and archaeological bone with a high organic content the specimens proved too tough to grind effectively. To obtain a finely divided sample, fine sawdust was created by cutting the specimen with a fine-toothed saw.

Where necessary, samples were further ground by hand in a small agate pestle and mortar. The resultant fine powder, amounting to approximately 50mg, was placed onto one a glass slide and wetted with acetone. For some of the later samples acetone was replaced by methanol in accordance with the introduction of more stringent safety requirements. The resulting slurry was distributed over one half of the slide in a thin film and set aside to dry. Care was taken to ensure that the slurry dried to a thin film since thick or uneven films can cause angular displacement of the diffraction peaks from their correct positions.

X-ray diffractograms were obtained using a Philips PW1130, 3 Kilowatt X-ray generator/diffractometer assembly using cobalt Kα radiation. The assembly was fitted with a 1 degree divergent slit, 0.1 degree receiving slit and a 1 degree scatter slit. The detector was scanned at a speed of 1 degree of 2θ per minute and the output recorded on a chart at a rate of 10mm per minute. The majority of samples were examined with the X-ray tube set to a voltage of 40kV and a current of 25mA. Tube current and voltage were occasionally varied according to the samples under investigation or in an attempt to improve the signal to noise ratio but where samples were to be directly compared, these parameters were kept constant.

Experience demonstrated that the majority of the more intense diffraction peaks due to bone apatite and any other contaminant species could be recorded by scanning samples over the range 12 to 44 degrees 2θ. The position of each peak was read off the diffractograms and the angle in degrees 2θ translated into the equivalent 'd' spacing using standard conversion tables for cobalt Kα radiation.

These values of 'd' spacing were then be used to identify the crystal species present and assign Miller indices to each peak.

5.3 Results

Diffractograms of some of the samples investigated are shown in Figures 5.2 to 5.8. Figure 5.2 shows the diffractograms for synthetic hydroxyapatite (Aldrich Catalogue ref. 23, 093-6), fresh bovine bone, and deproteinized sheep metatarsal. The individual peaks in the diffractogram of hydroxyapatite (fig. 5.2a) are identified by their Miller indices. The low signal to noise ratio in the diffractogram for synthetic hydroxyapatite suggests that the crystal dimensions in the synthetic sample are close to the 5-10μm limit suggested for powdered specimens (Hardy & Tucker 1988). It is clear from Figure 2 that there is considerable peak broadening in the spectrum of fresh untreated bone (5.2b) and that of the deproteinized bone (5.2c) compared to synthetic hydroxyapatite. This peak broadening demonstrates that bone apatite crystallites are considerably smaller than the crystals present in synthetic hydroxyapatite and previous studies have shown that in bone apatites, the crystallites have maximum dimensions of 25-35nm (see section 1.5)very much smaller than the 5-10μm limit.

The effects of poor crystallinity in hydroxyapatites can be demonstrated by a crude experiment. Figure 5.2d shows the diffractogram of the precipitate resulting from dissolving synthetic hydroxyapatite in 0.1mol HNO_3 and subsequently adding aqueous KOH to raise the pH to 7. The extremely fine suspension was repeatedly washed and centrifuged before drying at 105°C. The close similarity between the diffractogram of this precipitate and that of bone mineral demonstrates that hydroxyapatite (and by implication bone apatites) may be dissolved by an acidic aqueous solution and re-precipitated by subsequent increase in the local pH. The similarity in the diffractograms also indicates that in this crude experiment, the availability of atmospheric and dissolved CO_2 probably resulted in the formation of a carbonate containing hydroxyapatite. In the case of dissolution and re-precipitation of bone apatites in the burial environment, the growth of the resulting hydroxyapatite crystals and their ultimate sizes will be influenced by such factors as the rate at which the pH rises or rate at which the solution becomes concentrated at a drying front. This latter observation has important implications for the remodelling of bone apatites whilst buried in sediments.

Experiments in the deproteinization of fresh bone (see section 4.1.1) highlighted the possibility that bone mineral contains components of different solubilities. In addition to the use of hydrazinolysis to remove the organic fraction from bone, it is possible to strip out proteins by alkaline hydrolysis using hot aqueous sodium hydroxide. The use of hot NaOH results in cracking and warping of the specimen however, suggesting that there is some structural damage or modification. One feature of alkaline hydrolysis is that the percentage weight loss after treatment is higher than that after hydrazinolysis. This difference in weight loss according to the use of aqueous and non-aqueous

protein removal regimes (24.63% compared to 23.58% respectively) suggests that there is a water soluble component to bone mineral. This interpretation is in agreement with figures published by Eastoe & Eastoe (1954) quoting a water soluble inorganic component amounting to 1.25% of dry bovine bone.

To investigate whether a soluble component persisted in bone mineral isolated by hydrazinolysis, a simple experiment was performed to determine any weight loss as a result of prolonged washing in distilled water. Table 5.1 shows the results of hydrazinolysis and water washing on five samples of sheep metatarsal. The first figures in column 3 refer to the soluble inorganic matter expressed as weight percent of dry whole bone whereas the figures in brackets refer to soluble inorganic matter in weight percent of the bone mineral isolated by hydrazinolysis.

Sample	Protein (wt.%)	H_2O sol. mineral (wt.%)
1	23.28	1.62 (2.12)
2	25.98	1.75 (2.36)
3	23.65	1.43 (1.87)
4	23.07	1.52 (1.97)
5	22.64	2.90 (3.75)
Average	23.72	1.84 (2.02)

Table 5.1 Water soluble inorganic material in sheep metatarsal

The solubility of a crystalline salt is related to the size of the individual crystals with large crystals less readily dissolved than microcrystalline or amorphous solids. If this water soluble inorganic material represents amorphous or poorly crystalline calcium phosphate, it might be expected that its loss would be accompanied by an increase in the crystallinity of the remaining, insoluble matter. Figure 5.3 shows diffractograms for untreated fresh bone (fig. 5.3a), bone treated with hydrazine (fig. 5.3b), bone treated with hydrazine and washed (fig. 5.3c) and bone deproteinized using hot NaOH (fig. 5.3d). Sheep metatarsals were used in all samples. The diffraction pattern for untreated bone shows very poor crystallinity with the 002 peak barely visible above the background noise and the unresolved 211, 112 and 300 forming a single asymmetric peak. The hydrazine deproteinized bone shows some increase in crystallinity but once again the 211, 112 and 300 peaks are unresolved. The diffraction pattern for the deproteinized bone washed in water shows a similar slight increase in the peak heights. By comparison, the bone treated with hot NaOH (fig. 5.3d) shows a diffractogram in which the region between 36 and 41 degrees 2θ is resolved into three distinct peaks. This visible increase in the crystallinity of the mineral phase could be the result of one of two possible mechanisms. Either, prolonged washing at elevated temperatures caused the dissolution of part of the mineral fraction not normally soluble in water at room temperature, or the high concentration of hydroxide ions in the NaOH has allowed substitution of OH^- for CO_3^{2-} in the bone apatite, resulting in a restructuring of the crystal lattice into one with a more crystalline nature.

Figure 5.4 shows the XRD spectra of fresh bovine bone after anhydrous and aqueous treatment methods. All samples were in sealed separate Sterilin tubes at 70° C for 100 hours. Figure 5.4a shows the diffractogram of the original, untreated bone for reference. The other traces show the XRD spectra for bone treated with hot distilled water (fig. 5.4b), hydrazine (fig.5.4c) and sodium acetate buffer (fig. 5.4d). Sodium acetate buffer (acetic acid/sodium acetate buffered to pH 5.5) is an aqueous treatment frequently employed to remove carbonate inclusions from samples of sediment. Figure 5.4e shows the diffractogram for bone that has been hydrazine deproteinized and washed in distilled water. It is clear that it is not possible to distinguish any change in crystallinity in the bone apatite after treatment with hydrazine to strip out the organic matter. Nor is the crystallinity enhanced by heating in water for prolonged periods. However, the bone treated with hot sodium acetate shows a slight increase in crystallinity and that washed after hydrazine treatment an even more pronounced sharpening of the diffraction peaks. It is possible that the slightly acidic sodium acetate buffer (intended to remove carbonates from the bone mineral) may have hydrolysed some of the collagen in the bone, exposing some of the more soluble components of the bone mineral to potential dissolution and recrystallization.

The obvious differences in crystallinity between the diffractograms in Figures 5.4c and 5.4e, and the slight mass loss on washing bone mineral would suggest that there is a direct relationship between loss of the more readily soluble bone mineral and an increase in the average crystal size as determined by XRD peak broadening studies. It does seem likely that the removal of the organic matrix from bone tissue exposes a water soluble component of the inorganic fraction with a lower crystallinity than the insoluble bone mineral. Two factors may be involved in this behaviour. The first is that small, immature crystallites would be expected to have slightly greater solubility than larger, more mature ones. In addition, amorphous calcium phosphate and brushite have been suggested as precursors to biological apatite (Francis & Webb 1971) and since both are more readily soluble than hydroxyapatite, it would be reasonable to expect these (if they were present) to be preferentially dissolved once the cellular arrangement had been destroyed. However, the weight lost on washing amounts to only approximately 2 percent of the total mass of the bone mineral and any resulting increase in crystallinity would invariably be lost in the background noise of the XRD spectrum. It is much more likely that the observed increase in crystallinity is the result of recrystallization of dissolved hydroxyapatite or other calcium phosphate minerals upon evaporation of the wash water. Addition of even a relatively small amount of larger (non-biological) hydroxyapatite crystals could considerably increase the average crystal size in a sample where typical crystal dimensions are in the nanometer range.

Many of the specimens of archaeological bone examined also exhibited increased crystallinity, reflected in a sharpening of their XRD spectra. Specimens that appeared tough, dense and well preserved had XRD spectra comparable to that of fresh bone. However, those specimens which

showed considerable diagenetic alteration (recognisable by an increase in porosity and friability) also had demonstrably enhanced crystallinity. This increase in intensity and sharpening of the diffraction peaks of diagenetically altered bone was roughly correlated to the remaining protein content. Figure 5.5(a-h) shows the XRD spectra for eight of the bones selected for chemical analysis in Chapter 4. The protein content for each sample (as determined by hydrazinolysis) is given in brackets. The spectra of those specimens that have lost comparatively little collagen (Figures 5.5b and 5.5c) are indistinguishable from that of fresh bone (Figure 5.5a). Specimens which have lost considerable collagen however (samples 5.2, 7, 9, 22 and 23) generally show more intense, well defined peaks similar to those seen in Figure 5.4e. Five of the spectra in Figures 5.5a-5.5h have clearly defined 002 peaks from which it is possible to derive some measure of their crystallinity. Relative crystallinity measurements were calculated by drawing a baseline across the bottom of each 002 peak and calculating its area by multiplying half the base by the peak high (refer to Figure 5.6). The diffractogram in the area of each 002 peak was smoothed by eye to reduce the effects of noise. Figure 5.7 shows a plot of peak area vs collagen content for the five samples. Although the small sample size makes this quantitative analysis far from conclusive, it is clear that there is a trend towards increasing crystallinity with progressive loss of bone collagen. A similar trend may also be interpreted from the infrared analysis of archaeological bone samples (Figure 6.11).

Several authors have reported increased crystallinity in archaeological and fossil bones (Schoeninger *et al.* 1989; Tuross *et al.* 1989) and increase in the sharpness of the XRD spectra of such bones has frequently been related to age since death. Although the evidence above points to a relationship between collagen loss and increased crystallinity, it is not clear whether there is a causal link between the two phenomena. If collagen loss is promoted by the action of micro-organisms and that hypermineralization or 'cuffing' around areas of microfocal destruction (see Chapter 3) is also a consequence of fungal or bacterial metabolites, then there is a direct link between collagen content and crystallinity. However, it is possible that collagen loss by simple hydrolysis causes an increase in the water permeability of the bone and that this increases its susceptibility to dissolution and recrystallization. The dissolution of bone apatite and its recrystallization a short distance away in another area of the same bone is consistent with the local reduction in pH by acid-secreting micro-organisms. By contrast, the slow hydrolysis of collagen and leaching away of amino acids by percolating ground waters could equally well by accompanied by complete loss of dissolved bone apatites from the vicinity of the buried bone. The fact that recrystallized hydroxyapatite can be identified by electron microscopy (see section 3.1.4 and Plate 3.56) testifies that the observed increases in crystallinity can be attributed to such inclusions and that consequently the mechanism is a local one, *i.e.* dissolved apatite is not altogether lost from the bone to the surrounding soil.

In at least two cases of bone from waterlogged archaeological deposits (sample 5 and sample 6) there was a very obvious difference in the preservation of bone at the surface, where it was in contact with the soil, and that of the interior (see Plates 10.3 and 10.4). In these cases of differential preservation, the periostial and endosteal surfaces (and to a lesser extent broken surfaces) are tough, dark and well preserved with a high collagen content (refer to results for sample 6 in Table 4.2) whereas the interior is pale cream in colour, very powdery and brittle. Figures 5.8a and 5.8b show the diffractograms of the surface (5.1) and interior (5.2) of sample 5. The increased crystallinity of the material taken from the interior graphically illustrates the relationship between collagen loss and peak sharpening although the reason for preferential preservation at the surface has yet to be established. This type of bone preservation is rarely reported by researchers investigating ancient bone but a similar pattern of differential dissolution has been recognised during research into dental caries. Quantitative scanning microradiography (SMR) of thin sections of caries-free tooth enamel that have been demineralized using 0.1mol acetic acid (buffered to pH 4) display subsurface loss of mineral below an apparently intact surface layer (Anderson & Elliot 1993). Similar behaviour is seen in specimens of compressed hydroxyapatite aggregate when exposed to dimineralising solutions.

X-ray diffraction is frequently used for the identification of mixtures of different crystalline solids and is particularly suited to the detection of traces of contaminant (non-apatitic) minerals in archaeological bone. If the contaminant mineral is well crystalline and has sharp diffraction peaks, the sensitivity of the technique can be high. Microscopy has demonstrated that bones from waterlogged deposits often contain one or more contaminant minerals. In addition, XRF studies have demonstrated that certain bones have a low Ca:P ratio (section 4.2 and Figure 4.16), suggesting that bone apatite has been transformed to a calcium phosphate with a different stoichiometry or that either calcium or phosphorus is present in combination with other elements. High levels of iron, manganese and sulphur were also detected in these samples, potentially increasing the range of possible mineral species.

Vivianite is frequently visible as bright blue deposits on bones from waterlogged conditions and occurred on several of the specimens analysed (including sample 6). The interior of sample 6 was particularly friable and bore no evidence of any of the histological features associated with normal bone. Figure 5.9a shows the diffractogram of this yellow, powdery bone in the interior of sample 6 (from a Roman well at Rothwell, England). All of the bones from this deposit had tough, dark brown, delaminating surfaces overlying pale yellow, friable cores and wedges of massive vivianite. Figure 5.9a shows that the yellow core material is essentially amorphous with little more than a rise in background at the position of the apatite peaks. Figures 5.9b and 5.9c show diffractograms of massive vivianite and efflorescent blisters on bones from the same well. Characteristic peaks for vivianite can be seen on both the latter diffractograms. Pye *et. al.* (1990) have reported framboidal

pyrite and vivianite crystals in small numbers in siderite-iron sulphide concretions formed in muddy sediments.

It is known that if fresh bone is immersed in an acidic solution for a period of weeks the bone mineral is transformed into brushite $CaHPO_4.2H_2O$ (Lee-Thorpe *et. al.*, 1991). Brushite has also been identified in archaeological bone using X-ray diffraction and infra-red spectroscopy (Piepenbrink 1989; Newesely 1989). One might therefore expect to find brushite in bone recovered from acid, waterlogged environments. However, the XRD and infrared spectroscopy studies of samples from these environments show that gypsum $CaSO_4.2H_2O$ is commonly found as a contaminant in such material and may be confused with brushite. Figures 5.10a and 5.10b show diffractograms for sample 22 and crystals dissected from the surface and pores of the same sample. Diffractograms for synthetic gypsum and synthetic brushite are shown in Figure 5.10c and Figure 5.10d respectively. The peaks 020, 021 and 041 are very similar for both gypsum and brushite and may be confused when superimposed on a background of poorly crystalline bone. However, the presence of the 040 line in the diffractograms 5.10a and 5.10b clearly identify the contaminant mineral as gypsum (see also Figure 6.14). Electron microscopy of embedded and polished specimens, combined with elemental dot mapping show characteristic lenticular crystals of calcium sulphate which are also visible in electron micrographs of broken surfaces (Plates 3.40 to 3.42).

Figure 5.11a shows the XRD spectrum of sample 9, a human long bone excavated from a Byzantine cemetery in Cyprus. Microscopic, chemical and infrared studies of this specimen demonstrated that calcium carbonate filled many of its pore spaces and voids. Figure 5.11b is the diffractogram of synthetic calcite. Although the 012, 110 and 006 peaks for calcite are almost lost in the background noise of the diffractogram for sample 9, the 104 peak conclusively demonstrates the presence of calcite.

The results described above demonstrate that XRD studies can make two major contributions to the understanding of diagenetic processes in fossil bones. Firstly, it is useful for the identification of crystalline, inorganic contaminants arising either from the migration and recrystallization of mineral salts while in the burial environment or from the subsequent oxidation and hydration of those salts. Secondly, it provides a rapid and economical means of monitoring changes in the crystallinity of apatites in bone specimens. Due to the small sizes of both the original crystallites and those that occur due to dissolution and recrystallization of bone apatites, the technique is unable to discriminate between hydroxyapatites, fluorapatites and strontium apatites. Nevertheless, there is some considerable potential for the quantization of crystallinity changes by measuring the area of the 002 peak for comparative studies of a statistically significant sample number. This proposal is discussed further in Chapter 10.

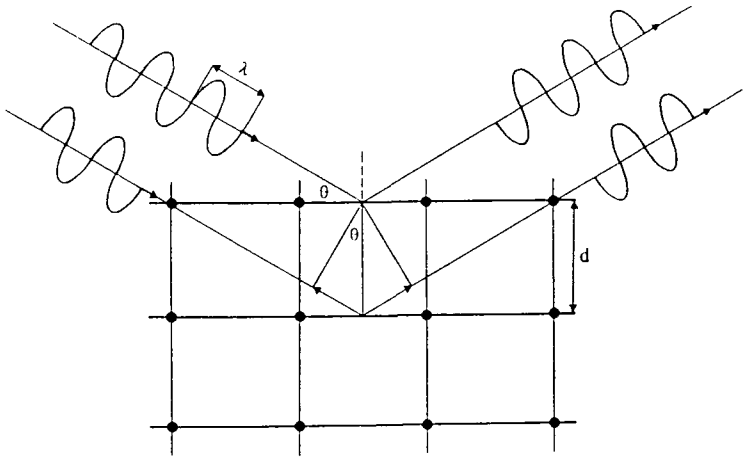

Figure 5.1 Principle of X-ray diffraction. Constructive interference occurs when $n\lambda = 2d \sin \theta$ (the Bragg equation)

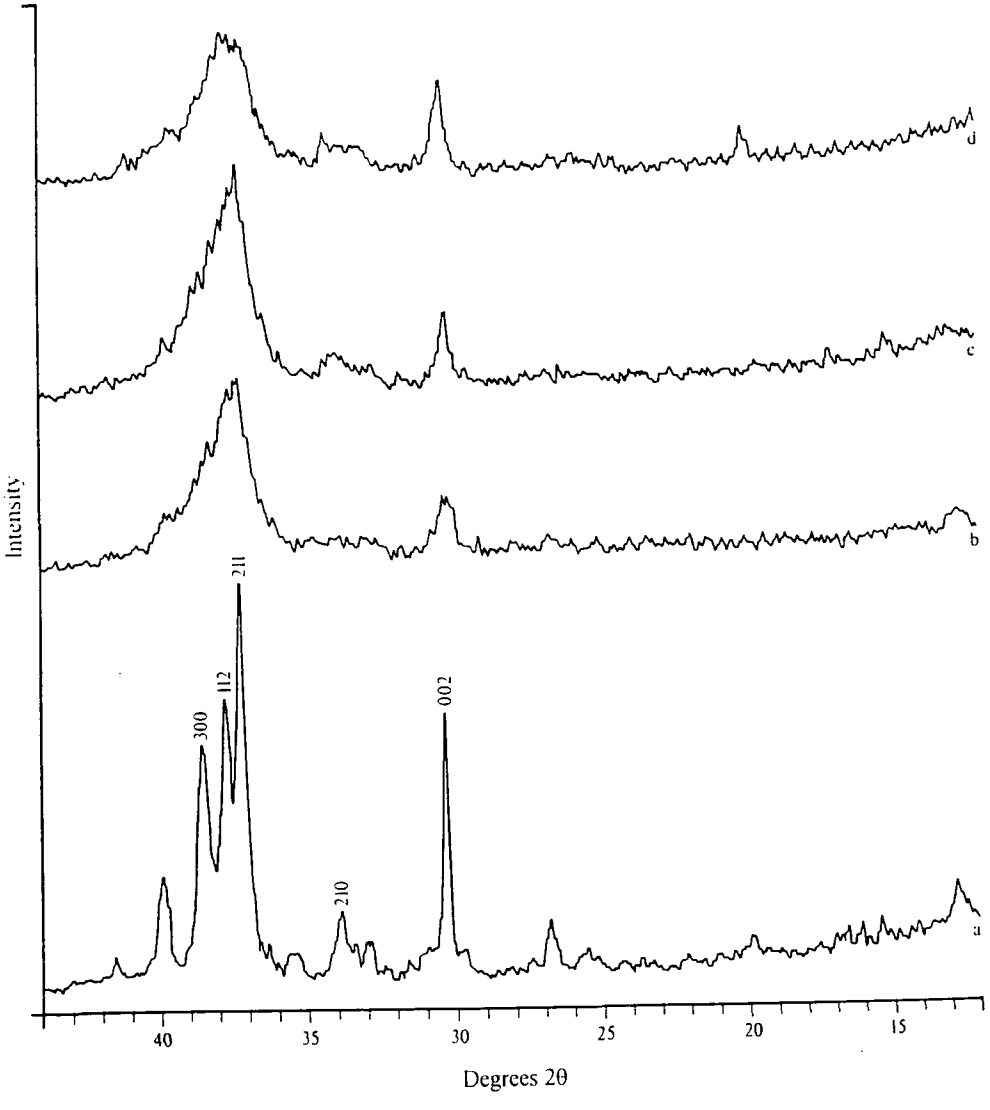

Figure 5.2 Diffractograms for: **a** synthetic hydroxyapatite; **b** untreated fresh bone; **c** deproteinized fresh bone; **d** reprecipitated synthetic hydroxyapatite

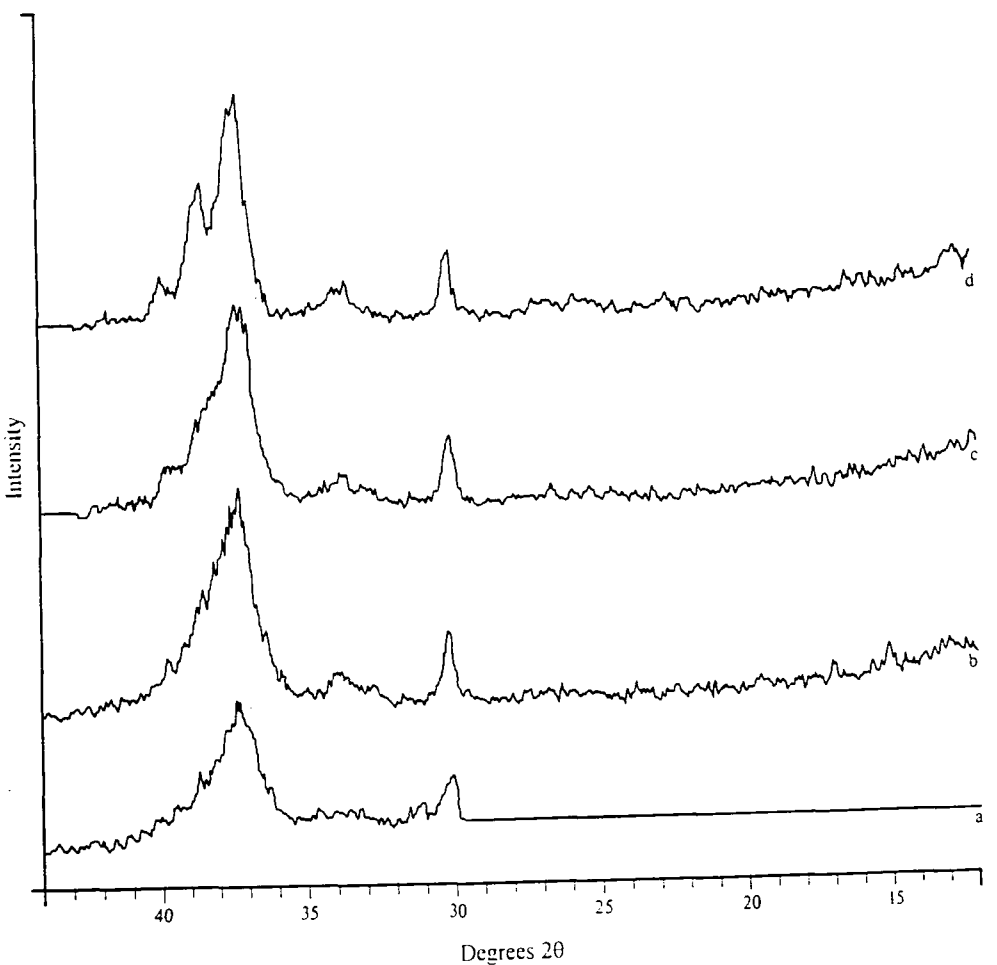

Figure 5.3 Diffractograms for: **a** untreated fresh bone (sheep) **b** hydrazine deproteinized bone; **c** hydrazine deproteinized and water washed bone; **d** fresh bone deproteinized with hot NaOH

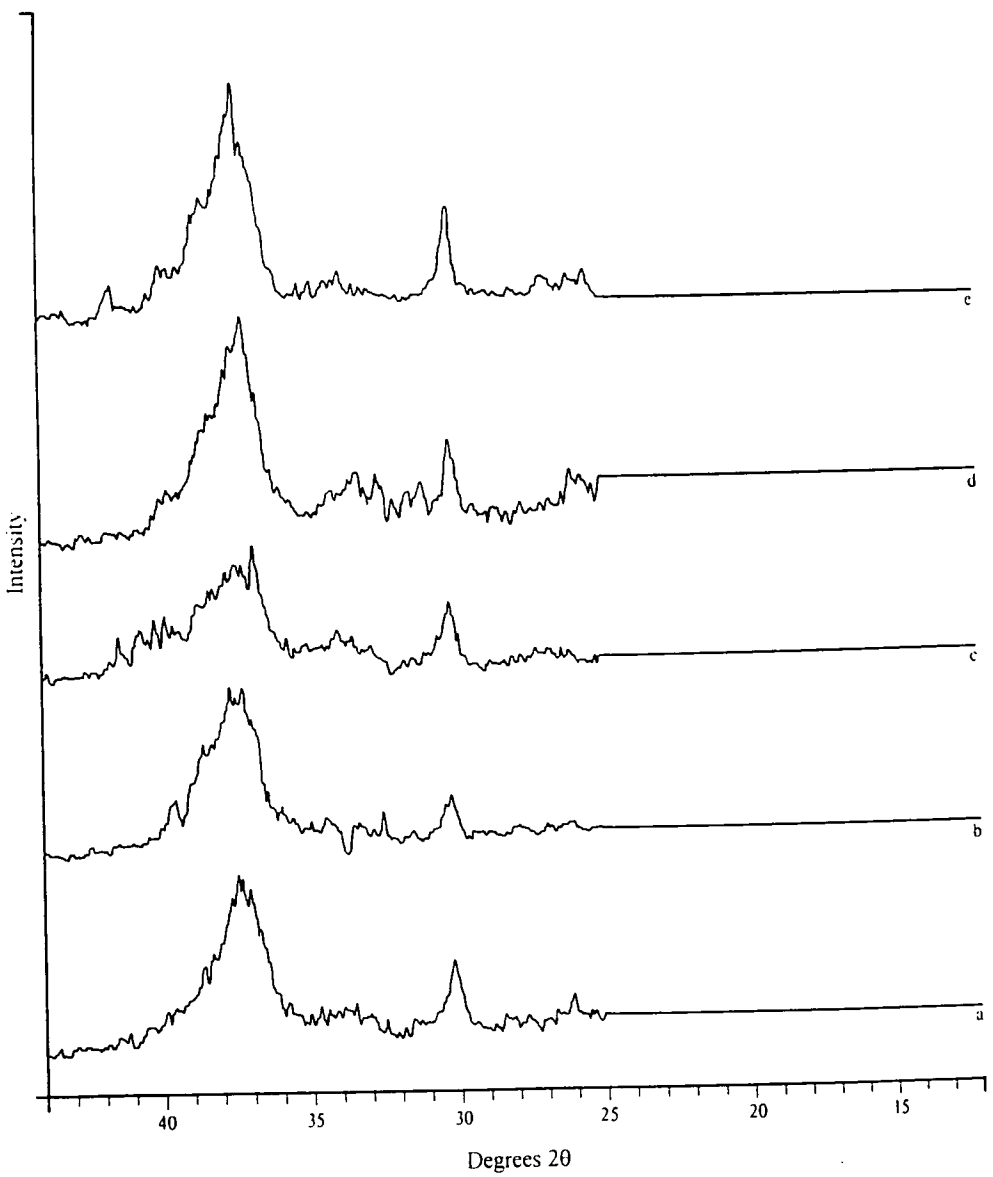

Figure 5.4 Diffractograms for: **a** untreated fresh bone (bovine); **b** fresh bone treated with hot distilled water only; **c** hydrazine deproteinized bone; **d** fresh bone treated with sodium acetate buffer; **e** bone deproteinized with hydrazine and washed in distilled water

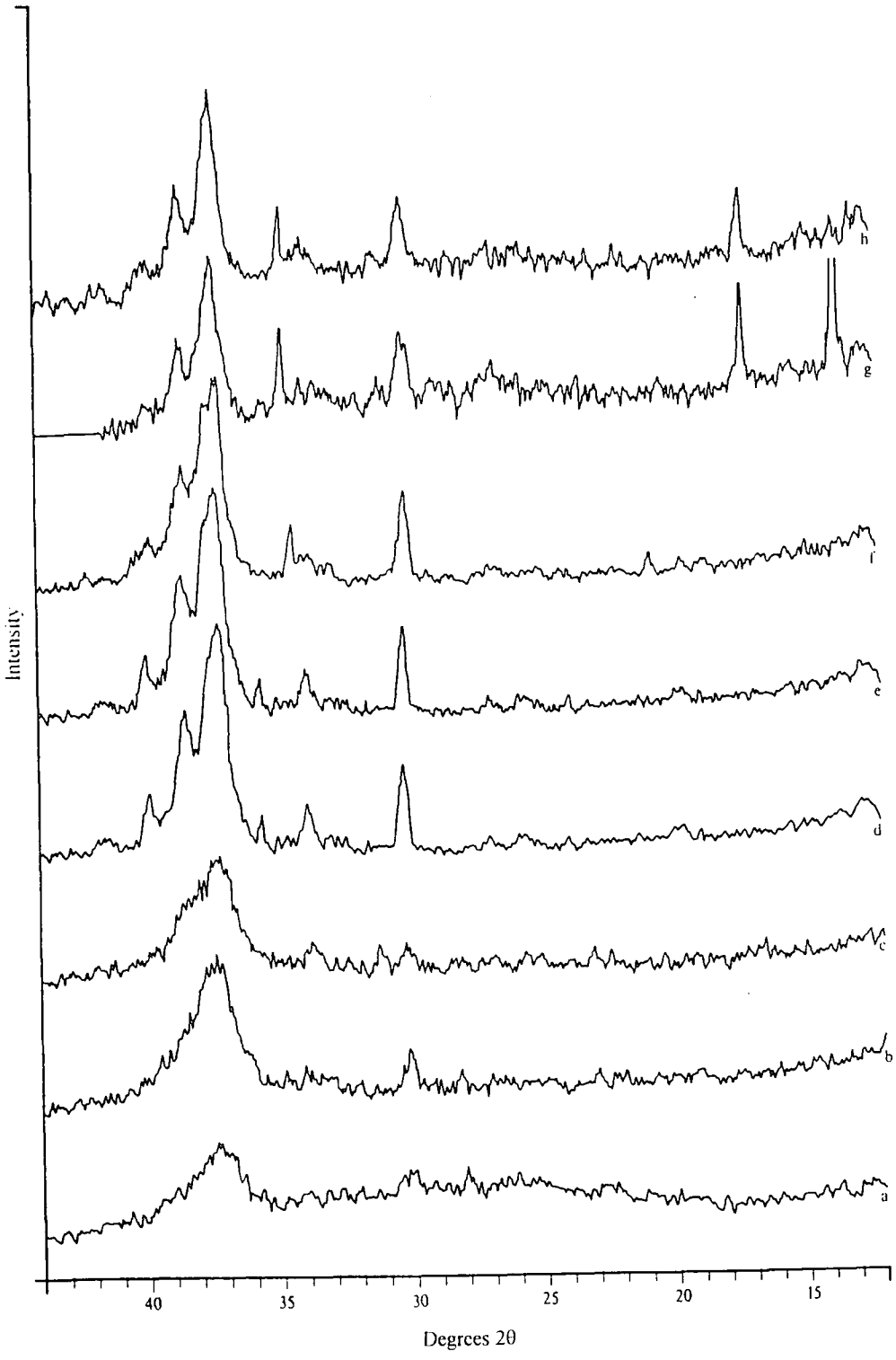

Figure 5.5 Diffractograms for: **a** Sample10 (23.02% protein: **b** Sample12 (21.78 % protein): **c** Sample 13 (22.56% protein): **d** Sample 5.2 (% protein): **e** Sample 7 (5.80% protein): **f** Sample 9 (0.02% protein): **g** Sample 21 (17.16% protein): **h** Sample 22 (5.49% protein)

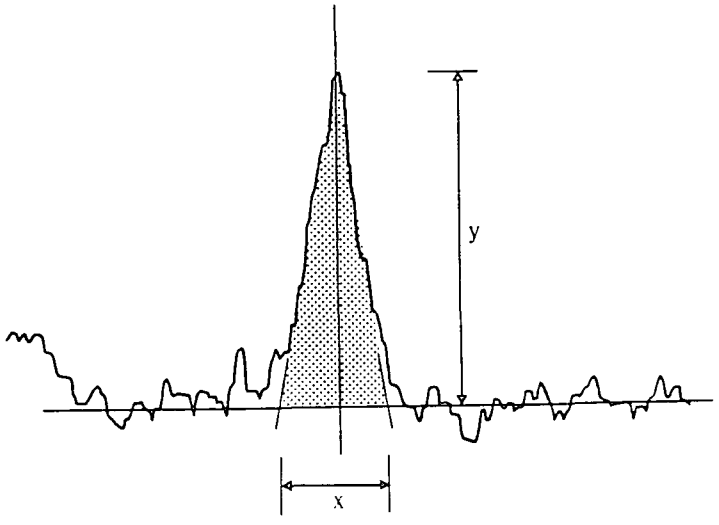

Figure 5.6 Determination of crystallinity by measurement of 002 peak area
peak area =x/2 x y

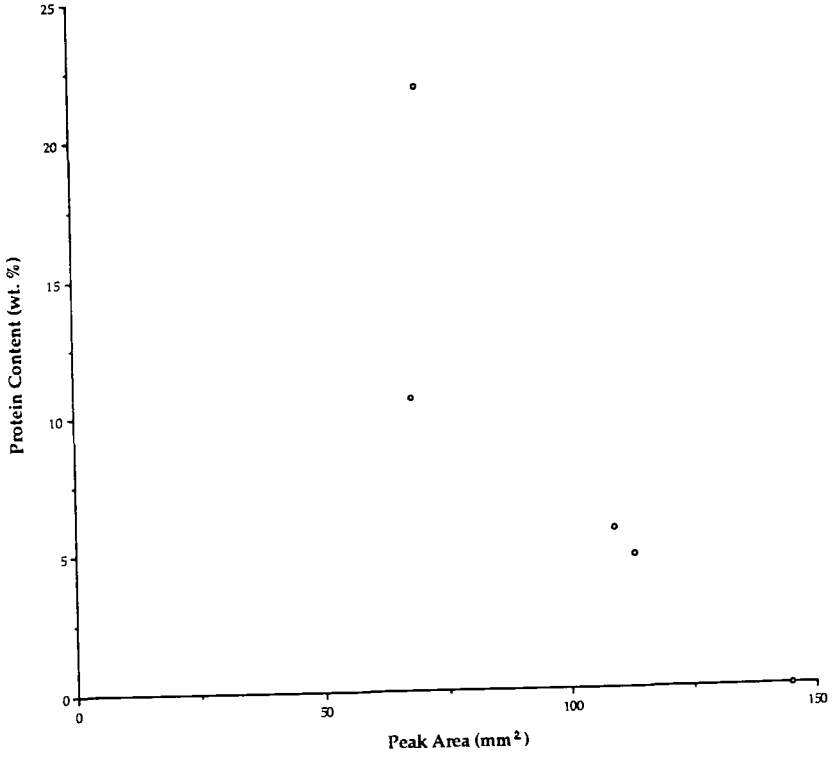

Figure 5.7 Plot of protein content vs peak area for five of the samples in Figure 5.5

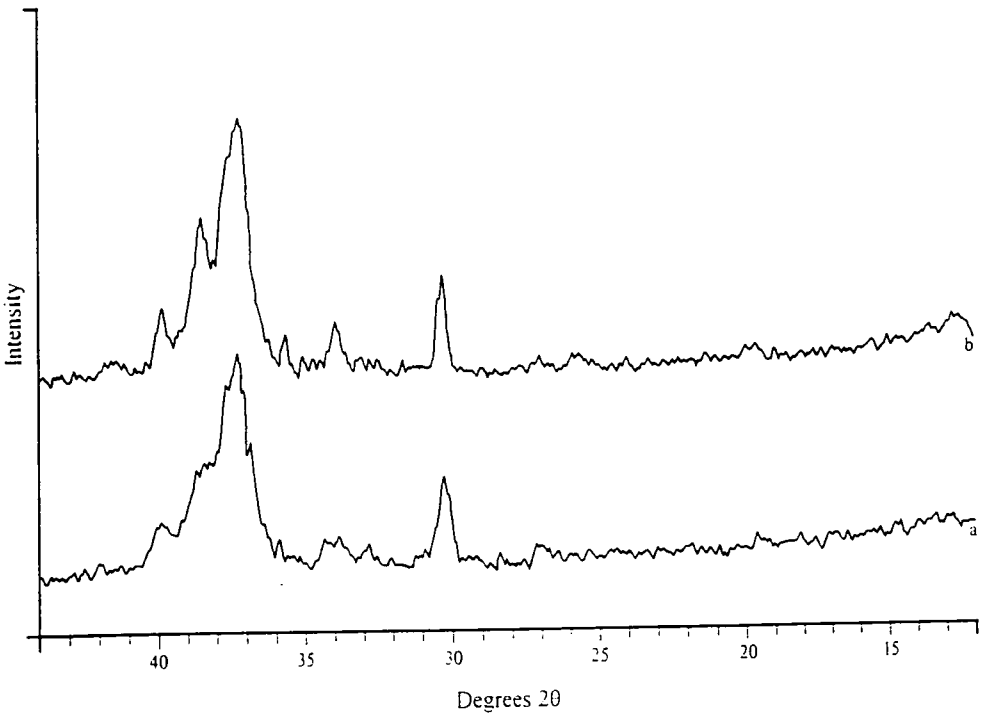

Figure 4.8 Diffractograms for: **a** surface of Sample 5 (5.1); **b** interior of Sample 5 (5.2)

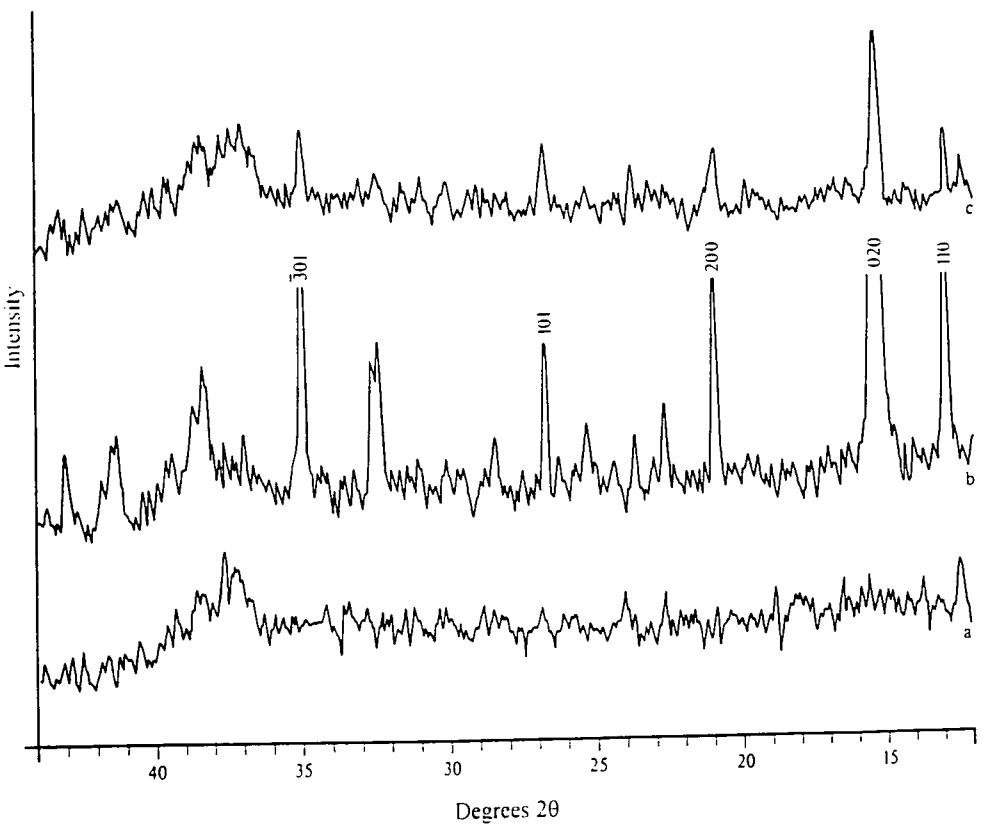

Figure 5.9 Diffractograms for: **a** powdery interior of Sample 6; **b** massive vivianite within waterlogged bone; **c** efluorescent blisters on waterlogged bone

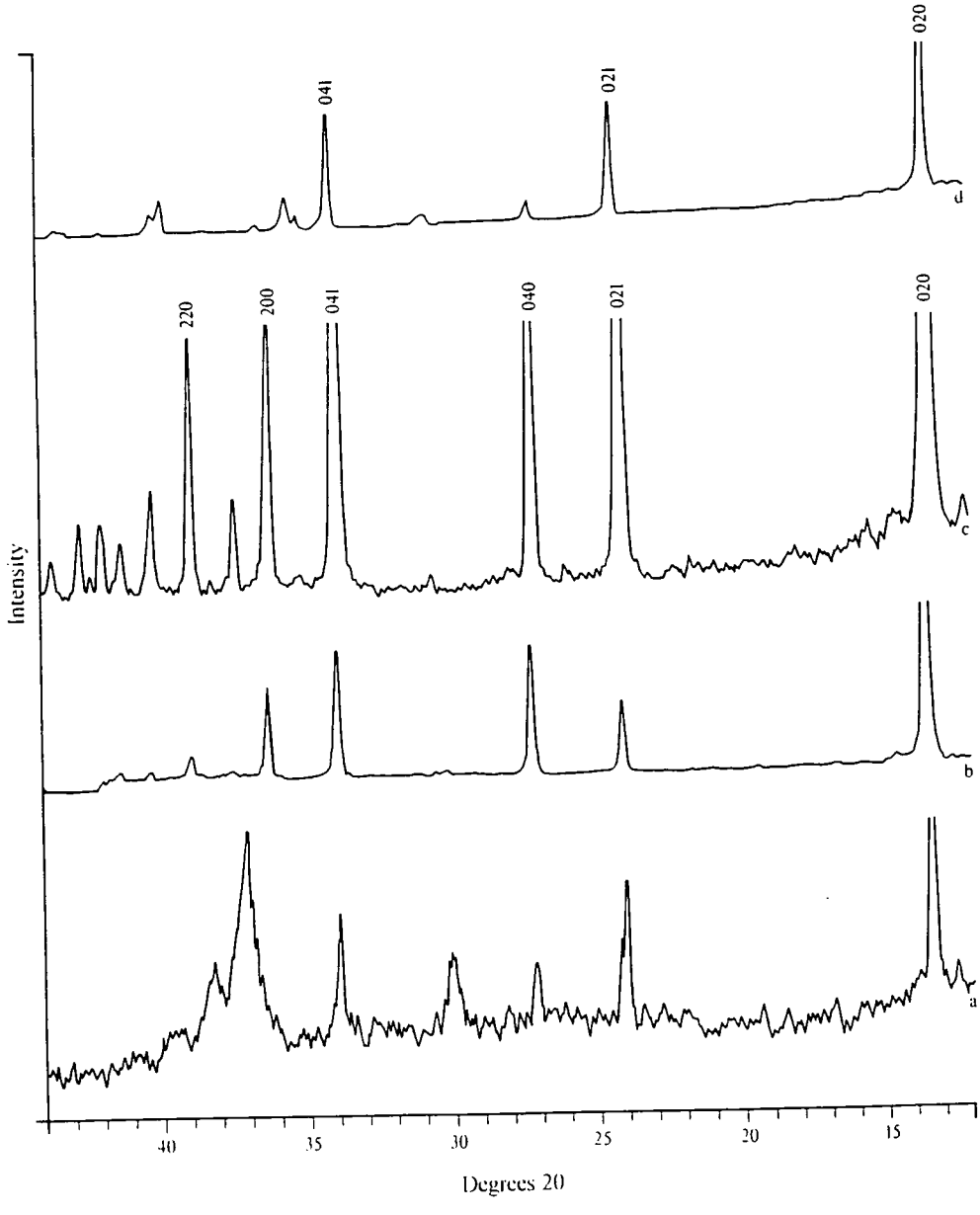

Figure 5.10 Diffractograms for: **a** Sample 22; **b** crystals from Sample 22; **c** synthetic gypsum; **d** synthetic brushite

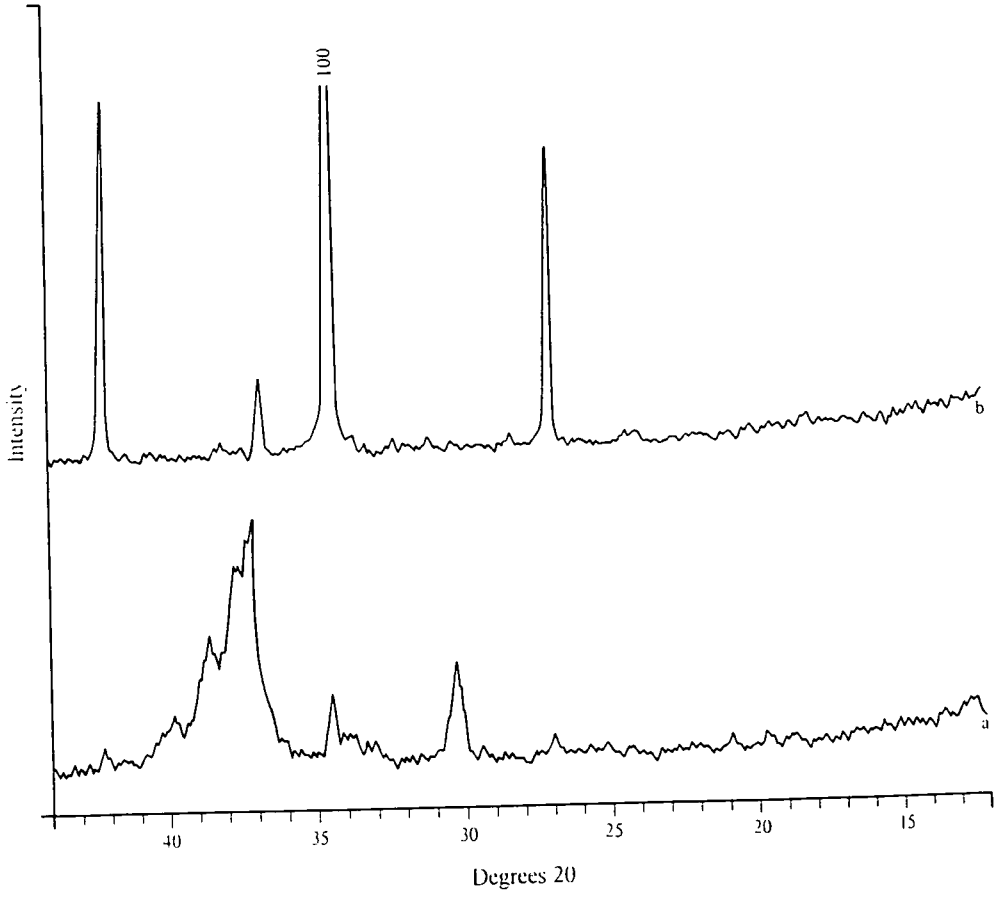

Figure 5.11 Diffractograms for: **a** Sample 9: **b** synthetic calcite

6. Infrared Spectroscopy of Fossil Bone

Infrared studies have been used extensively in the investigation of both the mineral structures in living bone (Posner 1985a, 1985b; LeGeros *et al.* 1987; Rey *et al.* 1990; Bigi *et al.* 1992) and the changes that take place in bone apatites as a result of taphonomic processes (Hassan *et al.* 1977; Newesely 1989; Sillen 1989; Weiner and Bar-Yosef 1990; Lee-Thorpe *et al.* 1991).

Because of the increasingly common use of calcium phosphate ceramics in surgery involving prosthetic implants, especially hip replacements, several research projects have also studied the changes that synthetic hydroxyapatites undergo in biological conditions (Orly *et al.* 1989; Dalcusi *et al.* 1990). Infrared analysis has also been used to examine the nature of other biomineralized tissues such as the shells of bivalves and the hard, rasp-like teeth of molluscs.

All of the above studies have contributed enormously to an understanding of the nature of biological apatites, the physical and chemical features that distinguish bioapatites from synthetic apatites, and how bioapatites may be modified by their environment.

The role of infrared studies in this research was to examine the potential of infrared spectroscopy as a tool to:

compare the relative contributions of bone mineral and the organic fraction to the overall spectrum of fresh and diagenetically altered bone

compare the infrared spectra of archaeological and fossil bones and relate any obvious differences to other physical and chemical characteristics of each sample

evaluate the use of infrared studies to identify foreign or diagenetically altered mineral species in ancient bone

attempt to quantify any visible differences in the infrared spectra.

6.1 Principles of Infrared Spectroscopy

The field of spectroscopy is divided into emission and absorption spectroscopy. As the name suggests, emission spectroscopy concerns the study of light or other radiation produced by an incandescent source such as a flame or electric arc, in which atoms are excited by thermal energy and emit characteristic wavelengths as a result. An absorption spectrum is obtained by introducing a sample material between a light source and detector. Dark lines of characteristic wavelength appear in the detected radiation when atoms within the sample absorb radiation and are promoted into an excited state as a result.

In the infrared region, molecular bonds rather than atoms are excited due to the lower energies

involved. The molecules themselves may be imagined as ball and spring models in which the springs are excited into vibrating when radiation is absorbed. This vibration may take the form of either *stretching* or *bending* of the spring and the wavelength of the absorbed radiation depends upon the strength of the bond. Some of the simple stretching and bending vibrations that are possible in a molecule are shown in Figure 6.1. For any particular bond, each *mode* of vibration will have its own particular frequency (or wavelength) with bending modes usually requiring less energy than stretching modes. Other wavelengths are possible however due to the presence of harmonics to the fundamental frequency of vibration (Dyer 1965). In infrared spectroscopy the position of any absorption band is often expressed in terms of its *wavenumber* or the reciprocal of its wavelength (in cm^{-1}).

6.2 Materials and Methods

Fresh bone, deproteinized bone and archaeological bone were examined using infrared spectroscopy. The archaeological bone examined was selected from the samples numbered 1 to 32 previously examined using X-ray fluorescence spectrometry. In addition, samples of visibly altered or contaminant material were also taken from a number of bone specimens, particularly those from waterlogged environments.

Spectra were also taken from the commercially available synthetic minerals hydroxyapatite, calcite and gypsum. Samples of the iron phosphate mineral, vivianite, were carefully dissected from specimens of archaeological ironwork excavated from waterlogged environments. These spectra were compared with those from archaeological and fossil bones in an attempt to recognise diagenetically derived, contaminant minerals. Some infrared spectra were also prepared from the acid-insoluble residues of powdered bone samples used in titration determinations of the carbonate content of bone (see 4.1.3). Sample preparation for these residues was complicated by the tough, gelatine-like film that they formed upon drying and the difficulty of grinding such residues.

Sample preparation for the powdered bone specimens was essentially very simple. Bone specimens were oven dried at 105°C, hand ground in a ceramic pestle and mortar and the resulting powder sieved through a 130μm mesh to remove larger particles and any sand or grit inclusions. These powdered bone samples were then ground with dry potassium bromide (KBr) mull at a KBr:sample ration of 3:2. Small silver gauge measures were used to standardise the amounts of sample and KBr and the mixture was ground and re-mixed three times with an agate pestle and mortar to ensure an even dilution of sample in the mulls. The sample:KBr mixture was loaded into a 15mm die which was then connected to a vacuum pump and set in a manually operated hydraulic press. The powder was evacuated for 4 minutes and then pressed under vacuum for a further 4 minutes at a load of 10 tonnes. After some practice it was possible to produce good, transparent discs with a thickness of

less than 1mm that could then be mounted in the analyser beam of the spectrometer. Infrared spectra were made with a Perkin-Elmer Model 377 Spectophotometer. Samples were scanned between 4000 and 400 wavenumbers (cm^{-1}) over a period of 5 minutes. For each sample the gain on the chart recorder was adjusted so that the baseline lay at approximately 90% transmittance. In cases where heavy staining of the original sample produced a dark disc, it proved necessary to introduce an attenuator into the reference beam in order to obtain a sufficiently strong signal in the spectrum.

6.3 Results

Infrared spectra for fresh, washed bone (sheep metapodial), hydrazine deproteinized fresh bone (see 4.1.1) and synthetic hydroxyapatite are shown in Figures 6.2a-6.2c respectively. It can be seen that the spectra share many features in common, although the fresh bone specimen has additional absorption bands (troughs), probably due to the presence of complex organic molecules such as mucopolysaccharides and lipids.

The spectrum shown in Figure 6.2b is typical of poorly crystalline hydroxyapatite and biological apatites. The broad absorption band in the region between $3600cm^{-1}$ and $3300cm^{-1}$ can be attributed to the O-H stretching mode of H_20 hydrogen bonded to the highly reactive surfaces of either the bone mineral or collagen. Since this feature also occurs in the spectrum for deproteinized bone this must represent water molecules adsorbed onto the surface of the bone mineral crystallites or residing in pores within the bone micro architecture (see section 7.2). The smaller absorption band at $1630cm^{-1}$ that occurs in Figure 6.2a, Figure 6.2b and to a lesser degree in the spectrum for synthetic hydroxyapatite (Figure 6.2c) may be attributed to the H-O-H bending mode of surface adsorbed water molecules.

The infrared absorption bands for phosphates in bone are much more complex than those for adsorbed water. The orthophosphate ion (PO_4^{3-}) is tetrahedral and presents four modes of vibration. In amorphous calcium phosphates, when this regular tetrahedral symmetry is preserved, two of these vibrations, the ν_1 and ν_2 modes are inactive in the infrared region, so that only the ν_3 and ν_4 modes are observed in infrared spectra. The ν_3 symmetric stretching mode of the PO_4^{3-} ion occurs between $1300cm^{-1}$ and $900cm^{-1}$. In amorphous mineral phosphates, the local electric field of the phosphate ion is symmetrical in three axes and the ν_4 antisymmetric bending mode produces a single absorption between $600cm^{-1}$ and $500cm^{-1}$. However, in crystalline calcium phosphate minerals the proximity and geometry of neighbouring ionic species lead to an anisotropic local electric field. This anisotropy of the local environment leads to additional bands in the infrared (Rey *et al.* 1990). The electric field surrounding the orthophosphate ion is asymmetric with the fields parallel to a- and b-axes of the unit cell equivalent whereas that parallel to the c-axis has a different value. This discrepancy results in the splitting of certain absorption band into two modes (Sillen 1989, 217).

The single, broad and symmetric ν_4 absorption band seen in amorphous calcium phosphate is split into a well defined doublet with twin absorption bands at $600cm^{-1}$ and $560cm^{-1}$. In highly crystalline apatites the ν_1 mode appears as a sharp, narrow band between $1000cm^{-1}$ and $950cm^{-1}$. In the poorly crystalline biological apatites however, this absorption is represented by a slight shoulder on the ν_3 band at approximately $960cm^{-1}$. The ν_2 vibration mode appears as a faint, barely distinguishable absorption around $470cm^{-1}$.

The absorption band between $1550cm^{-1}$ and $1350cm^{-1}$ is due to the ν_3 symmetric stretching vibration of the CO_3^{2-} ion present in the form of bone mineral carbonate. The small, sharp absorption band at $873cm^{-1}$ results from the ν_2 carbonate ion out-of-plane stretching mode. The spectra of all the bone samples (whether fresh or fossil) show a slight kick or discontinuity at $710cm^{-1}$. This marks the position of the ν_4 absorption for crystalline carbonate in the form of calcite or aragonite. This feature also occurs in the spectrum for synthetic hydroxyapatite (Figure 6.2c) suggesting that it contains a slight trace of calcite as an impurity.

Figure 6.2c shows additional absorption bands at $3580cm^{-1}$ and $630cm^{-1}$ that do not appear in the spectra of fresh or deproteinized bone. These represent hydroxyl ion absorption bands that are masked in finely divided hydroxyapatites and bioapatites due to the presence of water molecules hydrogen bonding to the surfaces of the small crystallites. This covering of tightly held, adsorbed water up to two molecules deep, restricts and perturbs the OH bending and stretching modes sufficiently to render the hydroxyl ions on bone apatite invisible. When bone mineral is heated or ashed (Figure 6.2d), this adsorbed water is lost and there is an increase in the size of the crystallites, a transformation that exposes OH groups, rendering them visible in infrared spectra (Posner 1985a, 91-92).

In addition to the hydroxyl ion bands at $3580cm^{-1}$ and $630cm^{-1}$ the spectra for synthetic hydroxyapatite and ashed bone both show an distinct increase in the distances between the maxima and minima of the PO_4^{3-} anti-symmetric bending mode absorption with a resultant sharpening of the bands. This sharpening or 'peak splitting' becomes more marked with increased crystallinity of the mineral (*i.e.* the size and order of the individual crystallites). This phenomenon is analogous to the sharpening of XRD diffraction peaks (see Chapter 5) with similar increases in crystallinity.

6.3.1 Determination of Crystallinity Index

Several researchers have used the degree of peak splitting as a measure of increased crystallinity in biological and synthetic apatites. Termine and Posner (1966) used quantitative analysis of infrared spectra to support their claim that amorphous calcium phosphate constituted a major component of bone mineral. Using ground and sieved synthetic calcium phosphate samples in a KBr mull,

Termine and Posner used the ν_4 antisymmetric bending vibration to explore the relationship between the degree of peak splitting and the relative proportions of amorphous and crystalline calcium phosphate. They were able to demonstrate a linear relationship between the 'splitting fraction' calculated directly from the infrared spectrum and the crystallinity defined as weight fraction of crystalline apatite in amorphous calcium phosphate. Termine and Posner calculated the splitting fraction by drawing two straight lines (a-a' and b-b') between the points of minimum transmittance of the ν_4 bands and from 450cm^{-1} to 700cm^{-1} (as a baseline) respectively (see Figure 6.3). They defined the splitting fraction as the ratio of the area enclosed by the transmittance minima and line a-a' and the area enclosed by the doublet and line b-b'. In none of the samples studied did the spectrum contain a hydroxyl ion absorption on the shoulder of ν_4 band (Termine and Posner 1966, 1523). They also prepared a plot of splitting fraction vs crystallinity for 'bone mock-up' by adding measured quantities of EDTA demineralized bone protein to their synthetic calcium phosphates.

When discussing diagenetic changes in bone mineral, Sillen briefly describes the derivation of crystallinity measurement as the vertical distance between the transmittance maximum and minima of the split ν_4 doublet (Sillen 1989, Figure 8.4). However, such a single measurement, without reference to other parameters can only be arbitrary. In addition, Sillen's Figure shows the height difference as both the distance between the minimum at 600cm^{-1} and the maximum at 580cm^{-1} and the minimum at 560cm^{-1} and 580cm^{-1}. Such inconsistencies can only serve to make comparisons between different samples and different data sets impossible.

Weiner and Bar-Yosef describe a similar but more stringent technique for the measurement of bone mineral crystallinity (Weiner & Bar-Yosef 1990, 190). They estimated the 'crystallinity index' by drawing a baseline from 750cm^{-1} to 494cm^{-1} and then measuring the distances from this line to the maxima transmittance at 603cm^{-1} (line a-a') and 565cm^{-1} (line b-b') and the minimum between (c-c') them (see Figure 6.4). They then defined the crystallinity index as:

$$I = \frac{(a-a')+(b-b')}{c-c'}$$

Hassan *et al.* (1977) used measurements taken from infrared spectra to determine the carbonate content of bones by measuring the areas enclosed by the absorption bands 1550cm^{-1} to 1350cm^{-1} (CO_3 ν_3 mode) and 800cm^{-1} to 450cm^{-1} (PO_4 ν_4 mode). By taking their ratio and comparing unknown specimens with a standard for which the carbonate content was determined by wet chemistry, they assessed the potential for carbonate ion substitution for bone mineral phosphate during burial.

Similar quantitative techniques to those described above were applied to the present study. The infrared spectra for bone samples 1 to 32 are shown in Figure 6.5 to Figure 6.8. Apart from some obvious exceptions such as sample 10 (fresh sheep bone) and samples 6.2, 20 and 21 where the PO_4

ν_4 mode is absent, the spectra are remarkably similar. Although there are obvious visible differences in the degree of peak splitting in the PO_4 ν_4 band, attempts to calculate the crystallinity indices or assign other numerical values to these differences were complicated by the problems of setting an objective baseline. Applying the simplest formula, that described by Weiner and Bar-Yosef (Weiner and Bar-Yosef 1990, 190), it proved possible to obtain the crystallinity index for each spectrum except samples 6.1, 20 and 21. However, rather than draw a baseline between the intercepts of the curve at 750cm^{-1} and 495cm^{-1}, a straight line was chosen that was tangential to the curve at the transmittance maximum on the high wavenumber side of the PO_4 ν_4 band (approximately 800-770cm^{-1}) and the transmittance maximum on the low wavenumber side of the PO_4 ν_2 band (approximately 430-400cm^{-1}). The crystallinity index was then calculated according to the equation above (refer to Figure 6.4). The results are shown in Table 6.1 together with the protein contents as determined by hydrazinolysis. The range of crystallinity indices shown in Table 6.1 covers a much narrower range that those quoted by Weiner and Bar-Yosef who obtained values ranging from a minimum of 2.8 for modern bone up to a maximum of 5.3 for 9,700-9,400 year old bone.

Although the crystallinity index for each pressed disc was exactly reproducible, the calculated figure varied for different discs and different sample:KBr ratios. Figure 6.9 shows the PO_4 ν_4 region for two successive runs of the infrared spectrum of deproteinized bone (sample 7) in which only the gain on the chart recorder has been changed. For both of the traces the calculated crystallinity index is 2.25. Figure 6.10 shows the spectra of untreated archaeological bone (sample 2) with sample to KBr ratios of 1:2 and 2:3. Although the spectra appear to be very similar they give crystallinity indices of 2.64 and 2.45 respectively.

It would appear then that the crystallinity index, as calculated by equation 6.1, is sensitive to changes in the sample:KBr ratio. If consistent results are to be obtained, accurately weighed proportions of sample material and mull must be carefully ground together and all of the resultant mixture incorporated into a single disc. Since previous work has demonstrated that the 'splitting fraction' decreases with the addition of bone protein (Termine and Posner 1966, 1524), only deproteinized bone should be examined. Despite these minor problems, quantitative infrared spectroscopic analysis holds considerable promise for the investigation of bone mineral crystallinity, since the signal to noise ratio is considerably higher than in XRD spectra.

Sample	I (crystallinity index)	Protein (%)
1	2.51	20.56
2	2.45	06.14
3	2.39	21.13
4	2.41	21.78
5	2.41	10.56
6.1	2.47	23.10
7	2.20	05.80
8	2.41	15.42
9	2.64	00.20
10	2.33	23.02
11	2.36	26.79
12	2.45	21.78
13	2.42	22.54
14	2.58	10.00
15	2.50	15.17
16	2.45	01.90
17	2.54	18.69
18	2.48	08.24
19	2.57	05.53
22	2.59	05.49
23	2.92	04.76
24	2.51	04.54
25	2.63	00.55
26	2.67	00.51
27	2.46	19.31
28	2.46	17.10
29	2.53	15.31
30	2.78	13.37
31	2.49	05.11
32	2.53	03.35

Table 6.1 Crystallinity indices and protein contents: samples 1-32

Figure 6.11 shows a plot of crystallinity index vs protein content for the bone samples examined. The considerable scatter in the data points almost certainly reflects the differences in the calculated crystallinity index as a result of differences in the sample KBr mull ratios. Despite this scatter, there is an underlying trend suggesting that crystallinity increases with progressive loss of bone collagen. This in turn suggests that remodelling of bone mineral is associated with, or dependant upon, the processes that degrade bone collagen.

6.3.2 Other Changes in Bone Mineral

In addition to changes in the peak splitting of the PO_4 ν_4 mode, several other subtle changes may be identified in the spectra shown in Figures 6.5 to 6.8. Many of these changes occur in the region 1800cm^{-1} to 1350cm^{-1} that includes the CO_3 ν_3 mode and O-H-O bending mode. In normal bone mineral the CO_3 ν_3 band appears as a poorly resolved doublet with absorption maxima at 1450cm^{-1}

and 1415cm^{-1}. After burial this doublet frequently becomes more pronounced and one of the absorption bands may become stronger and deeper. In the case of sample 32 the absorption at 1450cm^{-1} has become stronger whereas in sample 26 the 1415cm^{-1} band has become more pronounced and the 1450cm^{-1} is barely distinguishable. These changes probably reflect subtle differences in the local electric field surrounding the carbonate ion in bone mineral. In addition to changes in the CO_3 ν_3 vibrational mode, there are clear changes in the relative strengths of the CO_3 ν_3 mode and O-H-O bending mode. In some samples the O-H-O absorption at 1640cm^{-1} is much less intense and may be reduced to a flattened shoulder on the carbonate absorption (sample 25). Reduction in the strength of this absorption is accompanied by a corresponding reduction in the O-H stretching mode and must reflect a decrease in the amount of water hydrogen-bonded to the surfaces of the apatite crystallites. Instances in which there is a dramatic increase in absorption in the region of the O-H-O bending mode, as in samples 6.1, 20, 21 and 22 can be attributed to the presence of other mineral species and will be discussed in section 6.3.4.

Some samples (particularly sample 6.1) show a faint absorption at approximately 1550. This does not correspond to any of the known vibrational modes for calcium phosphates and remains enigmatic.

6.3.3 Residual Bone Collagen

Figure 6.12a shows the infrared spectrum for bovine tendon collagen and is identical to that for the acid insoluble (0.1 molar HCl) fraction of fresh sheep bone (Figure 6.12b). Figures 6.12d-6.12g show the spectra for the acid insoluble fraction of various bone samples (7, 11, 14 &15)and demonstrate that the non-mineral component of ancient bone is closely related to collagen. In their work on the acid insoluble residues of fossil bones, Weiner and Bar-Yosef describe the absorption bands at 1653cm^{-1}, 1539cm^{-1} and 1457cm^{-1} as characteristic of collagen (Weiner & Bar-Yosef 1990, 193). They also stress that the acid soluble fraction in fossil bones contains high molecular weight proteinaceous material in addition to dissolved mineral species so it is unsurprising that the acid insoluble residue contains only (or primarily) collagen. For comparison, figure 6.12c shows the infrared spectrum for finely ground archaeological leather taken from a Roman shoe found in waterlogged deposits. This spectrum also contains the characteristic absorption bands for collagen.

The fact that these broad absorption bands do not feature in the spectra for buried bone, even bone with a high collagen content, demonstrates the extent to which the infrared spectrum of bone is dominated by the mineral fraction. This probably reflects the manner in which the bone apatite crystallites permeate and surround the collagen fibrils. The intimate bonding between active sites on the collagen molecule and the reactive surface of the apatite crystallites presumably mask the vibrational modes in the same way that water molecules mask the hydroxyl ion vibration.

6.3.4 Other Mineral Species in Fossil Bone

Evidence from microscopic examination, XRF and XRD studies indicates that certain, specific mineral species occur in fossil bones (see Chapters 3, 4 and 5). At least two of these minerals, calcite and gypsum may be identified in the infrared spectra of some of the bone specimens examined. It was seen in Chapters 3 and 5 that calcium carbonate in the form of calcite was present in the pores and cracks of sample 9. Figure 6.13 shows the infrared spectra for both calcium carbonate (synthetic) and sample 9. In the spectrum for synthetic calcium carbonate the CO_3 ν_3 doublet is absent and is replaced by a very broad absorption at 1425cm^{-1}. The spectrum for sample 9 shows an increase in absorption at 873cm^{-1} (the CO_3 ν_2 mode) and between 1550cm^{-1} and 1350cm^{-1} (the CO_3 ν_3 doublet). In addition, there is a sharp absorption at 710cm^{-1} (CO_3 ν_4) and a weak absorption at 1800cm^{-1}. The absorption at 710cm^{-1} in particular is characteristic of both aragonite and calcite. However, since the CO_3 ν_2 mode in aragonite occurs at 842cm^{-1} or 852cm^{-1} (Hassan *et al.* 1977, Table 1) the carbonate inclusions can be positively identified as calcite.

Figures 6.14a and 6.14b show the infrared spectra for sample 22 together and the spectrum for white crystals dissected out from pores within the bone specimen. Figure 6.14c is the spectrum for synthetic hydrated calcium sulphate (gypsum). The obvious similarities between Figures 6.14b and 6.14c confirm that the white crystals are gypsum. However when the spectrum for sample 22 is examined, the sole clues to the presence of small quantities of gypsum in the specimen are a slight deepening of the broad absorption at 1650cm^{-1} and a small absorption at 660cm^{-1} on the shoulder of the PO_4 ν_4 doublet. The presence of gypsum in other bones from Mesolithic peat deposits is indicated by the infrared spectra for samples 20 to 23 (Figure 6.7). In Figures 6.7d and 6.7e, the PO_4 ν_4 doublet is not visible and that region of the spectra resembles that in Figure 6.14b. In Figures 6.7f and 6.7g, the PO_4 ν_4 doublet appears normal but the gypsum band at 660cm^{-1} can be detected on the shoulder. Where the gypsum absorption at 660cm^{-1} and is clearly distinguishable (sample 21) there is a pronounced deepening of the O-H-O bending mode due to the strong absorption at 1620cm^{-1} and an absence of the carbonate ion absorption band.

Figure 6.14d shows the infrared spectrum for brushite. Although there are similarities between the X-ray diffractograms for gypsum and brushite (Figures 5.10c and 5.10d respectively) there is little potential for confusion in their infrared spectra (Figures 6.14c and 6.14d). Several researchers have claimed to have identified brushite in fossil bones (Piepenbrink 1986; Piepenbrink 1989; Newesely 1989). Although Newesely used infrared spectroscopy to identify an efflorescence on post-Medieval bones (Newesely 1989, Figure 1) Piepenbrink relied upon X-ray diffraction patterns (Piepenbrink 1986, 421). The similarity between the diffraction patterns for gypsum and brushite, particularly when overlain upon the pattern for bone apatite, makes independent corroboration by infrared or X-ray fluorescence analysis essential for a positive identification.

Infrared spectroscopy has applications for the investigation of fossil bone. In common with X-ray diffraction, it is quick, economical and requires little sample preparation. Furthermore, bone specimens may be examined in the solid phase without having to dissolve the sample in acids to obtain a solution. In contrast to XRD studies however, the signal to noise ratio is high although interpretation of the resulting spectra is considerably more difficult. However, using hydrazine deproteinized specimens, careful sample preparation to ensure constant sample:KBr ratios and the application of Fourier transform infrared spectroscopy, there is considerable potential for overcoming many of the problems encountered above. A well-structured program of research may well reveal a relationship between collagen loss and diagenetic reworking of the mineral component of fossil bones.

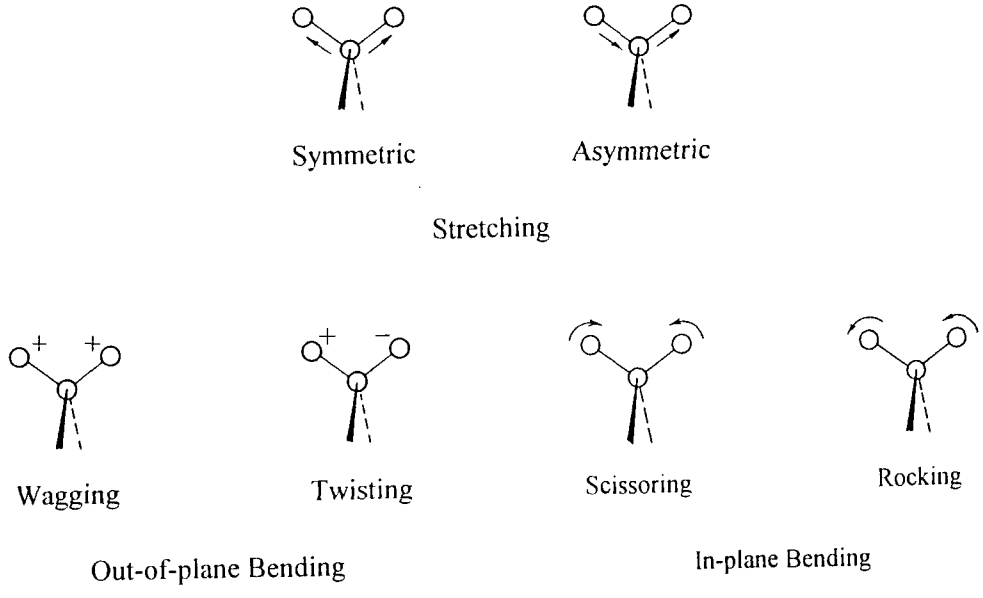

Figure 6.1 Principle vibrational modes of molecules

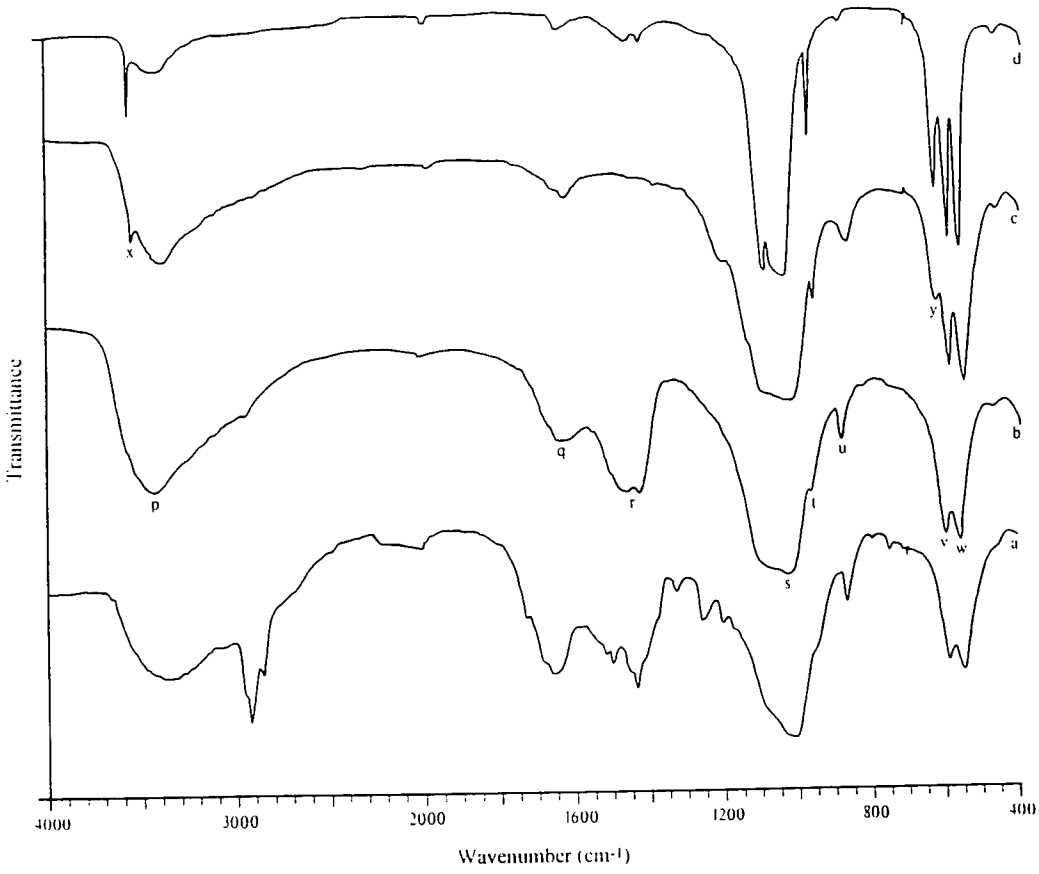

Figure 6.2 Infrared spectra for: **a** fresh untreated sheep bone; **b** hydrazine deproteinized bone; **c** synthetic hydroxyapatite **d** burnt bone

Vibration assignments: **p** O-H stretch; **q** O-H-O bend; **r** $CO_3\nu_3$; **s** $PO_4\nu_3$; **t** $PO_4\nu_1$; **u** $CO_3\nu_2$; **v** & **w** $PO_4\nu_4$; **x** O-H; **y** O-H

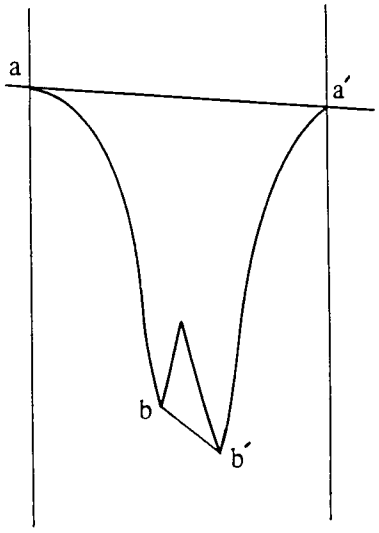

Figure 6.3 Determination of infrared splitting factor (Termine & Posner 1966)

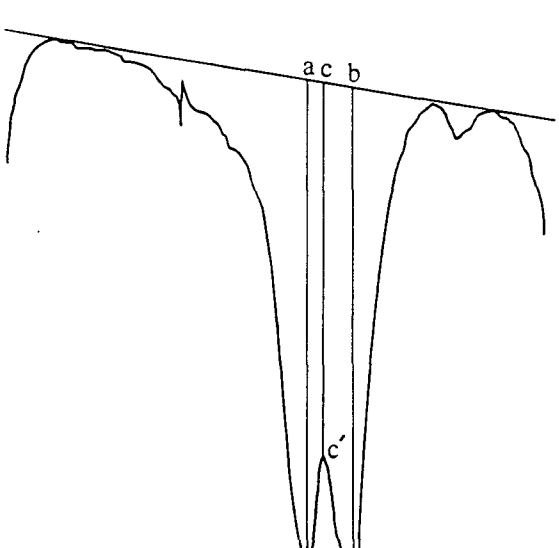

Figure 6.4 Determination of crystallinity index
(Weiner & Bar-Yosef 1990)

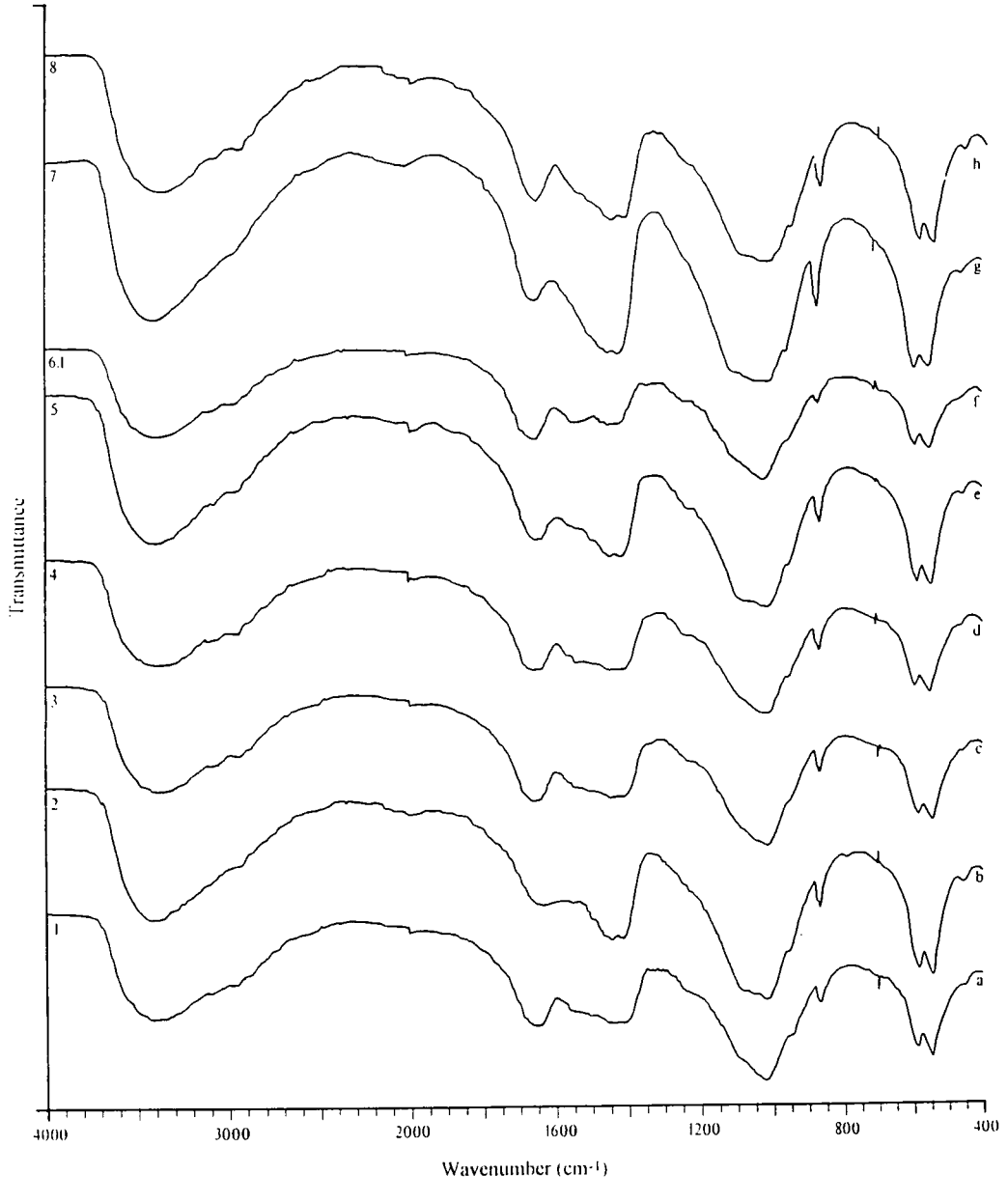

Figure 6.5 Infrared spectra for Samples 1 to 8

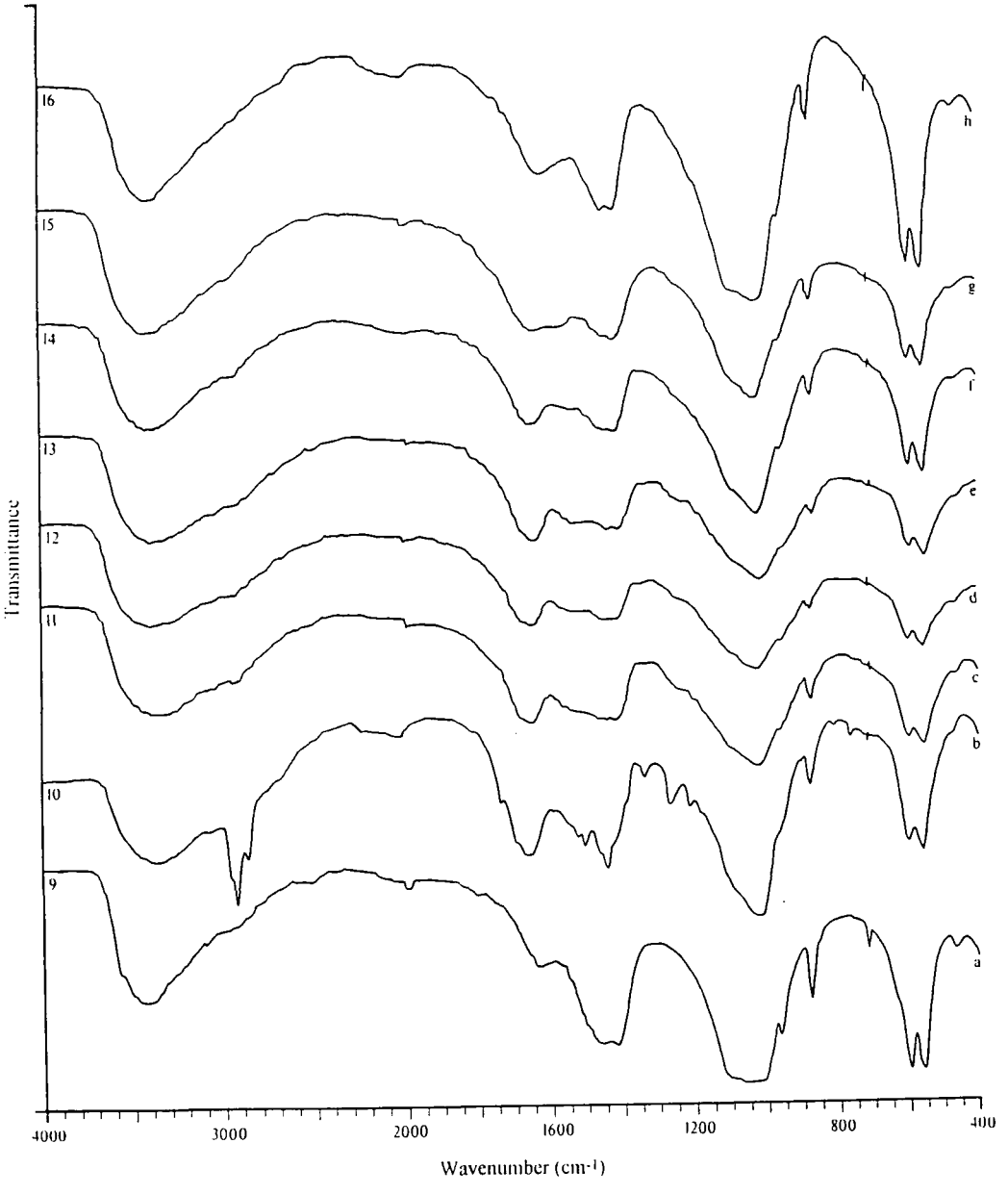

Figure 6.6 Infrared spectra for Samples 9 to 16

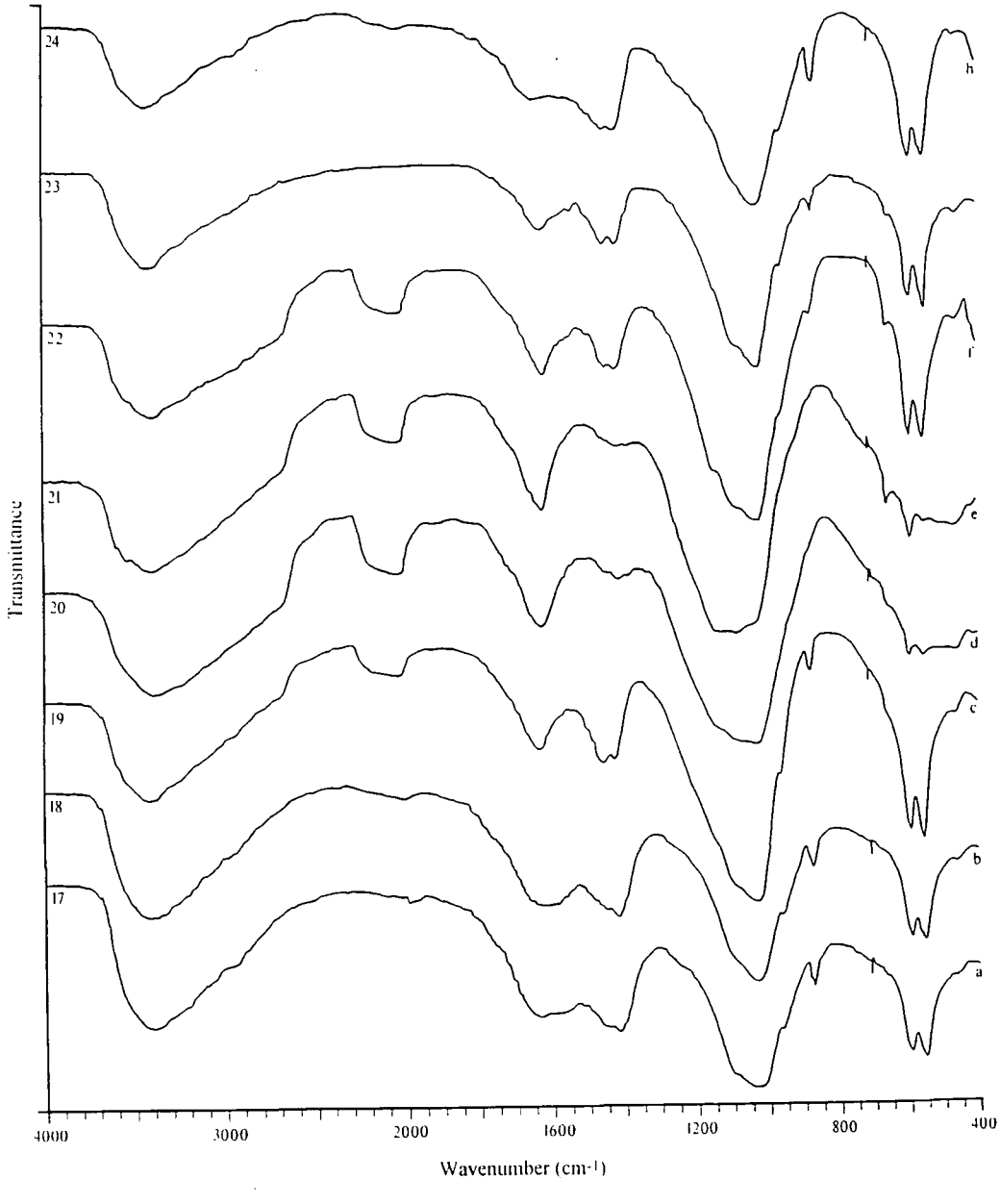

Figure 6.7 Infrared spectra for Samples 17 to 24

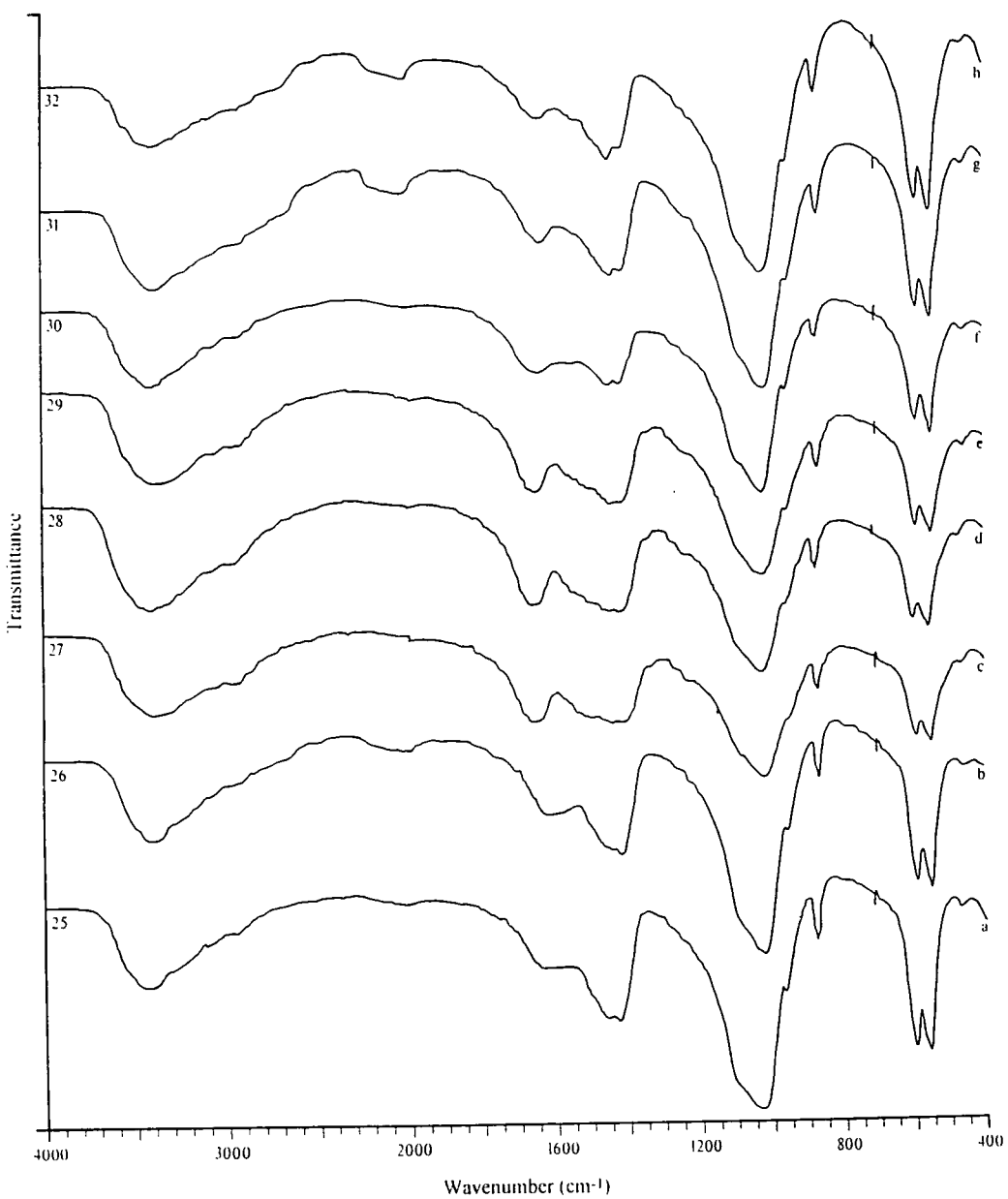

Figure 6.8 Infrared spectra for Samples 25 to 32

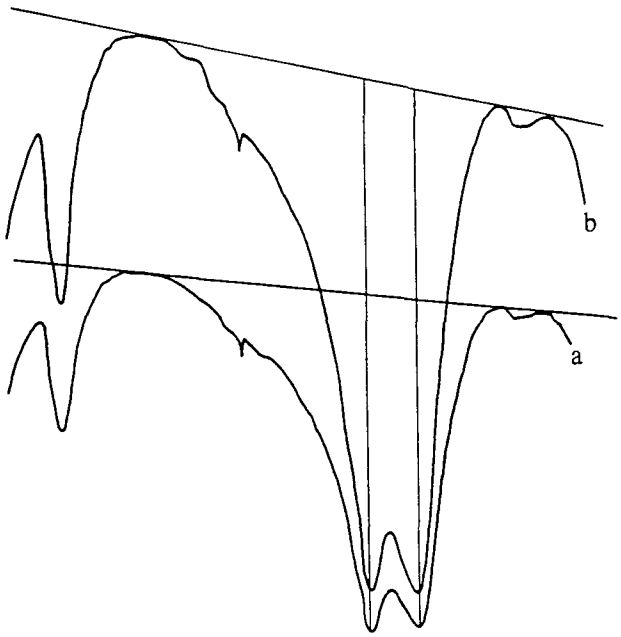

Figure 6.9 Two successive runs of the infrared spectrum for Sample 7. Only the gain on the chart recorder was altered between runs

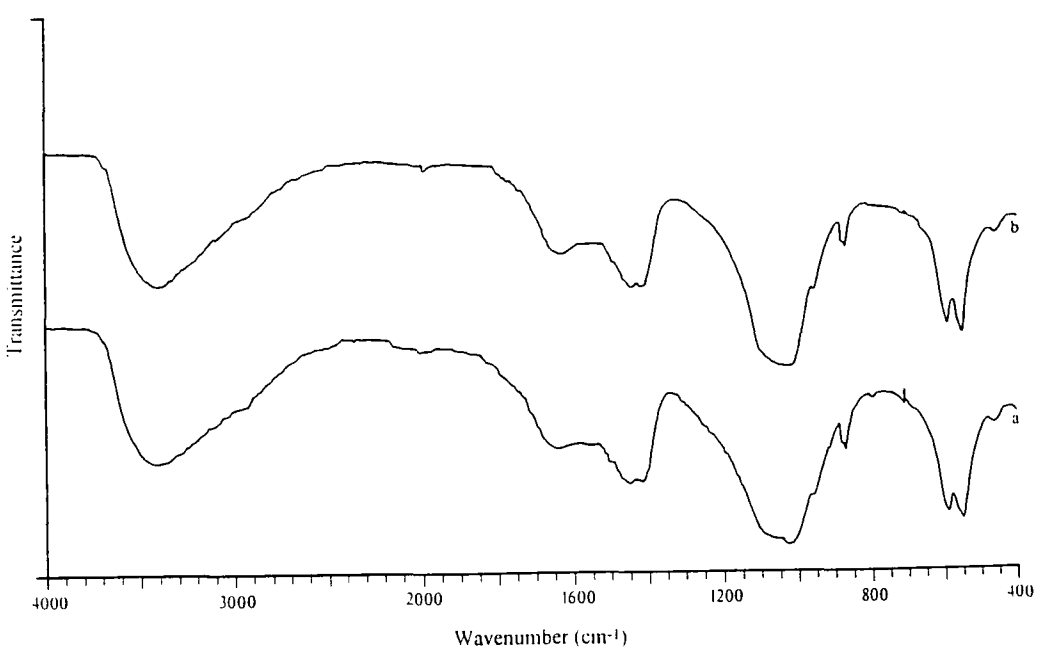

Figure 6.10 Two successive runs of the infrared spectrum of Sample 2: **a** sample:KBr ratio1:2; **b** sample:KBr ratio 2:3

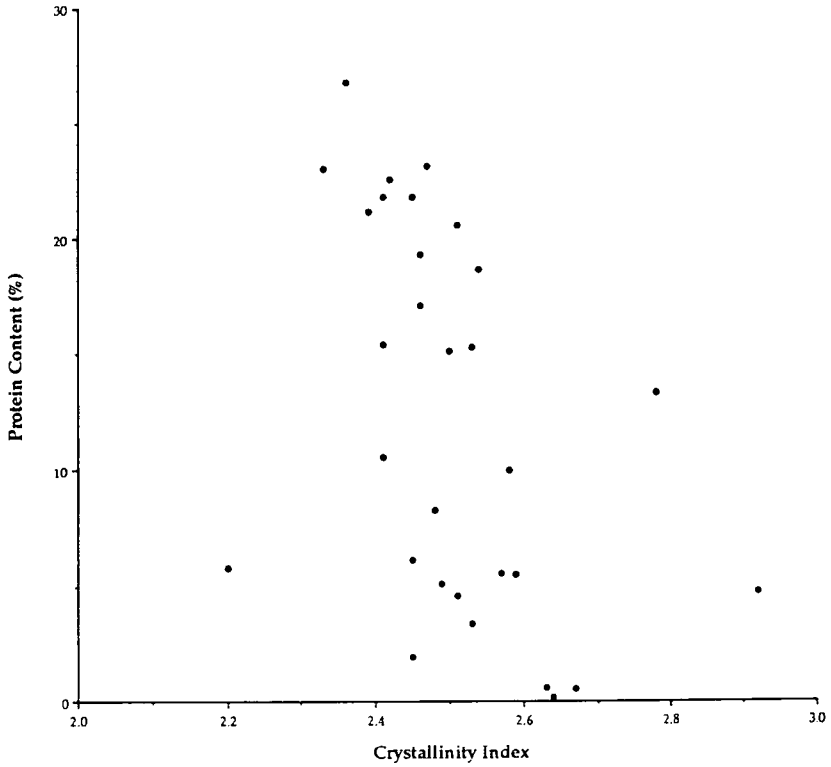

Figure 6.11 Plot of protein content vs crystallinity index (Samples 1 to 32)

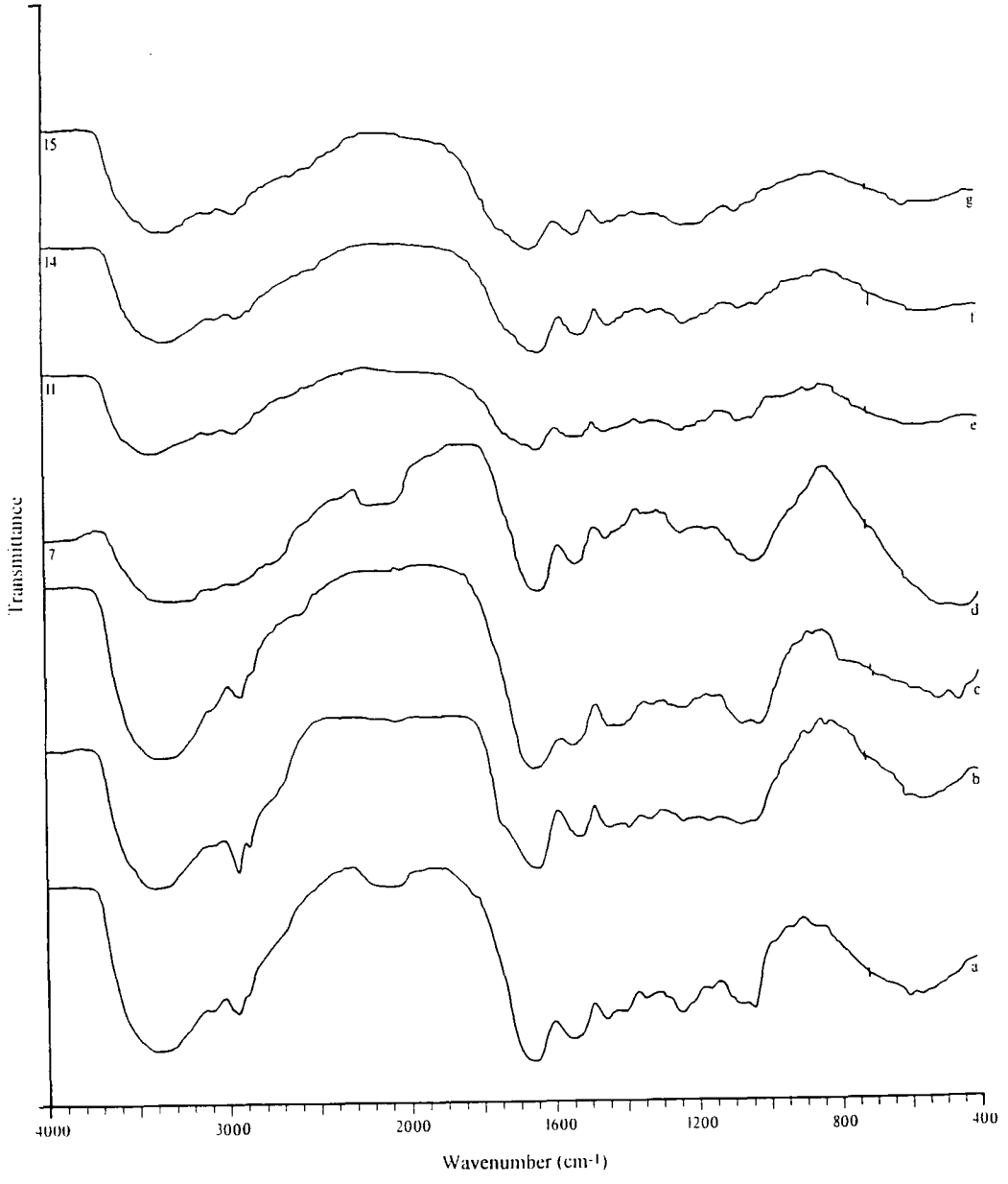

Figure 6.12 Infrared spectra for: **a** collagen; **b** acid-insoluble fraction of fresh bone; **c** archaeological leather; **d-g** acid-insoluble fraction of fossil bones

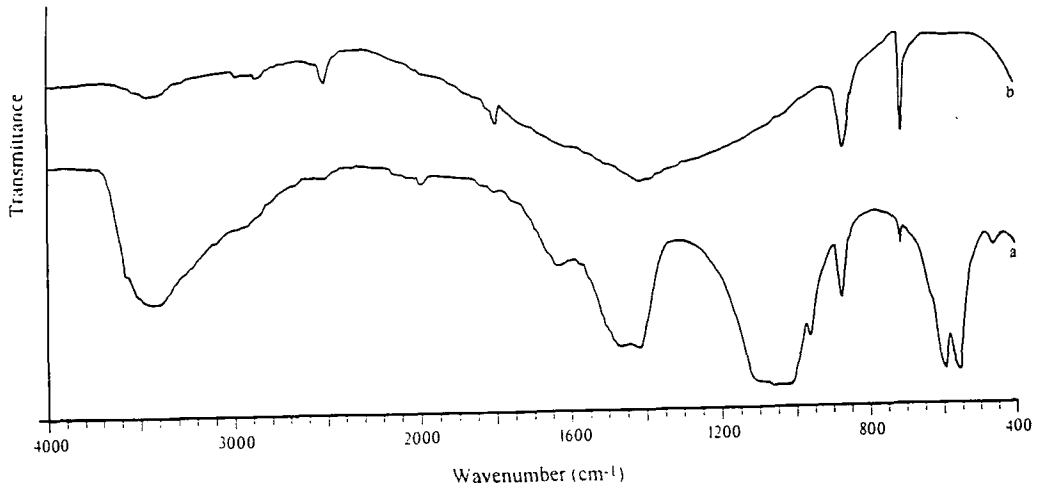

Figure 6.13 Infrared spectra for **a** Sample 9: **b** synthetic calcite

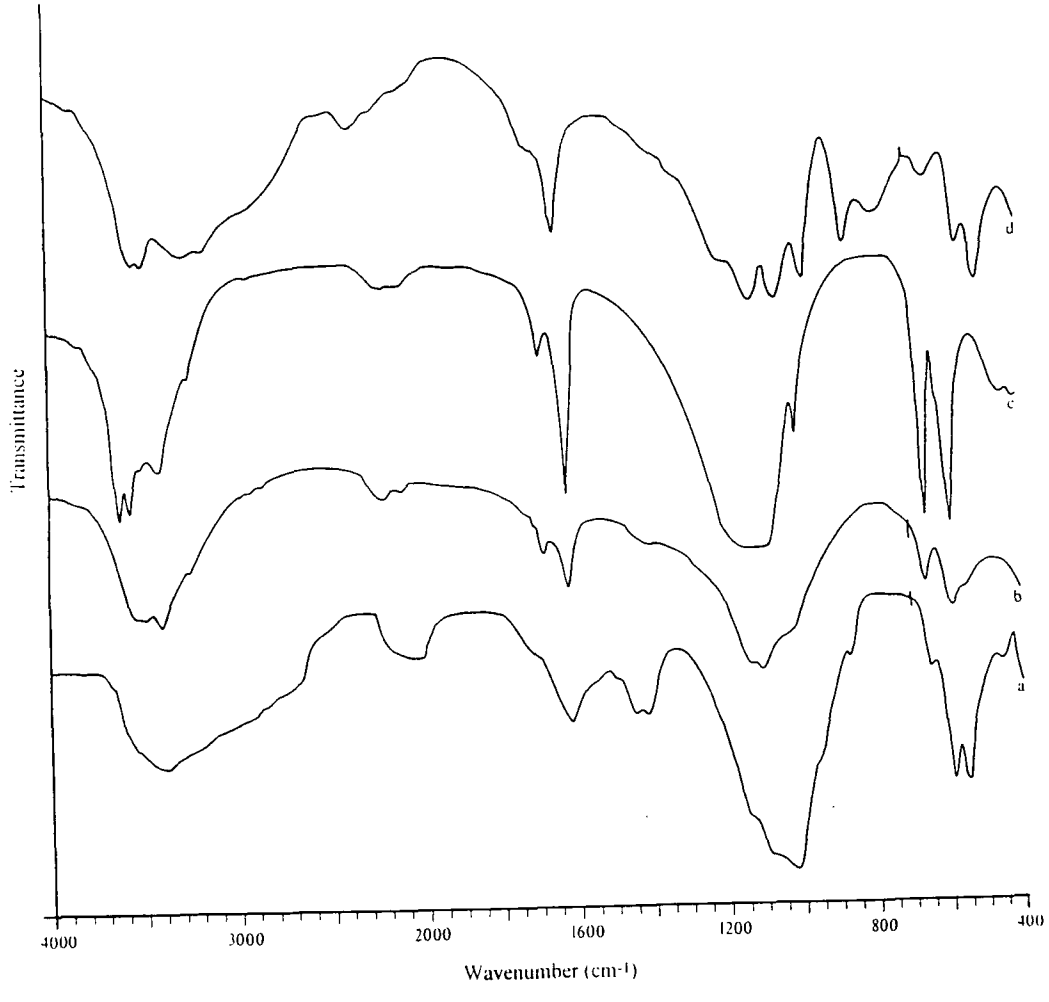

Figure 6.14 Infrared spectra for **a** Sample 22: **b** crystals from Sample 22: **c** synthetic gypsum: **d** synthetic brushite

7. Sorption of Water by Bone (Adsorption/Desorption Isotherms)

Organic materials such as wood, paper and leather are much more sensitive to atmospheric water vapour than inorganic materials, such as metals or ceramics, and can respond dramatically to changes in relative humidity (RH). Such materials, which have the ability absorb water from the air are termed *hygroscopic*. Absorption of water in organic hygroscopic materials is frequently accompanied by changes in the physical properties of these materials, such as dimensional changes, increase in flexibility and increased weight. The sensitivity to atmospheric water vapour arises from the polymeric nature of organic materials, the importance of hydrogen bonding to their structure, the polar nature of the organic molecules themselves and the natural porosity of most organic materials. This is true for undegraded materials (Stamm 1944) but the effects are considerably increased after chemical deterioration by light, water or microbial activity.

During life the structural elements of any organism, whether the cellulose walls of plant cells or the collagen network of skin and bone, are bathed in an electrolyte or other aqueous fluid, which in addition to performing roles essential for the life and growth of the organism also interacts with the surfaces of these structural elements. On death these electrolytes are removed, either intentionally as in the case of leather tanning and the seasoning of wood, or incidentally as the discarded or buried material adjusts to a new environment.

Because of its obvious importance as a structural material, wood has been the focus of numerous studies into the protection and preservation of cellulosic materials. In the field of archaeological conservation there has been considerable work on the behaviour of degraded wood and leather since these materials are frequently preserved in waterlogged deposits and invariably exhibit disastrous shrinkage if allowed to air-dry in uncontrolled circumstances. These studies (Ambrose 1970; Christensen 1970; Laidlaw 1970; Stamm 1970; Barkman 1975; Rosenqvist 1975; Grattan 1981 and Bunn 1985) have concentrated largely on the problems of waterlogged wood and had two main aims:

> to understand the structure and behaviour of degraded organic materials at a molecular level
>
> and to devise conservation treatments to overcome the problems of shrinkage during drying.

It has been found that the shrinkage of waterlogged wood on drying is strongly correlated with the amount of water that the structure contains on excavation and that this in turn is related to its degree of degradation at a cellular and molecular scale.

Bone is clearly a very different type of material to either wood or leather, being a composite composed of inorganic as well as organic structures. In contrast to leather and other collagenous materials (parchment, wool *etc.*) within bone the collagen fibres are surrounded by apatite crystallites that limit the access of water vapour and constrain any dimensional changes in the bone matrix. Despite its rigidity, fresh bone can take up a considerable quantity of water when exposed to high humidities and this capacity appears to increase after prolonged burial.

Lafontain and Wood studied the response of ivory (both elephant and walrus) to changes in atmospheric moisture by monitoring the changes in relative weight and dimension over time and at different relative humidities (Lafontain & Wood 1982). Similar experiments to investigate the behaviour of degraded bone and related materials when exposed to different relative humidities are described below. These experiments hoped to achieve two ends;

> to investigate and account for the behaviour of bone when exposed to water vapour
>
> to determine if this behaviour could be exploited to quantify the condition of archaeological bones.

7.1 Principles of Vapour Adsorption by Solids

Absorption of water by any substance is a general term which describes the ability of a material to hold water, usually liquid water, within its structure. Sponges are able to *absorb* water but this statement makes no attempt to describe the mechanism or mechanisms involved, *e.g.* does water react reversibly with the sponge substrate to form a different chemical compound or is it merely physically held within its pores? Chemists use the term *adsorption* to describe the reaction between molecules of a gas or vapour (the adsorbate) and the surface of a solid or *adsorbent*. Since it is not always possible to distinguish between adsorption and absorption by experiment, the general term *sorption* is sometimes used to describe the uptake of gas by solids. The amount of gas that a solid can hold (when in equilibrium) depends upon the nature of the sorption, the pressure of the surrounding vapour and the temperature. Graphs that illustrate the variance of amount adsorbed with the pressure of the surrounding gas at constant temperature are called adsorption *isotherms*.

There have been a number of attempts made to develop mathematical expressions and theoretical models to explain the observed adsorption phenomena. The three principle equations, proposed by Freundlich, Langmuir and the group comprising Brunauer, Emmett and Teller all assume equilibrium conditions where a vapour at constant pressure is in dynamic equilibrium with that adsorbed onto the adsorbent surface (Brunaur *et al.* 1938; Shaw 1968, 112-114). The resulting equations are solved for the volume of gas adsorbed, V and the pressure P of the surrounding vapour.

The Freundlich or classical adsorption isotherm is described by the empirical equation

$$V = kP^{1/n}$$

where k and n are constants. Taking logarithms this may be expressed

$$\log V = \log k + \frac{1}{n}\log P$$

This predicts a logarithmic relationship between the volume of gas adsorbed and the pressure (or partial pressure) of gas above the adsorbent surface.

In a dynamic situation where the adsorbent surface and the surrounding vapour are not in equilibrium the rate of change in the volume of adsorbed gas at any time depends upon the rate of adsorption, the rate of desorption and the number of available adsorption sites. If the temperature and pressure of the vapour surrounding the adsorbent surface are constant then the rate of adsorption is also constant since the number of molecules striking the adsorbent surface per unit time is constant. However, the rate of desorption from the surface will increase and the number of available adsorption sites decrease with increase in the volume of adsorbed gas.

For the sake of simplicity, it is assumed that all those gas molecules that strike the adsorbent surface are adsorbed, *i.e.* the sticking probability, s, defined as :

$$s = \frac{\text{rate of adsorption of molecules}}{\text{rate of collision of molecules}}$$

is one (Atkins 1982, 1021). It is also assumed that the adsorbed molecules form a monolayer and that once an adsorption site is filled then it becomes unavailable for further adsorption. For unit area of bare adsorbent surface with total number of available sites N_0 and a rate of impacts per unit area of k_i, then after a time interval dt the number of sited occupied by adsorbed molecules is:

$$dN = k_i . dt$$

or

$$\frac{dN}{dt} = k_i$$

this may be integrated to give the number of sites occupied after time t as:

$$N_t = \int_0^t k_i$$

$$N_t = N_0 . e^{kit}$$

Since the number of sites occupied is equivalent to the molar volume of the adsorbed gas, this may be expressed:

$$m \propto \log_e k_i t$$

where m is the weight of adsorbed gas.

Slight variations from this idealised behaviour can be explained by the fact that the sticking probability is rarely equal to unity and for many solids several hundreds of collisions may be needed before one molecule is adsorbed. It is also clear that multi-layer adsorption is probable, especially in the case of adsorption of polar molecules such as water.

Adsorption isotherms may be classified according to their shapes, which are in turn dependant upon the mechanism by which gasses are adsorbed onto the substrate. Brunauer's classification of adsorption isotherms (taken from Shaw's Introduction to Colloid and Surface Chemistry, 1968) is shown in Figures 7.1a & 7.1b. Type II isotherms result from the physical adsorption or *physisorption* of gas onto the substrate (Moore, 1972) in which the forces involved are restricted to relatively weak, van der Waal's forces and there is no chemical reaction between the gas and substrate. Physical adsorption is therefore considered to be reversible. Nitrogen gas on silica is an example of physisorption. In the case of chemical adsorption, or *chemisorption*, a chemical bond forms between the adsorbed gas and the adsorbent. These reactions involves much stronger forces such as those in the chemisorption of oxygen on charcoal. Chemisorption generally produces Type I isotherms, although Type I isotherms have also been found for physical adsorption on solids which contain a very fine pore structure (Shaw 1968, 109). Type III and Type V isotherms show no initial rapid uptake of gas molecules and occur when the forces involved in the first monolayer are small. Such isotherms are rare for most solids. Type IV isotherms tend towards a maximum value before the saturation vapour pressure and are considered to reflect capillary condensation in porous solids.

The van der Waal's forces involved in physisorption are undirected and relatively non-specific. They ultimately lead to condensation of vapour to liquid on the surface of the substrate and there may be several superimposed layers of adsorbate (in this case water molecules) on the surface before this condensation occurs.

Three phenomena may therefore be involved in physical adsorption:

monomolecular adsorption

multimolecular adsorption

condensation in pores and capillaries.

Physisorption often produces Type II isotherms which result from either multilayer adsorption on non-porous solids or microporous solids. In the case of microporous solids the point B in Figure 7.1b represents both monolayer adsorption on the surface as a whole and condensation in fine pores. The remainder of the curve represents multilayer adsorption as for non-porous solids.

7.2 Materials and Methods

A range of related materials was selected for investigation to determine those physical or chemical characteristics that determine the hygroscopicity of bone both before and after burial. The samples selected included:

fresh (washed and de-fatted) bovine bone

fresh (washed and de-fatted) bovine collagen

hydroxyapatite (synthetic)

archaeological bone

archaeological leather.

In their raw states the samples exhibited a wide range of available surface areas. For example, the hydroxyapatite was in the form of a fine powder whereas the bone and leather samples were irregular solids with undefined surface areas and pore volumes. To overcome this problem and to reduce the number of potential variables the samples were all reduced to a finely divided powder. The archaeological bone samples could be hand-ground to fine powder in a pestle and mortar. Fine sawdust from fresh bone was collected for the experiments since this proved impossible to grind. Both the bovine collagen and the archaeological leather were shredded in an electric grinder and the shorter strands of the resulting fibrous mass selected for use in the experiments.

The relationships between the mass of water absorbed and two separate variables were investigated by two groups of experimental procedures. For one group the partial pressure of water vapour in the air (equivalent to the relative humidity) was kept constant and the weight gain over time was monitored. For the second group, samples were allowed to come into equilibrium with different

atmospheres whose relative humidities were constant and known. In this way the dependence of adsorbed water content with RH was determined.

The experimental method in both cases were essentially very simple. Plastic petri dishes and lids were individually labelled and weighed before addition of the powdered samples that were spread evenly to a depth of approximately 5mm. These were then placed, on their lids, in an airtight polyethylene box whose atmosphere was maintained at approximately 0% RH by the presence of 750g of oven-dried silica gel. Silica gel is a common desiccant and when dried at 105°C is generally considered to maintain an enclosed volume of air at less than 5% RH. The dry weights of the samples were taken to be their masses after there was no further loss in weight. All weight measurements were made using a Mettler P161 electronic balance which was switched on 30 minutes before any weights were recorded to allow it to stabilize. On removal from their sealed environments, all samples were quickly covered by their plastic lids to minimise adsorption or desorption during the weighing procedure. The two different experimental regimes are described below.

7.2.1 Water Uptake vs Time

In this group of experiments the rate of water uptake of the sample materials was monitored by the increase in weight of the samples when transferred from equilibrium at 0% RH to an atmosphere saturated with water vapour (100% RH). The petri dishes containing the samples were transferred to an airtight plastic box containing approximately 150ml of distilled water. An empty plastic petri dish was also included as a control to determine if there was any increase in weight due to the adsorption of water on the surface of the plastic. A galvanised wire platform suspended above the base separated the petri dishes from the reservoir of water that covered the bottom of the box to a depth of approximately 5mm. Each sample was weighed every hour for the first eight hours then every two hour up to fourteen hours. Subsequent measurements were taken at increasingly long intervals as the samples approached equilibrium.

When the samples had reached equilibrium with this water vapour saturated atmosphere (indicated by zero or negligible increase in weight) they were transferred again to the box containing dried silica gel and the subsequent losses in weight monitored in a similar fashion to that described above.

7.2.2 Water Uptake vs Relative Humidities

In the second group of experiments small, lidded plastic dishes containing collagen, archaeological leather, synthetic hydroxyapatite and three different samples of archaeological bone (including sample 7 and sample 9) were allowed to come into equilibrium with atmospheres of different relative

humidities. The water uptake was again monitored by an increase in the weight of each sample. Environments of different relativities were provided by a number of Stewart plastic boxes. each containing approximately 450g of silica gel that was pre-conditioned to a particular relative humidity. The size of the box was selected to keep the volume of air above the silica gel to a minimum thereby reducing losses on opening the box to monitor the weights of each sample and maintaining a constant RH for each environment.

The relative humidity of the atmosphere within each box was measured by inserting a combined humidity and temperature probe (Vaisala HM 34. humidity and temperature meter) through a 10mm hole in the end of each box. This hole was sealed by a small rubber bung between measurements. Both humidity and temperature were recorded before opening the boxes to remove the sample dishes for weighing.

When each sample maintained a constant weight, indicating that it had come into equilibrium with the water vapour in the sealed environment, all six samples were transferred into a different box. conditioned to a higher relative humidity.

7.3 Results

It was quickly demonstrated that the plastic dishes did not gain weight as a consequence of storage at high relative humidities, nor was there any visible deterioration in the surface of the plastic that may have suggested a chemical reaction between the polystyrene and water. It was therefore assumed that any weight increase in each sample was due to absorption of water from the atmosphere in the sealed box. In those samples with a high organic content (the fresh collagen and fresh bone) mould could be identified on their surfaces after prolonged exposure to high relative humidities. These mould colonies. recognisable initially as circular patches of white filaments, later became darker areas from which fruiting bodies developed. Visible proliferation of these discoloured areas was accompanied by an additional increase in the weight gain of those samples affected following a period during which their weights had almost stabilized.

Results from the experiments described above are shown in the graphs below. In these results. water adsorbed or desorbed by the samples is expressed according to the following formulae:

$$\text{percentage water adsorbed or desorbed} = \frac{(w_t - w_0) \times 100}{w_0}$$

where w_0 is the weight of the sample at 0% RH and w_t is the weight after time t, and

$$\text{percentage water adsorbed or desorbed} = \frac{(w_{RH} - w_0) \times 100}{w_0}$$

where w_0 is the weight of the sample at 0% RH and w_{RH} is the weight at equilibrium with a particular RH.

Figures 7.2 to 7.4 illustrate the results of the water adsorption experiments. In these graphs the slopes of the curves represent the rate of water adsorption. The curves for collagen and bone (both fresh and archaeological) demonstrate that there is an initially rapid uptake of water after initial exposure to increased humidity, followed by a decrease in the rate of adsorption until a maximum is achieved. In the water adsorption behaviour for fresh bone and fresh collagen (Figures 7.2a and 7.3b respectively) there is a slight 'kick' in the curve as it approaches a maximum value due to the growth of mould on the surfaces of the samples. The water desorption results are illustrated in Figures 7.5 to 7.7. All the desorption curves show a trend similar to that of the adsorption behaviour of the organic samples. The water adsorption and desorption results for the bone and collagen samples (fresh and archaeological) are in excellent agreement with the results obtained by Lafontain and Wood (1982 Figure 2 and Figure 3) for the adsorption of water by walrus ivory. Their results are reproduced in Figure 7.8 and Figure 7.9.

The equation derived in section 7.2 to describe the mass of adsorbed gas as a function of time:

$$m \propto \log_e k_i t$$

predicts a logarithmic relationship between water uptake and time. If the adsorption results are plotted with time on a log. scale, a linear relationship can be seen, demonstrating that the observed behaviour is close to that predicted by the theoretical model.

Comparing the water adsorption curves in Figures 7.2 and 7.3 it is clear that there are differences in the rate of water adsorption and quantity of water adsorbed between fresh and archaeological adsorbents. In the case of the archaeological leather sample, this difference can be accounted for by part of the total mass of the sample represents inorganic matter such as fine soil particles and oxides of iron and manganese. Certainly the archaeological leather was heavily stained and upon ashing left a considerable ash residue. Inclusion of this inert matter effectively reduces the percentage weight change by increasing w_0. The difference between the fresh and archaeological bone samples

is more complex because more factors are involved. In Figure 7.2 the archaeological bone adsorbs more water than the fresh bone. This may be because loss of bone collagen by hydrolysis has increased the available surface area of the apatite crystallites or because the action of micro-organisms has increased the diameters of the capillaries allowing them to hold a greater volume of water.

The adsorption behaviour of synthetic hydroxyapatite (Figure 7.4) is very different to that of bone and collagen. The hydroxyapatite sample continues to adsorb water over a long period without showing any tendency to reach a maximum. This sample adsorbed as much as 65 percent of its dry weight in water over a period of 3000 hours, after which time the adsorption cycle was bought to an end. When the water adsorption as a function of water vapour pressure (relative humidity) for the hydroxyapatite sample was analysed, this too was very different from the other samples. The interpretation of these differences will be discussed later.

Adsorption and desorption curves for the bone samples are plotted together in Figures 7.10 and 7.11. In these graphs the desorption curves have effectively been inverted by substituting (700-t) for t on the horizontal axis and (M_{final}-M_t) for M on the vertical axis. These samples exhibit adsorption hysteresis, *i.e.* the desorption curve does not follow the same path as the adsorption curve. Capillary condensation theory provides an explanation for this observed adsorption hysteresis in the behaviour of bone and collagen which also displays this phenomenon.

It is known that the vapour pressure over a convex liquid surface is greater than that over the corresponding flat surface. This is a surface tension effect and for a curved surface with principle radii of curvature r_1 and r_2 the pressure difference is given by the Laplace-Young Equation:

$$dP = y\left(\frac{1}{r_1} + \frac{1}{r_2}\right)$$

which for a spherical surface reduces to

$$dP = \frac{2y}{r}$$

where y is the surface tension of the liquid and r is the radius of the surface (Shaw 1968, 51). This can be applied to a concave capillary meniscus, in which case the radius is negative and dP is also negative, *i.e.* a vapour pressure lowering is predicted. A liquid that wets the wall of a capillary will have a concave liquid-vapour interface and, consequently, a lower vapour pressure. Condensation can therefore take place in narrow capillaries at lower vapour pressures than the normal saturation vapour pressure. It was suggested by Zsigmondy in the early 1900's that this phenomenon may also

apply to microporous solids. Capillary forces in these solids may be assumed to be so great that pores are either filled or empty, though it is probably the case that an adsorbed monolayer of liquid covers the pore surface before condensation occurs. When liquid is advancing over a dry surface (adsorption) the contact angle is greater than that during retreat or desorption, i.e. the liquid-vapour interface surface will be more concave during desorption than adsorption and the value of r will be smaller. From the Laplace-Young equation it is clear that the pressure difference dP is inversely proportional to r and that as a consequence the difference in vapour pressure across the surface of a capillary meniscus will be greater during desorption than that during adsorption. Molecules will therefore leave the liquid surface more readily and the rate of desorption will be greater than the rate of adsorption.

Figures 7.10 and 7.11 graphically demonstrate that water is lost from bone that has been removed from an environment of high humidity to a low humidity much faster that it adsorbs moisture. It is therefore inevitable that these drying bones have a steep gradient in moisture content between the interior and the drying surfaces. This situation has important implications for the behaviour of drying bone regarding dimensional stability and movement of soluble ions. Lafontain and Wood (1968) demonstrated that there can be appreciable dimensional changes in ivory under conditions of different humidity. Their experiments demonstrated very effectively the detrimental effects of low RH conditions on both walrus and elephant ivory, which cracked severely under drying conditions. Their results also show that walrus ivory exhibits hysteresis in its water adsorption/desorption behaviour when moved between environments of high and low RH (Figure 7.12).

Results from the second series of experiments, to investigate the water content of bone and related materials at equilibrium with different atmospheres are shown in Figures 7.13 to 7.18. Again there is a clear difference between those curves for bone and collagen and that for the synthetic hydroxyapatite. These graphs of mass of adsorbed gas (here expressed as percent of dry weight of adsorbent) plotted against RH (which is proportional to partial pressure of water vapour) are true adsorption isotherms. Figures 7.13 to 7.15 (the archaeological bone samples) represent Type IV isotherms, representing capillary condensation in porous adsorbents. This observation is in excellent agreement with the results of the previous experiments to monitor the rate of adsorption. In capillary condensation, the upper limit of adsorption is largely determined by the total pore volume (Shaw 1968, 110). The adsorption isotherms for collagen and leather (Figures 7.16 and 7.17) are of Type II and can be interpreted as multilayer adsorption on a non-porous adsorbent. The isotherm for synthetic hydroxyapatite is of Type III (Figure 7.18) and demonstrates that the energy involved in adsorption of the initial monolayer is small. This is consistent with the presence of a hydration layer of tightly bound water molecules even in dry specimens of hydroxyapatite. Results of infrared analysis of both hydroxyapatite and bone apatites suggest that water is present on the active sites of apatite crystallites even in oven dried specimens (see section 6.3).

Results of the experiments described above indicate that the dominant factor in the ability of bone to adsorb water from the atmosphere and the rate of adsorption is the nature of the samples porosity, rather than its chemical composition. Bone specimens with higher pore volumes can adsorb more water and at a faster rate. However, the dimensional stability of the bone and the possible migration or transformation of soluble salts do depend strongly on the chemical composition of the sample.

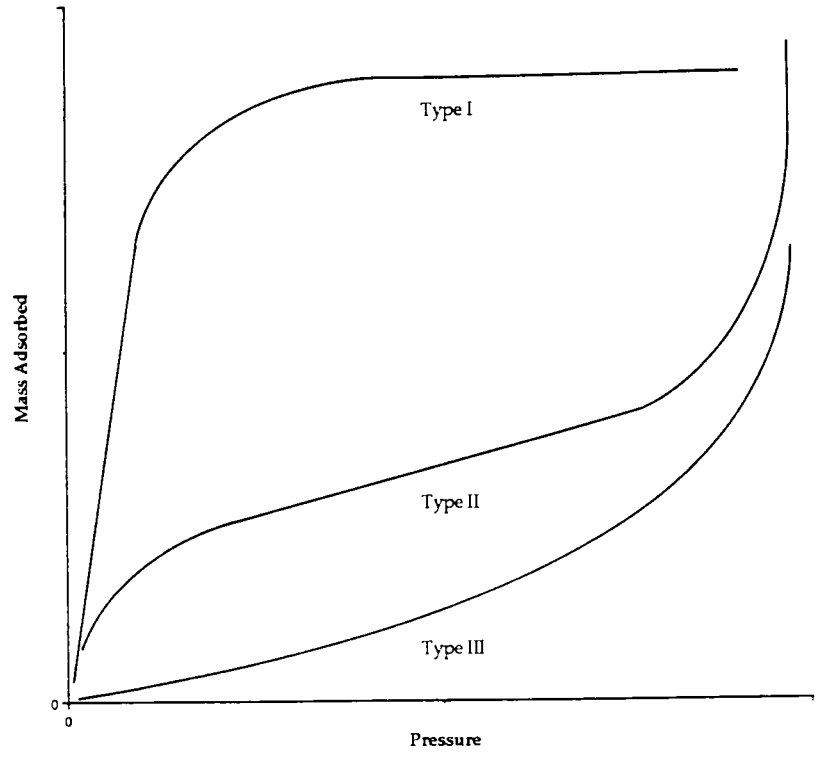

Figure 7.1a The forms of adsorption isotherms: Type I to Type III (taken from Shaw 1966)

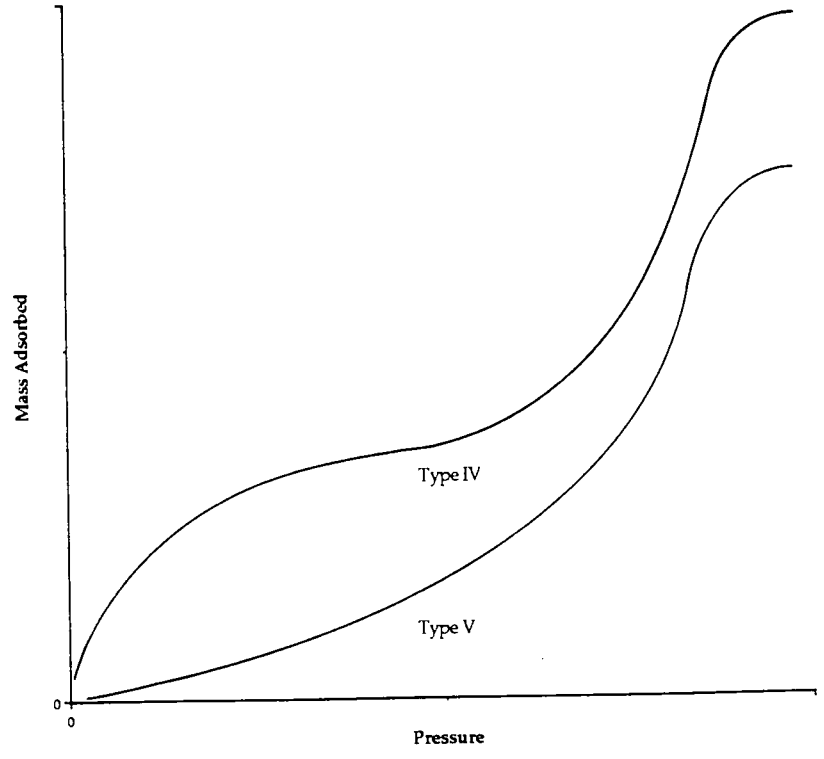

Figure 7.1b Adsorption isotherms Type IV and Type V

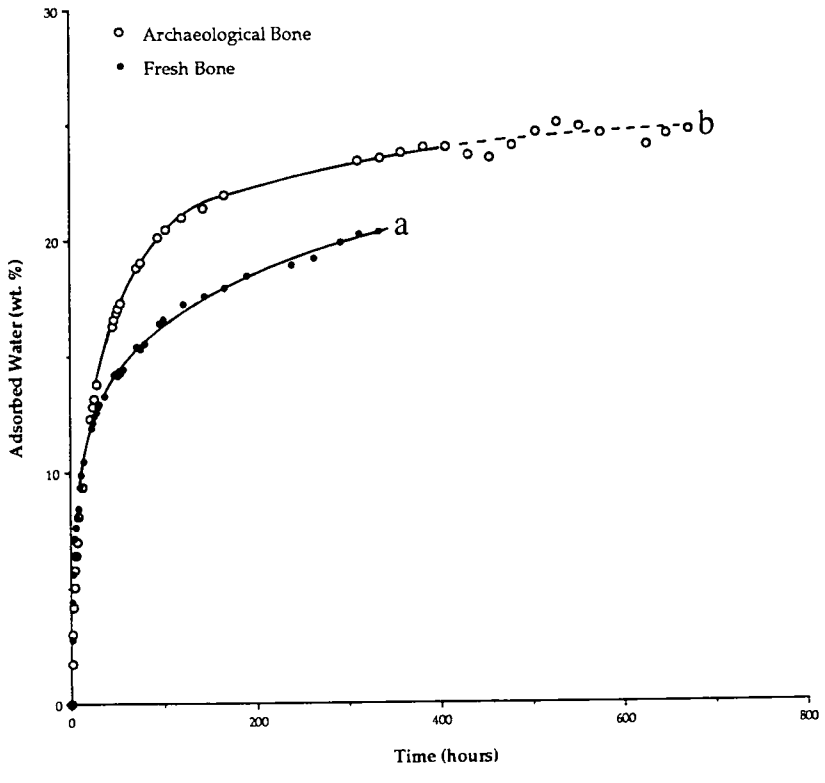

Figure 7.2 Adsorbed water vs time for fresh and archaeological bone

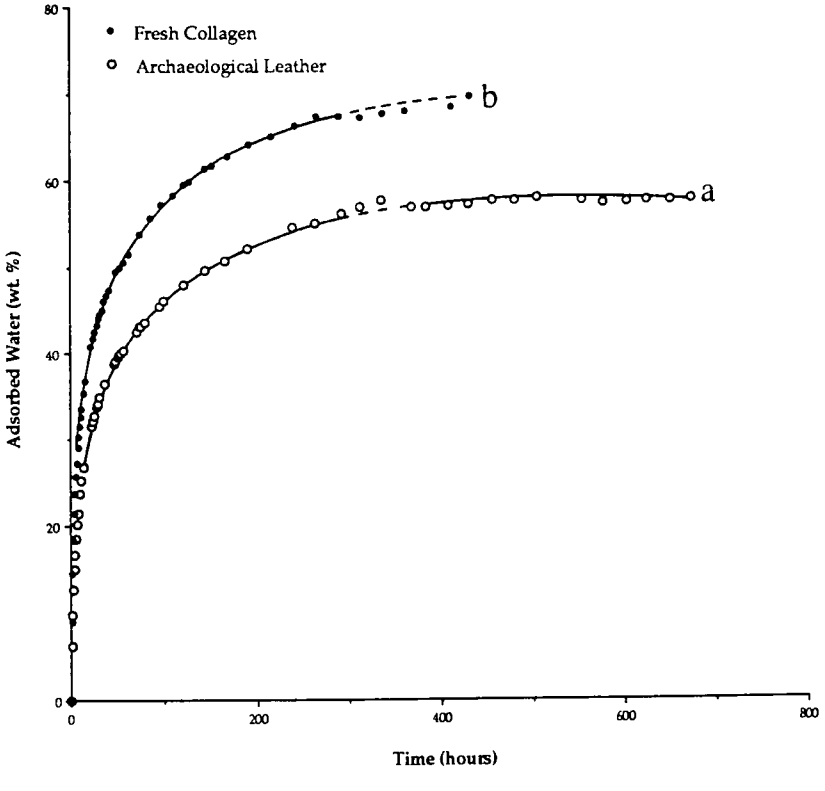

Figure 7.3 Adsorbed water vs time for collagen and archaeological leather

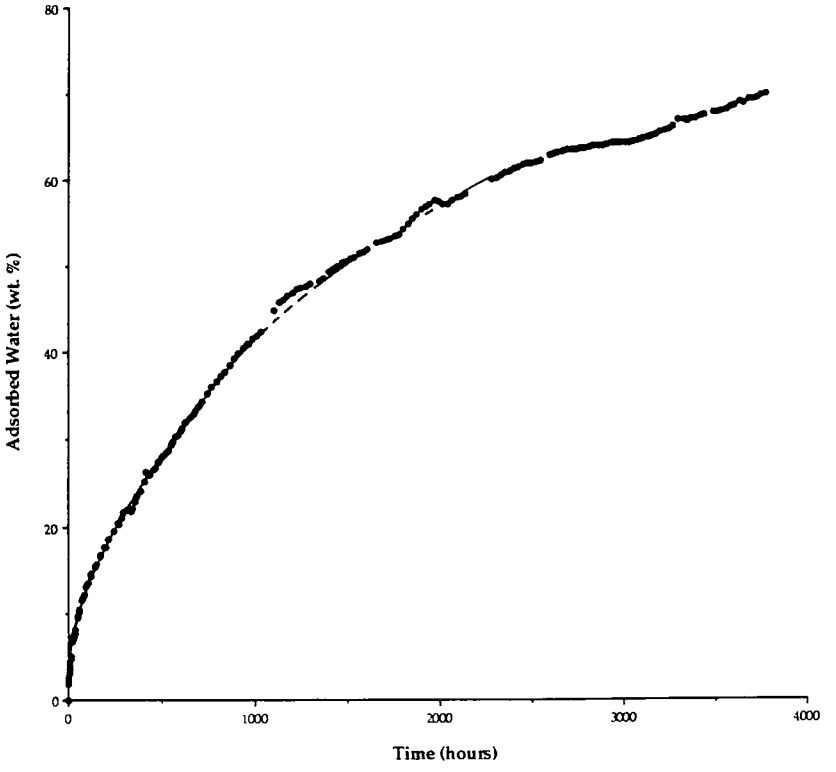

Figure 7.4 Adsorbed water vs time for synthetic hydroxyapatite

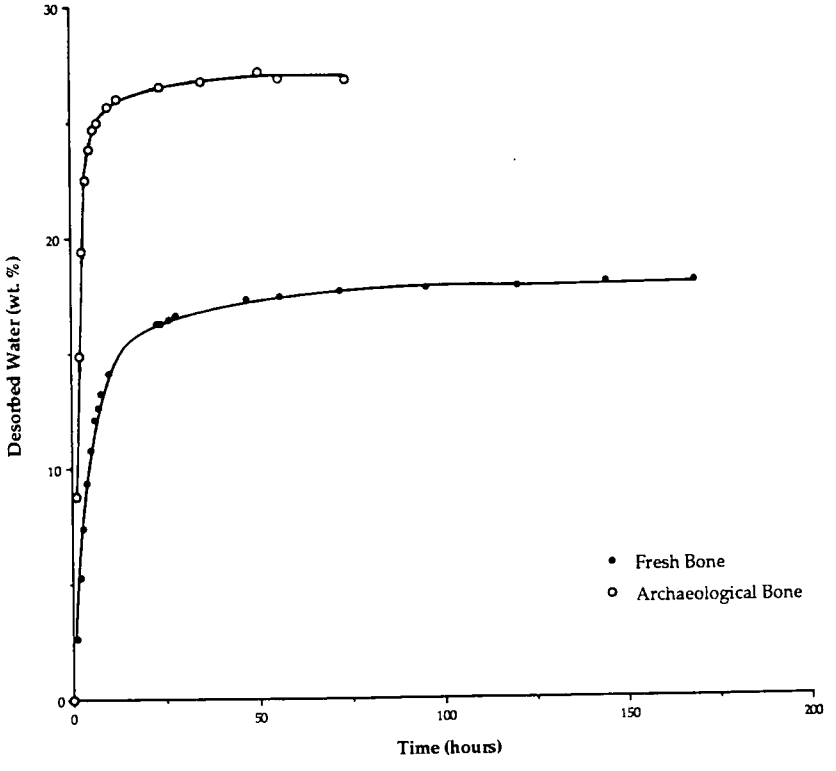

Figure 7.5 Desorbed water vs time for fresh and archaeological bone

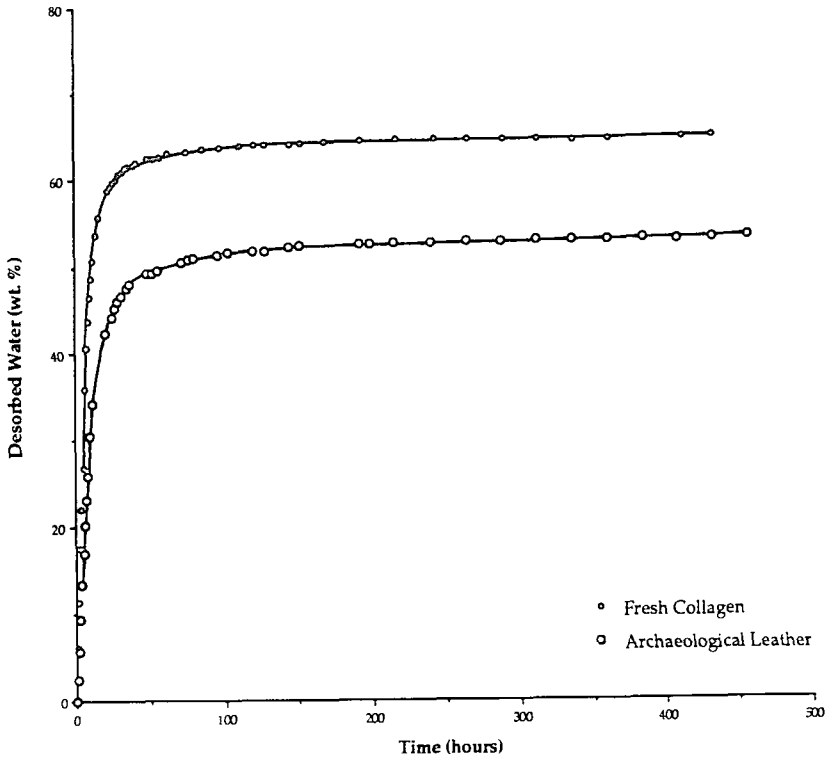

Figure 7.6 Desorbed water vs time for collagen and archaeological leather

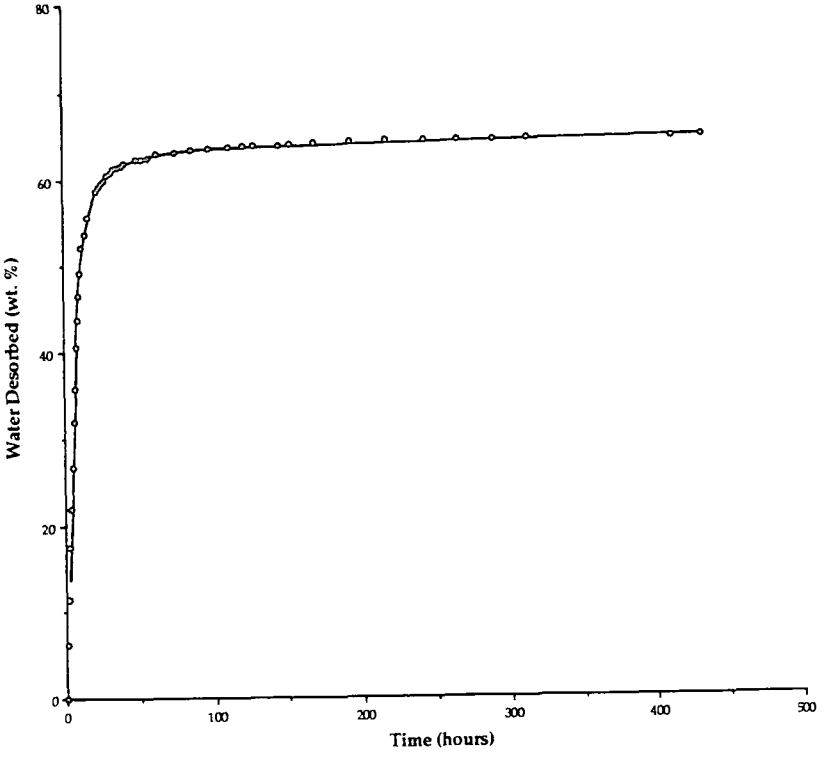

Figure 7.7 Desorbed water vs time for synthetic hydroxyapatite

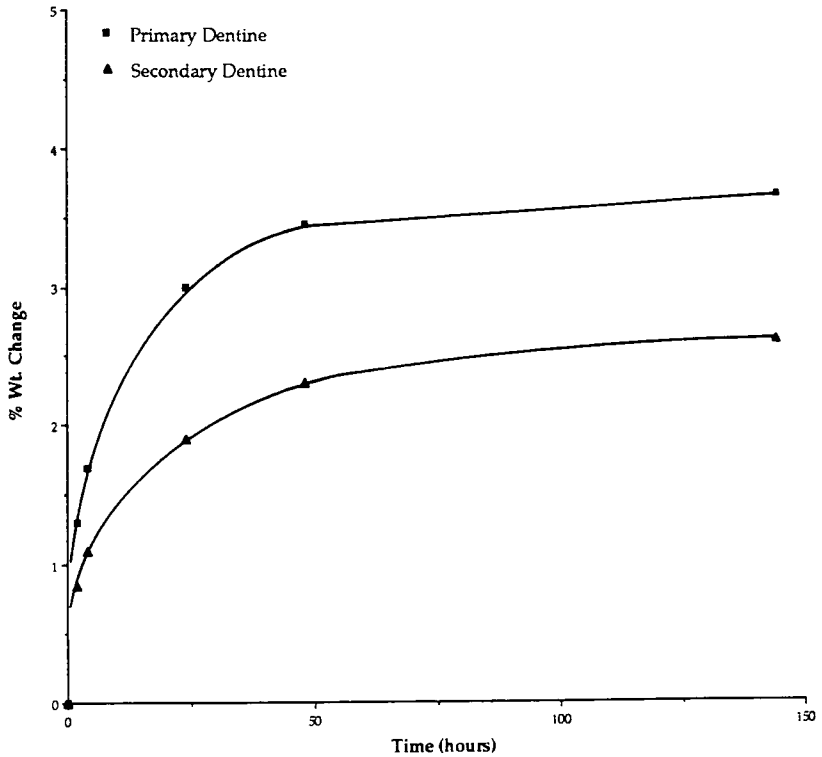

Figure 7.8 Adsorbed water vs time for walrus ivory
(after Lafontain & Wood 1982)

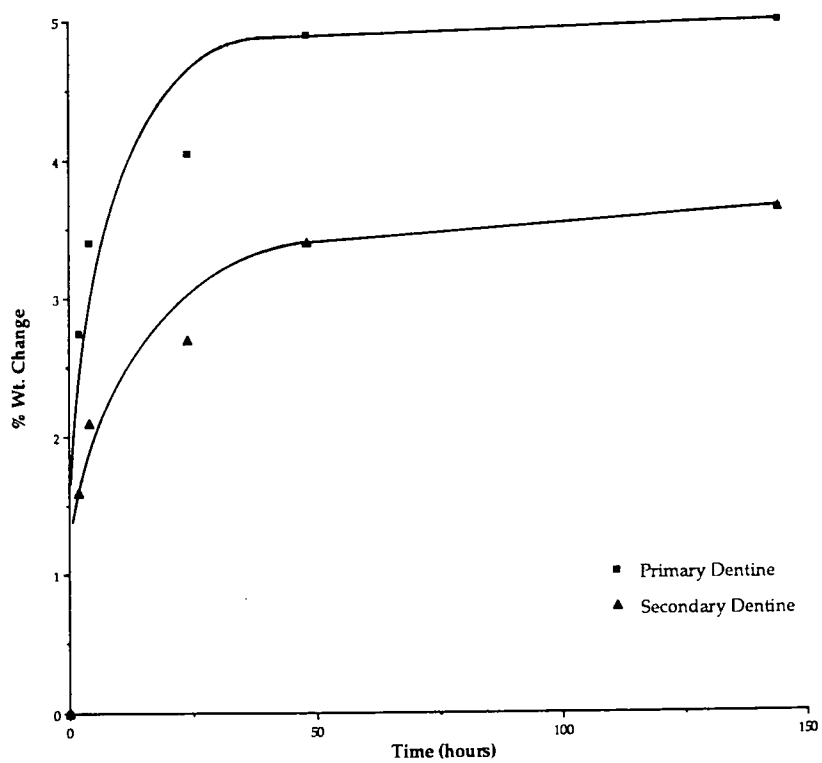

Figure 7.9 Desorbed water vs time for walrus ivory
(after Lafontain & Wood 1982)

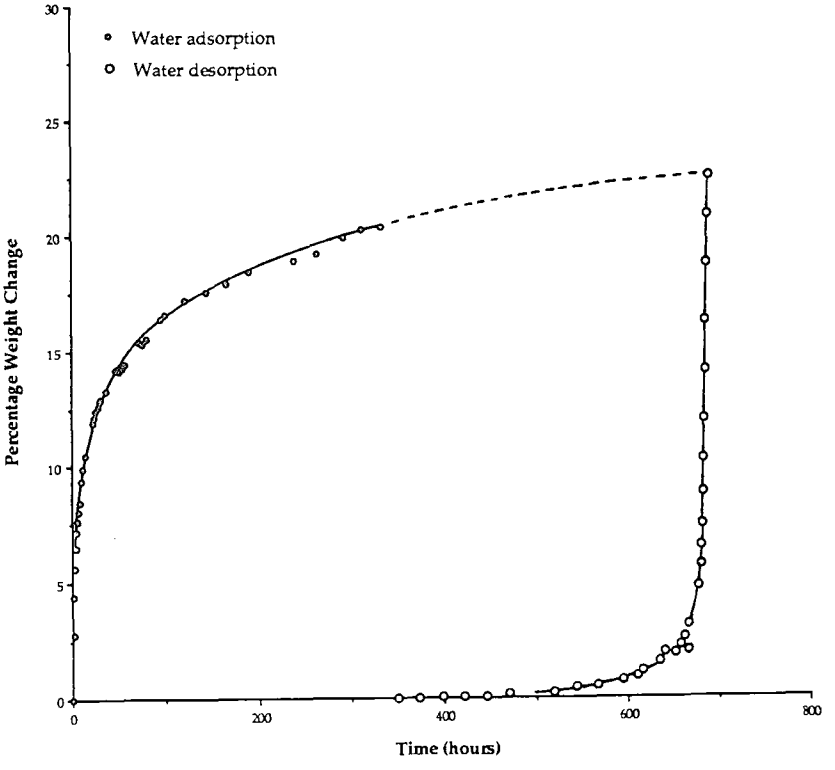

Figure 7.10 Adsorption/desorption curves for fresh bone

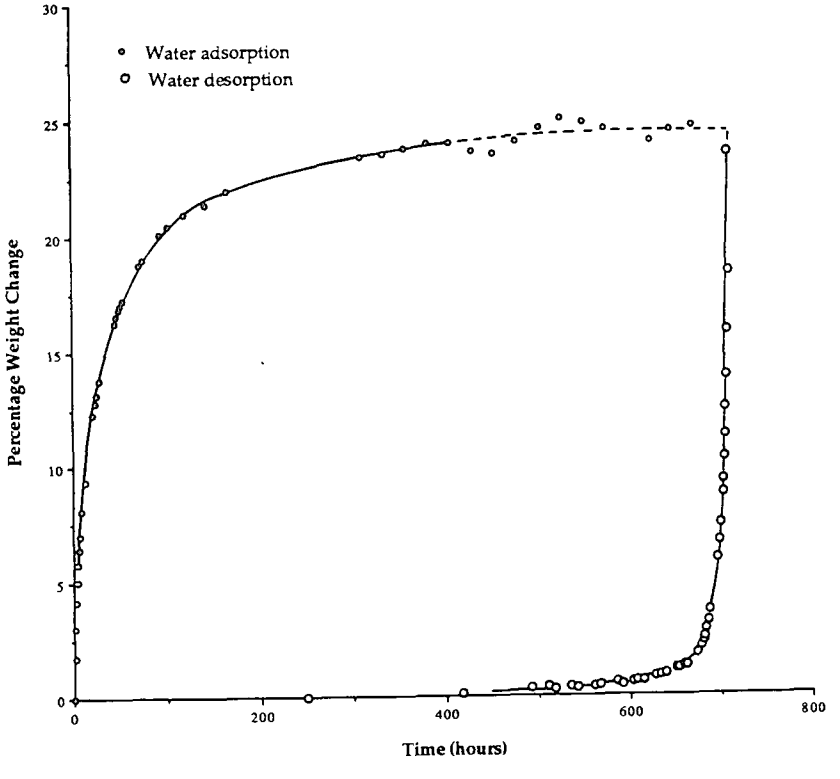

Figure 7.11 Adsorption/desorption curves for archaeological leather

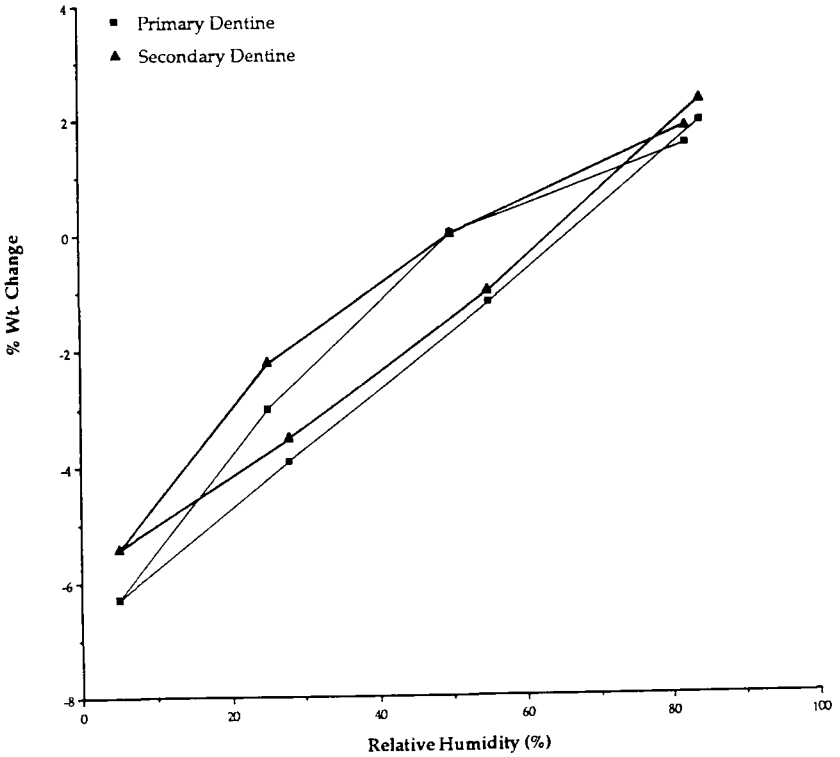

Figure 7.12 Adsorption/desorption vs RH for walrus ivory (after Lafontain & Wood)

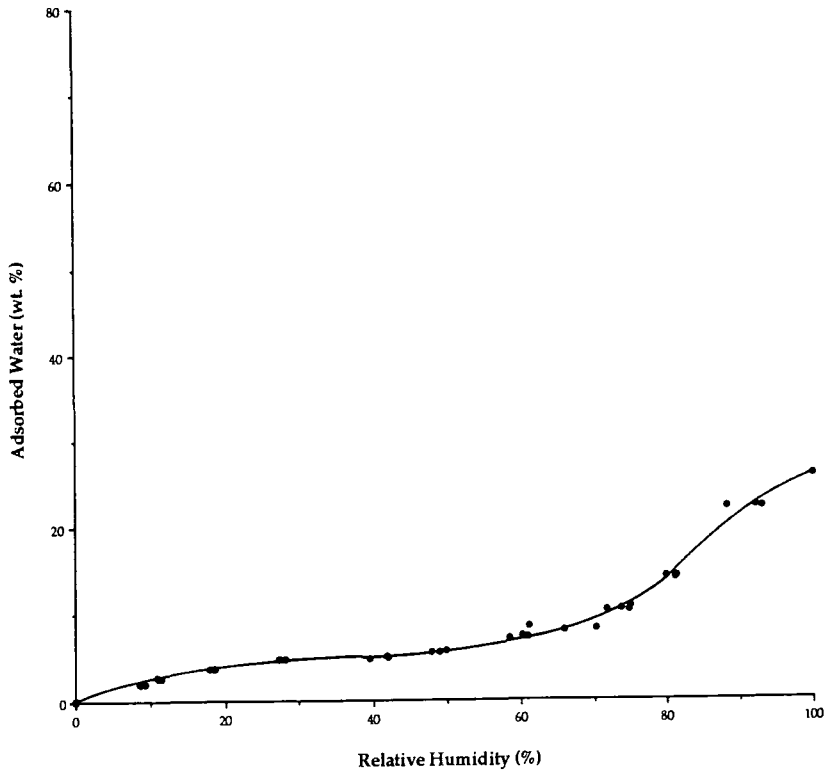

Figure 7.13 Adsorption vs RH for archaeological bone #1

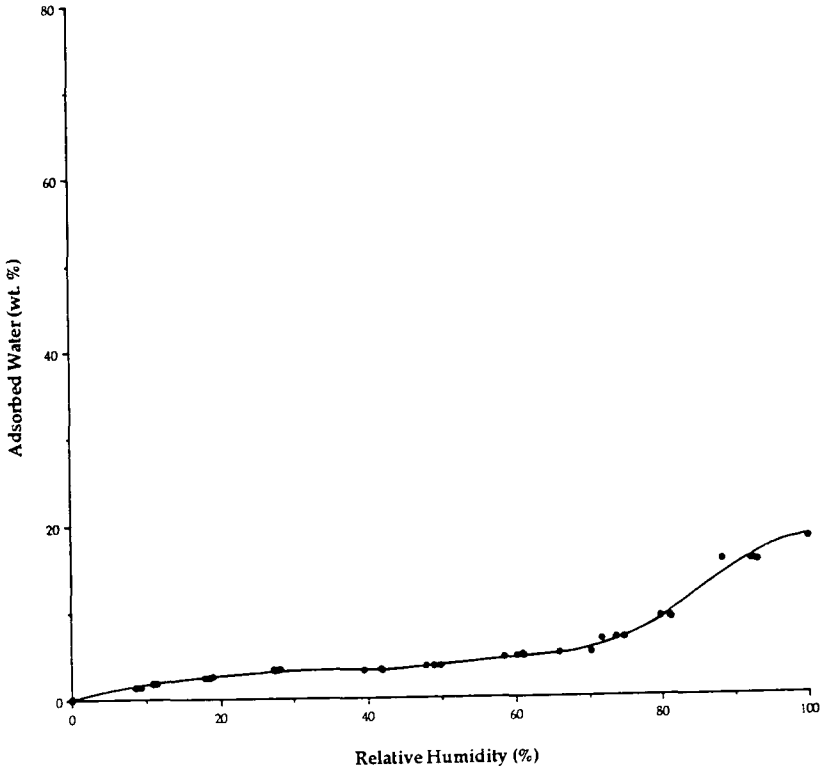

Figure 7.14 Adsorption vs RH for archaeological bone #2

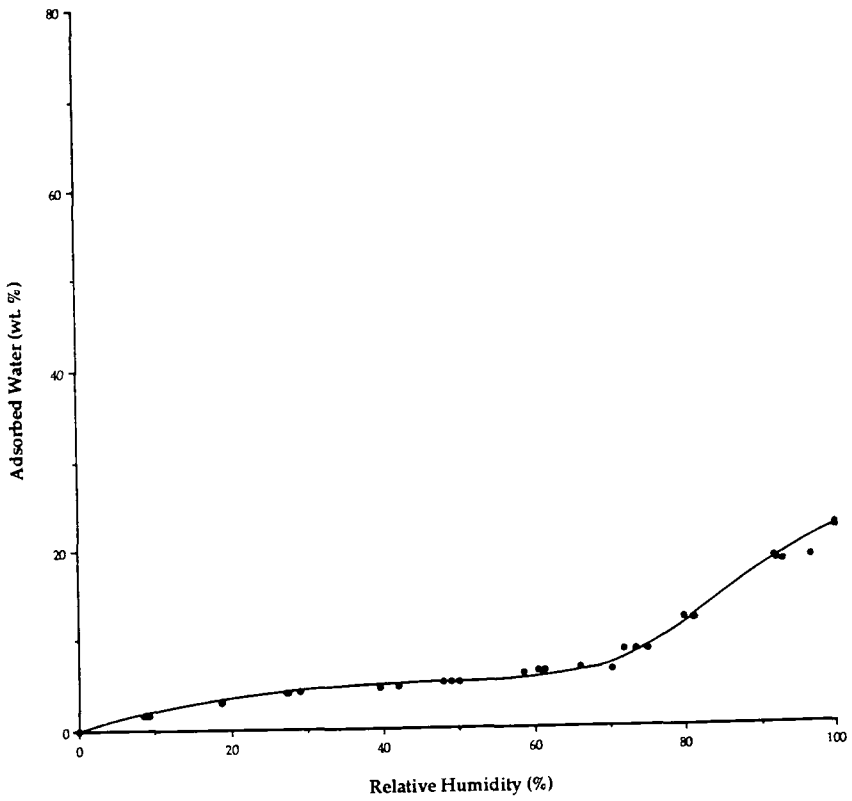

Figure 7.15 Adsorption vs RH for archaeological bone #3

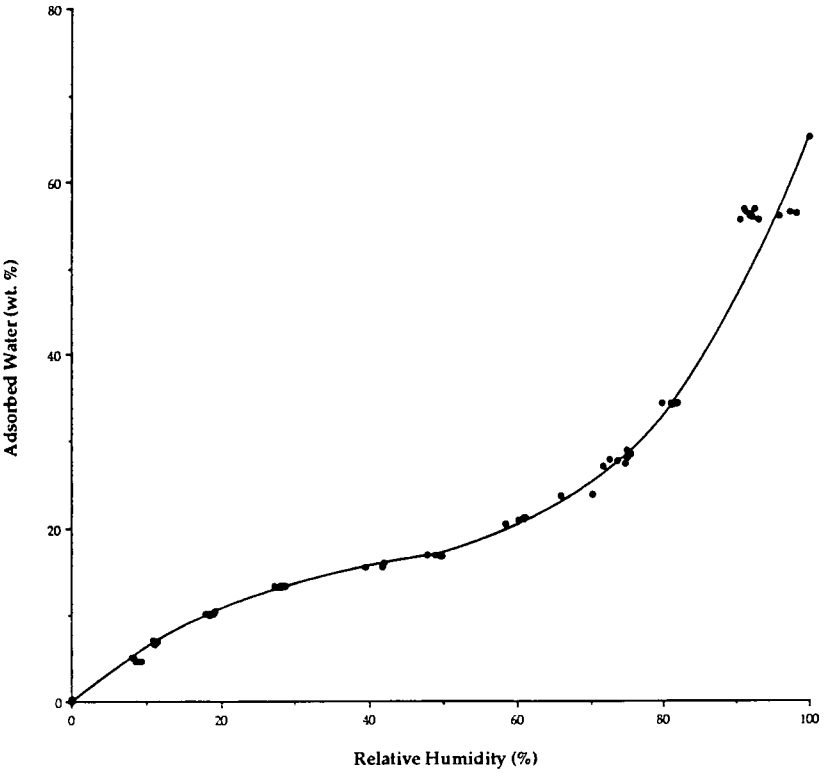

Figure 7.16 Adsorption vs RH for fresh collagen

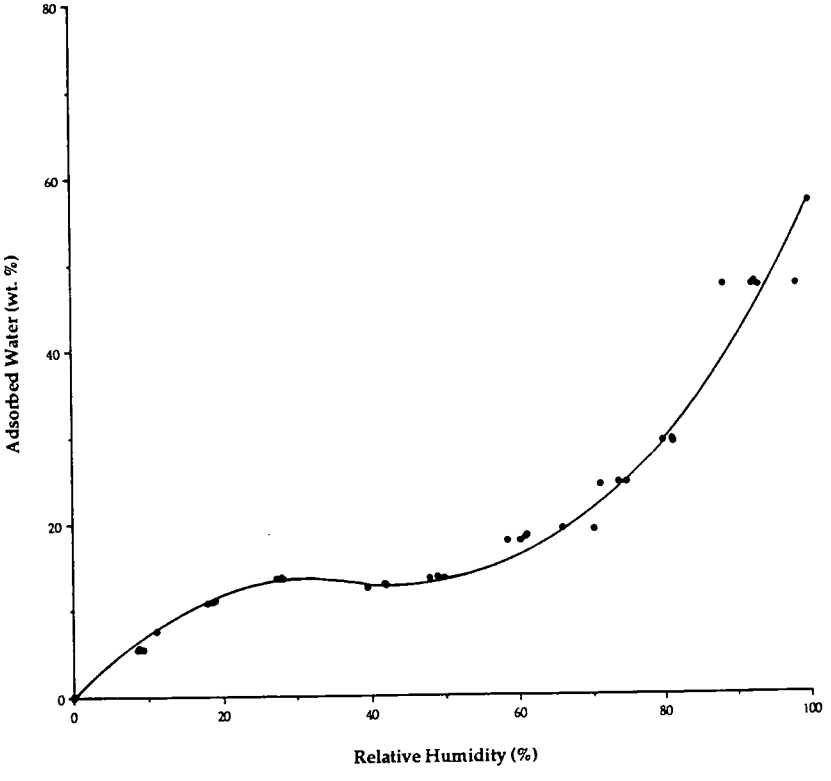

Figure 7.17 Adsorption vs RH for archaeological leather

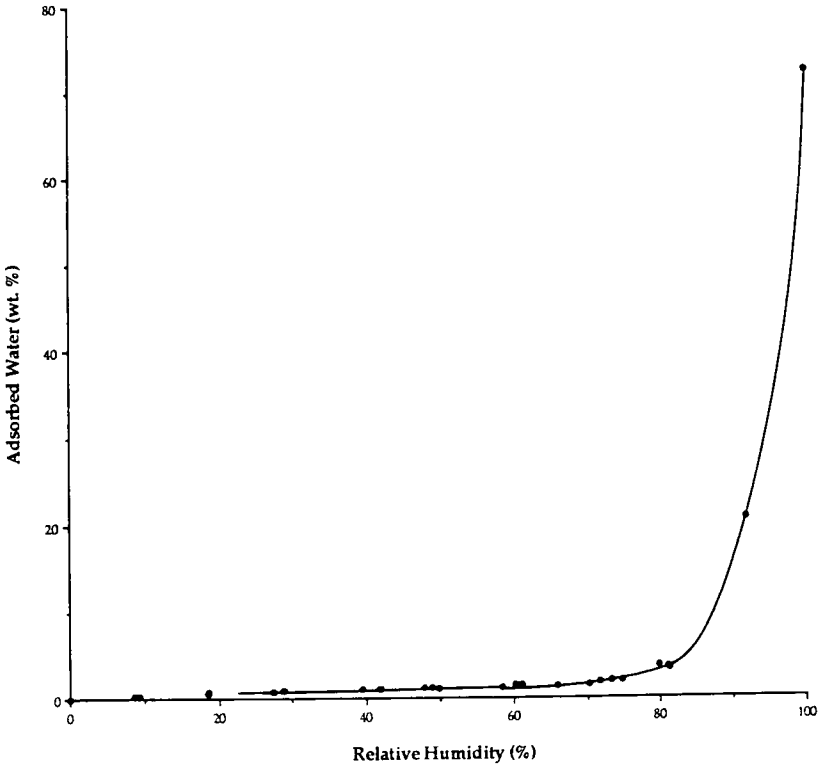

Figure 7.18 Adsorption vs RH for synthetic hydroxyapatite

8. The Tensile Strength of Fossil Bone

Although recent years has seen a rapidly expanding body of published work concerning the chemical composition and mineral nature of archaeological bone, there has been little investigation of its mechanical properties. Considering the wealth of potential information that can be recovered from ancient bone this is hardly surprising. Archaeological and fossil bones are known to preserve evidence of past diet, environment, date and genetic information (see Chapter 2). By comparison, studies of the mechanical properties of archaeological bone offer few rewards but are nevertheless important to obtaining an understanding of the survival of bone both in the burial environment and during post excavation treatment or storage.

There has been intensive work on the tensile strength and other properties of 'living' bone (Yamada, 1970; Currey, 1984, 1988; Vincent, 1982) but there have been relatively few similar investigations of 'dead' or ancient bone (MacGregor and Currey, 1983; Battaglia, 1985). Hand specimens of excavated bone can exhibit a wide range of states of preservation but are invariably brittle or friable when compared to living or fresh bone. Excavated bone is also frequently inhomogeneous with parts of the same bone having apparently suffered different degrees of degradation since burial.

The strength of structural materials is frequently expressed in terms of tensile strength or the stress required to pull a sample of the material apart. Stress is defined as force per unit area and is frequently quoted in terms of Newtons per square metre ($Nm^{-2} = kgm^{-2}$) or Pascals ($1Nm^{-2}$ equals 1Pa). For many engineering materials, tensile strength expressed in these units generates extremely high numbers and units of MNm^{-2} or MPa are often used as a consequence. If strong materials are stretched in controlled experiments, the relationship between load and deformation or strain (expressed as a percentage of the original length) is found to obey a linear relationship in accordance with Hooke's law. When the load is removed the sample can return to its original dimensions and this is termed elastic behaviour. For ductile materials, such as many metals, this relationship is found to be true only if the applied stress is well below the yield strength of the material. Beyond this it undergoes irreversible deformation termed plastic flow. Figure 8.1a represents a typical graph of stress vs strain for a ductile material. The initial straight line represents elastic deformation in which the solid behaves in accordance with Hooke's law. At higher stresses, this linear behaviour is replaced by plastic deformation represented by the curved portion of the graph. In this region, the test specimen suffers progressively higher deformations for unit increases in stress. For brittle materials such as glass, ceramics and concrete, there is no region of plastic deformation and the plot is very nearly linear up to the point of fracture which is sudden and catastrophic (Figure 8.1b). The slope of the linear part of the graph reflects the Modulus of elasticity or stiffness of the material under test. For very stiff materials like metals, a comparatively large load is required to produce a certain increase in length. By comparison, a similar increase in length may be achieved for a much

lower load in the case of plastics or some biological materials. The slope of the straight line portion of a stress-strain diagram is characteristic of different materials and is represented by Young's modulus, defined as:

$$E = \frac{\text{stress}}{\text{strain}} = \text{constant}$$

The brittleness of archaeological bone presents problems for its tensile strength determination. The direct tension testing of brittle materials, although desirable, is notoriously unreliable due to the difficulties associated with sample preparation and alignment during testing. For example, if twisting or shear loads are imposed on the sample during the test, it may fail prematurely. Many of these potential problems can be avoided if an indirect method of tensile strength determination is used. The diametral compression or 'Brazilian test' involves the compression of a thin, disc-shaped specimen across its diameter until it fails, usually by cracking along the line of the applied load. Obviously, a compressive stress distribution is simultaneously produced in the sample but this is a minimum at the disc's centre where failure occurs. Figure 8.2 illustrates how a compressive force across the specimen's diameter is translated into a tensional force at right angles to the line of compression. In addition to orthogonal compressive stresses, the sample also experiences shear stresses that have a maximum at approximately 45° to the applied load. These additional forces mean that the diametral compression test invariably underestimates the tensile strength of the material by as much as 50% in some cases (Hondros 1959; Parry *et al.* 1989).

The maximum tensile stress (σ_{max}) at failure can be calculated from the compressive load (P) at failure using the formula:

$$\sigma_{max} = \frac{2P}{\pi d.t}$$

where d is the diameter of the disc and t is its thickness (Parry & Wronski 1990). Failure along the vertical diameter may also be accompanied by crushing at the loading points if flat jaws or anvils are used. This problem can be considerably reduced by the use of cylindrically concave loading anvils of the appropriate diameter (see Figure 8.2).

Bone is a composite material which some researchers have likened to glass reinforced plastics (see Chapter 1, section 1.8). Bone also has a distinct anisotropy in the arrangement of its structural components so that, in the mid-shafts of long bones, the collagen fibres and associated apatite crystals run parallel to their long axes. Although it is the collagen fibres that provide bone's resistance to tensile forces, for the purposes of this research, it was decided to determine the tensile strength at right angles to the long axes of the bone specimens. It was expected that it should be

much easier to pull adjacent fibres apart than to break the collagen strands themselves. Directions normal to the presumed orientation of the collagen fibres should therefore represent planes of weakness in much the same way as the grain in wood forms planes of weakness along which it breaks easily.

8.1 Materials and Methods

Samples of fresh (recently dead) bovine bone and archaeological bone from a variety of burial environments were selected for tensile strength investigation. The near cylindrical sections of long bones were chosen to ensure that any directionality in the samples could be predicted and preserved during testing. Cow femur was used for the fresh bone samples due to its ready availability from local butchers. Cow metapodials were selected for testing from the archaeological specimens since these are common in the archaeological record (in North West Europe) and often survive intact whereas larger long bones were often broken for marrow extraction. One example of archaeological human femur was also included for comparison.

The mid-shafts of the bone samples were sawn into 50-60mm lengths which were then cut longitudinally into 3 sections. Fresh bone and archaeological bone which exhibited exceptional preservation was sufficiently tough to cut and shape without cracking or crumbling. However, the majority of the archaeological bone was too friable to machine without splintering and as a consequence was consolidated by vacuum impregnation with 10% Paraloid B72 (an ethyl methacrylate/methyl acrylate copolymer) in 50:50 acetone and toluene. The sawn lengths of bone were embedded in a proprietary car-body filler paste contained in small plastic moulds. When this had cured the upper surfaces of the bone samples were ground flat on a metallographic polishing disc, ensuring that this surface was normal to the faces of the plastic box in each case. This mounting and grinding procedure allowed the bone samples to be held firmly in an engineer's vice whilst cores were drilled. After clearly marking the long axes of the bones on each sample, several small, cylindrical cores were drilled from each using a purpose made tubular drill manufactured from silver steel. Water was used as a coolant and lubricant during drilling. The resulting cores had diameters of approximately 6.5mm. Parallel ends were polished on these cylinders while holding them in specially prepared stainless steel plates. Thicknesses of the discs ranged from 0.8 to 4.8mm. Care was taken to preserve the orientation of each specimen throughout. All the discs were finally washed in two changes of acetone and allowed to air dry. This washing in acetone had the dual purpose of removing consolidant from those samples impregnated with B72 and of dehydrating the discs without any possible shrinkage or distortion from circular. The discs were then dried in an oven at 105°C, transferred to a vacuum desiccator to cool and then weighed on an electronic balance. The diameters (parallel to and at right angles to the long axis of the bone) and the thickness of each disc were determined using a vernier micrometer.

Tensile strength determinations on 'living' bone are usually undertaken on wet bone samples in order to mimic the physiological condition of bone in the organism. In the initial experiments, bone specimens were tested either wet or dry in order to compare the behaviour of bone under different conditions. Subsequent tests were carried out on discs that had acclimatised to ambient conditions of humidity.

Concave loading anvils with a radius of curvature of 5mm were used in a Lloyd 6000R computer controlled testing machine at a load rate of 0.1mm per minute and a load capacity of 30kN. For some of the more friable samples a load cell measuring a maximum of 1kN was used. Load and cross-head displacement were monitored autographically and stored in the memory of the dedicated personal computer. Disc failure was determined by a sharp fall in load on the autographic trace and was frequently accompanied by an audible crack from the sample. Once an effective testing regime was devised, a total of 105 discs from 20 different bone specimens was tested. In each case the maximum load at failure was determined from the autographic trace on the monitor screen using a movable cursor. For those discs which produced stepped curves (as in Figure 8.3b) the failure point was taken to be the maximum value.

8.2 Results

Initial results demonstrated that those bone specimens tested dry exhibited much higher tensile strengths than equivalent samples tested wet. The behaviour of the samples under loading were also very clearly different in each case. Figure 8.3 shows a graph of test results for two fresh bone samples and compares their behaviour when tested wet (8.3a) and dry (8.3b). The discs tested had equivalent diameters (6.81mm and 6.61mm respectively) and an identical thickness (3.04mm) so that the traces may be compared directly. The curves in Figure 8.3 do not represent true stress-strain diagrams since applied compressive load (P) vs the diametral compression, measured as cross-head displacement, are plotted rather than the equivalent stress vs strain. Nevertheless, such diagrams are useful for the purposes of comparison and the determination of σ_{max}. Figure 8.3b shows that after a short curve between the origin and point A (probably representing local failure of the bone at the point of loading; see Plate 8.1) the dry specimen underwent a period of linear, elastic behaviour (A to B) followed by progressive plastic deformation (B to C) before failing abruptly at point C. In contrast to this behaviour, the specimen tested wet (Figure 8.3a) demonstrated a comparatively short region of elastic deformation followed by a complicated series of plastic deformations and partial recoveries. This sample also exhibited no identifiable point of failure and the end of the test sequence the wet sample appeared compressed and delaminated rather than exhibiting a single failure along the vertical diameter. This plastic deformation and indistinct failure in the samples tested wet was much less marked in the case of visibly degraded archaeological bone.

Living bone, in common with many other biological materials, is viscoelastic in that deformation is not instantaneous but depends upon the rate of application of the load (see section 1.8). Viscoelastic materials can creep under a constant load but will return to their original shapes once a deforming force has been removed even though this recovery may take some time. If however bone is loaded at a speed higher than the rate at which it can accommodate the resulting deformation by viscous flow, fracture may occur (Vincent 1982, 157). The behaviour of fresh bone samples tested wet suggests that, during diametral compression, certain regions of the disc undergo either plastic or viscous flow until the majority of the applied stress is taken up by other areas in the sample. These areas in turn display elastic deformation until they too undergo plastic deformation. This behaviour could account for the cycles of elastic and plastic deformation seen in Figure 8.3a. If a higher rate of cross-head displacement had been employed it is possible that Figure 8.3a may have resembled the trace in Figure 8.3b. However, at the strain rates chosen for the experiments, experience showed that for discs taken from the same bone, results from dry testing were much more self-consistent than the results from wet testing which showed considerable variation in the calculated value of σ.

Figure 8.4 shows graphs of load verses diametral compression for dry discs taken from four archaeological bones exhibiting apparently different states of preservation. In each case the curves have been normalized to compensate for differences in disc thickness and to give each sample an equivalent thickness of 3mm. Trace 8.4a represents a disc cut from a human femur of unknown date recovered in Cyprus. Although this sample has a much lower tensile strength than that of recent cow bone, the trace is very similar to that in Figure 8.3b. Human bone is noted for its high density of Haversian systems and several researchers have commented that the presence of Haversian systems is associated with weakness in tension (Currey 1959, 93). The reduced value of tensile strength calculated from Figure 8.4a may be attributed as much to the presence of Haversian systems as diagenetic change. Figures 8.4b and 8.4c both show steps in their curves. The specimen in trace 8.4c represents a disc taken from a bone excavated from waterlogged Roman site at Carlisle. Trace 8.4b is from bone excavated from an Iron Age ditch at Stanwick, North Yorkshire. Both bones were tough, compact and appeared to be well preserved. The sudden drops or steps in these curves probably represent the initiation of small cracks in the discs. It was stated in section 1.8 that the microstructure of bone contains a large number of crack-stoppers created by the multitude of lamellae, osteocyte lacunae and canaliculi. The presence of these crack-stoppers greatly increases the toughness of living bone and must influence the behaviour of dead or buried bone. Crack initiation and growth will permit the relaxation of stored energy in the viscoelastic bone and it must be this that accounts for the sudden drop in the measured load. If crack growth is subsequently halted, the surrounding bone is forced to bear the load once again and the specimen once again acts as a Hookean material until the disc finally fails. The sample represented by trace 8.4d (from Stanwick) shows a behaviour almost indistinguishable from that of the fresh bone in Figure 8.3b.

Experiments on fresh bone have determined that its mechanical properties (tensile and compressive strengths and Young's modulus) vary with a number of different factors. It has already been stated that bones are weakened by the presence of Haversian systems but it has not always been established whether this is due to a general reduction in the amount of bone tissue present or whether the reduction in strength is due to a lower concentration of bone mineral (Currey 1969). Later work by Curry established that the Young's modulus of bone (tested wet) depended upon both the porosity and the total calcium content (Curry 1988). Numerous other researchers (reported in Burr 1980) have identified that other parameters such as crushing strength increase with increasing ash or mineral content (Bartley *et al.* 1966; Burstien *et al.* 1975). Carter and Hayes (1977) reported that strength of human femur and tibia varied with 'apparent local density' squared, and compressive modulus with apparent density cubed. Table 8.1 shows the calculated disc volume and mass for each of the specimens illustrated in Figure 8.4, together with the compressive load at failure for each. The *apparent density* (ρ) of the bone specimens, defined as the mass divided by the volume contained within each disc are shown in column 4.

Sample	Volume (mm^3)	Mass (g)	ρ (gcm^{-3})	σmax (Nm^{-2})
2M	100.52	0.156	1.555	8.191
7K	50.09	0.086	1.717	14.750
11H	74.09	0.147	1.984	54.195
13E	108.24	0.206	1.903	24.593

Table 8.1 Apparent disc densities and indirect tensile strength

It can be seen from Table 8.1 that there is a general trend of increasing tensile strength (perpendicular to the long axis) with increasing apparent density. Dimensions, masses and test results for all samples are shown in Tables 8.2 to 8.4. For convenience, the apparent densities for all the bone discs are given in units of gcm^{-3} to avoid large numbers and because this is equivalent to specific gravity.

Sample	d1 (mm)	d2 (mm)	r Mean (mm)	Depth (mm)	Mass (g)	ρ (gcm^{-3})	Pmax (N)	σmax (MPa)
1F	6.55	6.53	3.27	0.80	0.028	1.042	37.38	4.548
1L	6.53	6.51	3.26	2.91	0.112	1.153	137.02	4.598
1M	6.45	6.46	3.23	1.98	0.063	0.972	83.31	4.150
1N	6.62	6.60	3.31	2.59	0.098	1.103	121.61	4.522
1O	6.61	6.57	3.30	2.80	0.107	1.120	121.46	4.191
1P	6.53	6.54	3.27	2.40	0.081	1.006	115.66	4.695
2H	6.64	6.62	3.32	3.24	0.174	1.556	856.86	25.394
2I	6.67	6.72	3.35	1.66	0.082	1.403	183.26	10.498
2K	6.59	6.56	3.29	3.32	0.175	1.552	513.31	14.970
2L	6.55	6.53	3.27	3.20	0.166	1.544	584.87	17.791
2M	6.59	6.64	3.31	2.92	0.156	1.555	497.51	16.397
4G	6.61	6.59	3.30	3.04	0.209	2.010	2075.96	65.869
4H	6.62	6.68	3.33	2.83		0.000	1881.41	63.644
4I	6.58	6.57	3.29	3.11		0.000	1945.50	60.570
4J	6.37	6.32	3.17	2.75	0.200	2.300	1584.03	57.793
4K	6.61	6.59	3.30	3.46	0.233	1.968	1712.04	47.728
4L	6.53	6.50	3.26	3.32	0.220	1.988	1879.12	55.307
4M	6.58	6.56	3.29	3.09	0.210	2.005	1746.37	54.764
5J	6.30	6.26	3.14	2.88	0.094	1.054	92.39	3.252
5K	6.46	6.44	3.23	2.56	0.094	1.124	130.08	5.015
5M	6.41	6.39	3.20	1.91	0.065	1.058	69.35	3.612
8A	6.20	6.22	3.11	2.68	0.108	1.330	283.97	10.862
8B	6.16	6.20	3.09	2.49	0.102	1.366	280.46	11.603
8C	6.22	6.22	3.11	3.47	0.145	1.375	350.65	10.343
8D	6.22	6.24	3.12	2.87	0.119	1.360	321.35	11.442
8E	6.25	6.26	3.13	1.80	0.077	1.392	220.34	12.459
8F	6.25	6.25	3.13	2.53	0.106	1.366	302.89	12.194
8G	6.23	6.21	3.11	2.61	0.109	1.374	214.23	8.401
9A	6.21	6.19	3.10	2.73	0.123	1.492	278.24	10.465
9B	6.24	6.22	3.12	2.46	0.103	1.374	192.26	7.986
9C	6.10	6.08	3.05	1.59	0.059	1.274	120.32	7.910
9D	6.22	6.19	3.10	2.25	0.093	1.367	203.09	9.261
9E	6.11	6.21	3.08	1.87	0.078	1.400	194.55	10.752
9F	6.23	6.19	3.11	1.86	0.074	1.314	143.89	7.931
9G	6.21	6.20	3.10	2.36	0.100	1.401	202.94	8.823
9H	6.13	6.12	3.06	1.69	0.066	1.325	172.04	10.581
9I	6.25	6.22	3.12	1.72	0.065	1.238	115.43	6.852
9J	6.23	6.23	3.12	1.45	0.056	1.267	110.70	7.801
9K	6.24	6.22	3.12	2.43	0.105	1.417	318.91	13.411
9L	6.26	6.19	3.11	2.4	0.095	1.301	198.90	8.475
9M	6.22	6.19	3.10	1.98	0.085	1.420	169.91	8.804
9N	6.22	6.2	3.11	2.54	0.107	1.391	215.99	8.717
9O	6.17	6.15	3.08	1.79	0.063	1.181	153.81	8.880
9P	6.19	6.17	3.09	2.04	0.078	1.275	171.13	8.641
10A	6.75	6.75	3.38	1.69	0.111	1.835	414.28	23.120

Table 8.2 Results of diametral compression. samples 1-10.

Sample	d1 (mm)	d2 (mm)	r Mean (mm)	Depth (mm)	Mass (g)	ρ (gcm^{-3})	Pmax (N)	σmax (MPa)
13A	6.35	6.15	3.13	3.40	0.186	1.783	844.57	25.302
13B	6.47	6.3	3.19	3.36	0.205	1.905	997.92	29.612
13C	6.34	6.13	3.12	2.93	0.165	1.844	727.84	25.364
13D	6.41	6.25	3.17	3.19	0.191	1.903	997.92	31.462
13E	6.40	6.24	3.16	3.45	0.206	1.903	842.29	24.593
13F	6.27	6.11	3.10	3.48	0.199	1.900	1293.18	38.218
13G	6.33	6.17	3.13	2.93	0.169	1.880	791.93	27.531
13H	6.39	6.24	3.16	2.54	0.155	1.948	569.92	22.620
13I	6.33	6.25	3.15	2.31	0.135	1.881	436.16	19.110
13J	6.33	6.14	3.12	3.62	0.216	1.954	1146.70	32.343
13K	6.27	6.14	3.10	2.43	0.138	1.878	904.08	38.171
13L	6.31	6.1	3.10	3.15	0.179	1.879	746.15	24.303
14A	6.22	6.14	3.09	3.18	0.175	1.835	787.35	25.505
14B	6.21	6.19	3.10	2.73	0.153	1.856	704.96	26.515
14D	6.22	6.16	3.10	3.00	0.166	1.839	1142.12	39.154
14E	6.21	6.19	3.10	3.12	0.173	1.837	718.69	23.652
14F	6.23	6.15	3.10	2.03	0.117	1.915	771.33	39.078
14G	6.26	6.16	3.11	3.56	0.188	1.744	899.51	25.903
14H	6.25	6.18	3.11	2.28	0.133	1.923	947.57	42.571
14I	6.22	6.16	3.10	3.28	0.179	1.813	977.33	30.645
14J	6.26	6.19	3.11	2.22	0.124	1.835	759.89	35.006
14K	6.29	6.16	3.11	3.04	0.167	1.805	878.91	29.567
14L	6.18	6.11	3.07	3.31	0.180	1.834	1011.66	31.664
17A	6.24	6.21	3.11	3.09	0.089	0.946	156.25	5.171
17B	6.17	6.14	3.08	2.92	0.081	0.932	103.30	3.659
17C	6.15	6.1	3.06	2.38	0.062	0.884	112.99	4.934
17D	6.24	6.16	3.10	1.64	0.043	0.868	61.34	3.840
17E	6.12	6.1	3.06	3.09	0.088	0.971	151.29	5.101
17F	6.16	6.11	3.07	2.96	0.096	1.097	320.89	11.249
17G	6.28	6.2	3.12	2.42	0.077	1.040	128.86	5.432
17H	6.17	6.19	3.09	3.1	0.082	0.882	126.88	4.216
17J	6.12	6.20	3.08	2.33	0.064	0.922	105.44	4.677
17K	6.13	6.12	3.06	2.32	0.062	0.907	105.96	4.747

Table 8.3 Results of diametral compression. samples 13-17.

Sample	d1 (mm)	d2 (mm)	r Mean (mm)	Depth (mm)	Mass (g)	ρ (gcm^{-3})	Pmax (N)	σmax (MPa)
18A	6.28	6.29	3.14	2.08	0.091	1.410	200.42	9.760
18B	6.21	6.20	3.10	2.24	0.080	1.181	128.17	5.871
18C	6.28	6.25	3.13	2.37	0.099	1.355	188.45	8.080
18D	6.15	6.18	3.08	2.35	0.084	1.197	128.25	5.636
18E	6.28	6.19	3.12	2.33	0.097	1.363	93.84	4.112
18F	6.20	6.10	3.08	1.81	0.074	1.376	205.08	11.729
18G	6.29	6.19	3.12	1.98	0.073	1.206	91.55	4.717
18H	6.14	6.15	3.07	2.56	0.098	1.291	161.29	6.527
18I	6.18	6.15	3.08	2.54	0.099	1.306	145.57	5.918
19A	6.10	6.10	3.05	2.57	0.072	0.959	173.95	7.064
19B	6.09	6.07	3.04	2.17	0.067	1.063	180.82	8.725
19C	6.20	6.21	3.10	3.08	0.086	0.923	210.57	7.014
19D	6.21	6.16	3.09	1.83	0.073	1.328	210.57	11.844
19E	6.09	6.1	3.05	2.52	0.064	0.870	167.08	6.925
19F	6.02	6.05	3.02	2.05	0.05	0.853	130.46	6.713
19G	6.17	6.15	3.08	1.89	0.049	0.870	116.73	6.383
19H	6.32	6.22	3.14	1.21	0.036	0.964	103	8.643
19I	5.90	5.98	2.97	2.2	0.051	0.837	139.62	6.802
19J	6.10	6.08	3.05	1.85	0.05	0.928	119.02	6.725
19K	6.16	6.15	3.08	1.69	0.044	0.875	86.98	5.323
20A	6.32	6.12	3.11	2.48	0.104	1.380	224.3	9.257
20B	6.29	6.12	3.10	1.64	0.065	1.311	167.08	10.452
20C	6.29	6.2	3.12	1.84	0.076	1.348	192.26	10.652
20D	6.35	6.27	3.16	2.19	0.097	1.416	192.26	8.857
20E	6.23	6.22	3.11	1.69	0.052	1.011	68.66	4.155
20F	6.24	6.21	3.11	1.37	0.05	1.199	75.53	5.638
20G	6.11	5.91	3.01	1.09	0.031	1.003	43.49	4.226

Table 8.4 Results of diametral compression, samples 18-20.

In Tables 8.2 to 8.4 the density in column 7 refers to the apparent density or *bulk density* of each disc (in gcm^{-3}). This measurement of density should not be confused with the true density *microstructural density* of bone tissue since the measured volume of each disc also contains a considerable amount of air spaces in the form of voids. This 'empty' space is termed the *pore volume* and may be expressed in terms of the percent of the total volume. Some researchers use the term volume fraction which refers to 1-porosity (Curry 1988).

It can be seen that for fresh bone (sample 4) the tensile strength normal to the direction of the long axis of the bone falls between 47MPa and 66MPa. If it is assumed that the collagen fibres run parallel to the long axis of the bone, then this can be compared to a figure of 116.5MPa for the tensile strength of osteons at 90° to the orientation of the fibres (Vincent 1982, Table 6.11). Measurement of tensile strength by the Brazilian test therefore underestimates the true tensile strength by approximately 50%.

Figure 8.5 shows a plot of tensile strength against bulk density for all the samples tested dry. Despite some scatter in the case of discs with higher densities (archaeological bone from water-logged deposits) the values conform to a curve that shows a dramatic initial fall in the tensile strength of bone after only modest losses in bone density. Figure 8.6 shows a plot of tensile strength vs disc bulk density expressed on a log scale and demonstrates that the relationship is approximately logarithmic. This finding is in agreement with the observation by Carter and Hayes (1977) that in fresh human femur the strength varied with the square of the local 'apparent density'. Another feature of Figure 8.5 is that the data falls into two distinct groups. With the exception of four of the discs cut from a human femur, the data fall into one of two groups; those discs with bulk densities between $1.72gcm^{-3}$ and $2.0gcm^{-3}$ and discs with bulk densities between $0.8gcm^{-3}$ and $1.4gcm^{-3}$. Those discs in the first group exhibit a wide range of tensile strengths and follow a trend consistent with a rapid loss of strength for modest reductions in bulk density. By contrast, those discs in the second group show almost negligible decrease in strength even though the bulk densities vary by a factor of almost two. No samples of bovine bone have a bulk density between $1.5gcm^{-3}$ and $1.7gcm^{-3}$. This suggests that two mechanisms may be responsible for differences in both the bulk density and tensile strength of ancient bones. Alternatively, the absence of intermediate specimens may suggest that bones buried in even moderately aggressive environments suffer a rapid loss in density and a corresponding reduction in strength shortly after deposition.

The bulk density of archaeological bone samples may be influenced by a number of variables. The first, and probably most important of these, is the micro-architecture of the bone, *i.e.* the size and distribution of osteocyte lacunae, canaliculi and Haversian canals in the specimen. Since the sites from which the discs were taken were rigorously controlled during sample preparation, each disc can be assumed to have a very nearly similar micro-architecture so that differences in bulk density cannot be attributed solely to such variability. A dominant controlling factor must be the amount of additional porosity due to microfocal destruction or 'tunnelling' by micro-organisms (see section 3.1.4). Other factors include variability in the chemical composition of the bone tissue itself. This embraces both natural differences in the degree of mineralization of bone tissues and differences brought about by diagenetic change. Even in essentially neutral soils there is considerable evidence for the slow hydrolysis of collagen and its loss from buried bones. Similarly, there is evidence that in acid soils there is a loss of bone apatite leading to collagen rich areas in bones (see section 4.2). The chemical analysis of archaeological bones in Chapter 4 also indicates that the infiltration of bone by metal salts and diagenetic minerals may also influence the bulk density.

To investigate the relationship between bulk density and pore volume a further series of experiments were undertaken on discs drilled from archaeological bone specimens. These were prepared, dried, measured and weighed in the same way as before but in addition were weighed wet. To ensure that water penetrated the entire pore structure the discs were immersed in distilled water and left under

vacuum overnight to exclude any air trapped in the smallest cavities. On removal from the water each disc was blotted briefly to remove any surface water and weighed. Table 8.6 shows the blotted and oven dried weights of discs. The pore volume was calculated from the difference between the wet and dry weights and the volumes of the discs, assuming that the density of water at room temperature is $1gcm^{-3}$. Bulk density was calculated from the oven dried weights. Figure 8.7 shows a plot of pore volume vs apparent density for the samples. Many of the discs lie on a straight line showing that there is a direct (linear) relation between bulk density and pore volume. This line intersects the pore volume axis at 100% for zero bulk density. The graph also demonstrates that for zero pore volume the density is $2.4gcm^{-3}$. This figure must represent the true density of bone tissue. Those samples (marked by circles) that lie off this straight line and appear to show an increase in pore volume for no additional increase in bulk density derive from waterlogged burial conditions. This deviation from the predicted behaviour may be interpreted as water being absorbed by collagen exposed by demineralization in the soil. This water would be absorbed by swelling of the collagen fibres rather than the filling of pores in the structure allowing considerable uptake of water despite having a low pore volume (see section 7.3). It should be noted that the bulk densities of these samples are close to that of fresh bone.

To explore what other factors may influence the tensile strengths of bones, twenty discs that failed satisfactorily along the vertical diameter were selected for carbon, hydrogen and nitrogen analysis. The results of these analyses are shown in Table 8.5.

Sample	σmax	Carbon (%)	Hydrogen (%)	Nitrogen (%)
1M	4.150	6.10	1.24	1.27
1L	4.598	5.85	1.23	0.91
2M	16.397	9.21	1.66	2.72
4M	54.764	11.24	2.04	3.50
4K	47.728	11.53	2.13	3.62
5J	3.252	5.11	1.11	0.85
5K	5.015	4.16	0.95	0.62
8A	10.862	5.36	1.08	1.13
8E	12.459	5.32	1.19	0.82
9A	10.465	3.72	0.89	0.44
9C	7.910	4.43	1.00	0.54
9K	13.411	3.82	0.95	0.54
13A	25.302	13.29	2.30	4.47
13J	32.343	11.31	2.22	3.69
13L	24.303	12.73	2.35	4.21
14E	23.652	11.32	2.14	3.73
14H	42.571	11.93	2.17	3.94
14K	29.567	11.01	2.04	3.62
17D	3.840	6.13	1.19	1.23
17F	11.249	8.72	1.59	2.32

Table 8.5 Results of carbon, hydrogen and nitrogen analyses on test discs

Sample	Blotted wt. (g)	Dry wt. (g)	Difference (g)	Volume (mm^3)	ρ ($g\ cm^{-3}$)	Porosity (%)
1A	0.077	0.049	0.028	48.81	1.00	57.37
1B	0.144	0.094	0.050	86.93	1.08	57.52
1D	0.162	0.106	0.056	97.76	1.08	57.28
1E	0.120	0.075	0.045	74.2	1.01	60.65
1I	0.043	0.028	0.015	26.87	1.04	55.82
1N	0.148	0.099	0.049	88.88	1.11	55.13
1O	0.160	0.107	0.053	95.5	1.12	55.50
1P	0.129	0.081	0.048	80.16	1.01	59.88
1Q	0.081	0.050	0.031	49.94	1.00	62.07
4B	0.260	0.232	0.028	127.04	1.83	22.04
4D	0.220	0.192	0.028	108.94	1.76	25.70
4F	0.212	0.183	0.029	111.06	1.65	26.11
6E	0.176	0.120	0.056	106.49	1.13	52.59
6G	0.126	0.096	0.030	73.37	1.31	40.89
8C	0.187	0.140	0.047	105.44	1.33	44.58
8D	0.156	0.116	0.040	87.49	1.33	45.72
9A	0.122	0.092	0.030	67.33	1.37	44.56
9E	0.101	0.076	0.025	55.73	1.36	44.86
9G	0.130	0.097	0.033	71.37	1.36	46.24
9H	0.085	0.063	0.022	49.8	1.27	44.18
9I	0.089	0.063	0.026	52.52	1.20	49.50
9J	0.072	0.053	0.019	44.2	1.20	42.99
9L	0.127	0.093	0.034	73.04	1.27	46.55
9M	0.111	0.082	0.029	59.78	1.37	48.51
9N	0.138	0.102	0.036	76.93	1.33	46.80
9P	0.106	0.076	0.030	61.19	1.24	49.03
11G	0.160	0.144	0.016	75.42	1.91	21.21
11H	0.155	0.137	0.018	74.08	1.85	24.30
11I	0.107	0.096	0.011	50.48	1.90	21.79
13F	0.215	0.184	0.031	104.73	1.76	29.60
13G	0.183	0.157	0.026	89.89	1.75	28.92
13I	0.144	0.127	0.017	71.78	1.77	23.68
13K	0.150	0.128	0.022	73.48	1.74	29.94
14C	0.204	0.162	0.042	101.42	1.60	41.41
14F	0.127	0.106	0.021	61.09	1.74	34.38
14G	0.221	0.170	0.051	107.83	1.58	47.30
14I	0.202	0.162	0.040	98.71	1.64	40.52
14J	0.141	0.114	0.027	67.57	1.69	39.96

Table 8.6a Determination of pore volume for test discs

15A	0.148	0.116	0.032	72.98	1.59	43.85
15B	0.170	0.138	0.032	85.02	1.62	37.64
15C	0.150	0.122	0.028	71.07	1.72	39.40
15D	0.181	0.146	0.035	90.19	1.62	38.81
15E	0.135	0.109	0.026	67.01	1.63	38.80
15F	0.184	0.152	0.032	90.32	1.68	35.43
15H	0.143	0.117	0.026	69.93	1.67	37.18
15I	0.170	0.139	0.031	80.82	1.72	38.36
15J	0.153	0.128	0.025	77.87	1.64	32.10
15K	0.120	0.096	0.024	57.38	1.67	41.83
15L	0.130	0.107	0.023	61.88	1.73	37.17
17A	0.144	0.088	0.056	94.04	0.94	59.55
17H	0.141	0.080	0.061	92.99	0.86	65.60
17I	0.159	0.101	0.058	97.79	1.03	59.31
17K	0.103	0.061	0.042	68.36	0.89	61.44
17L	0.115	0.076	0.039	71.89	1.06	54.25
17M	0.099	0.057	0.042	66.89	0.85	62.79
18E	0.128	0.095	0.033	71.14	1.34	46.39
18I	0.136	0.097	0.039	75.82	1.28	51.44
18J	0.122	0.088	0.034	67.91	1.30	50.07
18K	0.083	0.058	0.025	47.93	1.21	52.16
18L	0.159	0.117	0.042	86.73	1.35	48.43
18M	0.106	0.072	0.034	62.57	1.15	54.34
18Z	0.080	0.055	0.025	46.46	1.18	53.81

Table 8.6b Determination of pore volume for test discs

To determine whether there was a relationship between mechanical strength and protein content in archaeological bones, tensile strength was plotted against nitrogen content of the disc (Figure.8.8). Although it is possible to see a general trend of increased tensile strength with higher nitrogen content the correlation is poor when compared with Figure 8.5. However, Figure 8.8 does demonstrate that for well preserved bones (*i.e.* bones with nitrogen contents above 3.5%) there is a wide range of tensile strengths of samples with very similar nitrogen (protein) contents. If a plot of bulk density vs nitrogen content is examined (Figure 8.9) it can be seen that these well preserved bone samples all have bulk densities of around $2.0gcm^{-3}$. Thus, for well preserved bones the major factor determining tensile strength is their protein or collagen content rather than porosity. Table 8.5 also demonstrates that there is considerable variation in the carbon, hydrogen and nitrogen contents of the same bone sample. To verify that this scatter results from real variations in the bone samples rather than random experimental error, graphs of hydrogen vs carbon and nitrogen vs carbon are shown in Figures 8.10 and 8.11 respectively. These graphs show very similar patterns to those in Figures 4.13 and 4.14, indicating that experimental error is unlikely to account for the variation in nitrogen content within a single bone. The similarity between Figures 8.10 and 4.13 also suggests that a negligible residue of acrylic consolidant remains within the sample discs after washing in acetone.

The results above suggest that shortly after burial there is an initial rapid decrease in the mechanical strength of bone and that this decrease occurs without appreciable loss of collagen or increase in porosity. In the majority of burial environments this initial rapid modification of the bone is followed by a much slower weakening of the structure brought about by an increase in porosity rather than a gradual loss of its organic fraction. This gradual loss of strength is probably attributable to an increase in the number of microscopic voids that can act as initiation sites for cracks and subsequent failure. Furthermore, the high number of natural channels (e.g. Haversian canals) running parallel to the long axes of bones facilitates propagation of these cracks. This interpretation is confirmed by scanning electron microscopy of the fracture surfaces of discs. Plates 8.2 and 8.3 show a disc in which failure was initiated by, or followed, a plane of weakness caused by several tunnels or canals. From their geometry it is probable that these channels represent Haversian canals and canals of Volkman. Small crystals line these channels and at high magnification can be seen to be small rhomboids with a maximum dimension of 2μm. Although the small size of the crystals and heavy gold coating of the specimen precluded any microanalysis, from their shape it is probable that they represent small calcite crystals.

Plates 8.4 and 8.5 show the fracture surface of a specimen taken from an archaeological bone with a high collagen content (excavated from Iron Age deposits at Stanwick, North Yorkshire). The surface has a distinctly grained appearance, like wood, and at high magnification clearly shows the structure of lamellar bone (for comparison, see Weiner *et al.* 1991, Figure 1). Plates 8.6 and 8.7 show the

fracture surface of a disc cut from an archaeological bone specimen from Stanwick which was considerably degraded with a low bulk density and visibly high porosity. At high magnification it can be seen that there has been complete loss of microstructure and that the originally dense bone tissues have been replaced by a very spongy texture. There were no obvious signs of any pathological condition in the hand specimen. In this specimen the structure of the bone has been considerable weakened by the numerous voids, any of which could act as crack initiators

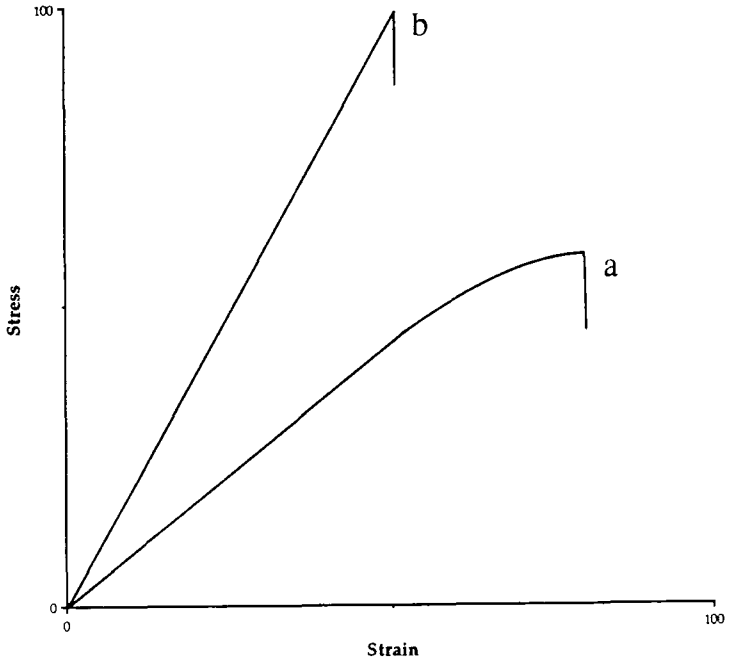

Figure 8.1 Typical stress vs strain diagrams for **a** a ductile material; **b** a brittle material

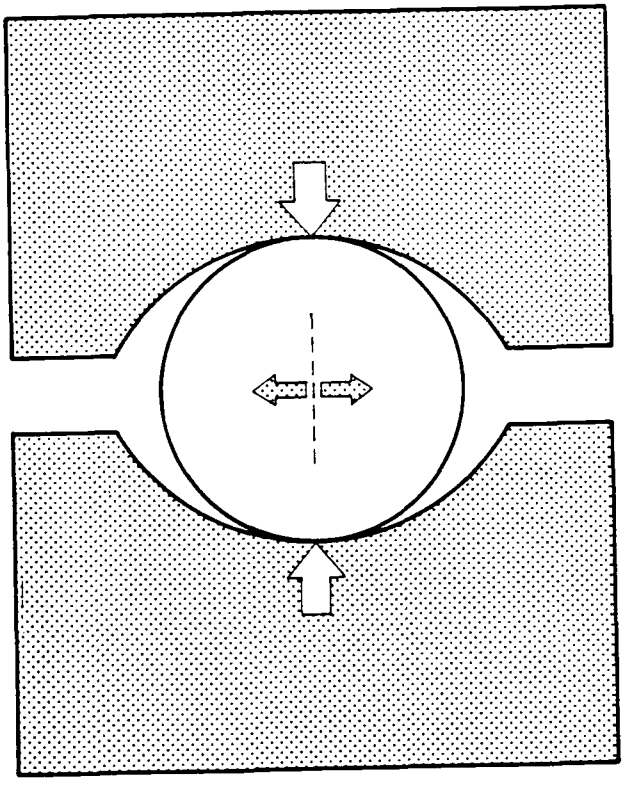

Figure 8.2 Principle forces in the diametral compression (Brazilian) test

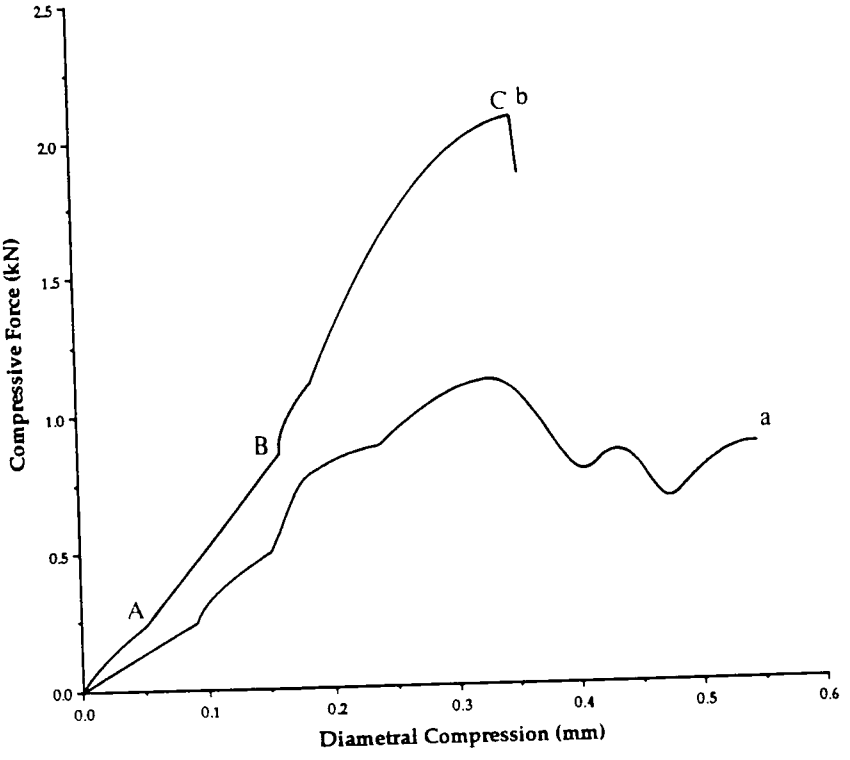

Figure 8.3 Compressive force vs diametral compression for **a** wet bone: **b** air dried bone

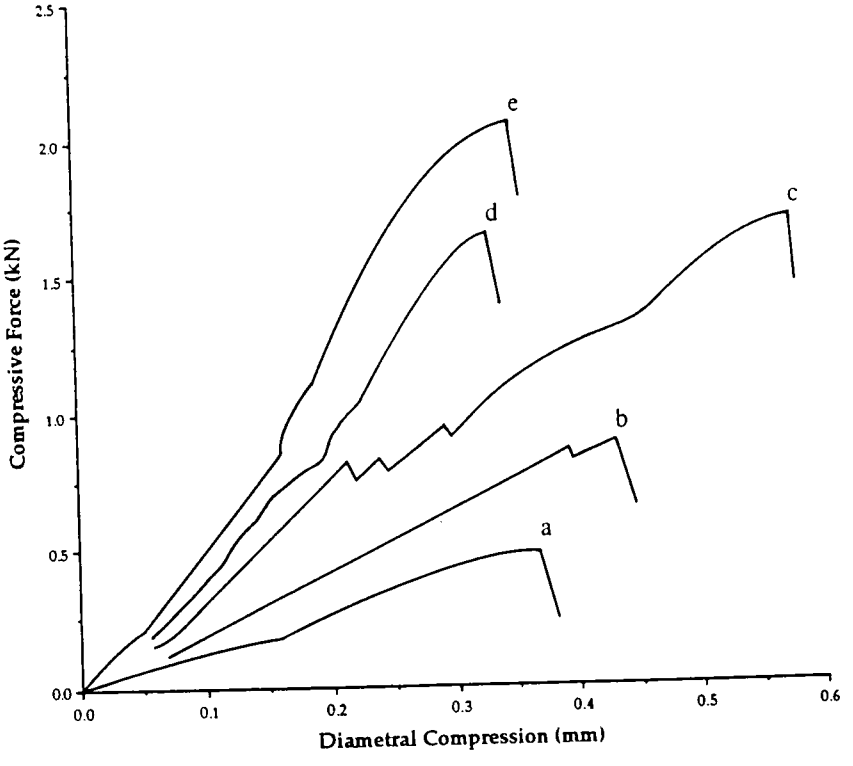

Figure 8.4 Compressive force vs diametral compression for various bones (corrected for differences in disc thickness)

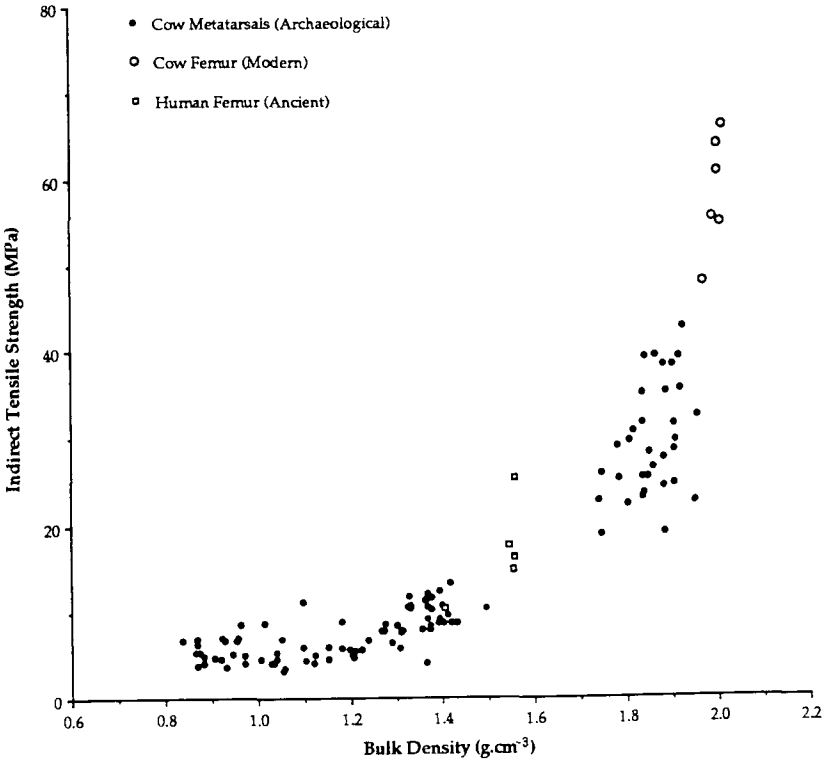

Figure 8.5 Indirect tensile strength vs bulk density for sample discs tested dry

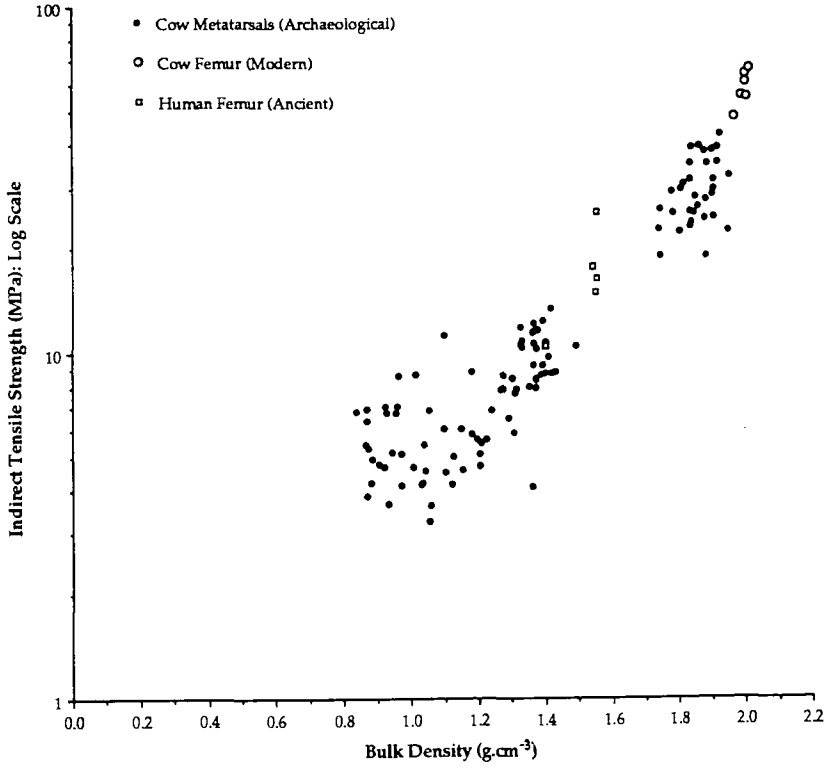

Figure 8.6 Plot of log sigma vs bulk density. Fossil bone specimens approximate to log-linear relationship

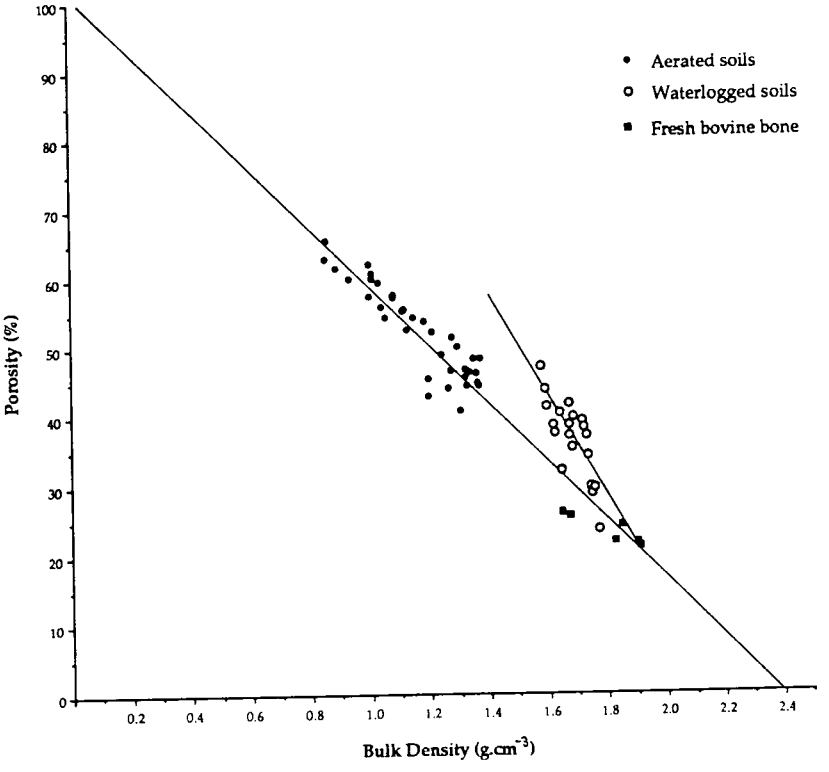

Figure 8.7 Plot of porosity vs bulk density for bones from aerated (closed circles) and waterlogged (open circles) contexts. Note intercept at bulk density of 2.4gcm^{-1}

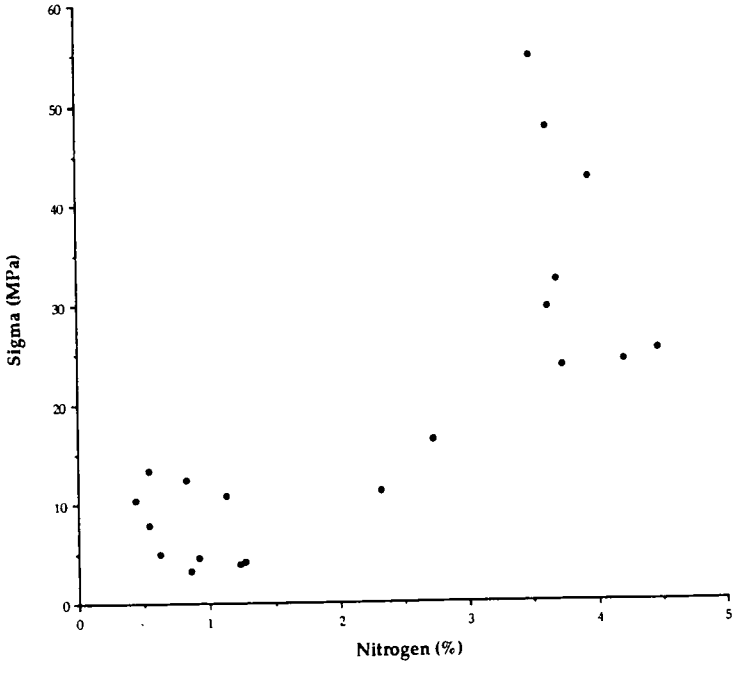

Figure 8.8 Plot of tensile strength vs nitrogen

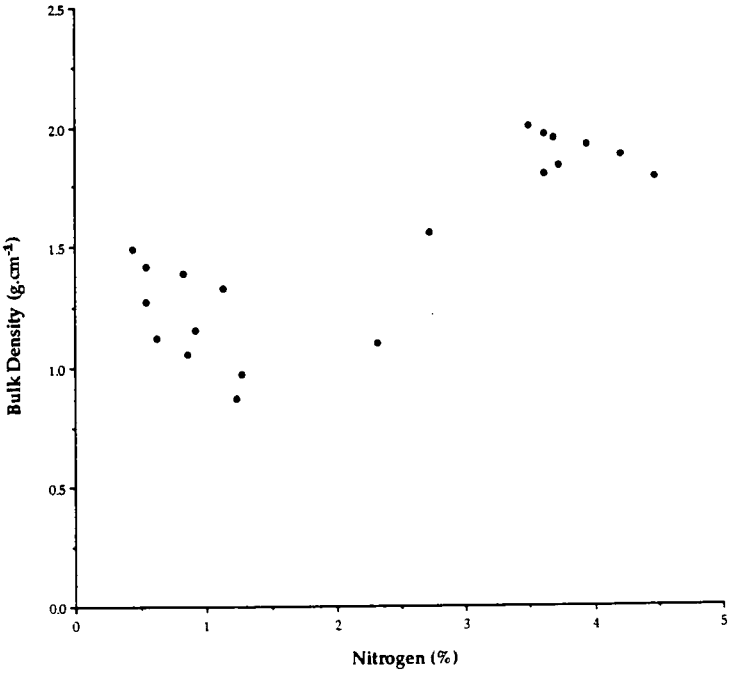

Figure 8.9 Plot of bulk density vs nitrogen

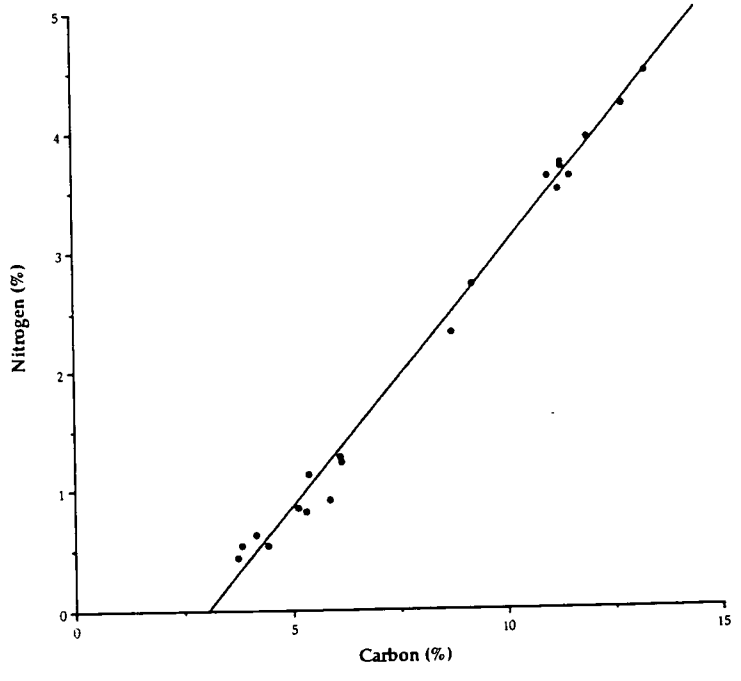

Figure 8.10 Plot of nitrogen vs carbon for test discs

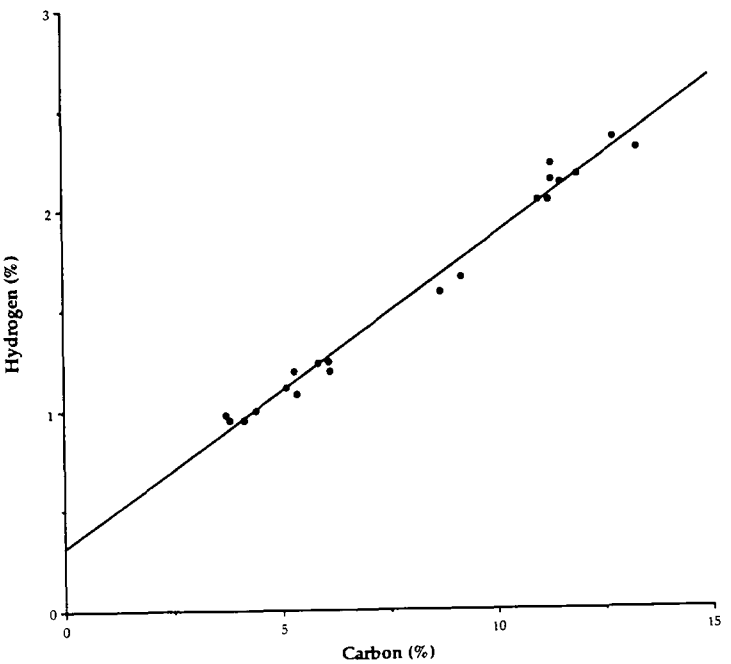

Figure 8.11 Plot of hydrogen vs carbon for test discs

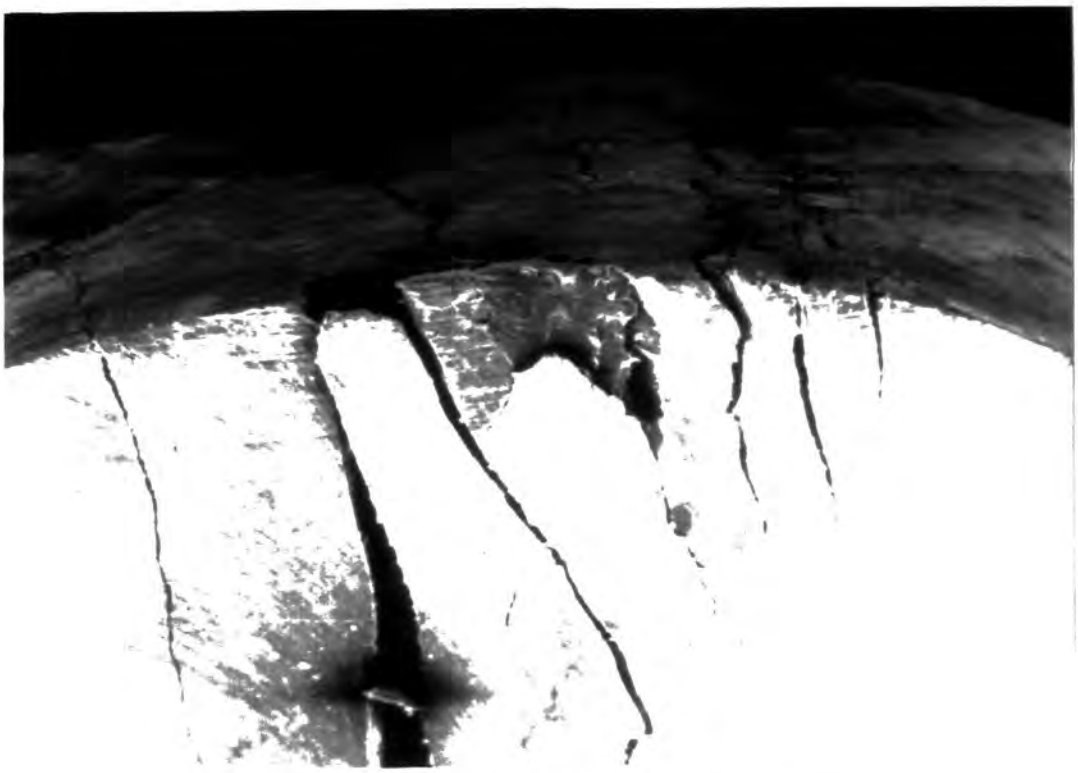

Plate 8.1 Local failure of disc at point of loading

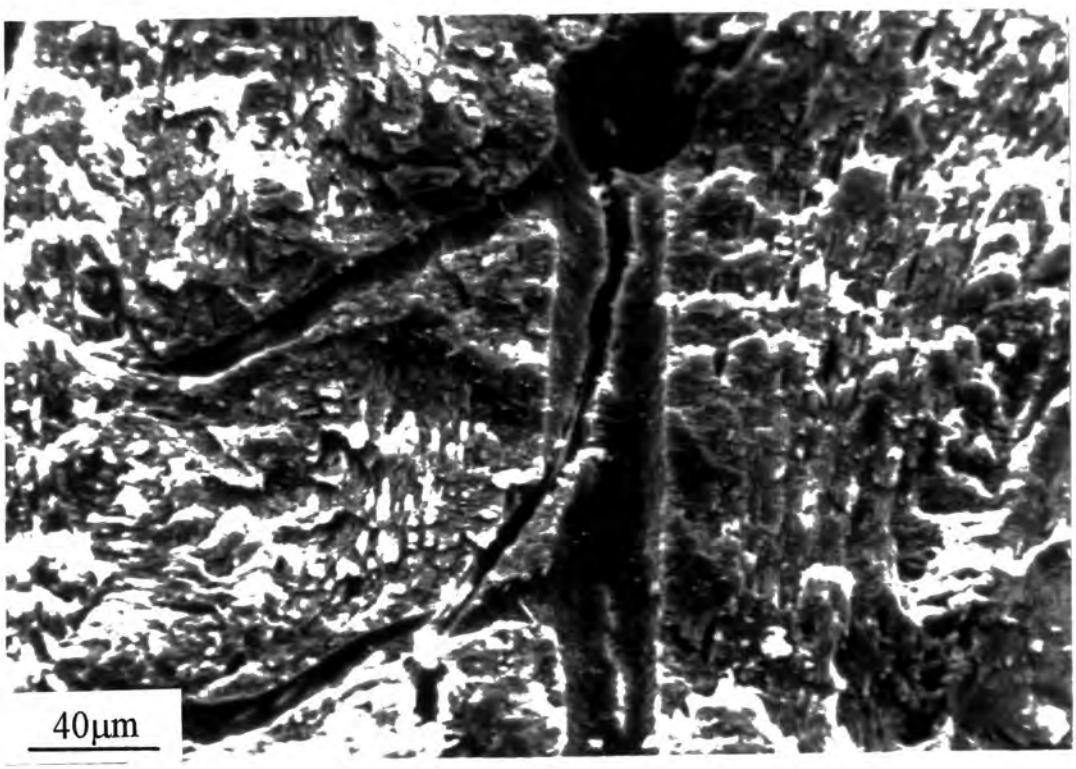

Plate 8.2 Fracture surface of 'well preserved' bone showing that path of failure respects the original microstructure of bone (Haversian & Volkman's canals)

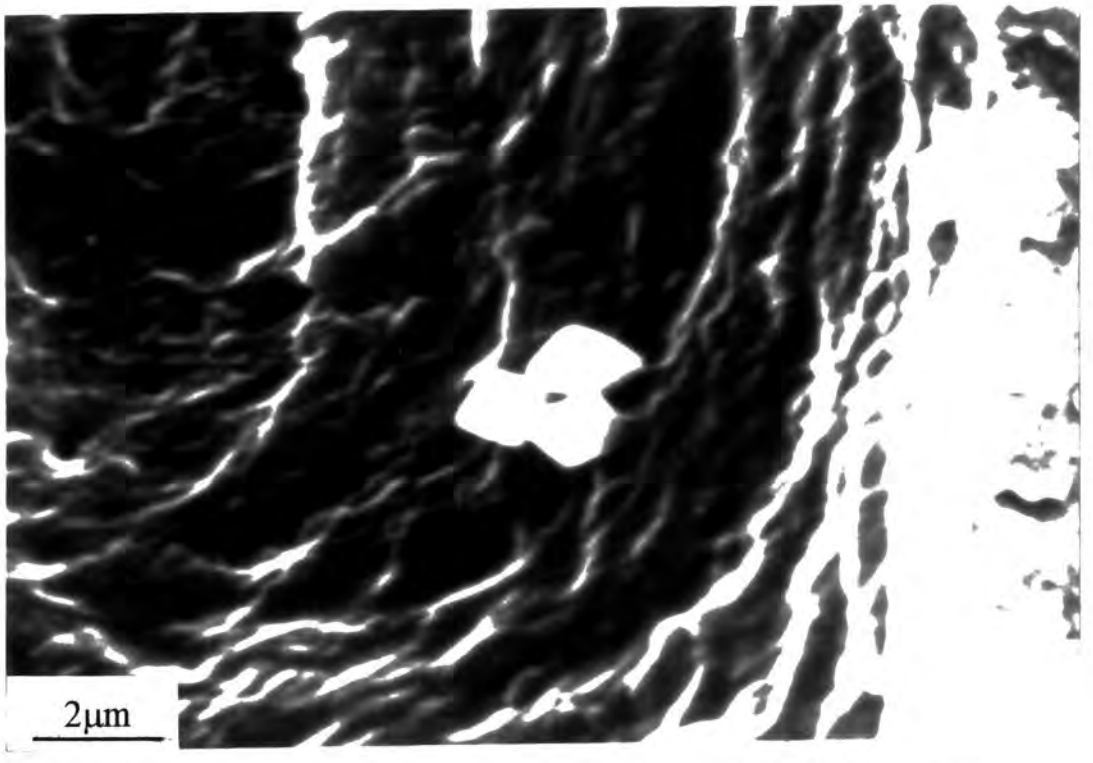

Plate 8.3 High magnification view of Plate 8.2. Note small rhomboidal crystals (possibly calcite) Approximately 2μm long

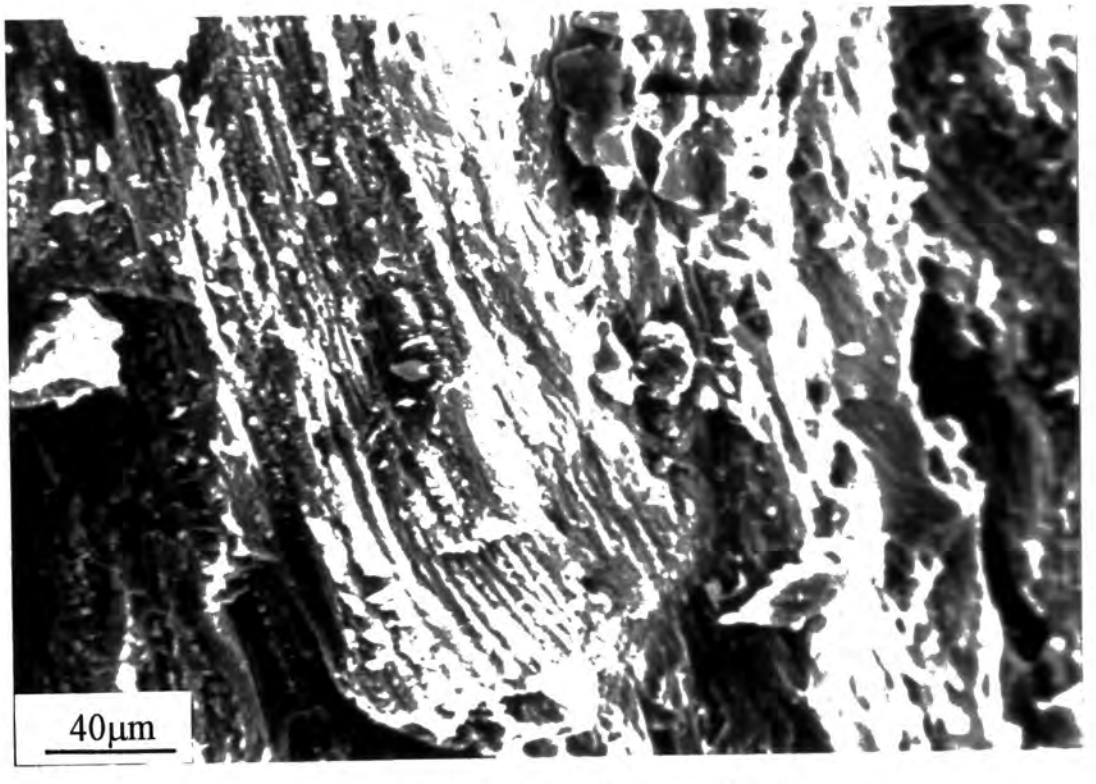

Plate 8.4 Fracture surface of test disc with high collagen content, demonstrating fibrous nature of bone

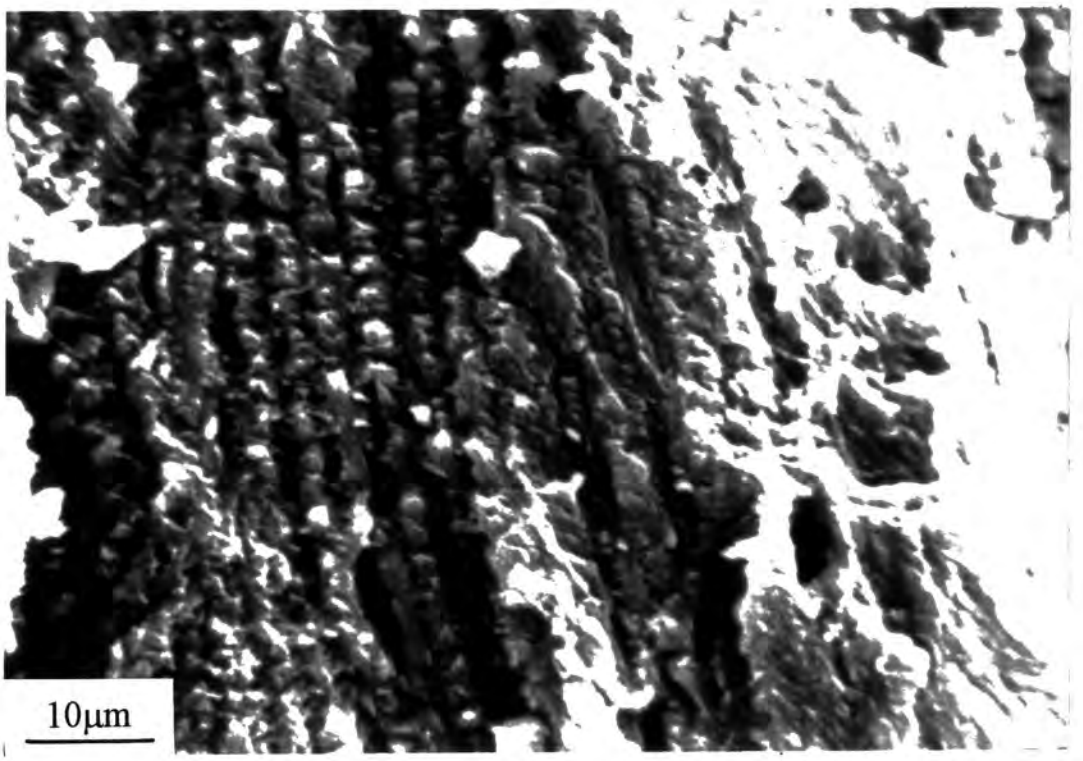

Plate 8.5 High magnification view of Plate 8.4 showing successive lamellae approximately 4μm across (see Weiner *et al.* 1991, Fig 1)

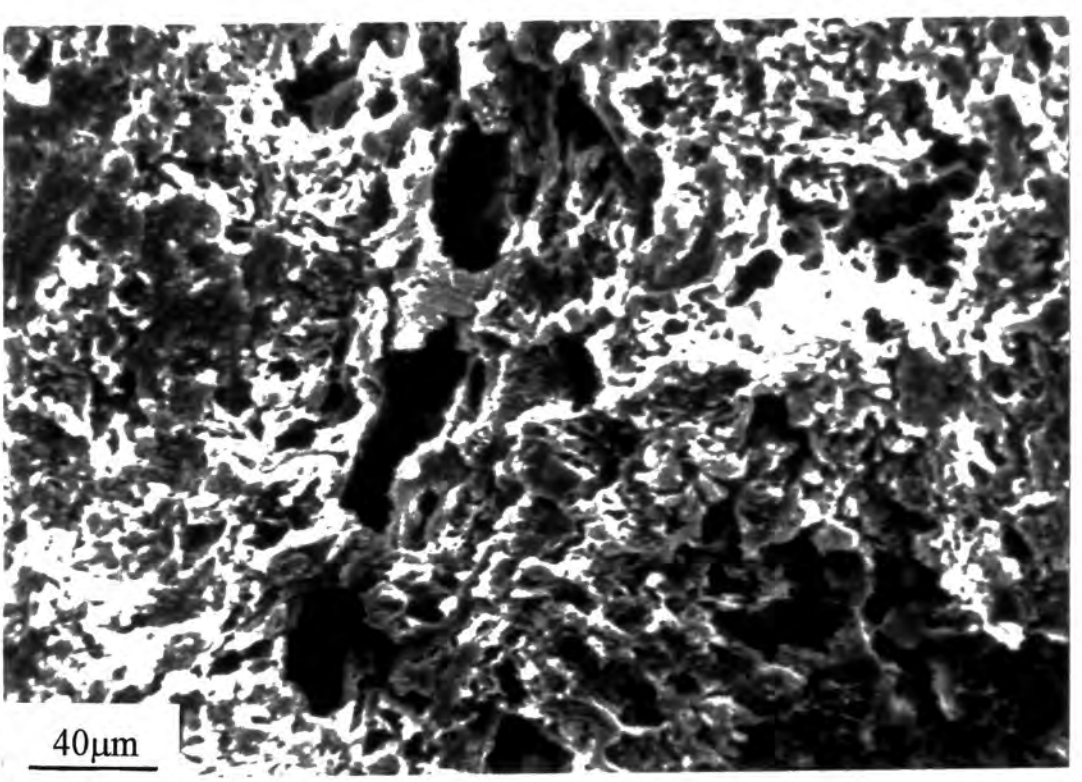

Plate 8.6 Fracture surface of test disc with low collagen content. Note loss of fibrous structure and increased porosity

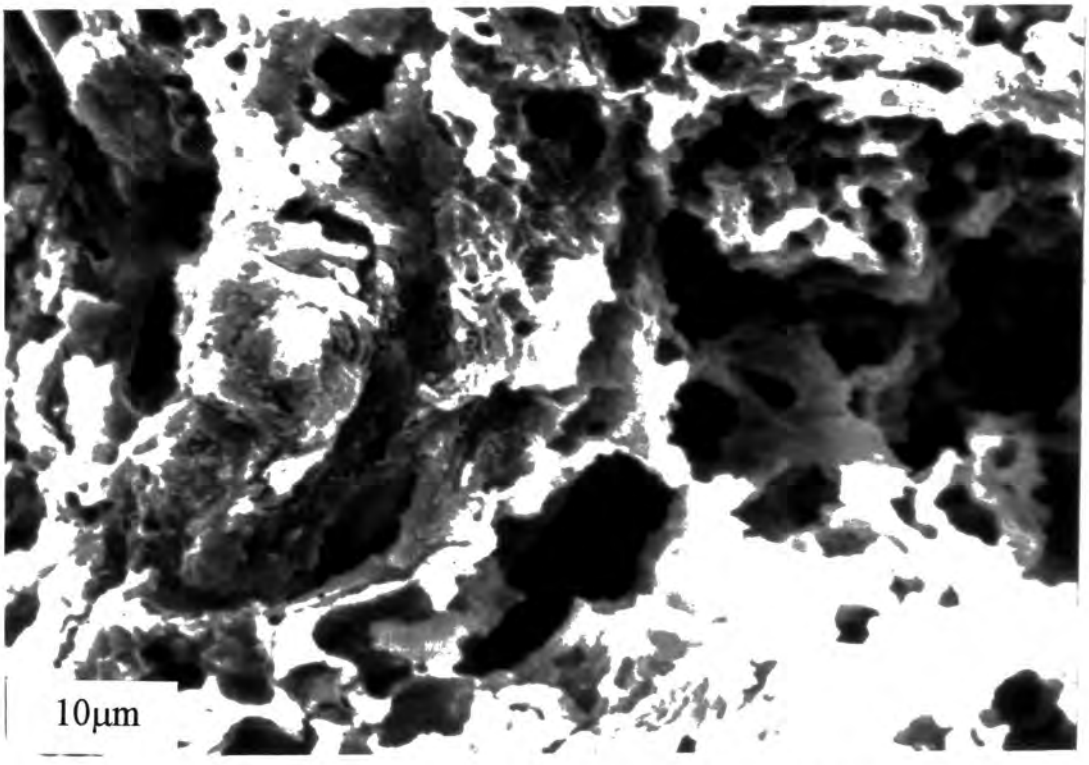

Plate 8.7 High magnification view of Plate 8.6. Note erosion of bone tissues (Possibly by micro-organisms) and dramatic increase in porosity

9. Biomolecules in Fossil Bone

In the light of recent research and developments in biomolecular palaeontology and the essentially interventionist approach to the conservation or preservation of fossil bones, it was considered imperative to investigate the potential for recovering complex macromolecules from excavated bones and consider the possible interferences from post-excavation treatments. The term biomolecular palaeontology has been used to describe the rapidly expanding disciplines concerned with the detection, analysis and interpretation of biological molecules preserved in the geological, fossil and archaeological records. These biological markers or *biomarkers* include a wide range of biologically synthesised molecules of low, moderate and high molecular weights such as amino acids, lipids, proteins, nucleic acids (DNA and RNA), biologically derived pigments (chlorophyll and carotenoid degradation products) and immunologically active protein fragments. Two areas of the rapidly expanding field of research were chosen for particular attention, the analysis of lipid or fatty residues in excavated bones and the extraction of DNA. Building upon his past experience with bog bodies, Dr Richard Evershed (current address: Department of Biochemistry, University of Liverpool) agreed to examine a small number of archaeological bones for their lipid content. Dr Evershed had previously examined specimens of skin and adipocere (a breakdown product caused by the hydrolysis of adipose or fatty tissue) from a number of bog bodies, including Lindow man (Connolly *et al.* 1986; Evershed 1988, 1990, 1991, 1992). The DNA extraction and amplification was undertaken by Dr Martin Richards (Institute of Molecular Medicine, John Radcliffe Hospital, Oxford).

9.1 Lipid Analysis

Lipids are a group of organic compounds that are soluble in organic solvents. They have moderate molecular masses (containing typically 14 to 28 carbon atoms) as opposed to some other biomolecules such as DNA (deoxyribonucleic acid; the carrier of the genetic code in living organisms) which have molecular masses in the thousands. Because of their modest sizes, they are readily extracted and purified, and as a consequence fossil lipids have provided some of the best examples of molecular preservation over geological time. Lipid molecules exhibit a wide variety of molecular architectures and may comprise straight or branched chains or cyclic structures. They are usually fully saturated and very insoluble in water. The latter is of crucial importance when considering their potential for preservation in the archaeological or fossil record.

A total of ten samples were analysed for lipid content, six bone specimens and four samples of soil taken from the immediate vicinity of the bones where this was possible. The bone specimens comprised specimens of cow, horse and pig from the Roman site at Ribchester (Lancashire) and three unidentified bone fragments from the Mesolithic site in the Vale of Pickering (Table 9.1).After excavation, all samples had been transferred to the laboratory and stored, with their adhering soil at

either 4°C or -20°C. A specimen of fresh (modern) bovine cortical bone was also analysed for comparison with the archaeological material. Sample preparation for the lipid extractions was carried out by the author at the University of Liverpool under the supervision of Dr Evershed and following the standard procedure developed for the extraction of lipid residues from archaeological pottery and other specimens (Evershed *et al.* 1992). This procedure is summarized below.

Sample	Sample type	Site data
A	Cow femur	Modern
B	Cow femur (+fat)	Modern
C	Horse	RB 9583 670
D	Cow	RB 9582 684
E	Pig	RB 9582 684
#1	unidentified	VP86AB 5099 2686
#2	unidentified	VP86AB 2711 1016
G	Soil	RB 9582 684 (cow)
H	Soil	RB 9582 684 (pig)
I	Soil	RB 9583 (horse)
	Soil	VP86AB 1014

Table 9.1 Samples submitted for lipid analysis

9.1.1 Experimental Procedure

All surfaces of the bone fragments were abraded using a small, hand-held drill to remove any bone material which may have become contaminated with endogenous lipids from adhering soil or due to inadvertent post-excavation handling. After cleaning, the abraded samples were crushed, dried and weighed. All tweezers, glassware *etc.* were carefully washed and similarly degreased to minimise the risk of contamination with natural oils contained in fingerprints. Each sample was then dried, crushed and weighed. The sizes of the samples ranged from approximately 0.2g to 3g. After addition of 20μl of internal standard (n-tetratricontane for the bone specimens; 100μl 5α-cholestane and 30μl pregnanol for the soils) the lipid components of the samples were extracted with a mixture of chloroform and methanol (2:1 v/v, 2 x 15 minutes ultrasonication). After leaving to settle overnight the extracts were pipetted off and centrifuged (at this point two of the bone samples were lost by breakage of the vials). The supernatants were decanted and evaporated to dryness by rotary evaporation. Following dissolution with a minimum volume of chloroform and methanol, the extracts were transferred to small glass vials (2ml), blown to dryness under a stream of nitrogen, capped and stored in a deep freeze until required for analysis.

The modern bovine bones were mechanically cleaned of soft tissue and marrow, washed in distilled water at about 60°C and then oven dried at 70°C for 1-2 hours. One of these samples was a section cut from the jointed end of the bone and included part of the spongy, trebaculate bone tissue, from which it was impossible to remove the marrow fat. This had become absorbed into the structure of

the bone. The other section analysed was cut from the mid-shaft of the bone. where the endosteal surface is smooth and easily cleaned. This sample contained no absorbed marrow fat.

Aliquots of the total lipid extracts were derivatised (60°C for 10 minutes) in screw-capped vials by treating with N,O-bis(trimethylsilyl)trifluoroacetamide (BSTFA). containing 1% v/v trimethylsilylchloride (Pierce Chemical Co.). The resulting trimethylsilyl (TMS) derivatives were diluted with cyclohexane and analysed by gas chromatography (GC) and gas chromatography/mass spectrometry (GC/MS).

The GC analyses were performed on a Hewlett-Packard 5890A gas chromatograph, coupled to an Opus V PC using Chemstation software. Samples were introduced by on-column injection into a 12m x 0.22mm fused-silica capillary coated with BP-1 stationary phase. Helium was used as the carrier gas at a column head pressure of 20psi. The temperature programme consisted of a 2 minute isothermal hold at 50°C on injection followed by an increase in temperature from 50°C to 350°C at 10°C per minute. The temperature was then held at 350oC for 10 minutes. Flame ionisation was used to monitor the column effluent.

The GC/MS instrument comprised a Pye Unicam 204 GC, equipped with a S.G.E. OCI III on-column injector. The chromatograph was linked to a VG 7070H double-focusing magnetic-sector mass spectrometer. Data acquisition and processing were on a Finnigan INCOS 2300 data system. An Opus V PC equipped with Finnigan DataMaster software was linked to the INCOS to provide additional data-processing. The MS was operated in the electron-ionisation mode (70eV) while maintaining an ion source block temperature of approximately 300°C. An acceleratoer voltage of 4kV was used in scanning the *m/z* range 40-700 in a total scan cycle time of 3 minutes.

9.1.2 Results of Lipid Analysis

The high temperature GC analyses of the trimethylsilylated total lipid extract of the modern bone samples are shown in Figures 9.1a and 9.1b. Figure 9.1a shows the sample with absorbed marrow fat and Figure 9.1b shows that without absorbed marrow fat. The methods employed in this analysis only provide information on the composition of the non-polar lipid fraction in the samples and do not provide evidence of phospholipids for example. Significantly, the GC profile obtained from the sample with absorbed marrow fat is clearly different from that without marrow fat. Figure 9.1b shows substantially lower acyl lipid content than Figure 9.1a, demonstrating that marrow fat is the major source of apolar acyl lipids in bone. The GC analysis of fresh bovine bone without absorbed marrow fat shows cholesterol as the major constituent (Figure 9.1b). The concentration of cholesterol is similar in both of the samples (Table 9.2), suggesting that this compound is more closely associated with the bone tissues rather than the marrow fat. This indicated that the acyl

lipids in bones are associated with the marrow fat whereas the cholesterol is restricted to the bone tissues. The free fatty acids, palmitic ($C_{16:0}$), stearic ($C_{18:0}$) and oleic ($C_{18:1}$) were evident at shorter retention times than cholesterol, while at longer retention times cholesteryl esters were detected. Their presence was confirmed by GC/MS.

Sample	Total lipid yield ($\mu g\ g^{-1}$)	Conc. of C27 steroids ($\mu g\ g^{-1}$)	Conc. of cholesterol ($\mu g\ g^{-1}$)
Modern			
Cow femur	155.4	74.0	74.0
Cow femur + marrow fat	2500.9	78.6	78.6
Archaeological			
Horse	80.4	58.6	46.5
Pig	61.3	41.4	24.6
Cow	56.7	40.9	19.8
VP Sample 1	139.3	32.7	26.8
VP Sample 2	41.4	3.9	1.8

Table 9.2 Total lipid yields and steroid concentrations for modern and archaeological bones

In general, the results of the lipid extraction of the archaeological specimens correlated well with the preservation of the bone specimens as assessed by visual inspection. The two samples from the Roman deposits for which analyses were obtained appeared well preserved with dense, compact bone tissue and no obvious tunnelling. These samples were extremely difficult to crush by hand. The same general trends in lipid composition were seen in all the archaeological samples. More significantly, the composition of the total lipid extract from the archaeological bones most closely resembled that of the modern bone without marrow fat. The high temperature GC analysis of the Roman horse metapodial is shown in Figure 9.2. This profile is dominated by a compound with a similar retention time to cholesterol. GC/MS confirmed this assignment (M^+ 458) in addition to revealing the presence (at slightly longer and shorter retention times) of several degradation products of cholesterol (Figure 9.3). Eluting as a shoulder on the cholesterol peak at longer retention time is 5α-cholestanol (M^+ 460), the expected product of anaerobic reduction of cholesterol. Eluting at shorter retention time and with a lower abundance is a peak corresponding to 5β-cholestanol (coprostanol; M^+ 460). Co-eluting with 5β-cholestanol is the corresponding C27 steroidal ketone, 5β-cholestan-3-one (M+ 386). Also present between this and the cholesterol peak is a peak corresponding to 5α-cholestan-3-one (M^+ 386).

The total lipid extract of the substantially older, Mesolithic, samples (Samples 1 & 2) are shown in Figures 9.4a and 9.4b. Although both these samples were poorly preserved compared to the Roman horse metatarsal, the data obtained from sample 1 was analogous to that from the Roman sample. Sample 1 had a relatively high abundance of cholesterol (26.8mg g^{-1}) and cholesterol degradation products (5β-cholestanol, 5β-cholestanol, 5β-cholestan-3-one and 5α-cholestan-3-one) although the

latter were present in much lower relative abundances than those seen in the Roman bone. At short retention time, free fatty acids were evident and monoacylglycerols, diacylglycerols, triacylglycerols and cholesteryl fatty acids were all seen at longer retention times. All the above assignments were confirmed by GC/MS. In contrast to Sample 1, the other Mesolithic bone (Sample 2) had a much lower abundance of cholesterol (1.8mg g^{-1}) which was exceeded by the abundance of 5α-cholestanol. Other cholesterol degradation products, 5β-cholestanol, 5β-cholestan-3-one and 5α-cholestan-3-one were present in smaller quantities than cholesterol. Although free fatty acids and cholesterol esters were detected, there was no evidence for mono-, di- or triacylglycerols.

This analysis was intended as a preliminary investigation only and does not show the full range of potential lipid residues. The experimental procedure outlined above would not, for example, reveal the presence of phospholipids. However, it is clear from the data reported above that lipids do persist in archaeological bones, or at least bones from waterlogged, anoxic environments since the bones from Ribchester and the Vale of Pickering examined came from such conditions. Most significant of those lipids present are cholesterol and its degradation products. These compounds have been observed in other archaeological remains, particularly the tissues of bog bodies (Evershed 1990, 1991; Evershed & Connolly 1987) which also represent finds from waterlogged sites where anoxic conditions have prevailed for the major part of the period of burial. The presence of 5α- and 5β-cholestanol and 5α- and 5β-cholestan-3-one are significant since these compounds represent two separate pathways for the diagenetic reduction of cholesterol. The 5α- and 5β-cholestan-3-ones represent the intermediates in the pathways for the conversion of cholesterol to 5α- and 5β-cholestanol respectively. In the case of the skin tissues from Lindow Man, the occurrence of unexpectedly high levels of 5β-cholestanol and 5β-cholestan-3-one were attributed to the action of gut flora released during the early phases of decay. 5β-steroids were present in all of the archaeological bones examined above but in substantially smaller amounts than cholesterol, suggesting that these quantities represent the natural abundances arising though the action of micro-organisms in the burial environment. The relative contributions to these decay processes by the action of cellular enzymes or micro-organisms active in animal tissues at the time of death, and the activities of micro-organisms in the burial environment are difficult to separate however. Further complications arise from the fact that the preservation of biomolecules is seriously influenced by the nature of the physico-chemical environment in which the tissues have been buried. In addition, preservation of lipids in bone will be determined by any pre-burial taphonomic processes, *e.g.* mechanical cleaning, boiling or cooking, method and time of discard *etc.*

Taphonomic processes have a bearing on the low abundances of free fatty acids and acyl lipid in the archaeological samples. There are two possible explanations; the bone specimens contained low concentrations of acyl lipid at the time of burial or discard, or the bones contained substantial amounts of these lipids but these were subsequently degraded during their period of burial. The

archaeological record certainly contains considerable evidence for the processing of animal long bones to remove marrow (which contains high levels of acyl lipids *cf.* Table 9.2) in the form of cut marks and characteristic spiral fractures. Removal of the marrow in this manner would seriously reduce the quantities of lipid in processed bones at the time of burial or discard.

The samples examined above were extracted from untreated bone specimens without any attempt at subsequent extractions from demineralized tissues. Previous studies by Shapiro and others have demonstrated that after initial extraction from whole bone, additional lipid residues may be extracted following demineralization to remove the hydroxyapatite component (Shapiro 1973). Vaughan quoted Shapiro as reporting that of the total lipids released from bone, 65% were removed prior to decalcification (Vaughan 1975, 83) and that cholesterol esters formed the bulk of the post-demineralized extract. By comparison, 94% of the pre-demineralized lipid extract was made up of triglycerides. Although Shapiro postulated that a small fraction of the lipids, approximately 8% were covalently bound to the collagen molecules, it is also possible that lipids and other biomolecules are either tightly bound to the surfaces of the hydroxyapatite crystals or are actually locked away inside the crystallites. If the lipid molecules are in fact irreversibly bound to the bone mineral crystallites. then a combination of gas chromatography/mass spectrometry holds enormous potential for dating and isotopic evidence even in cases where practically all of the other organic components of bone tissues have degraded and been lost or corrupted.

The finding of cholesterol in all of the bone samples studied so far has significant implications for its use in other archaeometric studies. The possibility arises for its use as a new palaeodietary indicator in studies involving the measurement of $\delta^{13}C$. The availability of on-line GC/isotope ratio monitoring MS instruments and the relatively high abundances of cholesterol present in the samples (even without demineralization) permits the comparison of lipid $\delta^{13}C$ measurements with those of $\delta^{13}C$ and $\delta^{15}N$ from collagen. This could potentially provide a confirmation that the isotopic signatures from collagen are unaltered by diagenesis. The possibility of making such measurements on cholesterol is appealing since its identification assures that it is undegraded and therefore accurately reflects the original isotopic composition of the lipid. It may even be possible to use the 5α- and 5β- cholestanol component of the lipid extract since although these are degradation products of cholesterol, their carbon skeletons are fully intact and once again represent the original isotopic ratios. Cholesterol has the additional advantage of a possibly higher turnover rate during the life of the organism than does collagen and therefore represents the isotopic composition of diet more faithfully.

In parallel with future work on fossil lipid analysis, some research must be directed to the problems of contamination, both due to diagenesis of the bones themselves or by humans handling the specimens. The latter can be easily overcome by strict adherence to good excavation and laboratory

practice. For example, post-excavational contamination can be reduced by the use of gloves by the excavator and by the swift transfer of bagged samples to a refrigerator or freezer to reduce contamination by the growth of bacteria or fungi on the bones. However, the problem of diagenetic contamination is more serious. The sediments surrounding bones are an obvious source of chemical contamination, either by material diffusing into the fabric of the bone from the soil or through the growth of fungi or bacteria on the specimen. This problem has already been examined with regards to the contamination of another porous, archaeological material- pottery. Lipid extracts from pottery sherds have been compared to the total lipid extract from the soil adhering to the specimens (Evershed *et al.* 1992, 1993). Figures 9.5a and 9.5b show the GC 'fingerprint' from an analysis of the total lipid extract of the Roman pig bone specimen and the corresponding GC 'fingerprint' from the lipids in the surrounding soil. The major components of the soil are long-chain alcohols, alkanes, fatty acids and wax esters. These are in contrast to the presence of cholesterol and its diagenetic degradation products in the bone specimen. This observation indicates that it is indeed possible to distinguish between lipids endogenous to the bone specimen and those arising from the action of micro-organisms either in the porosity of the bone or the surrounding soil. Lipid analysis holds great promise, therefore, as a secure biomarker.

9.2 DNA Analysis

Recent years have seen a proliferation of papers published on the extraction of DNA from ancient tissues and often each successive publication pushes back even further the earliest date from which genetic material has been recovered. The driving force of this revolution in extracting and identifying DNA was the development in 1985 (Mullis 1990) of the polymerase chain reaction (PCR). Previous to the development of PCR it was necessary to use difficult and lengthy cloning techniques to obtain sufficient DNA to sequence. In 1986, attempts to isolate DNA from the tissues of the (Roman Iron Age) bog body found in Lindow Moss using conventional techniques (without cloning) were unsuccessful (Hughes *et al.* 1986). Within four years however, DNA was identified and sequenced from Magnolia leaves 17-20 million years old by amplifying fragments of the surviving DNA using PCR although in some respects this work is controversial(Golenberg 1990). More recently still, DNA has been amplified and sequenced from a 120-135 million-year-old extinct nemonychid weevil preserved in amber (Cano *et al.* 1993) and the discovery of possible red blood cells in a fossilized *Tyrannosaurus rex* bone has sparked considerable debate about the potential for extracting and sequencing dinosaur DNA (Morrell 1993).

The polymerase chain reaction permits the amplification of trace amounts of DNA into quantities that can be analysed by submitting them to successive cycles of controlled heating, breaking the hydrogen bonds within the double helix, and enzymatic copying of the isolated strands. With each successive cycle, the amount of target DNA increases exponentially allowing analysis from a single

strand of hair or droplet of blood taken from an individual (Higuchi *et al.* 1988). The use of PCR therefore dramatically speeds the study of genetic information in forensic detection or the investigation of living populations. PCR amplification of DNA from ancient remains however has first to overcome two distinct problems, one inherent to the nature of the material examined and one which rests in the experimental methodology. Unlike modern blood and hair samples, ancient material is invariably bound up in the specimen with an array of organic and inorganic substances which may alter the results of the subsequent analysis. For example, the inability to extract DNA from a particular specimen may reflect inhibition of the PCR reaction rather than the absence of any suitable DNA template. Secondly, any surviving endogenous DNA may be far outnumbered by contaminant DNA from the human experimenters during excavation, handling or during PCR itself.

Humic acids are frequently present in fossil bones and other archaeological materials and may be extracted and purified along with the surviving DNA. Their presence in DNA extracts is demonstrated by a marked blue-white fluorescence under ultraviolet light. The term 'humic acids' is used to describe a complex heterogeneous class of stable, large molecules derived from decaying organic matter and generally believed to result from the reaction between proteins and carbohydrates. These humic acids are implicated in the inhibition of the PCR reaction since they are known to form cross-links with proteins and have been demonstrated to cause inhibition when added to reaction mixtures at concentrations known to occur in excavated bones (Richards *et al.* 1993). The inhibition in PCR can be overcome by the addition of anti-inhibitory agents such as chelex (a chelating resin) and bovine serum albumin (BSA) to the solutions. The problem of contamination by exogenous DNA is critical when examining human tissues or skeletal remains since modern contaminant sequences may be indistinguishable from ancient sequences, although a particularly strong signal will arouse suspicions. Modern DNA will almost certainly be amplified in preference to ancient DNA since it is undegraded and much better preserved than material that has undergone prolonged burial. If the only source of contamination was the person attempting PCR then it would be a simple matter to identify authentic and contaminant sequences. However, if the source of contamination is within the laboratory equipment or the skeletal remains are already contaminated (perhaps by several handlers) when they arrive at the laboratory then authentic sequences will be impossible to recognise. Contamination by experimenters or their equipment can be avoided by careful laboratory procedures but the problem of casually handled bones clearly lies outside of the experimenters' control and can be particularly serious in skeletons excavated perhaps several years previously. Analysis of animal bones is a good indicator of whether contamination by human DNA has occurred. Independent analyses by Hagelberg and Clegg (1991) and Richards *et al.* (1993) have demonstrated that endogenous DNA may be extracted and sequenced from animal bones by examining a pig rib from the wreck of the *Mary Rose* which had lain undisturbed in the mud off Portsmouth harbour since 1545. However it must be concluded that this sample from waterlogged and anoxic conditions is exceptionally well preserved compared to the majority of ancient bones.

9.2.1 Experimental Procedure

Seven bone samples were submitted for analysis, covering a wide range of ages from Mesolithic to late medieval (Table 9.3). All sample preparation, analysis and interpretation was done by Martin Richards of the Institute of Molecular Medicine, John Radcliffe Hospital, Oxford. A simplified description of the experimental procedure is summarized below.

Sample	Sample type	Site data
1	Horse	RB89 9583 670
2	Cow	RB89 9582 684
3	Pig	RB89 9582 684
4	Unidentified	RO329
5	Unidentified	VP86 2551 1007
6	Unidentified	SW84
7	Human	Surface collection

Table 9.3 Samples submitted for DNA analysis

Bone samples were initially air-abraded to remove the outer surface and any potential contamination, then ground and washed in sterile water. The resulting powder was demineralized by incubating in 0.5 Molar ethylenediamene-tetra-acetic acid (EDTA) at 37°C for one day before adding 0.5% Sarkosyl and 100mg ml^{-1} of proteinase K for a further day. The solution was then extracted with phenol, phenol-chloroform and again with chloroform/iso-amyl alcohol to remove proteins and other matter. The DNA was then separated from the remaining EDTA by successive rounds of centrifugal dialysis. The concentrated DNA extract was then purified using a genomic purification column.

The DNA extracts were treated with 5% Chelex-100 resin for 10 minutes at room temperature, then microcentrifuged at 13000g for three minutes and the DNA taken off. The DNA was amplified in 10mM Tris-HCl, pH 8.3, 50mM KCl, 1.5mM $MgCl_2$, 200mM of each dNTP, 12 pmol of each primer and 1.2 units of *Taq* polymerase for 40 cycles. To enhance the sensitivity of the reaction, a period of 4 minutes pre-treatment at 94°C and a further 8 minutes post-treatment at 72°C were employed. Each cycle comprised one minute at 55°C, 1 minute at 72°C and one minute at 94°C. BSA at 160$\mu g ml^{-1}$ was added to the PCR mixture. Direct sequencing of the single-stranded DNA products was performed using a Dynal system.

All samples were initially amplified for 40 cycles with the universal primers cytbL1-B and cybtH2 (Table 9.4), from the mitochondrial DNA cytochrome b region. This gives a 96-bp product in a wide range of mammalian species. To enhance the signal 10μl aliquot of the product was run into a 3% Nuseive low-melting temperature agarose gel and re-amplified for 30 cycles from a 1-5 dilution of the fragment in the agarose cut from the gel (about a 1 in 10 dilution of the product). Single

stranded DNA was prepared from the biotinylated product using the Dynal method (binding of DNA to streptavidin-coated magnetic beads and removal of non-biotinylated strand by denaturation with 0.15 molar NaOH whilst retaining the biotinylated strand on the beads with a magnet). This was sequenced with 1 pmol of cytbH2 by the dideoxy chain termination method using the Sequenase 2.0 kit (United States Biochemicals).

9.2.2 Results of DNA Analysis.

All of the samples examined amplified with the exception of the human bone specimen from Cyprus. An extraction blank run in parallel with the bone samples also failed to amplify indicating that there was no significant contamination of the archaeological samples during preparation of the DNA. The Mesolithic bone sample (VP86P 2551 1007) amplified only weakly, probably as a result of heavy inhibition by humic acids. The extract from this sample retained a slight brown colouration even after column purification. Despite being short and indistinct, the sequences obtained were all clearly human. The samples were therefore re-amplified with human-specific primers (con LC and conH2-B) to give a 232-base pair product from the first hyper-variable segment of the mitochondrial control region. Again, all amplified except for the Mesolithic sample. The human specimen from Cyprus amplified only after dilution. The six samples that did amplify were sequenced with conLC in an attempt to identify the contaminating sequence. Three of the samples were readable from 16,250-16,390, two were readable only up to 16,367 and the Cyprus sample was unreadable. There was no detectable variation from the standard reference sequence (Anderson *et al.* 1981). This is the 'consensus' sequence for Europeans and is the result that would be obtained by mixing a lot of individuals together (Richards *et al.* 1993, 22-23). This may mean that the bones were handled by several individuals or simply became contaminated with dust, much of which is made up of sloughed off skin cells.

Subsequent attempts were made to amplify the extracts with primers (AN1 and AN2) that specifically target parts of the mitochondrial control region and designed to be cow-specific, although they also amplify pig DNA (Table 9.4). These primers offer a method of bypassing the problems associated with the human contamination of samples. Only the cow bone from Roman Ribchester (RB9582 684) and the unidentified bone (probably bovine) from Stanwick (SW84) gave positive results with this primer. Despite apparently excellent preservation of the bone, the pig specimen from Ribchester and the other cow specimen from Rothwell failed to amplify. In future analyses these primers offer a means of distinguishing between species when combined with sequencing.

Primer	Sequence
cytbH2	GTA GTG TAT TGC TAG GAA TAG GCC TG
conLC	CCC CAT GCT TAC AAG CAA G
ConH2-B	B TTG ATT TCA CGG AGC ATG GT
AN1	ACG CGG CAT GGT AAT TAA GC
AN2	GCC CCA TGC ATA TAA GCA AG

Table 9.4 Primers used in amplification of samples

There still remains considerable work to be done in the analysis of ancient DNA, particularly that from bones. Improvements in laboratory procedures and the handling of bone specimens are rapidly overcoming the problems of contamination during sample preparation and analysis. However, the problems of potential contamination in the ground, during excavation and during post-excavation processing remain to be investigated thoroughly. Regimes for the sterile lifting and handling of bone specimens from waterlogged archaeological deposits have already been implemented so that promising specimens may be recovered and frozen for prompt analysis. Despite scrupulous excavation and storage, it is possible that contamination may occur during burial since faecal matter might be expected to contain blood or tissue residues and archaeological deposits frequently include midden material. The work described above indicates that future work should concentrate on freshly excavated material from sites that produce 'well preserved' bones, using samples that have been collected specifically with DNA and other biomarker analysis in mind, and that soil samples taken from adjacent to the bone specimens should also be analysed as controls. Here of course, the question of 'What is a well preserved bone?' arises. Hagelberg *et al.*(1991b) examined the relationships between the survival of extractable DNA and the macroscopic and microscopic preservation of human bones from the 17th century Civil War cemetery at Abingdon, Oxfordshire (Hagelberg *et al.* 1991). Their results demonstrated that there can be considerable variation in the macroscopic, microscopic and DNA preservation within a single archaeological site, even for burials of approximately the same date. They also concluded that even in bone specimens that appeared poorly preserved, there were regions of the bone with good histological preservation. Hagelberg *et al.* proposed that bones to be submitted for DNA analysis should be histologically screened to select the best preserved specimens and those areas of individual bones with un-remodelled tissue (Hagelberg *et al* 1991b, 406).

Experimental projects to correlate the survival of DNA with the presence of other biomarkers such as lipids and proteins may also throw some light on where the DNA actually resides in ancient bones and thus aid the selection process. Although surviving blood cells have been reported in fossil bones (Wilby 1992; Morrell 1993; the author, section 3.1.4) these may not be necessary for the preservation of DNA since in common with many other proteins DNA is strongly bound by the surface of hydroxyapatite.

9.3 Humic Acids in Fossil Bones

The mobility of many metal ions, including iron and manganese, in the burial environment is influenced by their ability to form soluble complexes with 'organic matter' in the soil. This organic matter is formed during the accumulation of soils and peat by the action of micro-organisms on organic compounds of plant and animal origin. The resulting complex structures are known by the general term 'humic material'. Humic material may be classified into three groups:

humic acids; dark brown compounds that tend to predominate in neutral to alkaline soil.

fulvic acids; light straw or tea coloured compounds that dominate in acid soils and peats

humins; dark brown residues with a high ash content that are insoluble in both acids and alkalis.

Humic acids have high molecular weights and a high carbon content (see Table 9.5). Humic acids play an important role in the formation of peat deposits and humic soils and the dark brown colouration of these deposits is due to the presence of humic acids. It has been demonstrated that mould and fungi (*e.g. aspergillus & penicillium*) can produce dark, red and brown coloured compounds when grown in media composes of glucose and mineral salts. The 'humic acids' created in these experiments contained 45-51% carbon, 6-6% nitrogen and approximately 3% nitrogen. Certain bacteria (myxobacteria) have been demonstrated to create humic acids by the decomposition of cellulose (Manskaya & Drozdova 1968).

Acids	C (%)	H (%)	N (%)
Humic acids	52-62	3.0-4.5	3.5-4.5
Fulvic acids	44-48	4.0-5.5	1.5-2.5

Table 9.5 Carbon, hydrogen and nitrogen analyses of peat and various soils (from Manskaya & Drozdova 1968, 41)

The enormous numbers of micro-organisms in soils have a considerable influence on the chemistry of the burial environment by their participation in the decomposition of proteins, carbohydrates and fats, including relatively stable, high molecular weight structures such as lignin, tannins, waxes and pitch. Following decomposition of these organic compounds, considerable quantities of simpler molecules such as amino acids, phenolic compounds, sugars and organic acids are liberated into the soil solution. In turn these simple compounds are synthesised into the dark-coloured compounds that comprise humic acids. At elevated temperatures, amino acids react with reducing sugars to form dark-coloured, amorphous, nitrogen-containing condensation products called melanoidins (Manskaya & Drozdova 1968, 58). This reaction is known as the Maillard Reaction and is analogous to the formation of caramels during the cooking of food although evidence points to the formation of melanoidins at much lower temperatures. Among the many intermediate compounds

formed during the synthesis of melanoidins is a substance that fluoresces under ultraviolet light (Manskaya & Drozdova 1968, 67). If bisulphite is present during the reaction, this fluorescent species tends to accumulate and the dark colouration characteristic of melanoidins and humic acids does not appear.

Most bones excavated from the soil or terrestrial sediments are brown in colour and those from waterlogged or acidic environments tend to be darker than those deriving from relatively neutral soils. Generally, only bones excavated from noticeably alkaline soils remain white or cream (refer to the Munsel colours in Table 4.1). Although histological study and XRF analysis of fossil bones has demonstrated that there is considerable infiltration of iron and manganese ions, which both form dark oxides or oxyhydroxides when exposed to the air, there is evidence to suggest that mineral salts do not account for all the discolouration of the bones. During the hydrazinolysis of bone samples 1 to 15, one obvious feature distinguishing different samples was the colour of the supernatant hydrazine extracts (Table 9.6).

Well preserved bone specimens (10 and 11) produced a white or slightly pink solution following protein extraction whereas the colours of the solutions for other samples ranged from straw yellow, through rose/tea coloured to dark brown or even green. Since hydrazine is a strong reducing agent and would reduce dark iron and manganese oxides or oxyhydroxides to pale green or pink respectively, it is unlikely that the colours of the extracts were attributable to metal ions. Furthermore, those hydrazine deproteinized samples that were originally dark brown remained stained after treatment (unfortunately the deproteinized samples were not subject to XRF analysis to determine their iron and manganese contents).

Sample	Colour of hydrazine extract	Munsell
1	pink/tea	2.5Y7/2
2	pink/tea	2.5Y8/2
3	straw yellow/brown	5Y8/1
4	white/cream	White
5.2*	yellow/brown	10YR8/3
6.1*	dark tea	10YR8/2
6.2*	green	
7	pink/brown	7.5YR5/2
8	straw yellow	White
9	white/cream	10YR8/1
10	white	White
11	white/cream	White
12*	pink/tea	10YR7/2
13*	pink/tea	10YR7/3
14*	dark tea	10YR4/3
15*	dark tea	10YR5/2

Table 9.6 Colours of hydrazine extracts (samples 1-15)
Those samples marked with an asterix derive from waterlogged environments

Those hydrazine extracts with a dark brown colour were found to fluoresce with a greenish tinge when viewed under ultraviolet light whereas that from fresh bone did not. Simple paper chromatography of the fluorescing extracts confirmed that the fluorescing species was different from the extracted protein (disclosed by spraying the chromatogram with ninhydrin). Hot alkali extracts of archaeological bone specimens were similarly found to fluoresce in ultraviolet light.

Recent experiments in the burial of bones and other organic and metallic artefacts in a raised peat bog (S. Kelly in preparation) have shown that bone rapidly takes up a red-brown stain from the soil and that this stain can penetrate up to several millimetres from the periosteal surface in a period of less than 12 months. The presence of humic acids has been reported by previous researchers on the evidence of infrared specrophotometry (Weiner & Bar-Yosef 1990) and the inhibiting effects of humic acids on the PCR reaction were mentioned above (section 9.2). However, there was no evidence from infrared analysis of either untreated archaeological bone samples or the acid insoluble residues of archaeological bone for humic or fulvic acids.

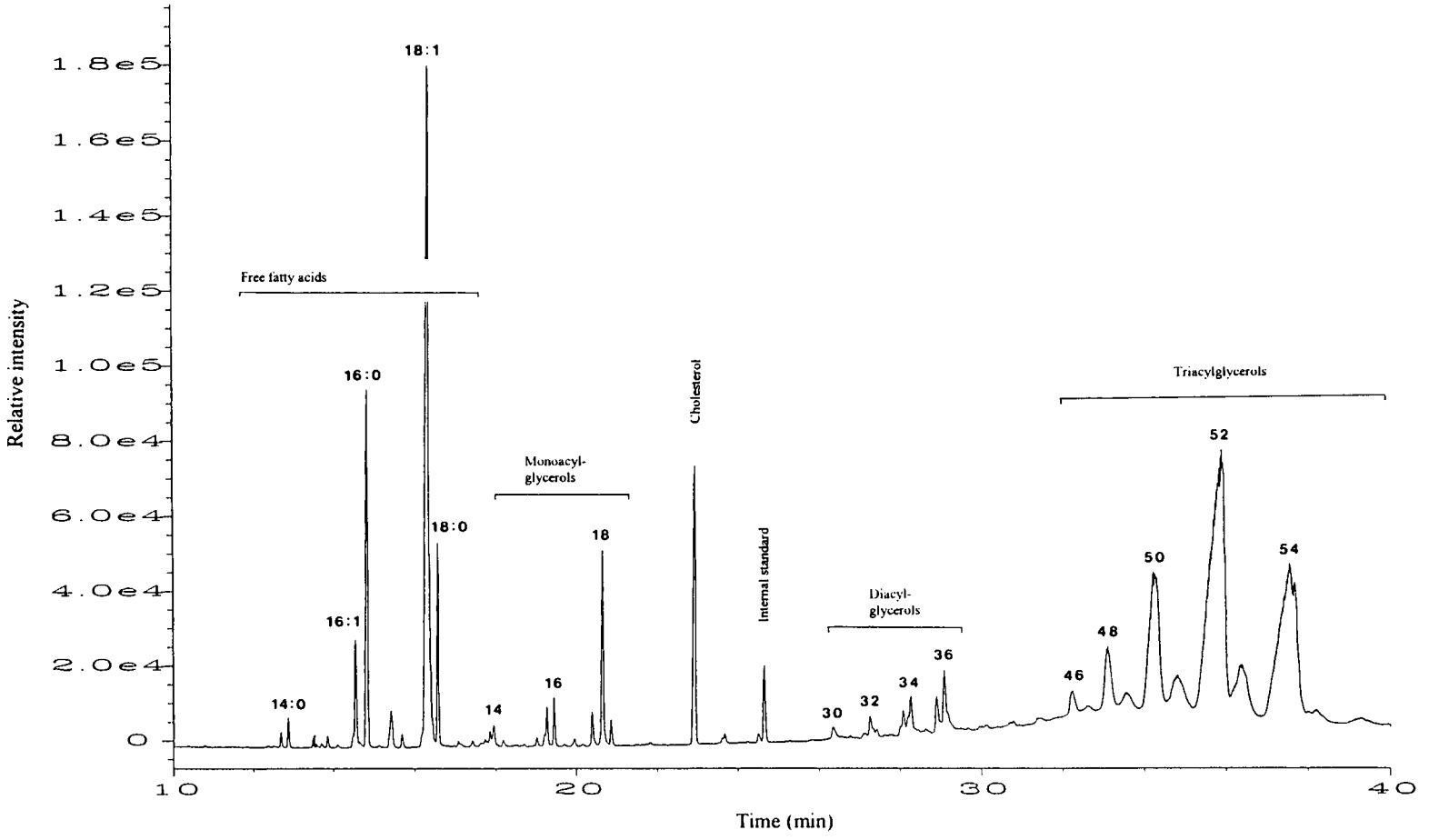

Figure 9.1a Gas chromatogram obtained for the trimethylsilated total lipid extract of modern bone with adsorbed marrow fat. The bracketed region denote the retention time windows for the fatty acids, monoacylglycerols, diacylglycerols, triacylglycerols and cholesteryl esters. The numbers on the peaks correspond to the number of acyl carbon atoms contained in the respective class of lipid.

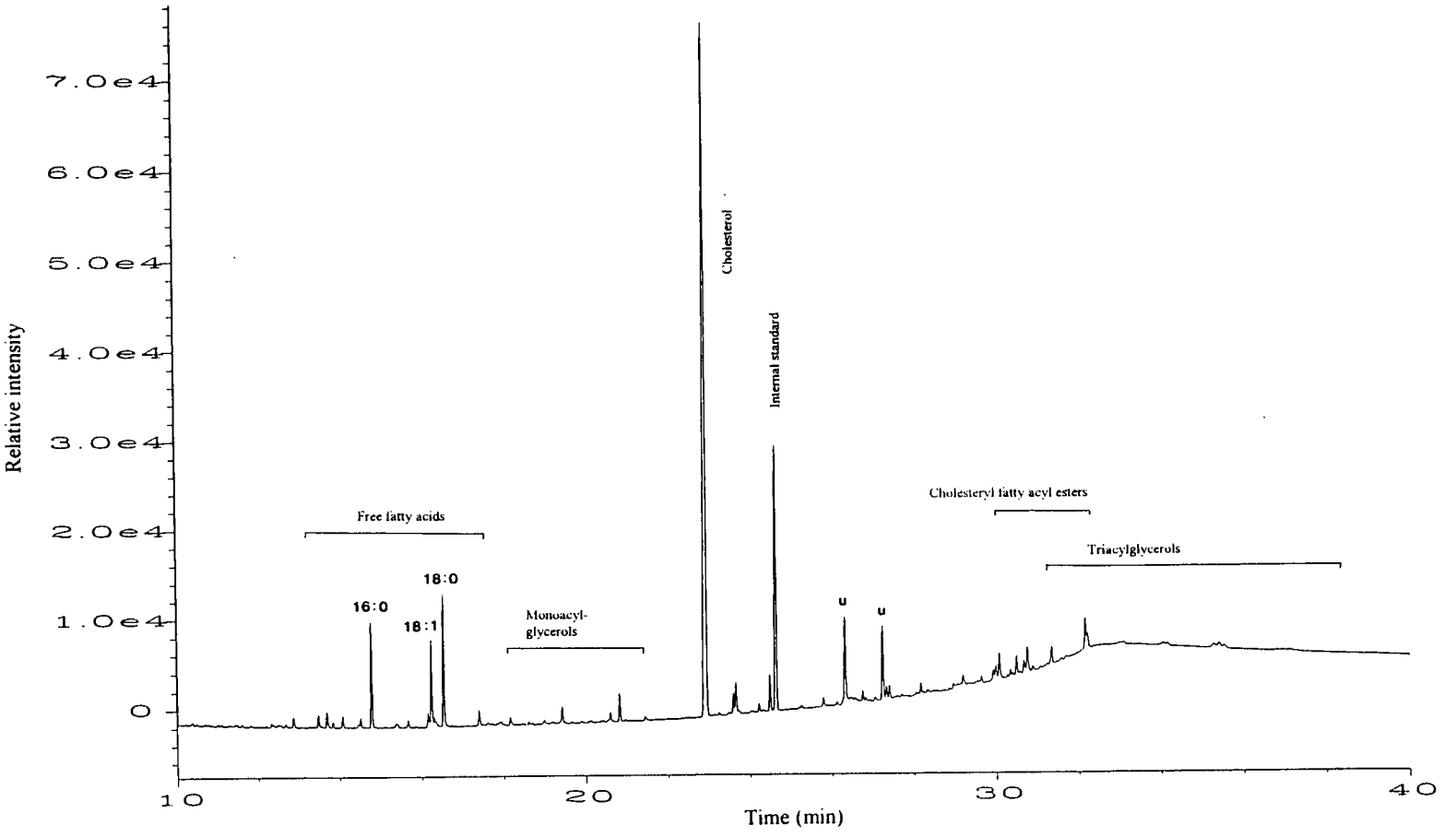

Figure 9.1b Gas chromatogram obtained for the trimethylsilated total lipid extract of modern bone without adsorbed marrow fat. The bracketed region denote the retention time windows for the fatty acids, monoacylglycerols, diacylglycerols, triacylglycerols and cholesteryl esters. The numbers on the peaks correspond to the number of acyl carbon atoms contained in the respective class of lipid.

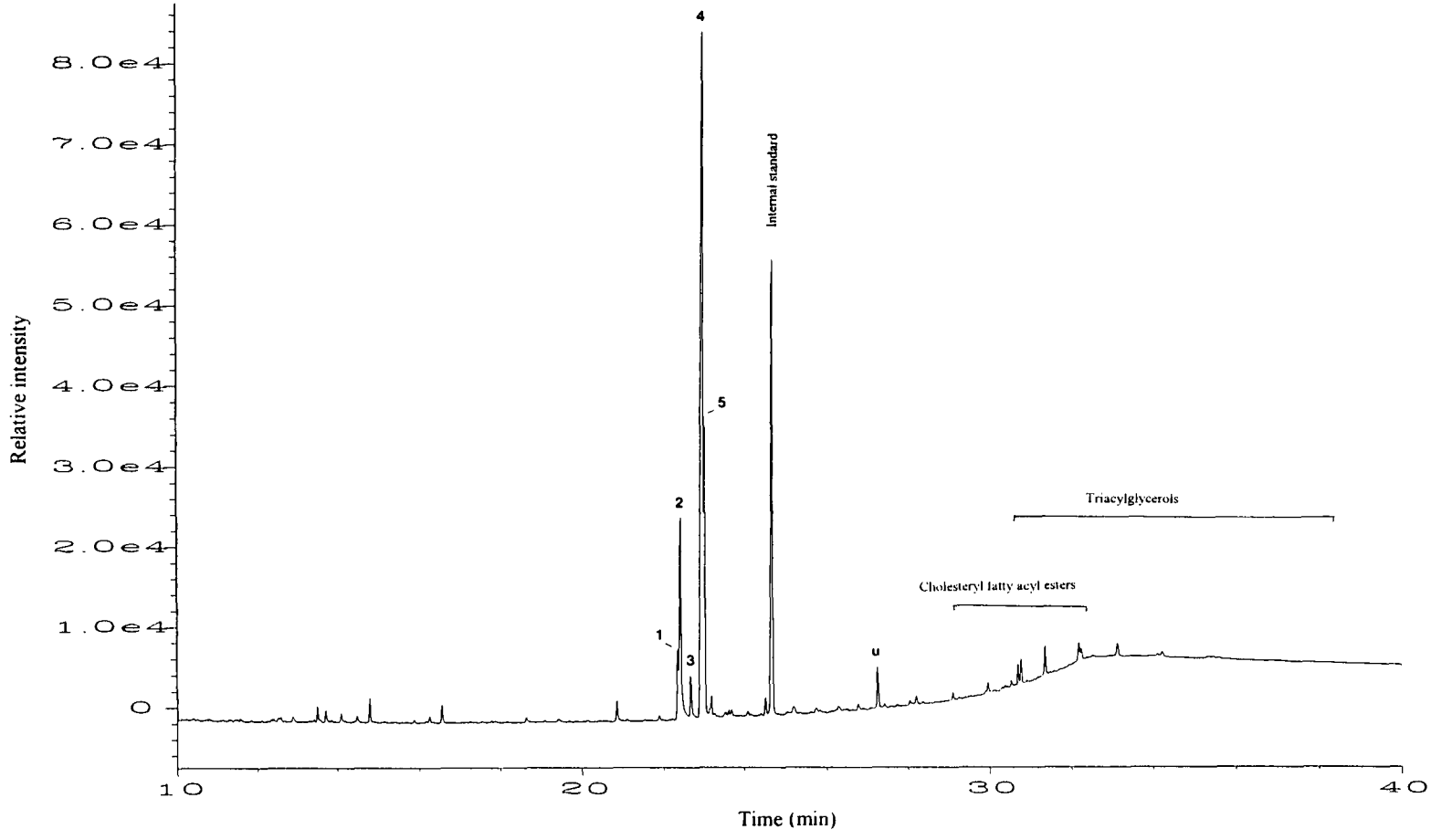

Figure 9.2 Gas chromatogram for the trimethylsilated (TMS) total lipid extract of the horse metapodial bone from the Roman excavation at Ribchester. Peak identities: 1 = 5β-cholestan-3-one; 2 = 5β-cholestanol; 3 = 5α-cholestan-3-one; 4 = cholesterol; 5 = 5α-cholestanol; u = unknown. The bracketed peaks correspond to cholesteryl fatty acid esters and triglycerols.

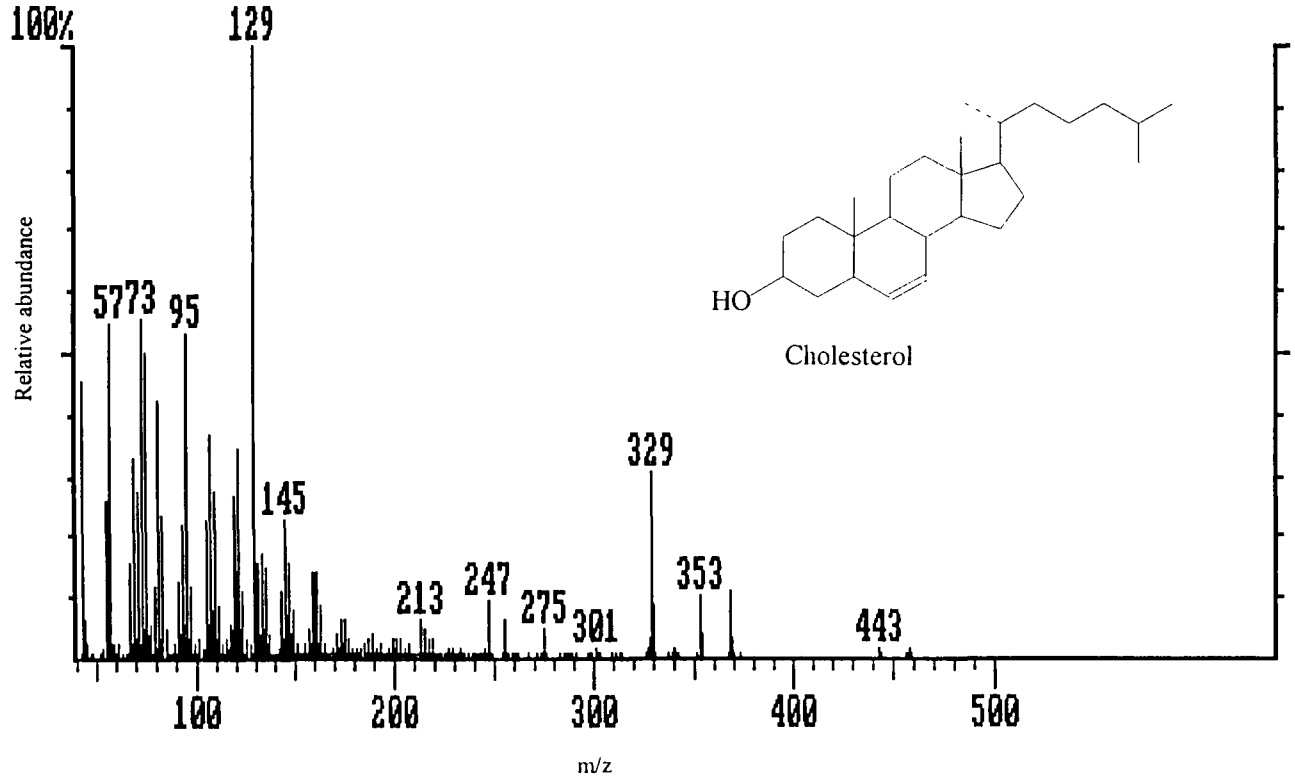

Figure 9.3 Electron ionisation (EI 70eV) mass spectrum of cholesterol (TMS ether derivative from the horse metapodial in Figure 9.2). The insert shows the chemical structure of cholesterol.

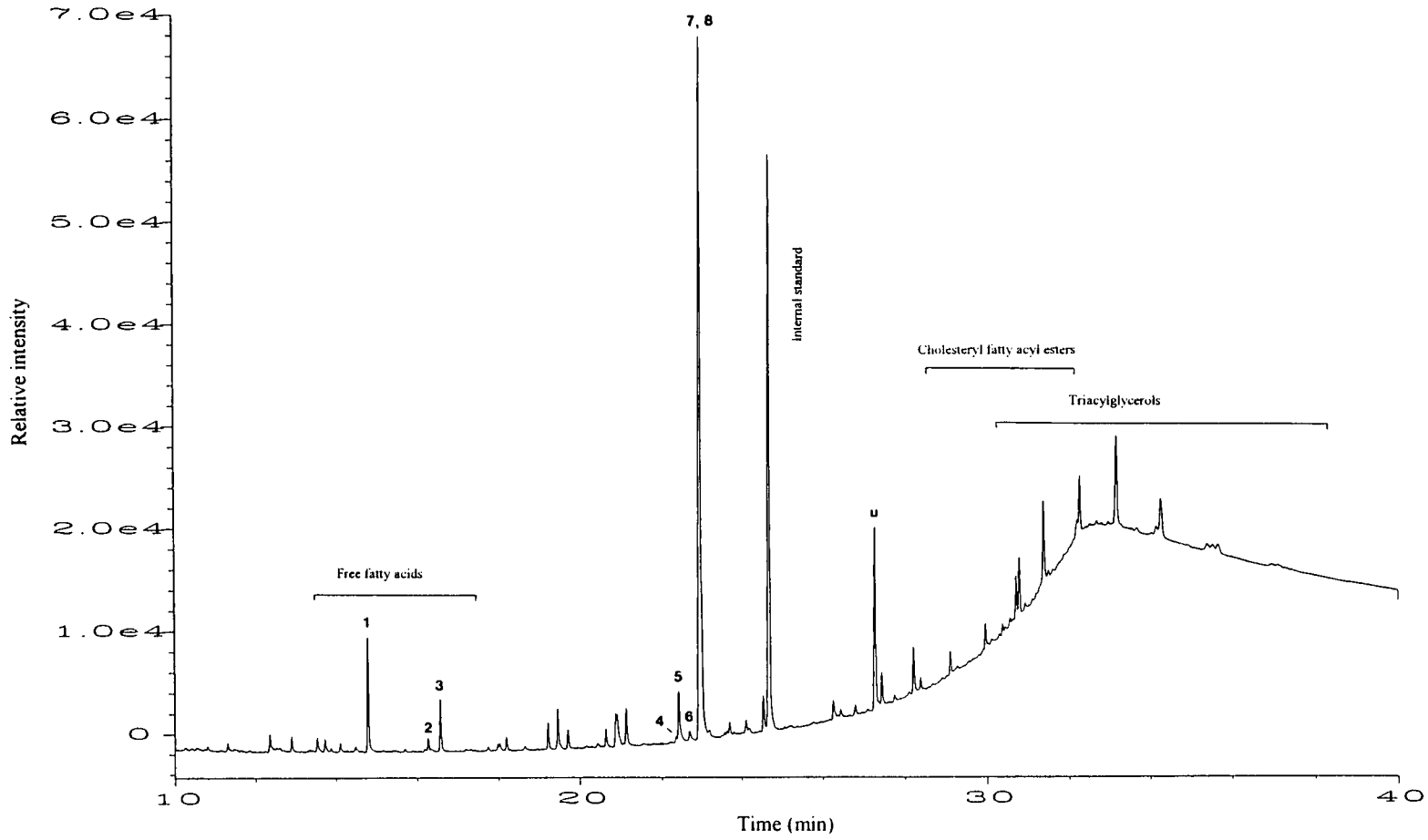

Figure 9.4a Gas chromatograms for the TMS total lipid extract of Mesolithic bone #1. Peak identities: 1 = hexadecanoic acid (C16:0); 2 = octadecanoic acid (C16:0); 3 = octadecanoic acid (C18:0); 4 = 5β-cholestanol; 5 = 5β-cholestanol; 6 = 5α-cholestan-3-one; 7 = cholesterol; 8 = 5α-cholestanol; u = unknown. The bracketed peaks correspond to cholesteryl fatty acid esters and triglycerols.

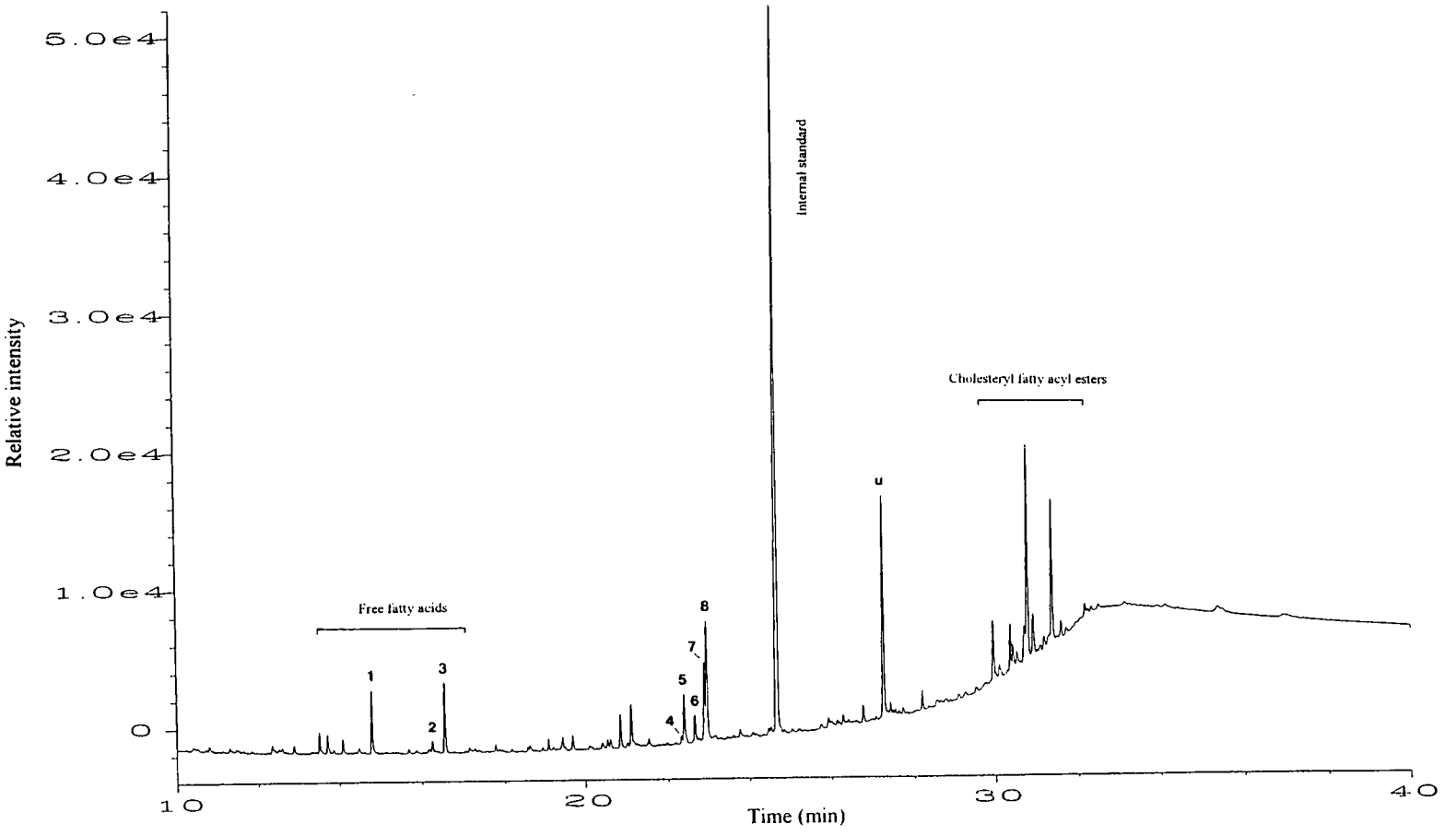

Figure 9.4b Gas chromatograms for the TMS total lipid extract of Mesolithic bone #2. Peak identities: 1 = hexadecanoic acid (C16:0); 2 = octadecanoic acid (C16:0); 3 = octadecanoic acid (C18:0); 4 = 5β-cholestanol; 5 = 5β-cholestanol; 6 = 5α-cholestan-3-one; 7 = cholesterol; 8 = 5α-cholestanol; u = unknown. The bracketed peaks correspond to cholesteryl fatty acid esters and triglycerols.

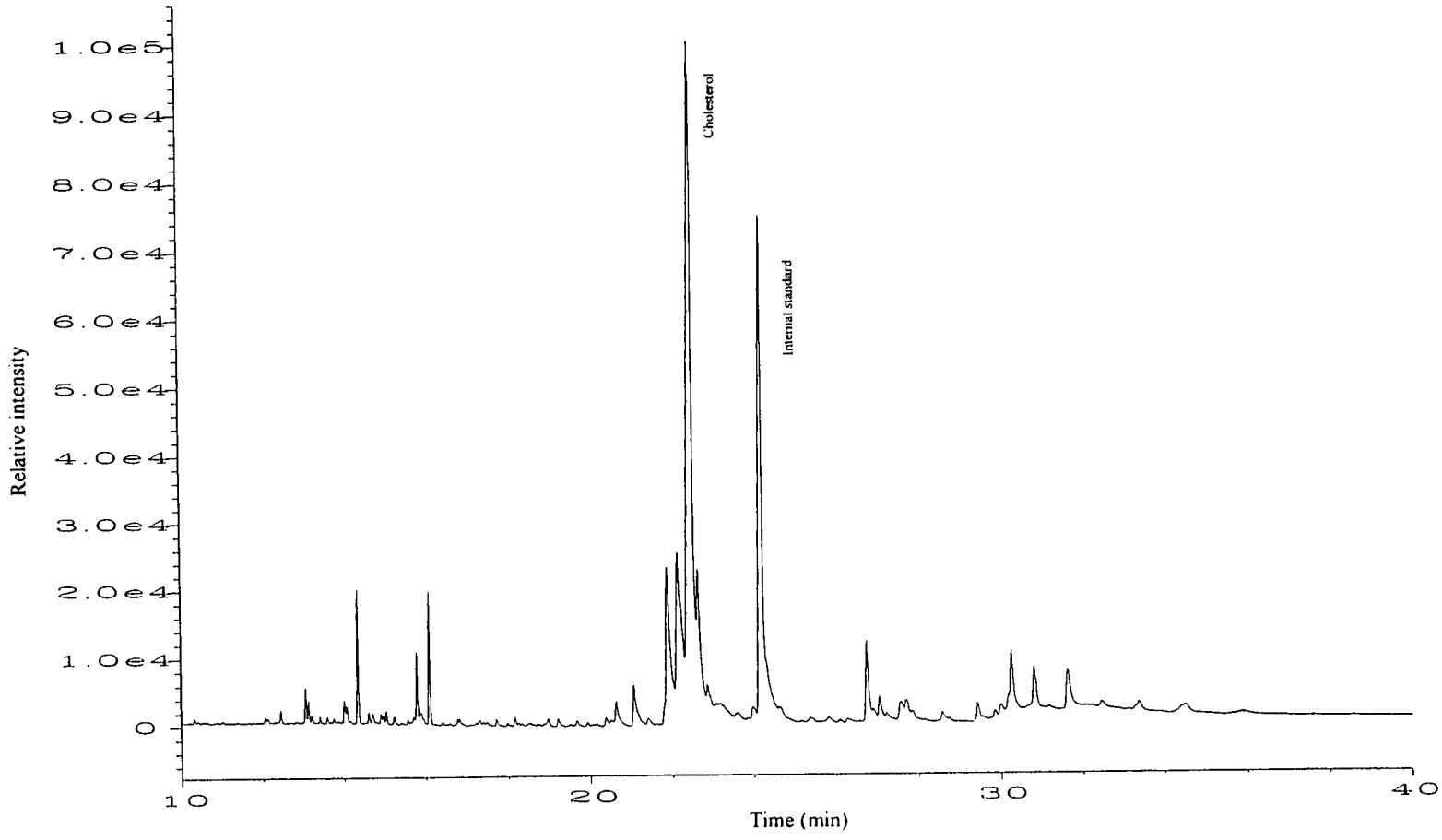

Figure 9.5a Gas chromatogram for the total lipid extract of the pig bone from Roman Ribchester.

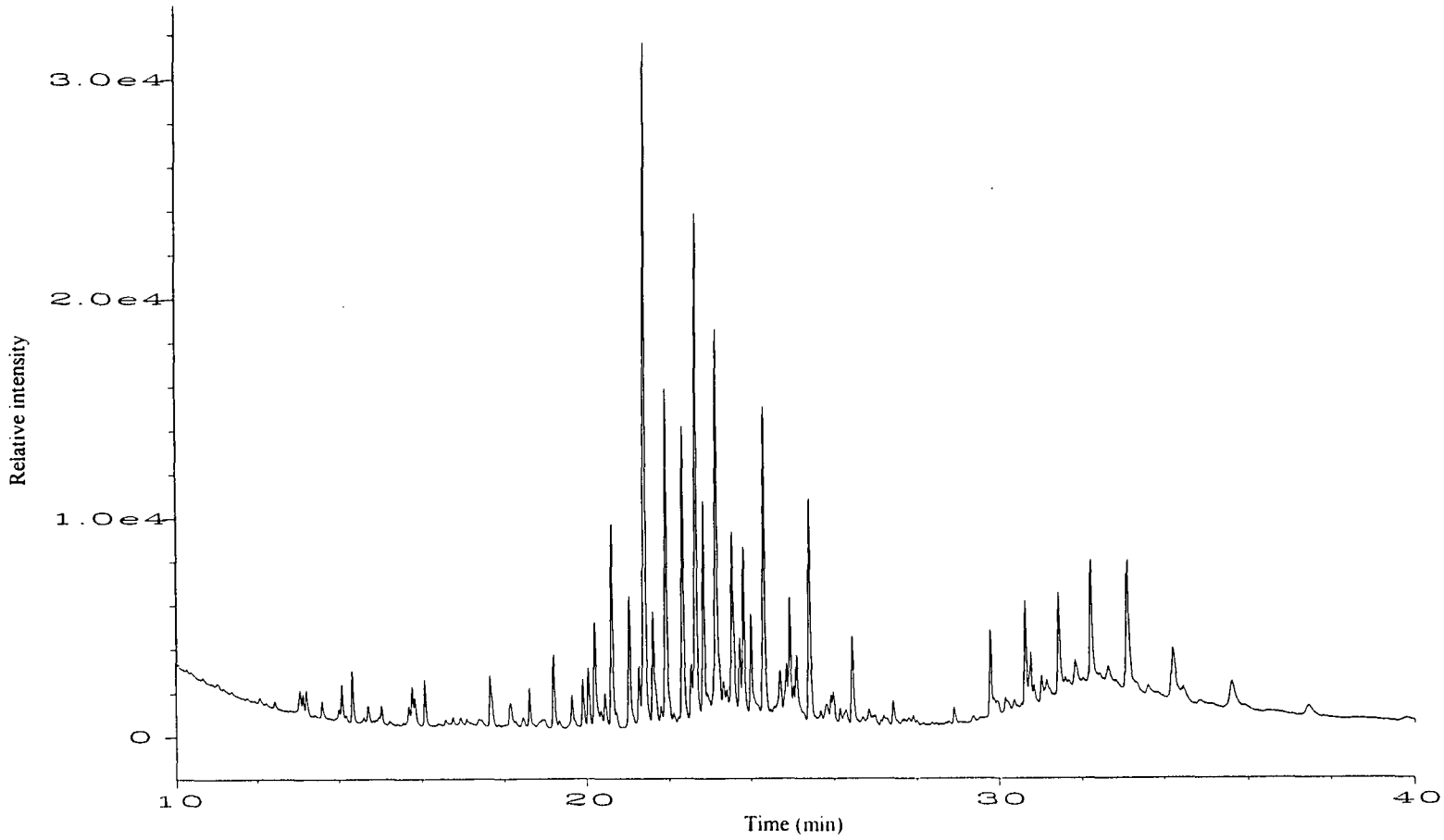

Figure 9.5b Gas chromatogram for the total lipid extract of soil adhering to the pig bone from Roman Ribchester.

10. Discussion and Conclusions

This research has shed new light on the gross physical and chemical changes undergone by bones whilst buried in a wide range of different environments. While many of these changes have been anticipated by previous researchers, some have not been demonstrated by experiment or widely published and others are new, unexpected or even counterintuitive. The results of this work have also highlighted the underlying reasons for the post-excavation deterioration of bones, particularly those from waterlogged deposits, and indicate which environments in particular are likely to produce skeletal remains in a poor state of preservation or subject to rapid deterioration on removal from their surrounding sediments. Furthermore the potential exists for the sampling of individual specimens to identify those bones requiring some sort of conservation treatment shortly after excavation. These latter two points are of particular importance because although fossilized bones are relatively rare in the geological record, archaeological sites frequently produce enormous quantities of animal or human remains, for which neither the resources nor finances exist for protracted conservation programmes. Perhaps equally important, the identification of those bones that require interventionist conservation treatments permits these to be separated from those which will survive long term storage and provide a resource for future scientific analysis. However, considerable work remains to be done in determining what parameters in the 'preservation' of bone tissues correlate with good preservation of biomarkers or isotopic evidence.

10.1 Diagenesis of Fossil Bones

Evidence from the microscopical examination of bones and their chemical analyses indicates that two mechanisms are involved in the gross degradation or diagenesis of bone tissues: the hydrolysis or partial hydrolysis of bone collagen and 'tunnelling' produced by the action of micro-organisms. The effects of both hydrolysis and 'tunnelling' are readily visible in light microscopy of thin sections of fossil bones. Loss of birefringence in bone, when viewed through crossed polars, clearly reflects some disruption of the complex architecture of collagen fibrils within the bone tissues. Birefringence in bone is the result of a strong preferred orientation of the bone apatite crystallites, which in turn are closely aligned with the collagen fibrils although these in turn do contribute to the optical properties of bone tissues. Loss of birefringence as a result of diagenetic alteration of buried bones may be attributable to a randomisation in the orientation of bone mineral crystallites as a direct consequence of chopping the collagen fibrils into shorter lengths or a disruption of the collagen-mineral bond. Although it is possible that the infiltration of other optically active molecular species such as humic or fulvic acids may be responsible for the observed loss of birefringence, these molecules are far too large to penetrate between the bone apatite crystallites and gain access to the collagen. Few molecular species appear to be small, and mobile enough to penetrate bone tissues and react with the collagen molecules. Water is certainly able to diffuse throughout the bone's structure and in life such

access would be crucial to maintaining the suppleness and strength of the collagen fibrils. It is also clear that hydroxyl ions can penetrate to the collagen and hydrolyse it into short peptide units since bone is rapidly deproteinized by hot alkali solutions (*e.g.* NaOH) although shrinkage or cracking of the remaining mineral pseudomorph and an increase in crystallinity of the mineral strongly suggests that some disruption of the bone apatite contributes to the ingress of hydroxyl ions. Although 'tunnelling' is frequently accompanied by loss of birefringence, the reverse is not seen to be the case, which suggests that initial hydrolysis of the collagen is a prerequisite for colonisation by or growth of micro-organisms. Although many soil micro-organisms produce collagenases, they are unable to utilise the collagen in bone directly since the collagenase enzymes are too large to gain access to the collagen fibrils while they are locked up within the mineral fraction (Child *et al.* in preparation). Once colonies of micro-organisms have become established, access to exposed collagen is facilitated by the demineralization of bone tissue, by acid metabolites, around the borders of existing cavities (canals of Volkman, canaliculi *etc.*). This mechanism is analogous to the resorption of living bone tissue by osteoclasts, which also demineralize bone tissue (possibly by citric or lactic acids) in advance of enzymatic digestion by collagenases, creating a characteristic 'ruffled' border around to the resorption bays where there is active remodelling of bone tissue. These ruffled or striated borders can be seen in high magnification light microscopy of modern histological sections and are caused by freed collagen fibrils protruding from the surfaces of demineralized bone (Ham & Leeson 1961, 292-296 and Figure 177).

This evidence suggests that following death and burial in aerated soils, colonisation by saprophytic micro-organisms is preceded by an interval in which water from the soil or from fluids originating in the animal itself hydrolyses the more readily accessible collagen molecules. The initial points of chemical attack may be either cross-links between adjacent collagen molecules in the collagen fibril or the bond between the mineral and the organic fractions. Glimcher has proposed that the mineralization of collagen in the body is regulated by phosphoproteins that form a substrate for the deposition of apatite (Glimcher 1984). The bridge between bone collagen and bone mineral formed by protein-bound phosphate bonds may represent the site of initial hydrolytic attack in bone shortly after the death of the organism. Destruction of this bridge would effectively decouple the two components of the organic-mineral composite and leave the bone matrix open to enzymatic degradation. This model is lent further support by the results of the tensile strength experiments. The tensile strengths of archaeological bone specimens do not correlate directly with protein content but fall into two groups; those with a nitrogen content close to that of fresh bone and those with nitrogen contents approximately 25% of that of fresh bone. 'Fresh' (bovine) bone and archaeological bovine metapodials exhibiting exceptional preservation have nitrogen contents ranging from 3.5 to 4.5 % but have tensile strengths covering a much wider range, from 23.7MPa to 54.8MPa (Table 8.5). Furthermore, Figure 8.5 shows that there is a rapid decrease from the maximum tensile strength of 'fresh' bone without any appreciable decrease in bulk density. These observations are

consistent with chain scissioning of collagen molecules or interruption of the collagen-mineral bond without any net loss of protein, and in the case of archaeological bone, with no appreciable tunnelling or increase in porosity. Once the collagen-apatite composite has become de-coupled, the bone is open to rapid decomposition by micro-organisms with a resultant increase in porosity due to tunnelling. This mechanism explains the absence of archaeological bone samples with bulk densities between 1.4g cm^{-1} and 1.8g cm^{-1}.

Evidence from the chemical analysis of fossil bones generally supports the theory that most of the collagen that is lost by bones whilst buried is lost as a result of hydrolysis. Inspection of the plots of hydrogen vs carbon and nitrogen vs carbon (Figures 4.13 and 4.14) together with the plot of phosphorus vs calcium for the same samples shows that nitrogen and carbon contents decrease in the same relative proportions whereas calcium and phosphorus contents increase in the same relative proportions.

Table 10.1 shows the collagen content as determined by hydrazinolysis, calcium and phosphorus contents as determined by XRF analysis for samples 1 to 32. Table 10.1 also shows these values normalized to 100 percent, although these calculations take no account of the oxygen content of the bone mineral. When these are plotted on a ternary diagram (Figure 10.2) a cluster of points can be seen centred on 37% collagen, 42% calcium and 21% phosphorus. Other points lie on a straight line running from this cluster and intersecting the line for zero collagen at a point corresponding to 68% calcium, 32% phosphorus. Points are distributed evenly along this line and there is no evidence for the two groups seen in Figures 8.8 and 8.9. This observation suggests that hydrolysis of collagen is a gradual, but not necessarily linear, process. Although the simplest interpretation of the evidence set out above is that collagen is lost by hydrolysis without any substantial alteration of the mineral component and that bone behaves as a two-component system during diagenesis, another possibility exists that would give the same analytical results. In this model, bone is demineralized by acidic secretions from saprophytic organisms in advance of enzymatic degradation of the collagen. Rather than there being a net loss of mineral from the structure of the bone by leaching ground waters however, the solubilized bone mineral is rapidly re-precipitated within the micro-porosity of the bone. Although this process certainly does take place during diagenesis and is very probably responsible for the increased crystallinity seen in fossil bones, there are arguments against this model as the main cause of collagen loss. Firstly, there are several examples of fossil bones in which the vast majority of collagen has been lost and yet there is no obvious sign of tunnelling and histological structures are preserved intact (Halstead 1974, Figure 10.4). Secondly, if in cases of bones with no detectable collagen, the whole of the mineral fraction had been systematically dissolved and re-precipitated, one might expect more dramatic changes in the crystal nature of the hydroxyapatite analogue. Finally, if the protein from bone collagen is utilised by and incorporated into the cells of growing micro-organisms, the question arises 'Why cannot these bacterial proteins also be detected

in carbon, hydrogen and nitrogen analyses as a skew away from the relative proportions for collagen?' The answer to this problem almost certainly lies in the nature of the proteins that make up the cell walls of the micro-organisms. These proteins are considerably more soluble than collagen, which in an undegraded form is highly insoluble.

Sample	Collagen (	Ca (%)	P (%)	Collagen	Ca	P
1	20.56	28.67	13.17	32.95	45.95	21.11
2	06.14	36.61	16.84	10.30	61.44	28.26
3	21.13	27.22	12.36	34.80	44.84	20.36
4	21.78	26.92	12.30	35.70	44.13	20.16
5.2*	10.56	38.03	17.52	15.97	57.53	26.50
6.1*	23.10	25.92	13.19	37.13	41.67	21.20
7	05.80	36.59	15.78	9.97	62.90	27.13
8	15.42	33.61	15.31	23.97	52.24	23.80
9	00.20	38.66	15.26	0.37	71.43	28.20
10	23.02	25.64	12.30	37.76	42.06	20.18
11	26.79	26.97	12.65	40.34	40.61	19.05
12*	21.78	28.88	12.24	34.63	45.91	19.46
13*	22.54	25.69	12.91	36.87	42.02	21.12
14*	10.00	32.13	15.31	17.41	55.94	26.65
15*	15.17	29.67	13.06	26.20	51.24	22.56
16*	01.90	35.27	16.65	3.53	65.53	30.94
17*	18.69	28.71	12.93	30.98	47.59	21.43
18*	08.24	30.11	13.32	15.95	58.27	25.78
19*	05.53	24.37	15.25	12.25	53.98	33.78
20*	09.82	6.65	11.05	35.68	24.16	40.15
21*	17.16	15.27	12.47	38.22	34.01	27.77
22*	05.49	32.32	16.36	10.13	59.66	30.20
23*	04.76	27.48	15.18	10.04	57.95	32.01
24*	04.54	32.65	16.36	8.48	60.97	30.55
25	00.55	27.48	15.18	1.27	63.60	35.13
26	00.51	37.30	16.49	0.94	68.69	30.37
27	19.31	29.56	12.85	31.29	47.89	20.82
28	17.10	30.90	13.41	27.85	50.32	21.84
29	15.31	28.05	12.83	27.25	49.92	22.83
30	13.37	30.32	14.46	22.99	52.14	24.87
31	05.11	35.26	16.58	8.97	61.91	29.11
32	03.35	30.17	14.42	6.99	62.93	30.08

Table 10.1 Percentages and normalized values of protein, calcium and phosphorus (samples marked by an asterix derive from waterlogged contexts)

Taking the second argument, the results of XRD analyses presented in Chapter 5 have demonstrated that within the resolution of the diffractometer used, fossil bone mineral is indistinguishable from a poorly crystalline hydroxyapatite with trace impurities of other mineral species dependant upon burial environment. Hydroxyapatite is thermodynamically one of the most stable forms of solid calcium phosphate. Simple 'bucket chemistry' experiments and the experience of the carbonate titrations (section 4.1.3) demonstrated that both bone and synthetic hydroxyapatite can be dissolved in mineral acids and re-precipitated once more to a paracrystalline powder on the addition of alkali.

In fact, carnivores which consume large quantities of bone routinely excrete finely divided hydroxyapatite in their faeces. X-ray diffraction studies on modern and ancient hyena coprolites demonstrate that their spectra are essentially the same as that of bone apatite (Horowitz & Goldberg 1989). Although calcium and phosphorus are excreted via the gut of all vertebrates (Berne & Levi 1990, 515-518) the bulk of the apatite in these coprolites will derive directly from bone dissolved in the stomach. It is therefore probable that bone mineral solubilized in the burial environment, either by the active intervention of micro-organisms or by the movement of ground waters over deproteinized bone, will be re-precipitated as a paracrystalline hydroxyapatite or carbonate apatite depending upon the local availability of dissolved carbon dioxide. If the burial environment contains organisms that undergo aerobic respiration then the dissolved CO_3^{2-} concentration will be high and carbonate apatites with a correspondingly small crystallite dimension would be expected. Certain bacteria are also capable of depositing hydroxyapatite from solutions. Streptococcus has been identified as being able to initiate the extracellular deposition of hydroxyapatite by the action of proteolipids and ion transfer (Mann 1992).

The XRD results provide tentative evidence that there is a inverse correlation between collagen content and crystallinity index (Figure 5.6). It has long been recognised that fossil bones show considerably sharper XRD spectra than fresh bones and that generally, the older the specimen the sharper and more defined the hydroxyapatite peaks. Bartsiokas & Middleton (1992) claim to have found a log/linear relationship between age and crystallinity index determined from the relative heights of the 202 and 300 diffraction peaks. Their samples ranged in age from recent to 2 million years old and exhibited crystallinity indices from zero up to 7.2. Interestingly some of the specimens with the highest crystallinity indices and of the greatest ages had well or moderately preserved histology (Bartsiokas & Middleton 1992, Table 1). Although there is potentially much more work to be done in this particular aspect of bone diagenesis, the evidence from the XRD investigation (Chapter 5) and microscopy (Plates 3.53-3.56) strongly suggest that increases in the crystallinity of fossil bones are due to the presence of precipitated, well crystalline hydroxyapatite in pore spaces in the bone structure. These crystalline masses have essentially the same chemical composition as bone apatite, although perhaps with a lower carbonate content and the inclusion of fluoride or uranium ions in the lattice, and consequently do not alter the calcium:phosphorus ratio substantially.

Future carefully controlled investigations using infrared analysis to determine the crystallinity indices of bones may confirm a relationship between crystallinity index and collagen content. Glimcher (pers. comm.) maintains that exposed bone mineral, once it has had its organic fraction stripped away is so susceptible to dissolution and alteration by water that he holds that the composition of fossil bone apatite cannot be said to represent that of the original bone mineral. Experiments with the water washing of hydrazine deproteinized bone confirm that parts of the bone mineral may be dissolved out of specimens and that this is accompanied by an increase in

crystallinity. Over geological time scales a similar mechanism may dramatically alter the ionic composition of fossil bone apatites. Deposits that contain quantities of skeletal remains are frequently highly phosphate rich and individual bone fragments (or fish scales) can act as nuclei for the secondary calcium phosphate to form nodules. Konta (1956) recorded fish scales from Permian deposits with a core of carbonate apatite surrounded by an outer layer of fluorapatite. Such processes are considerably more likely in the centres of bones where the dissolved calcium and phosphate ion concentrations are high.

It is thought that hydroxyapatite reacts with water to form a 'surface complex' that is in metastable equilibrium with the aqueous solution (Stumm & Morgan 1970) so that the equilibria of hydroxyapatite may be expressed:

$$Ca_{10}(PO_4)_6(OH)_2 = 10Ca^{2+} + 6PO_4^{3-} + 2OH^- \qquad \text{log. eq. const.} = -55.6$$

$$Ca_{10}(PO_4)_6(OH)_2 + 6H_2O = 4[Ca_2HPO_4(OH)_2]_{surface} + 2Ca^{2+} + 2HPO_4^{2-} \qquad \text{log. eq. const.} = -8.5$$

$$[Ca_2HPO_4(OH)_2]_{surface} = 2Ca^{2+} + HPO_4^{2-} + 2OH^- \qquad \text{log. eq. const.} = -27$$

Crudely, this can be imagined as the dissolution of the more soluble hydrogen phosphate from the surface of hydroxyapatite crystals. These considerations can be extended to cover fluorapatites, carbonate apatites and bone apatite. As pH falls in ground waters, the acid phosphates: HPO_4^{2-}, $H_2PO_4^-$ and H_3PO_4 become progressively more dominant. Also, as the pH falls below 7 the solubility of hydroxyapatite approaches that of the hydrogen phosphate but this solubility may be suppressed between pH 8 and 6 by the addition of more Ca^{2+} to the soil solution by the common ion effect. Hydroxyapatite rather than the hydrogen phosphate, brushite, is therefore the more likely stable solid to form in neutral ground waters and where calcium ions are in excess. In fact, in the absence of competing species such as CO_3^{2-} or SO_4^{2-}, then the local dissolution of bone mineral results in the precipitation of much larger crystals of pure hydroxyapatite in areas of bone where the pH rises and the solubility product for $Ca_{10}(PO_4)_6(OH)_2$ is exceeded.

In addition to local dissolution and re-precipitation of bone apatites, bone mineral may be significantly altered over geological time scales by ionic substitution without the requirement of total dissolution of individual crystallites. The simplest case of diagenetic modification of bone mineral is that of substitution of Ca^{2+} or PO_4^{3-} ions in the lattice with those of the same species in the soil solution. Here the chemical composition and consequently the Ca:P ratio remains essentially unaltered although the isotopic ratios, especially those of calcium and oxygen may change with important implications for the interpretation of some dating and dietary studies. The large surface

area of bone apatite results in a highly reactive colloidal interface, where up to one quarter of the surface ions are available for exchange (Posner 1985b). In life and in the soil, bone mineral crystallites are always surrounded by a thin layer of water with ions immediately adjacent to the crystallite surface much more tightly bound in this hydration shell than those in the plasma or soil solution filling pore spaces within the bone. Ionic species in the bulk solution may be removed by flushing with clean water and as a consequence are much more loosely bound to the mineral than those in the hydration layer which require an excess of another species to displace them and take their place at the crystallite surface. These ionic species must rely on diffusion processes to carry them from the bulk solution to the hydration layer. Some ionic species can enter the crystallite surface from the hydration layer. This relatively rapid exchange between ionic species in solution and surface sites in the bone mineral is followed by a much slower, solid state diffusion into the interior. Experiments have demonstrated that Ba^{2+}, Mg^{2+}, Pb^{2+}, Sr^{2+}, Na^{+}, CO_3^{2-} and F^{-} may enter the surface and Pb^{2+}, Sr^{2+}, CO_3^{2-} and F^{-} can penetrate further, into the interior (Pate *et. al.* 1989, 306). Various soluble cations can substitute for Ca^{2+} while CO_3^{2-} replaces PO_4^{3-} and F^{-} replaces OH^{-}. Electrical neutrality is maintained by coupled substitutions such as the gradual transformation of hydroxyapatite to carbonate fluorapatite by the exchange of PO_4^{3-} by $CO_3^{2-} + F^{-}$. Many cations are excluded from Ca sites in the interior because of excessive differences in ionic radii. Exchange is permitted if their ionic radii do not differ by more than 15%. Differences in ionic radii are therefore influential in exchange mechanisms between competing species. Thus, although strontium (ionic radius = 1.18Å) can occupy the calcium (ionic radius = 0.99Å) position in the apatite lattice, calcium is preferred when both are competing for the site. Because ions in solution are hydrated (*i.e.* surrounded by a shell of bound water molecules) their energies of hydration also influence the abilities of various cations to substitute into the lattice. For example, cations of the alkaline earth elements have larger ionic radii and lower charge densities than trivalent transition metal ions and consequently associate less strongly with water molecules. As a consequence the more hydrated or densely charged ionic species are less mobile in solution.

Unfortunately, such subtle changes in the ionic and chemical composition of fossil bone apatites lie beyond the range of sensitivity of the X-ray fluorescence technique used in this research. Nevertheless, there are some notable patterns of variability in the minor element compositions of the bone specimens analysed (Table 4.12). Sample 11 had an extraordinarily high sodium and a high chlorine content, consistent with heavy contamination by sea water since it was found on a beach. The other sample with a high chlorine content also came from Cyprus, a result that demonstrates the high chloride content of ground waters in Mediterranean countries (where tap water was also found to be heavily contaminated by chlorides). An examination of those elements widely considered to be dietary indicators, strontium, barium and zinc, shows that very few patterns emerge, although little variation in the pre-mortem concentrations may be expected since all but samples 8 and 9 (which were human bone specimens) came from vegetarian ungulates. Within the levels of accuracy of the

XRF analysis, there is little variation in the strontium content, elevated levels of which are generally accepted to indicate a diet low in meat and high in vegetable foodstuffs. The highest level of strontium (333ppm) was found in sample 11, once again reflecting the elevated concentration of strontium in sea water. Similarly there was no obvious pattern in the barium contents of the bone samples. However, five of the specimens (samples 5.1 & 5.2, 20, 21 & 23) had a zinc content more than ten times higher than the other specimens. Since both the surface and interior cortex of specimen 5 had comparable zinc concentrations (2228 compared to 2269) it is almost certain that these figures reflect the true compositions of the bones and do not arise from contamination or instrumental errors. High levels of zinc in bones are associated with a diet rich in meat but since these bones come from cattle and deer it is clear that diagenetic processes must be responsible for the observed zinc content. Separate qualitative analysis of Roman leather shoe leather also showed measurable quantities of both strontium and zinc, demonstrating that these elements along with others such as calcium, iron and manganese are readily taken up by collagen when buried. Although all of the samples with high zinc contents come from waterlogged deposits, reference to the protein contents in Table 10.1 show that there is poor correlation between zinc content and preferential preservation of collagen.

Reference to Table 4.12 shows that there are some general trends in the iron and manganese contents of the bones analysed. Of those samples with iron contents above one percent (16 samples in all) only two (samples 7 and 26) were not excavated from waterlogged deposits. Although as a rule, those samples with high iron contents also have enhanced manganese levels, there is no simple relationship between the amounts of these two elements in bones. Some samples with a high manganese content do not contain any appreciable iron (*e.g.* samples 7 and 27). Although it is certainly true that in most burial environments the availability of iron in the soil solution will be determined largely by pH, for example the two samples from arid, alkaline soils (samples 8 and 9) contained little iron, there are other factors which influence the mobility of iron in the soil.

Soluble salts of calcium, magnesium, sodium, and potassium are common in arid environments with low rainfall and high evaporation where the net flow of the soil solution is upwards. Here, chemical reactions in the burial environment should be dominated by the relatively more abundant carbonate and sulphate ions and as a result carbonates frequently dominate such soils. However, iron and manganese are usually dominant in acid soils and reducing environments and play an important role in soil chemistry (Stumm & Morgan 1970, Figures 5.8 and 10.4). Phosphorus is a major component of all organic matter, including bone, and is usually relatively immobile in the soil. As a consequence of this immobility, phosphate analysis has become a recognised tool in the prospection and surveying of archaeological sites. However, iron, manganese and phosphorus must be considered together because their dissolution, transport and accumulation in soils are strongly related.

Phosphorus occurs in nature almost exclusively in the fully oxidized state, forming the phosphate ion PO_4^{3-}. In natural waters this ion occurs as orthophosphates which can be either anionic or cationic:

$H_2PO_4^-$

HPO_4^{2-}

PO_4^{3-}

or

$FeHPO_4^+$ and $CaH_2PO_4^+$

Substantial fractions of the mobile phosphorus in the soil solution consist of dissolved or colloidal organic phosphorus. The distribution of acid and base species of orthophosphates in solution is governed by pH. The dominant dissolved orthophosphates at pH 5-9 are $H_2PO_4^-$ and HPO_4^{2-} (Stumm & Morgan 1970) and conform to the following equilibria:

$$H_3PO_4 = H_2PO_4^- + H^+$$

$$H_2PO_4^- = HPO_4^{2-} + H^+$$

$$HPO_4^{2-} = PO_4^{3-} + H^+$$

Phosphates are also known to form soluble complexes and chelates as well as insoluble salts with a number of metal ions. The extent of this complexing will depend upon the relative concentrations of phosphate and metal ions, the pH and the presence of other competing ligands such as SO_4^{2-}, CO_3^{2-}, F^- and various organic species, such as humic acids, in the ground water. Complex formation will have a small effect on the metal ion distribution but may significantly alter the distribution of phosphates. That is, the degree of complexation between phosphate and metal ions can significantly affect the solubilities of phosphates in soil waters. Therefore, in acid ground waters where iron and manganese are more likely to be present as cations, bone apatite may be more readily soluble. In addition, the low concentration of phosphorus in soils and the tendency of phosphate ions to be adsorbed on the surfaces of colloids such as clay minerals and iron oxides, combine to produce soil solutions generally deficient in phosphates, a situation which may also contribute to the solubility of bone apatites. The Fe^{3+} ion interacts with orthophosphate ion to form soluble complexes such as $FeHPO_4^+$. In slightly acidic environments this leads to the precipitation of pure $FePO_4$ (Stumm & Morgan 1970, 530). This mechanism is probably involved in the formation of vivianite deposits in bones from acid waterlogged environments. The mobility of iron and manganese in the burial environment is also influenced by their ability to form soluble complexes with 'organic matter' in the soil (see section 9.4). Ferric ions (Fe^{3+}) have a stronger tendency to form complexes than ferrous and manganous ions. Also, hydroxide ions often have a stronger affinity for Fe^{3+} than do many organic bases, with the result that complexation of Fe^{3+} is more prevalent in acidic environments. Stumm and Morgan state that natural waters with high a concentration of organic matter frequently have high concentrations of 'operationally soluble' ferric ion, and maintain that much of the natural colour of soil waters is due to the presence of this ion in 'highly stabilized colloidal dispersions' (Stumm &

Morgan 1970, 531). They attribute the yellow staining in soil to complex formation with hydrolysed ferric iron. It is therefore possible that the infiltration of iron into bones buried in soils occurs by its transportation in the form of colloidal matter or complexes rather than as free Fe^{3+} ions and that it later becomes fixated to either the bone mineral crystallites or the collagen template by simple chemisorption or some other, unknown, mechanism.

Manganese is known to have a strong affinity for decomposing organic matter and especially skeletal tissue. The manganese content of fossil bones is affected by the chemical reactions that take place between the burial environment, the organic fraction of skeletal tissue and the bacterial populations in buried bone (Parker & Toots 1974). Manganese concentrations have also been recognised as one of the distinguishing features in 'soil silhouettes' that represent the end point of bone degradation in certain human inhumation burials. Anglo-Saxon cemeteries, which are frequently located in soils where bone preservation is especially poor, have produced large numbers of these silhouettes, which take the form of dark stains in sediments corresponding to the positions of bodies. Keeley *et al.* reported that chemical analysis of soil samples from selected areas of graves at the multi-period site of Mucking showed that although the phosphate concentrations in silhouettes were less than 4% of that of the original bone, manganese contents were significantly higher than in the surrounding soil. In some cases the manganese concentrations were ten times greater than that in the adjacent soil but enhances manganese levels were only found where phosphate concentrations exceeded 1% (Keeley *et al.* 1977). Keeley *et al.* also found that areas of soil with high manganese did not necessarily correspond with areas of high iron content. However, they did demonstrate that high enhanced levels of manganese did coincide with relatively high levels of copper. This latter observation is interesting in the light of microscopic examination of the bone collected from the copper mine at Limni, Cyprus (Plates 3.23 and 3.24) which show that copper is apparently concentrated in the areas of active microbiological activity. It may also be significant that one of the bones from the copper mines at Great Orme has a high level of manganese although a high copper content can only be inferred from the colour of the bones.

Both X-ray diffraction analysis and infrared spectrophotometry proved invaluable in the identification of mineral contaminants in fossil bones. Calcite, gypsum and vivianite were all readily identified using a combination of XRD and X-ray fluorescence techniques. Moreover, the combined use of XRD and infrared analyses demonstrated that there existed the potential for confusion between the calcium phosphate mineral, brushite and the calcium sulphate mineral gypsum when only XRD is used for identification. Both gypsum and brushite belong to the monoclinic crystal system and have similar lattice constants resulting in similar, but not identical, XRD spectra (see Figure 5.10c and Figure 5.10d). This observation throws into question some claims for the detection of brushite in fossil and archaeological bones where the sole evidence for identification is X-ray diffraction, although there can be no doubt about those instances in which identification has been made on the

evidence of infrared analysis (Piepenbrink 1989). It should also be stressed that the detection of brushite, gypsum or vivianite in specimens of excavated bone, especially bones excavated from sediments containing free water (as opposed to well mineralized bone recovered from compact rock) does not provide proof that these minerals were present in the specimens while they were in the ground. Rather, there is considerable evidence, both experimental and apocryphal, that bone can undergo chemical change following excavation, whether as a result of oxidation or hydration of mineral species contained within its structure. This change is not restricted to the initial period of water evaporation and oxidation following exposure to the air but can continue in specimens that have already been well dried, either in air or through solvent baths, as evidenced by the growth of gypsum crystals on the exterior surface of a fragment of waterlogged bone previously gold-coated for SEM examination.

10.2 Post-excavational Changes in Fossil Bone

The post-excavation formation of these minerals can be accounted for by the oxidation of pyrite (especially framboidal pyrite) in bone specimens recovered from anoxic environments where the sediments are likely to contain colonies of sulphate reducing bacteria. The reduction of sulphate to sulphite by microbes, or 'sulphate respiration' involves the oxidation of organic matter with the transfer of electrons to sulphate rather than oxygen as in the case of normal respiration.

$$2CH_2O + SO_4^{2-} = + 2H_2O + 2CO_2 + S^{2-} \qquad \text{(Fisher, I. St. J. 1986)}$$

The energy released in this redox reaction is utilised by the organism. This sulphate respiration is a comparatively rare metabolic process and is restricted to only a few species of bacteria of the genera *Desulfovibrio, Desulfotomaculum* and *Desulfomonas* (Trudinger & Swaine 1979).

Sulphur occurs as a trace in bone and is present in much larger quantities in blood. However, in most cases it will be safe to assume that the majority of sulphur compounds found in buried bone derive from either the sediment or the soil solution. Both sulphates and sulphides have been identified in archaeological bone and other porous materials recovered from the waterlogged, anoxic and stagnant environments associated with shipwrecks and deep, terrestrial sediments (Watson 1981; Watson 1984; Ellam, 1985a). These environments have conditions of low pH and Eh. MacLeod quotes on-site pH values and corrosion potentials of concreted iron objects from the shipwreck 'Batavia' as in the range pH of 4.8±0.5 and Eh of -0.30±0.12 (MacCleod 1989). In these extreme conditions, only certain classes of micro-organisms may flourish. These microbes tolerate high acidity, high concentrations of sulphides and levels of metals that would be toxic to the majority of aerobic organisms. Almost any form of organic matter such as cellulose or sewage will support the growth of these sulphate reducing bacteria but experiments to investigate the production of H_2S in

deep marine sediments suggest that the complex organic matter produced by living organisms must first be degraded by fermentative or other saprophytic organisms before being available for the reduction of sulphate (Sorokin 1962). A major constraint on the growth of these sulphate reducing bacteria is their requirement for strict anoxic conditions so that these organisms are confined to sediments, aqueous basins and waterlogged soils where restricted water movement and oxidation of organic matter by aerobic organisms has depleted the available oxygen. These organisms can however be found in pockets or 'reduced microniches' in otherwise aerated soils.

The free sulphide ion generated by the reaction above is available to combine with soluble metal ions to form insoluble sulphides. Ferrous ions react with sulphide to form amorphous ferrous sulphide. Alternatively, the sulphide ion may oxidised by ferric ions to form elemental free sulphur.

$$Fe^{2+} + S^{2-} = FeS$$

$$2Fe^{3+} + S^{2-} = S^{0} + 2Fe^{2+}$$

The original amorphous or poorly crystalline iron sulphide is transformed to iron pyrite by reaction with excess free sulphur. Evidence suggests that at low Eh values, ferrous sulphide may be converted to pyrite by some organisms and intracellular pyrite has also been identified in sulphate reducing bacteria (Issatschenko 1929). A reaction between ferrous sulphide and hydrogen sulphide to produce pyrite and hydrogen, coupled with the reduction of sulphate to hydrogen sulphide has been proposed by ZoBell (ZoBell 1961) for its formation.

$$FeS + H_2S = FeS_2 + H_2$$

$$4H_2 + H_2SO_4 = H_2S + 4H_2O$$

These small, angular grains of pyrite are released on death and cell lysis to give the characteristic globular clusters of iron sulphide seen in pyrite framboids.
On excavation and exposure to atmospheric oxygen, these finely divided sulphides readily oxidise by a mechanism known as 'pyrite rot'.

This is a self catalyzing reaction and may be summarized:

$$FeS_2(s) + 7/2O_2 + H_2O = Fe^{2+} + 2SO_4^{2-} + 2H^+$$

$$Fe^{2+} + 1/4O_2 + H^+ = Fe^{3+} + 1/2H_2O$$

$$Fe^{3+} + 3H_2O = Fe(OH)_3(s) + 3H^+$$

$$FeS_2(s) + 14Fe^{3+} + 8H_2O = 15Fe^{2+} + 2SO_4^{2-} + 16H^+$$

Thus the oxidation of pyrite to sulphate releases ferric ions and acidity into the surrounding solution. This reaction is initiated by molecular oxygen (MacCleod & Kenna 1991) but will proceed even in the absence of further oxygen since the Fe^{3+} ions produced then act as the principle oxidising agent, driving the reaction. Figure 10.1 shows the model proposed by Stumm and Morgan to summarize the oxidation and decomposition of pyrite in coal mine waters:

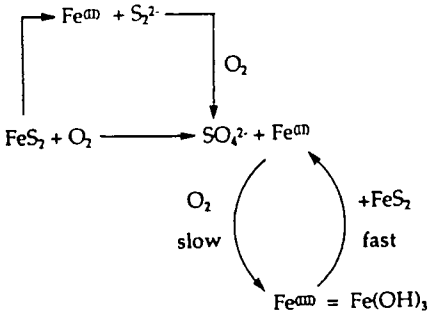

Figure 10.1 Proposed mechanism for oxidation of pyrite
(after Stumm & Morgan 1970)

The oxidation of pyrite can also be catalysed by the action of micro-organisms such as the *Thiobacillus thiooxidans*, *Thiobacillus ferrooxidans* and *Ferrobacillus ferrooxidans* (Zajic 1969, p 114). However, microbiological assays of pyritized fossils (Howie 1978) and waterlogged wood (MacCleod & Kenna 1991) have been unable to demonstrate significant bacterial activity and indicate that the oxidation of pyrite in excavated materials follows chemical rather than microbiological pathways.

The decomposition of pyrite is amongst the most acidic of all weathering mechanisms due to the extreme insolubility of $Fe^{(III)}$ compounds. The resulting low pH is extremely detrimental to bone mineral, dissolving bone apatite , decomposing carbonates and releasing Ca^{2+}, PO_4^{3-} and SO_4^{2-} ions into the surrounding pore spaces. There, concentration by drying fronts may cause crystallization of calcium sulphates and iron phosphates, accounting for the presence of gypsum and vivianite in some bones examined.

10.3 Conservation Strategies for Fossil Bones

There has been considerable work on the conservation of fossil bones, particularly the consolidation of geological specimens (Koob 1984; Howie 1984; Ellam 1985a, 1985b; Doyle 1986; Stone 1990). However, this work has normally been undertaken by museum curators and conservators rather and has focused on the problems of maintaining the physical integrity of the individual specimens rather than the potential information contained within them. Conservation has been interventionist in many cases (frequently because the conservator is only alerted to a potential problem when the specimen begins to disintegrate) and improvements in the conservation of fossil bones have usually involved the introduction of new synthetic resins with better properties and reversibility.

The research described in the preceding chapters has highlighted several mechanism by which fossil bone may deteriorate immediately after excavation and during subsequent storage. Bones from waterlogged conditions have presented particular problems when excavated and have rarely survives the initial 'drying out' without serious distortion and delamination without the application of a water-based consolidant, usually poly vinyl acetate (PVAc) but more recently an acrylic dispersal (Koob 1984). Warping, cracking and particularly delamination of the surface destroys a considerable amount of the information the bone preserves by virtue of its physical shape and texture *e.g.* species, sex, age and pathology in addition to taphonomic evidence such as cut or wear marks. Ellam's work on the freeze-drying of bones from waterlogged contexts represented a different and potentially valuable approach to the problem and freeze-dried bones pre-treated with a water soluble consolidant/humectant would, in principle, be more easily reversed than consolidation with a synthetic resin. However, unlike the majority of archaeological wood or leather specimens treated by freeze-drying, waterlogged bone has a considerable inorganic component comprising countless microscopic crystals which frequently have become de-coupled from their organic matrix. When waterlogged collagenous or cellulosic materials are allowed to dry in air, the strong surface tension forces in the liquid water draw together individual fibres or cell walls, pulling the structure of the material apart and creating tears or splits in the specimen. Often, the degraded surfaces of the collagen fibres in leather or cell walls in wood are irreversibly bound by cross-links or strong hydrogen bonds, ensuring that the damage done by air drying is largely irreversible. These problems can be overcome by pre-treatment with a suitable plasticiser/humectant such as glycerol or poly-ethylene glycol (PEG, a synthetic, water soluble wax) and freeze-drying. During freeze-drying, water is sublimed at low pressure from the solid phase, avoiding the shrinkage due to surface tension forces. The addition of glycerol or low molecular weight PEG before freeze-drying provides some additional support and lubrication to the organic substrate and buffers the specimen from rapid fluctuations in relative humidity.

In the case of bone that has been excavated from an acidic, waterlogged environment, the bone

matrix has frequently become demineralized to some extent (see Figure 8.7) with the result that these areas undergo considerable shrinkage if allowed to dry in air (Plate 10.1). Often it is the surface of the bones (not necessarily the periostial surface since the surfaces of broken edges can also show characteristic demineralization) that are affected by shrinkage whereas the underlying bone matrix is still supported by its hydroxyapatite content. This situation frequently results in the complete loss of the outer surface in such specimens (Plate 10.2). Preliminary experiments in the freeze-drying of waterlogged bones have demonstrated that the problems of shrinkage can be overcome but the integrity of the specimens is still compromised by the fragile nature of the bone. As a result of their mineral content, bones are considerably heavier than leather artefacts after freeze-drying and in severely degraded specimens the mineral content is represented by a loose aggregate of minute crystals. These problems can probably be overcome by the correct blend of PEG waxes in pre-treatment or the application of a consolidant subsequent to freeze-drying. Ellam conducted experiments in the freeze-drying of bones from two waterlogged sites, the Fenlands and Seamer Carr, using both glycerol solutions and various molecular weight PEG solutions at different concentrations (Ellam 1985a). Small samples of waterlogged bone were pre-treated with solutions of PEG 400, PEG 1500, PEG 2000 and PEG 400 at concentrations of 10, 20, 30, 40 and 50 percent, before freeze-drying in the conventional manner. Ellam found that although the appearances of the specimens after treatment were aesthetically acceptable for low concentrations of PEG (10% and 20%) they had acquired no additional strength and were extremely fragile. Good results were achieved at a solution concentration of 40% but at 50% the surfaces of the specimen appeared dark and sticky. All grades of PEG gave good results at 40% solution concentrations. For bones treated with PEG of molecular weights 400 to 2000, the bones retained a wide rage of wax after freeze-drying (4% up to 42%). Some of the Seamer Carr samples had visible gypsum deposits in their pore structure. A similar picture emerged for bone samples pre-treated with glycerol. The appearance of the specimens was good at low concentrations (10-30%) but the specimens took on a dark shiny appearance at concentrations of 40% and 50%. Improvements in strength were poor for samples pre-treated with 10% glycerol, slight for 20% but no real improvements were made below 30%. Good consolidation was achieved at 50% glycerol pre-treatment. Ellam's work illustrated that the major factors in the successful treatment of waterlogged bone by freeze drying were consolidant concentration (rather than molecular weight) and duration of pre-treatment. Specimens from Seamer Carr took up a total of between 15% and 18% glycerol whereas the specimens from the Fenland took up between 4% and 7% (Ellam 1985a, Tables 4-7). Further experiments with the treated samples demonstrated that the addition of PEG or glycerol substantially buffered the specimens against fluctuations in relative humidity (Ellam 1985a, 38). There were considerable variations in the success of the treatments described above, depending upon the sample. Since the size of each sample was small (1g) there is no way of predicting the outcome of treating large specimens which may display many different states of preservation.

Although the research presented in Chapter 9 demonstrated that some biomarkers survive even in degraded bones, it can be argued that the primary source of evidence in a bone specimen (i.e. species, sex, age at death and pathology) is represented by its physical form rather than its chemical composition. As such, one of the first priorities must be to preserve its physical integrity. It is therefore acceptable that in some instances freeze- or air drying may be supplemented by the application of a synthetic resin consolidant but only once its potential for surviving the drying process untreated has been assessed and any specimens singled out for further analytical procedures such as DNA, lipid or radiometric analysis. Simple measurements of pore volume and bulk density may provide a useful tool for the assessment of the degree of degradation of the bone mineral and resulting exposure of the collagen matrix (see section 8.2 and Figure 8.7). Specimens with bulk density and porosity measurements lying off the line representing the results of 'normal' aerobic diagenesis may be expected to suffer potentially catastrophic shrinkage on drying.

Even after specimens from anoxic, waterlogged contexts have been dried successfully, there still remains considerable risk of post-excavational deterioration due to the oxidation of diagenetic pyrite and resulting release of acidity and mobile ions into the pore structure or the bones. Dissolution, migration and recrystallization or hydration of mineral salts such as vivianite or gypsum can cause considerable damage to bones (Plates 10.3 and 10.4). 'Pyrite rot' in geological specimens, particularly pyritized fossils, is a problem that has attracted considerable attention over the years. Such specimens have been successfully treated in an atmosphere of ammonia to neutralise acidity and stabilize oxidation products (Waller 1987). Such treatment would be suitable for the treatment of fossil bones and would be considerably less invasive than the application of water or air resistant coatings to the specimens, although the effects of ammonia on subsequent analysis is, as yet, unknown.

10.4 Suggestions for Future Work on Fossil Bones

The findings of this research suggest several avenues for future analytical work and indicate the potential for some radical changes in the way skeletal material is handled, both at the point of excavation and at subsequent stages in its treatment , storage or eventual display. The results presented in Chapter 3 demonstrate that palaeohistological examination of fossil bones can reveal a great deal about a specimen's condition, chemistry and pathology. In particular it can reveal framboidal pyrite and contaminant minerals in the bone structure, although it is highly skilled, time consuming and expensive to undertake.

X-ray fluorescence spectrometry represents a simple, inexpensive and extremely robust analytical technique for the chemical analysis of bone specimens. With careful instrument calibration it may be possible to improve the accuracy of measurement (particularly in hydrazine deproteinized samples)

for trace elements such as copper, zinc, barium and strontium. The use of XRF on powdered. pelletized samples would circumvent the problems associated with dissolution of samples and separate analysis against known stock solutions.

There is considerable promise in the correlation of mineral crystallinity with protein content by measurement of the area of the 002 peak in X-ray diffractograms of hydrazine deproteinized bone. This in turn could be correlated with similar crystallinity measurements made from Fourier transform infrared spectroscopy.

The priority of bone specimens should be re-evaluated, particularly large assemblages from sites of relatively recent archaeological date. Although these assemblages are frequently large, difficult to handle and store, their large sample size and relatively good state of preservation means that they represent a considerable resource for the analysis of biomarkers such as lipids, DNA, blood residues and immunologically active molecular species (Hedges 1985). Provision should be made for a sampling strategy, suitable cold storage facilities, on-site expert guidance or gloves *etc.* and consultation with a relevant specialist at the design stage of the excavation.

Broader experiments should be conducted on 'safe' and appropriate conservation regimes for skeletal remains, using larger sample sizes and numbers. The long term effects of these treatments on future analysis should also be investigated. In addition to the implementation of less invasive conservation treatments, the potential for a simple assessment of individual specimens to determine which require treatment and what sort of treatment would be most effective should be explored.

Work on the potential applications of lipid analysis on bones for palaeodietary studies should be continued, in collaboration with similar studies on soils and diagenetic processes. Similarly, the isolation and amplification of DNA residues should be persuade in a structured programme of research in which the potential for contamination by organism and residues in the burial environment is explored.

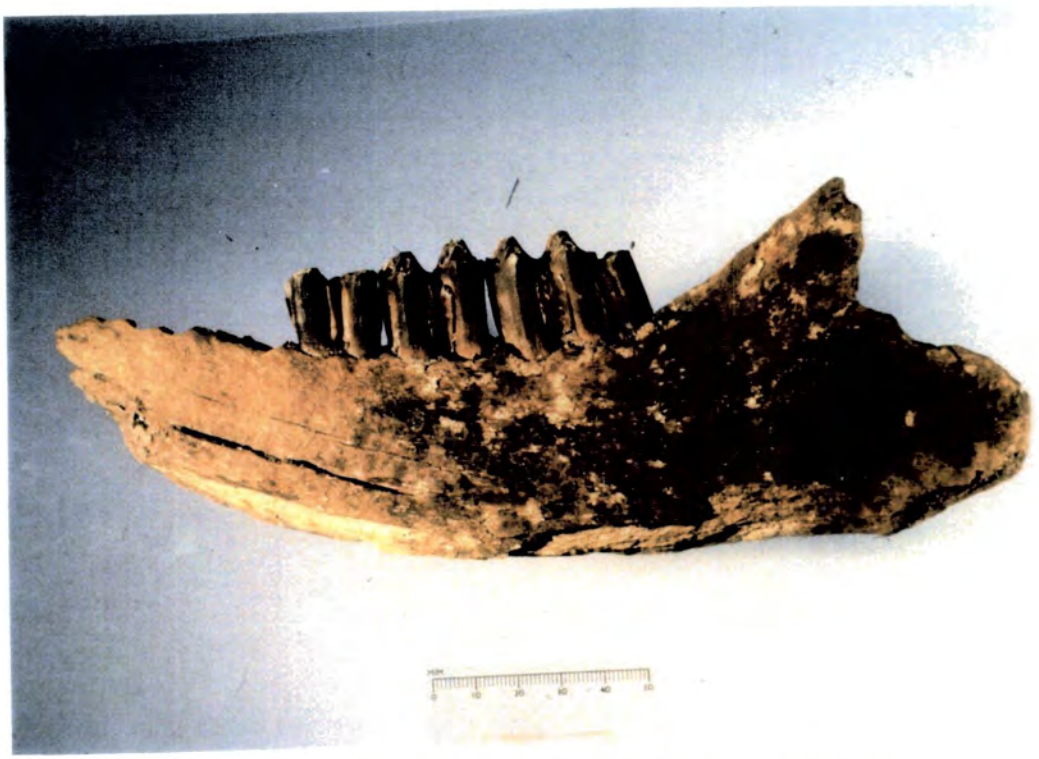

Plate 10.1 Exfoliation of outer surface of archaeological jaw bone from waterlogged deposits. Note also the efflorescence on the surface

Plate 10.2 Loss of periosteal surface on bone from waterlogged deposit. Note differential preservation showing high organic content on surface and paler, heavily degraded interior (*cf.* Sample 5)

Plate 10.3 Vivianite deposits in delaminating lamellar bone in specimen (bovine) from a Roman well

Plate 10.4 Loss of periosteal surface due to differential shrinkage and hydration/crystallization pressure of vivianite deposits

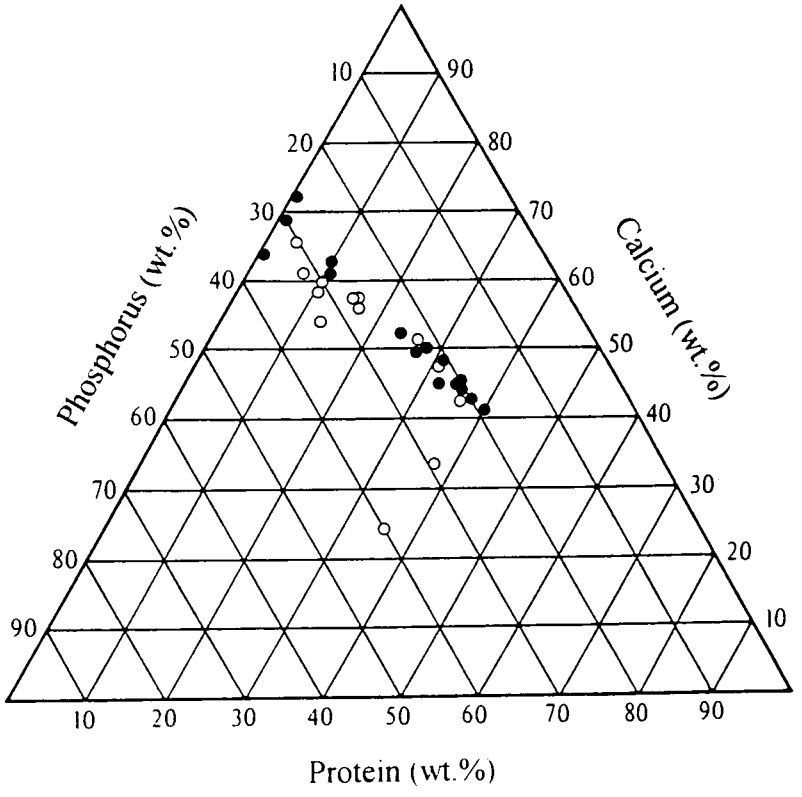

Figure 10.2 Ternary diagram of normalised values for protein, calcium and phosphorus.

Bibliography

Aitken, M. J. (1990) *Science-based Dating in Archaeology*. Longman Archaeology Series.

Ambler, R. P. & Daniel, M. (1991) Proteins and molecular palaeontology. *Molecules Through Time: Fossil Molecules and Biochemical Systematics*, 381-389.

Ambrose, S. H. (1986) Stable carbon and nitrogen analysis of human diet in Africa. *Journal of Human Evolution* **15**, 707-731.

Ambrose, S. H. (1990) Preparation and characterization of bone and tooth collagen for isotopic analysis. *Journal of Archaeological Science* **17**, 431-451.

Ambrose, S. H. (1991) Effects of diet, climate and physiology on nitrogen isotope abundances in terrestrial foodwebs. *Journal of Archaeological Science* **18**, 293-317.

Ambrose, S. H. & DeNiro, M. J. (1986) Reconstruction of African human diet using bone collagen carbon and nitrogen isotope ratios. *Nature* **319**, 321-324.

Ambrose, S. H. & DeNiro, M. J. (1989) Climate and habitat reconstruction using stable carbon and nitrogen isotope ratios of collagen in prehistoric herbivor teeth from Kenya. *Quaternary Research* **31**, 407-422.

Ambrose, W. (1970) Freeze-drying of swamp degraded wood. in *Proceedings of the 1970 IIC Conference on Waterlogged Wood.*

Andersen, S. R. & Geertinger, P. (1984) Bog bodies investigated in the light of forensic medicine. *Journal of Danish Archaeology* **3**, 111-119.

Anderson, P. & Elliot, J. C. (1993) Scanning microradiography. *Microscopy & Analysis* **34**, 29-31.

Anderson, S., Bankier, A. T., Barrell, B. G., de Bruijn, M. H. L., Coulson, A. R., Drouin, J., Eperon, I. C., Nierich, D. P., Roe, B. A., Sanger, F., Schteier, P. H., Smith, A. J. H., Staden, R. & Young, I. G. (1981) Sequence and organisation of the human mitochondrial genome. *Nature* **290**, 457-465.

Antoine, S. E., Dresser, P. Q., Pollard, A. M. & Whittle, A. W. R. (1988) Bone chemistry and dietary reconstruction in prehistoric Britain: examples from Wessex. Science in Archaeology (Proceedings of a conference on the application of scientific techniques to archaeology, Glasgow, September 1987), British Archaeological Reports **196** (Slater, E. A. & Tate J. O. ed.), 369-380.

Armstrong, W. D. & Singer, L. (1965) *Clinical Orthopaedics* **38**, 179.

Ascenzi, A. M., Brunori, M., Citro, G. & Zito, R. (1985) Immunological detection of haemoglobin in bones of ancient Roman times and of Iron Age and Neolithic Ages. *Proceedings of the National Academy of Sciences* **82**, 7170-7172.

Ascher, R. (1968) Time's Arrow and the archaeology of a contemporary community. In *The Weathering and Performance of Building Materials*, ed. J. W. Simpson & P. J. Horrobin, Medical and Technical Publishing, Aylesbury 1-40.

Atkins, P. W. (1982). *Physical Chemistry*. 2nd edition. Oxford University Press.

Bada, J. L. (1982) The racemization of amino acids in nature. *Interdisciplinary Science Reviews* **7**, 30-460.

Bada, J. L. (1985) Amino acid racemization dating of fossil bones. *Annual Reviews of Earth and Planetary Science* **13**, 241-268.

Bada, J. L. (1987) Palaeoanthropological applications of amino acid racemization of fossil bones and teeth. *Anthrop. Anz.* **45**, 1-8.

Bada, J. L. (1991) Amino acid cosmogeochemistry. *Molecules Through Time: Fossil Molecules and Biochemical Systematics*, 349-358.

Bada, J. L., Gillespie, R., Gowlett, J. A. J. & Hedges, R. E. M. (1984) Accelerator mass spectrometry radiocarbon ages of amino acid extracts from Californian palaeoindian skeletons. *Nature*, **312**, 442-444.

Bada, J. L., Herrmann, B., Payan, I. L. & Man, E. H. (1989) Amino acid racemization in bone and the boiling of the German Emperor Lothar I. *Applied Geochemistry* **4**, 325-327.

Badone, E. & Farquhar, R. M. (1982) Application of neutron activation analysis to the study of element concentration and exchange in fossil bones. *Journal of Radioanalytical Chemistry* **69**, 291-311.

Baker, J. & Brothwell, D. R. (1980) *Animal Diseases in Archaeology*. Academic Press.

Bakker, R. T. (1974) Experimental and fossil evidence for the evolution of tetrapod bioenergetics. In *Perspectives in Biophysical Ecology*. (Gates, D. & Shmerl, R. eds.) 365-399. Springer-Verlag, New York.

Barkman, L. (1975) The preservation of the warship Wasa. in Problems in the conservation of waterlogged wood, Nat. *Maritime Museum Monograph No. 16.*

Bartley, M. H., Arnold, J. S., Haslam, R. K. & Jee, W. S. S. (1966) the relationship of bone strength and bone quantity in health, disease and ageing. *Journal of Gerontology* **21**, 517-521.

Bartsiokas, A. & Middleton, A. P. (1992) Characterization and dating of recent and fossil bone by X-ray diffraction. *Journal of Archaeological Science* **19**, 63-72.

Battaglia, D. (1985) An investigation into the biomechanics and structure of archaeological bone. Unpublished dissertation, University of York.

Behrensmeyer, A. K. & Hill, A. P. (1980) *Fossils in the Making: Vertebrate Taphonomy and Palaeoecology*. University of Chicago Press

Bell, L. S. (1990) Paleopathology and diagenesis: an SEM evaluation of structural changes using backscattered electron imaging. *Journal of Archaeological Science* **17**, 85-102.

Bennike, P. & Ebbesen, K. (1986a) The bog finds from Sigersdal: human sacrifice in the Early Neolithic. *Journal of Danish Archaeology* **5**.

Bennike, P., Ebbesen, K. & Bender Jorgensen, L. (1986b) Early Neolithic skeletons from Bolkilde Bog, Denmark. *Antiquity* **LX**.

Berne, R. M. & Levi, M. N. (1990) *Principles of Physiology: International Student Edition.* Wolfe Publishing Limited, U.S.A.

Bigi, A., Foresti, E., Gregorini, R., Ripamonti, A., Roveri, N. & Shah, J. S. (1992) The role of magnesium on the structure of biological apatites. *Calcified Tissue International* **50**, 439-444.

Binford, L. R. (1981) *Bones: Ancient Men and Modern Myths*. Academic Press.

Bishop, A. C. (1972) *An Outline of Crystal Morphology*, London.

Blumenthal, N. C., Betts, F. & Posner, A. S. (1975) Effect of carbonate and biological macromolecules on the formation and properties of hydroxyapatite. *Calcified Tissue Research* **18**, 81-90.

Boddington, A. (1987) From bones to population: the problem of numbers. *in Death Decay and Reconstruction* (ed. Boddington A., Garland, A. N. & Janaway, R. C.). Manchester, 180-197.

Bohn, H. L., McNeal, B. L. & O'Connor, G. A. (1985). *Soil Chemistry*. John Wiley.

Bowie, S. H. U. & Atkin, D. (1956) An unusually radioactive fish from Thurso, Scotland. *Nature* **177**, 487-488.

Boyde, A., Maconnachie, E., Reid, S. A., Delling, G. & Mundy, G. R. (1986) Scanning electron microscopy in bone pathology: rewiew of methods, potentials and applications. *Scanning Electron Microscopy* **IV**, 1537-1554.

Brain, C. K. (1981) *The Hunters or the Hunted: An Introduction to African Cave Taphonomy*. University of Chicago Press.

Briggs, D. E. G. (1992) Conodonts: a major extinct group added to the vertebrates. *Science* **256**, 1285-1286.

Brothwell, D. R. (1968) *The skeletal biology of earlier human populations*, Pergamon.

Brothwell, D. R. (1969) The palaeopathology of pleistocene and more recent animals. in *Science in Archaeology* (Brothwell, D. R. & Higgs, E. eds) London, 310-314.

Brothwell, D. R. (1972) *Digging up Bones*. London.

Brothwell, D. R. & Higgs, E. (1969) (eds) *Science in Archaeology*. London.

Brown, W. E. (1966) Crystal growth of bone mineral. *Clinical Orthopaedics* **44**, 205-220.

Brunaur, S., Emmett, P. H. & Teller, E. J. (1938) Adsorption of gasses in multimolecular layers. *Journal of American Chemical Society* **60**, 309-319.

Buikstra, J.E., Frankenberg, S., Lambert, J. B. & Xue, L. (1989) Multiple elements: multiple expectations. in *The Chemistry of Prehistoric Human Bone*, (ed. Douglas T. Price). Cambridge, 155-210.

Bunn, M., (1985) Saran as a treatment for bone. in *Bone, Antler, Ivory and Horn: UKIC Occasional Paper*.

Burstein, A. H., Zika, J. M., Heiple, K. G. & Klien, L. (1975) Contribution of collagen and mineral to the elastic-plastic properties of bone. *Journal of Bone and Joint Surgery* **57A**, 956-961.

Burr, D. B. (1980) The relationships among the physical, geometrical and mechanical properties of bone, with a note on the properties of non-human primate bone. *Yearbook of Physical Anthropology* **23**, 109-146.

Cano, R. J., Poinar, H. N., Pieniazek, N. J., Acra, A. & Poinar, G. O. (1993) Amplification and sequencing of DNA from a 120-135-million-year-old weevil. *Nature* **363**, 536-358.

Carter, D. R. & Hayes, W. C. (1977) The compressive behaviour of bone as a two phase porous structure. *Journal of Bone and Joint Surgery* **59**, 954-962.

Casey, C. E. & Robinson, M. F. (1984) Some aspects of nutritional trace element research. in, *Metal Ions in Biological Systems* **16**, (ed. Sigel, H.), New York.

Chaplin, R. E. (1975) *The Study of Animal Bones from Archaeological Sites*, London.

Charters, S., Evershed, R. P., Heron, C. and Goad, L. J. (1991) Chemical analysis of organic residues in ancient pottery; methodological guidelines and applications. *Organic Residues in Archaeology; Their Identification and Analysis.* Proceedings of the conference organised by the U.K.I.C., Archaeology Section held at York, May 10th 1990. (Robert White & Hazelle Page eds.) Published by U.K.I.C.

Chen, T & Yuan, S. (1988) Uranium series dating of bones and teeth from Chinese Palaeolithic Sites. *Archaeometry* **30**, 59-76.

Child, A. M. & Pollard, A. M. (1990) Microbial attack on collagen. *Archaeometry* **90**, 617-625.

Child, A. M. & Pollard, A. M. (199) A review of the applications of immunochemistry to archaeological bone. *Journal of Archaeological Science* **19**, 39-47.

Chisholm, B. S. (1989) Variation in diet reconstruction based on stable carbon isotopic evidence. in *The Chemistry of Prehistoric Human Bone*, (ed. Douglas T. Price). Cambridge, 10-37.

Christensen, B. B., (1970) Developments in the treatment of waterlogged wood in the National Museum of Denmark during the years 1962-69.in *Proceedings of the 1970 IIC Conference on Waterlogged Wood.*

Clark, J. G. D. (1954) *Excavations at Star Carr.* Cambridge University Press.

Collins, M. J., Muyzer, G., Westbroek, P., Curry, G. B., Sandberg, P. A., Xu, S. J., Quinn, R. & MacKinnon, D (1991) Preservation of fossil biopolymeric structures: conclusive immunological evidence. *Geochimica et Cosmochimica Acta* **55**, 2253-2257.

Connolly, R. C., Evershed, R. P., Embery, G., Stanbury, J. B., Green, D., Beahan, P. & Shortall, J. B. (1986) The chemical composition of some body tissues, in *Lindow Man: The Body in the Bog.* (I. M. Stead, J. B. Bourke & Don Brothwell eds.).

Cornwall, I. W. (1974) *Bones for the Archaeologist.* London.

Currey, J. D. (1959) Differences in the tensile strength of bone of different histological types. *Quarterly Journal of Microscopical Science* 103, 111-122.

Currey, J. D. (1969) The mechanical consequences of variation in the mineral content of bone. *Journal of Biomechanics* **2**, 1-1.

Currey, J. D. (1970) *Animal Skeletons.* Edward Arnold, London.

Currey, J. D. (1984) *The Mechanical Adaptations of Bones.* Princeton University Press.

Currey, J. D. (1988) The effect of porosity and mineral content on the Young's modulus of elasticity of compact bone. *Journal of Biomachanics* **21**(2), 131-139.

Dalcusi, G., LeGeros, R. Z., Heughebaert, M & Barbieux, I. (1990) Formation of carbonate -apatite crystals after implantation of calcium phosphate ceramics. *Calcified Tissue International* **46**, 20-27.

Dallemagne, M. J. (1942) *These d'Agregation.* University of Liege.

Dallemagne, M. J. & Richelle, L. J. (1973) Inorganic chemistry of bone, in *Biological Mineralization.* (I. Zipkin, ed.). Wiley & Sons.

Damon, P. E., Donahue, D. J., Gore, B. H., Hatheway, A. L., Jull, A. J. T., Linick, T. W., Sercel, P. J., Toolin, L. J., Bronk, C. R., Hall, E. T., Hedges, R. E. M., Housley, R., Law, I. A., Perry, C.,

Bonani, G., Trumbore, S., Woelfli, W., Ambers, J. C., Bowman, S. G. E., Leese, M. N. & Tite, M. S. (1989) Radiocarbon dating of the Turin Shroud. *Nature* **337**, 611-615.

Day, M. H. & Molleson, T. I. (1973) The Trinil femora. *Human Evolution*, **XI**, 127-154.

de Jong, W. I. (1926) La substance minerale dans les os. *Recueil des Travaux Chimiques des Pays Bas* **45**, 445-448.

de Vries, H. & Oakley, K. P. (1959) Radiocarbon dating of the Piltdown skull and jaw. *Nature* **184**, 224-226

Dennison, K. J. (1980) Amino acids in archaeological bone. *Journal of Archaeological Science* **7**, 81-86.

Drury, R. A. B. & Wallington, E. A. (1980) *Carleton's Histological Technique*, 5th ed., Oxford.

Dyer, J. R. (1965) *Applications of Absorption Spectroscopy of Organic Compounds.* Foundations of Modern Organic Chemistry Series. Prentis-Hall, U. S. A.

Eanes, E.D., Termine, J. D. & Nylen, M. (1973) An electron microscope study of the formation of amorphous calcium phosphate and its transformation to crystalline apatite. *Calcified Tissue Research* **12**, 143-158.

Eastoe, J. E. (1960) Bone - The structure of a biological microcosm. *Journal of the Dental Association ofSouth Africa* **15**(10), 313-321.

Eastoe, J. E. & Eastoe, B. (1954) The organic constituents of mammalian compact bone. *Biochemical Journal* **57**, 453-459.

Edward, J., Fossey, J. M. & Yaffe, L. (1984) Analysis by neutron activation of human bone from the Hellenistic cemetery at Asine, Greece. *Journal of Field Archaeology* **II**, 37-46.

Efremov, I. A. (1940) Taphonomy: a new branch of palaeontology. *Pan-Am. Geol.* **74**, 81-93.

El-Kammar, A., Hancock, R. G. V. & Allen, R. O. (1989) Human bones as archaeological samples: changes due to contamination and diagenesis. *Archaeological Chemistry.* Published by the American Chemical Society.

Ellam, D. (1985a) Wet bone: the potential for freeze-drying. Unpublished thesis, Institute of Archaeology University of London, 1985.

Ellam, D. (1985b) Wet bone: the potential for freeze-drying. in *Bone, Antler, Ivory,and Horn: U K I C Occassional Paper.*

Elliott, T. A. & Grime, G. W. (1993) Examining the diagenetic alteration of human bone material from a range of archaeological burial sites using nuclear microscopy. *Nuclear Instruments and Methods in Physics Research* **B77**, 537-547.

Elster, H., Gil-Av, E. & Weiner, S. (1991) Amino acid racemization of fossil bone. *Journal of Archaeological Science* **18**, 605-617.

Enlow, D. H. & Brown, S. O. (1956) A comparative histological study of fossil and recent bone tissues. Part I. *The Texas Journal of Science* **8**(4), 405-443.

Enlow, D. H. & Brown, S. O. (1957) A comparative histological study of fossil and recent bone tissues. Part II. *The Texas Journal of Science* **9**(2), 186-214.

Enlow, D. H. & Brown, S. O. (1958) A comparative histological study of fossil and recent bone tissues. Part II. *The Texas Journal of Science* **10**(2), 187-230.

Ericson, J. E., West, M., Sullivan, C. H. & Krueger, H. W. (1989) The development of maize agriculturein the Viru valley, Peru. in *The Chemistry of Prehistoric Human Bone*, (ed. Douglas T. Price). Cambridge, 68-104.

Evershed, R. P. (1990) Lipids from samples of skin from seven Dutch bog bodies: preliminary report. *Archaeometry* **32**, 139-153.

Evershed, R. P. (1991) Bog body lipid taphonomy., in Archaeological Sciences 89 (P. Budd, B. Chapman, C. Jackson, R. Janaway & B. Ottaway eds) Oxbow Books, Oxford, 352-361.

Evershed, R. P. (1992) Chemical composition of a bog body adipocere. *Archaeometry* **34 2**, 253-266.

Evershed, R. P. (1993) Biomolecular archaeology and lipids. *World Archeaeology* **25**, 74-93.

Evershed, R. P. & Connolly, R. C. (1988) Lipid preservation in Lindow Man. *Naturwissenschaften* **75**, 143-145.

Evershed, R. P., Heron, C. & Goad, L. J. (1990) Analysis of organic residues of archaeological origin by high temperature gas chromatography and gas chromatography/mass spectrometry. *Analyst* **115**, 1339-1342

Evershed, R. P., Heron, C. Charters, S., & Goad, (1992) The survival of food residues in buried potsherds, new methods of analysis, interpretation and application. *Proceedings of the British Academy* **77**, 187-208.

Fischer, C. G., Ediger, R. D. & Delaney, J. R. (1981) An Automatic Sequential Multielement ICP Emission Spectrometer. *American Laboratory* **13**(2), 346-354.

Fisher, I., St. J. (1986). Pyrite replacement of mollusc shells from the Lower Oxford Clay (Jurassic) of England. *Sedimentology* **33**: 575-585.

Fleisch, H. (1964) Role of nucleation and inhibition in calcification. *Clinical Othopaedics* **32**, 170-180.

Francillon-Vieillot, H., de Buffrenil, V., Castanet, J., Geraudie, J., Meunier, F. J., Sire, J. Y., Zylberberg, L. & de Ricqles, A. (1990) *Microstructure and Mineralization of Vertebrate Skeletal Tissues*. In, Skeletal Biomineralization: Patterns, Processes and Evolutionary Trends. (ed. Joseph J. Carter).

Francis, M. D. & Webb, N. C. (1971) Hydroxyapatite formation from a hydrated calcium monohydrogen phosphate precursoe. *Calcified Tissue Research* **6**(4), 335-342.

Garland, A. N. (1987) A histological study of archaeological bone decomposition. *in Death Decay and Reconstruction* (ed. Boddington A., Garland, A. N. & Janaway, R. C.). Manchester, 109-126.

Garland, A. N. (1989) Microscopical analysis of fossil bone, *Applied Geochemistry* **4**, 215-229.

Garlick, J. D. (1971) Buried bone: The experimantal approach in the study of nitrogen content and blood group activity. *Science in Archaeology, 2nd edition*,(Don Brothwell & Eric Higgs eds.). Thames & Hudson, 503-510.

Gassman, T. (1911) quoted in: Dallemagne, M. J. & Richelle, L. J. (1973) Inorganic chemistry of bone, in *Biological Mineralization*. (I. Zipkin, ed.). Wiley & Sons.

Gillard, R. D., Pollard, A. M., Sutton, P. A. & Whittaker, D. K. (1990) An improved method for age at death determination from the measurement of D-aspartic acid in dental collagen. *Archaeometry* **32**(1), 61-70.

Giraud-Guille, M. M. (1988) Twisted plywood architecture of collagen fibrils in human compact bone osteons. *Calcified Tissue International* **42**, 167-180.

Glemser, M. S. (1963) Palaeoserology. in *Science in Archaeology. 1st edition* (Don Brothwell & Eric Higgs eds.) London, 437-446.

Glimcher, M. J. (1976) Composition, structure and organization of bone and other mineralized tissues and the mechanism of mineralization. *Handbook of Physiology-Endocrinology* 7, 25-116.

Glimcher, M. J. (1984) Recent studies on the mineral phase in bone and its possible linkage to the organic matrix by protein-bound phosphate bonds. *Philosophical Transactions of the Royal Society of London*, series B **304**, 479-508.

Glimcher, M. J., Hodge, A. J. & Schmitt, F. O. (1957) Macromolecular aggregation states in relation to mineralization: the collagen-hydroxyapatite system as studied in vitro. *Proceedings of the National Academy of Sciences of the United States of America* (New York), **43**, 860-867.

Glimcher, M. J. & Krane, S. M. (1968) The organization and structure of bone and the mechanism of calcification, in *Treatise on Collagen. Biology of Collagen* (ed. Ramachandran, G. N. & Gould, B. S.) Academic Press, New York.

Golenberg, E. M., Gianassi, D. E., Clegg, M. T., Smiley, C. J., Durbin, M., Henderson, D. & Zurawski, G. (1990) Chloroplast DNA sequences from a Miocene Magnolia species. *Nature* **344**, 656-658.

Gordon, J. E. (1983) *The New Science of Strong Materials: or Why You Don't Fall Through the Floor*. 2nd ed. Pelican, Middlesex.

Graf, W. (1949) Preserved histological structures in Egyptian and ancient Swedish skeletons. *Acta Anatomica* **8**, 236-250.

Grattan, D. W., (1981) A practical comparative study of treatments for waterlogged wood, Part II: The effect of humidity on treated wood. in *Proceedings of the ICOM Waterlogged Wood Working Group Conference, Ottowa*, 1981.

Gray, H. (1992) *Gray's Anatomy, 15th ed.* (ed. Pick, T. P. & Howden, R.)

Green, L. R. (1992) Low-fired ceramics and H_2S. *Museums Journal*, November 1992, 36.

Grün, R. & Stringer, C. B. (1991) ESR dating and the evolution of humans. *Archaeometry* **33 2**, 153-200.

Grupe, G. & Piepenbrink, H. (1989) Impact of microbial activity on trace element concentrations in excavated bones. *Applied Geochemistry* **4**, 293-298.

Grupe, G., Piepenbrink, H. & Schoeninger, M. J. (1989) Note on microbial influence on stable carbon and nitrogen isotopes in bone. *Applied Geochemistry* **4**, 299.

Hackett, C.J. (1981) Microscopical focal destruction (tunnels) in exhumed human bones. *Medicine, Science and the Law* **21**(4), 243-265.

Hagelberg, E. & Clegg, J. B. (1991a) Isolation and characterization of DNA from archaeological bone. *Proceedings of the Royal Society of London* B **244**, 45-50.

Hagelberg, E., Bell, L. S., Allen, T., Boyde, A. Jones, S. J. & Clegg, J. B. (1991b) Analysis of ancient bone DNA: techniques and applications. *Molecules Through Time: Fossil Molecules and Biochemical Systematics*, (G. Eglington & G. B. Currey eds) 399-407.

Hagelberg, E., Gray, I. E. & Jeffreys, A. C. (1991) Identification of the skeletal remains of a murder victim by DNA analysis. *Nature, London* **352**, 427-429.

Hagelberg, E., Sykes, B. & Hedges, R. E. M. (1989) Ancient bone DNA amplified. *Nature, London* **342**, 485.

Halstead, L. B. (1974) *Vertebrate Hard Tissues.* Wykeham Science Series, London.

Ham, A. W. & Leeson, T. S. (1961) *Histology*, 4th ed., Philadelphia & Montreal.

Hanson, D. B. & Buikstra, J. E. (1987) Histomorphological alteration in buried human bone from the Lower Illinois Valley: implications for palaeodietary research. *Journal of Archaeological Science* **14**, 549-563.

Hardy, R. & Tucker, M. (1988) X-ray powder diffraction of sediments. in *Techniques of Sedimentology* (Maurice Tucker ed.) Blackwell. Oxford, 191-228.

Hare, P. E. (1988) Organic geochemistry of bone and its relation to the survival of bone in the natural environment. in *Fossils in the Making* (Behrensmeyer & Hill eds), 208-222.

Hare, P. E. & Estep, M. L. F. (1983) Carbon and nitrogen isotopic composition of amino acids in modern and fossil collagens. *Carnegie Institution of Washington Yearbook* **82**, 410-414.

Hare, P.E., Fogel, M. L., Stafford , T. W. Jr. Mitchell, A. D. & Hoering, T. C. (1991) The isotopic composition of carbon and nitrogen in individual amino acids isolated from modern and fossil proteins. *Journal of Archaeological Science* **18**, 277-292.

Hassan, A. A. & Ortner, D. J. (1977) Inclusions in bone material as a source of error in radiocarbon dating. *Archaeometry* **19**(2), 131-135.

Hassan, A. A., Termine, J.D. & Haynes , C. V. Jr. (1977) Mineralogical studies on bone apatite and their implications for radiocarbon dating. *Radiocarbon* **19**(3), 364-374.

Haynes, V. (1968) Radiocarbon: analysis of inorganic carbon of fossil bone and enamel. *Science* **161**, 687-688

Hedges, J. W. (1982) An archaeodemographical perspective on Isbister. *Scottish Archaeological Review* **1**(1), 5-20.

Hedges, J. W. (1984) *Tomb of the Eagles: A Window on Stone Age Tribal Britain.* London, 174-200.

Hedges, R. E. M. & Law, I. A. (1989) The radiocarbon dating of bone. *Applied Geochemistry* **4**, 249-253.

Henning, W., Bell, W. A., Billquist, P. J., Glagola, B. G., Kutchera, W., Liu, A., Lucas, H. F., Paul, M., Rehm, K. E. & L'Yntema, J. (1987) Calcium-41 concentration in terrestrial materials: prospects for dating Pleistocene samples. *Science* **236**, 725-727.

Herring, G. M. (1973) The Mucosubstances in Bone, in *Biological Mineralization.* (ed. Zipkin, I). Wiley & Sons.

Higuchi, R., Bowman, B., Freiberger, M., Ryder, O. A. & Wilson, A. C. (1984) DNA sequences from the quagga, an extinct member of the horse family. *Nature, London* **312**, 282-284.

Higuchi, R., von Beroldingen, C. H., Sensabaugh, G. F. & Erlich, H. A. (1988) DNA typing from single hairs. *Nature* **332**, 543-546.

Hodge, A. J. & Petruscka, J. A. (1963) Recent studies with the electron microscope on ordered aggregates of the tmacromolecule. in, *Aspects of Protein Structure* (ed. Ramachandran, G. N.,) Academic Press, New York, 289-300.

Hondros, G. (1959) The evaluation of Poisson's ratio and the modulus of elasticity of materials of a low tensile resistance by the Brazilian (indirect tensile) test with particular reference to concrete. *Australian Journal of Applied Science* **10**, 243-268.

Horai, S., Gojobori, T. & Matsunaga, E. (1987) Mitochondrial DNA polymorphism in Japanese. II. analysis with restriction enzymes of six base pair recognition. *Human Genetics* **68**, 324-332.

Horai, S., Hayasaka, K., Hirayama, K., Takenaka, S. & Pan, I.-H. (1991) Mitochondrial DNA polymorphisms in three Japanese populations. in *Proceedings of Circum-Pacific Prehistory Conference, Seattle, 1989.*

Horai, S., Hayasaka, K., Murayama, K., Wate, N., Koike, H. & Nakai, N. (1989) DNA amplification from ancient human skeletal remains and their sequence analysis. *Proceedings of Japan Academy* **65**, 229-233.

Horowitz, L. K. & Goldberg, P. (1989) A study of Pleistocene and Holocene hyena coprolites. *Journal of Archaeological Science* **16**, 71-94.

Howie, F. M. P. (1984) Materials used for conserving fossil specimens since 1930: a review. *Adhesives and Consolidants Preprints, IIC 1984 Paris Congress*, 92-98.

Hue, E. (1907) *Musée Osteologique-étude de la faune Quaternaire. Osteometrie des mammifères.* I-II. Paris, Schleicher frères.

Hughes, M. A., Jones, D. S. & Connolly (1986) Body in the bog, but no DNA. *Nature* **323**, 208.

Iijima, M., Tohda, H., Suzuki, H., Yanagisawa, T. & Moriwaki, Y. (1992) Effects of F^- on apatite-octacalcium phosphate intergrowth and crystal morphology in a model system of tooth enamel formation. *Calcified Tissue International* **50**, 357-361.

Ikeya, M. & Miki, T. (1980) Electron spin resonance dating of animal and human bones. *Science* **207**, 977-979.

Issachenko, B. L. (1929). 'Zur frage der biogenischen bildung des pyrits'. *Int. Rev. Gesamten Hydrobiol. Hydrogr.* **22**, 99-101.

Jowsey, J. (1973) Autoradiographic and microradiographic studies of bone, in *Biological Mineralization.* (ed. Zipkin, I.). Wiley & Sons, 297-333.

Junqueira, L. C., Carneiro, J. & Long, J. A. (1986) *Basic Histology: 5th edition.* Appleton-century-Crofts, Conneticut.

Katzenberg, M. A. (1989) *Chemical Analysis of Prehistoric Human Bone from Five Temporally Distinct Populations in Southern Ontario.* National Museum of Man, Mercury Series. Ottowa: Archaeological Survey of Canada, Paper 129.

Keeley, H. C. M., Hudson, G. E. & Evans, J. (1977) Trace element contents of human bones in various states of preservation: 1. The soil silhouette. *Journal of Archaeological Science* **4**, 19-24.

Kemp, T. S. (1982) *Mammal-like Reptiles and the Origin of Mammals.* Academic Press, Oxford.

Konta, J. (1956) Regularly-oriented growth of two phosphates in the scales of Permian fishes (Palaeoniscidae). *Casopis pro Mineralogii a Geologii* **1**, 15.

Koob, S. (1984) The consolidation of archaeological bone. *Adhesives and Consolidants Preprints, IIC 1984 Paris Congress*, 98-102.

Kruose, H.R. & McCready, R.G.L. (1979). 'Reductive reactions in the sulfur cycle', in . *Biochemical Cycling of Mineral Forming Elements* (P.A. Trudinger & D.J. Swaine eds) Elsevier: 315-368.

Lafontain, R. H. and Wood, P. A., (1982) The stability of ivory against relative humidity fluctuations. *Studies in Conservation* **27**, 109-117.

Laidlaw, R. A., (1970) The dimensional stabilization of timber. in *Proceedings of the 1970 IIC Conference on Waterlogged wood.*

Lambert, J. B., Liang, X. & Buikstra, J. E. (1991) Inorganic analysis of excavated human bone after surface removal. *Journal of Archaeological Science* **18**, 363-383.

Lambert, J. B., Simpsom, S. V., Buikstra, J. E. & Hanson, D. (1983) Electron microprobe analysis of elemental distribution in excavated human femurs. *American Journal of Physical Anthropology* **62**, 409-423.

Lambert, J. B., Simpson, S. V., Weiner, S. G. & Buikstra, J. E. (1985). Induced metal ion exchange in excavated human bone *Journal of Archaeological Science* **12**, 85-92.

Lambert, J. B., Simpson, S. V., Szpunar, C. B. & Buikstra, J. E. (1985) Bone diagenesis and dietary analysis. *Journal of Human Evolution* **14**, 477-482.

Lambert, J. B., Szpunar, C. B. & Buikstra, J. E. (1979) Chemical analysis of excavated human bone from Middle and Late Woodland sites. *Archaeometry* **21**, 115-129.

Lambert, J. B., Vlask, S. M., Thometz, A. C. & Buikstra, J. E. (1982) A comparative study of the chemical analysis of ribs and femurs in Woodland populations. *American Journal of Physical Anthropology* **59**, 289-294.

Lambert, J.B., Simpson, S. V., Szpunar, C. B. & Buikstra, J. E. (1984) Copper and barium as dietary discriminants: the effects of diagenesis. *Archaeometry* **26**(2), 131-138.

Lee-Thorpe, J. & van der Merwe, N. J. (1991) Aspects of the chemistry of modern and fossil biological apatites. *Journal of Archaeological Science* **18**, 343-354.

Lees, S, Bonar, L. C. & Mook, H. A. (1984) A study of dense mineralized tissue by neutron diffraction. *International Journal of Biological Macromolecules* **6**, 321-326.

LeGeros, R., Balmain, N. & Bonel, G. (1987) Age-related changes in mineral of rat and bovine bone. *Calcified Tissue International* **41**, 137-144.

Legge, A. J. & Rowley-Conwy, P. A. (1988) *Star Carr Revisited.* London.

Leitner-Wild, E. & Steffan, I. (1993) Uranium-series dating of fossil bones from Alpine caves. *Archaeometry* **35**(1), 137-146.

Liboff, A. R. & Shamos, M. H. (1973) Solid state physics of bone. in *Biological Mineralization.* (I. Zipkin, ed.). Wiley & Sons.

Love, L. G. (1965). 'Micro-organic material with diagenetic pyrite from the Lower Proterozoic Mount Isa shale and carboniferous shale'. *Proceedings of the Yorkshire Geological Society* **35**, 187-202

Love, L. G. (1965). 'Micro-organic material with diagenetic pyrite from the Lower Proterozoic Mount Isa shale and carboniferous shale'. *Proceedings of the Yorkshire Geological Society* **35**, 187-202

Lowenstein, J. M. & Scheuenstuhl, G. (1991) Immunological methods in molecular palaeontology, in *Molecules Through Time: Fossil Molecules and Biochemical Systematics*, (G. Eglinton & G. B. Curry eds), The Royal Society, London, 375-380.

Luff, R. M. (1984) *Animals remains in archaeology.* Shire Archaeology Series.

MacGregor, A. G. & Currey, J. D. (1983) Mechanical properties as conditioning factors in the bone and antler industry of the 3rd to the 13th century A.D. *Journal of Archaeological Science* **10**, 71-77.

Macko, S. A. & Engel, M. H. (1991) Assessment of indigeneity in fossil organic matter: amino acids and stable isotopes. *Molecules Through Time: Fossil Molecules and Biochemical Systematics.* The Royal Society, 367-374.

MacCleod, I.D. (1989). Electrochemistry and conservation of iron in sea water. *Chemistry in Australia* **56**(7): 227-229.

MacCleod, I .D. & Kenna, C. (1991). Degredation of archaeological timbers by pyrite: oxidation of iron and sulphur species. *Proc. 4th ICOM Group on Wet Organic Archaeological Materials Conf., ICOM*, 133-142.

Manchester, K. (1986) Tuberculosis and leprosy in antiquity: an interpretation. *MASCA Journal* **4**, 1, 22-30.

Manchester, K. (1987) Skeletal evidence for health and disease. *in Death Decay and Reconstruction* (Boddington A., Garland, A. N. & Janaway, R. C. eds.). Manchester, 163-179

Manjo, G. (1975) *The Healing Hand: Man and Wound in the Ancient World.* Harvard University Press, London.

Mann, S. (1992) Bacteria and the Midas touch. *Nature* **357**, 358-360.

Manskaya, S. M. & Dorozdova, T. V. (1968) *Geochemistry of Organic Substances.* Pergamon Press.

Marchiafava, V., Bonucci, E. & Ascenzi, A. (1974) Fungal osteoclasia: a model of dead bone resorption. *Calcified Tissue Research* **14**, 195-210.

Marlow, M. & Winter, C. (1991) Kitchen chemistry? The use of microwaves in the analysis of human bone. *Proceedings of the Archaeological Sciences Conference, Bradford, 20-22 September 1989.* Oxbow Books.

Maron, S. H. & Prutton, C. F. (1972) Principles of Physical Chemistry, 4th Edition. Macmillan. New York.

McConnell, D. (1973) *Apatite, its Chrystal Chemistry, Mineralogy, Utilization and Geological and Biological Occurances.* Springer-Verlag, New York.

McGregor, A. (1980) *Skeletal materials.* Unpublished M. Phil. thesis, University of Durham.

Mehmel, M. (1930) quoted in: Eastoe, J. E. (1960) Bone - The structure of a biological microcosm. *Journal of the Dental Association ofSouth Africa* **15**(10), 313-321.

Middleton, R., Fink, D., Klein, J. & Sharma, P. (1989) ^{41}Calcium concentrations in modern bone and their implications for dating. *Radiocarbon* **31**(3)

Moore, K.M., Murray, M. T. & Schoeninger, M. (1989) Dietary reconstruction from bones treated with preservatives. *Journal of Archaeological Science* **16**, 437-446.

Morell, V. Dino DNA: the hunt and the hype. *Science* **261**, 160-162.

Mullins, K. B. (1990) The unusual origin of the polymerase chain reaction. *Scientific American* **262**(4).

Muyzer, G., Sandberg, P., Knapen, M. H. J., Vermeer, C., Collinc, M. & Westbroek, P. Preservation of the bone protein osteocalcin in dinosaurs. *Geology* **20**, 871-874.

Myers, T. P., Voorhies, M. R. & Carter, R. G. (1980) Spiral fractures and bone pseodotools at palaeontological sites. *American Antiquity* **45**, 483-490

Neuman, W. F. & Neuman, M. W. (1953) *Chemical Review* **53**, 1.

Neuman, W. F. & Neuman, M. W. (1958) *The Chemical Dynamics of Bone Mineral*. University of Chicago Press.

Neuman, W. F. & Neuman, M. W. (1973) In the beginning there was apatite, in *Biological Mineralization*. (ed. Zipkin, I.). Wiley & Sons.

Newseley, H. (1989) Fossil bone apatite. *Applied Geochemistry* **4**, 233-245.

Olson, E. C. (1980) Taphonomy: its history and role in community evolution. in *Fossils in the Making* (Behrensmeyer, A. K. & Hill, A. P. eds.), 5-19.

Orly, I., Gregoire, M., Menanteau, J. Heughebeart, M. & Kerebel, B. (1989) Chemical changes in hydroxyapatite biomineral under *in vivo* and *in vitro* biological conditions, *Calcified Tissue International* **45**, 20-26.

Otlet, R. L., Walker, A. J. & Dadson, S. M. (1986) Report on radiocarbon dating of the Lindow Man by AERE, Harwell. in *Lindow Man: the Body in the Bog* (Ian. M. Stead, J. B. Bourke, & Don Brothwell, eds.) British Museum Publications.

Oudermans, T. F. M., Boon, J. J. & Evershed, R. P. (1991) *Tracing vessel use: Mass spectrometry of (food) residues on Prehistoric pottery*, unpublished conference paper, York.

Paabo, S. (1985) Molecular cloning of ancient Egyptian mummy DNA. *Nature, London* **314**, 644-645.

Paabo, S., Gifford, J. A. & Wilson, A. C. (1988) Mitochondrial DNA sequences from a 7,000-year-old brain. *Nucleic Acids research* **16**, 9775-9787.

Paabo, S., Higuch, R. G. & Wilson, A. C. (1989) Ancient DNA and the polymerase chain reaction. *Journal of Biological Chemistry* **264**, 9709-9712.

Parker, R. B. & Toots, H. (1974) Minor elements in fossil bone: Applications to Quaternary studies. *Geological Survey of Wyoming*, 74-77.

Parkington, J. (1991) Approaches to dietary reconstruction in the Western Cape: Are you what you have eaten? *Journal of Archaeological science* **18**, 331-342.

Parry, T. V., Al-Allak, H. M., Russel, G. J. & Woods, J. (1989) The effect of aluminium on the electrical and mechanical properties of BaTiO3 ceramics as a function of sintering temperature. *Journal of Materials Science* **24**, 3478-3482.

Parry, T. V. & Wronski, A. S. (1990) The effect of hydrostatic pressre on transverse strength of glass and carbon fibre-epoxy composites. *Journal of Materials Science* **25**, 3162-3166.

Pate, F. D., Hutton, J.T. & Norrish, K. (1989) Ionic exchange between soil solution and bone: towards a predictive model. *Applied Geochemistry* **4**, 303-316.

Pauwels, F. (1980) Biomechanics of the Locomotor Apparatus: Contributions on the Functional Anatomy of the Locomotor Apparatus. (Maquet & Furlong trans.)

Perinet, G. (1964) Determination par diffraction X de la temperature de cuisson d'un ossement calcine. Application au material prehistorique. *Comptes-rendus des seances de l'Academie des Sciences, Paris* **258**, seance du 20 avril, 4115-4116.

Perinet, G. (1969) Etude cristallographique des ossements brules de la cabane acheuleenne de Lazarett, in Une cabane acheuleenne dans la grotte du Lazaret (Nice). *Memoires de la Societe Prehistorique Francais* **7**, 143-144.

Perinet, G. (1972) Etude cristallographique des ossements brules de la grotte de l'Hortus. *Etudes Quaternaires* **1**, 517-518.

Piekarski, K. (1973) *International Journal of Engineering Science*, **11**, 557-565 (Reference quoted in Vincent 1982).

Piepenbrink, H. (1986) Two examples of biogenous dead bone decomposition and their consequences for taphonomic interpretation. *Journal of Archaeological Science* **13**, 417-430.

Piepenbrink, H. (1989) Examples of chemical changes during fossilization. *Applied Geochemistry* **4**, 273-280.

Piperno, D. & Ciochon, R. (1990) Scratching the surface of evolution. *New Scientist*, 10 November.

Posner, A. S., Fabri, C. & Dallemagne, M. J. (1954) *Biochem. Biophys Acta* **15**, 304.

Posner, A. S. (1969). Chrystal chemistry of bone mineral. *Physiological Review* **49**, 760-792.

Posner, A. S. (1985a) The mineral of bone. *Clinical Orthopaedics* **200**, 87-99.

Posner, A. S. (1985b) The structure of bone apatite surfaces. *Journal of Biomedical Materials Research* **19**, 241-250.

Posner, A. S. (1987) Bone mineral and the mineralization process, in *Bone and Mineral Research*, (W. A. Peck, ed.) Oxford.

Posner, A. S., Fabry, C. & Dallemagne, M. J. (1954) *Biochemical and Biophysical Acta*, **15**, 304.

Price, T. D. (1989a). Bones, chemistry and the human past. in The chemistry of prehistoric human bone. Cambridge University Press.

Price, T. D. (1989b) Bones, chemistry and the human past. in *The Chemistry of Prehistoric Human Bone* (Douglas T. Price ed.). Cambridge, 1-9.

Price, T. D. (1989c) Multi-element studies of diagenesis in Prehistoric bone. in *The Chemistry of Prehistoric Human Bone* (Douglas T. Price ed.). Cambridge, 126-154.

Price, T. D., Schoeninger, M. J. & Armelagos, G. J. (1985) Bone chemistry and past behaviour: an overview. *Journal of Human Evolution* **14**, 419-448.

Probert, M. E. (1983). 'The sorption of phosphate by soils'. in *Soils: an Australian viewpoint.* (Division of Soils, CSIRO) Academic Press. 427-453.

Pye, K., Dickson, J. A. D., Schiavon, N., Coleman, M. L. & Cox, M. (1990). Formation of siderite-Mg-calcite-iron sulfide concretions in intertidal marsh and sandflat sediments, north Norfolk, England. *Sedimentology***37**: 325-343.

Rae, A., Hedges, R. E. M. & Ivanovich, M. (1989) Further Studies for Uranium-series Dating of Fossil bone. *Applied Geochemistry*, **4**, 331-337.

Ramachandran, G. N. and Kartha, G (1954) Nature **174**, 269.

Rey, C., Collins, B., Goehl, T., Dickson, I. R. & Glimcher, M. J. (1989) The carbonate environment in bone mineral: a resolution-enhanced Fourier transform infrared spectroscopy study. *Calcified Tissue International* **45**, 157-164.

Rey, C., Shimizu, M., Collins, B. & Glimcher, M. J. (1990) Resolution-enhanced Fourier transform infrared spectroscopy study of the environment of phosphate ions in the early deposits od a solid phase of calcium phosphate in bone and enamel, and their evolution with age. I: investigations in the ν_4PO_4 domain. *Calcified Tissue International* **46**, 384-394.

Richards, M., Smalley, K., Sykes, B. & Hedges, R. E. M. (1993) Archaeology and genetics: analysing DNA from skeletal remains. *World Archaeology* **25 1**, 18-28.

Ricqles, A. de (1974) Evolution of endothermy. *Evolutionary Theory* **1**, 51-80.

Rosedqvist, A.M., (1975) Experiments in the conservation of waterlogged wood and leather by freeze-drying.Problems in the conservation of waterlogged wood, *National Maritime Museum Monograph No. 16.*

Ross, P. E. (1992) Eloquent remains: trends in molecular archaeology. *Scientific American* **266**(5), 72-81.

Roufosse, A. H., Landis, W. J., Sabine, W. K. & Glimcher, M. J. (1979;) Identification of brushite in newly deposited bone mineral in embryonic chicks. *Journal of Ultrastructure Research* **68**, 235-255.

Roux, W. (1887) Uber eine knochen lebende gruppe von faderpilzen (*Mycelites ossifragus*). *Zeitschr Wiss Zoologic* **45**, 227-254.

Sales, K. D., Robins, G. V. & Oduwole, D. (1989) Electron spin resonance study of bones from the Palaeolithic site at Zhoukoudian, China. *Archaeological Chemistry*. American Chemical Society.

Sansom. I. J., Smith. M. P., Armstrong, H. A. & Smith, M. M. (1992) Presence of the earliest vertebrate hard tissues in conodonts. *Science* **256**, 1308-1311.

Schoeninger, M. J. (1989) Reconstructing Prehistoric human diet. in *The Chemistry of Prehistoric Human Bone* (ed. Douglas T. Price). Cambridge, 38-67.

Schoeninger, M. J., Moore, K. M., Murray, M. L. & Kingston, J. D. (1989) Detection of bone preservation in archaeological and fossil samples. *Applied Geochemistry* **4**, 281-292.

Schrenk, F. & Maguire, J. M. (1988) Actualistic SEM studies on the Makapansgat Limeworks Grey Breccia bone assemblage, Transvaal, South Africa. *Scanning Electron Microscopy in Archaeology. BAR International Series* **452**, 287-301.

Schubert, J. (1955) Radioactive Poisons. *Scientific American* **193**, 35-39.

Breccia bone assemblage, Transvaal, South Africa. *Scanning Electron Microscopy in Archaeology. BAR International Series* **452**, 287-301.

Schubert, J. (1955) Radioactive Poisons. *Scientific American* **193**, 35-39.
Schwarcz, H. P. & Grun, R. (1989) ESR dating of tooth enamel from Prehistoric archaeological sites. *Applied Geochemistry* **4**, 329-330.

Schwarcz, H. P. (1980) Absolute age determination of archaeological sites by Uranium series dating of travertines, *Archaeometry* **22**, 3-24.

Shapiro, I. M. (1973) The lipids of skeletal and dental tissues: Their role in mineralization, in *Biological Mineralization*. (Zipkin. I. ed.) Wiley & Sons.

Shaw, D.J. (1968). *Introduction to Colloid and Surface Chemistry*. Butterworths. London.

Shipman, P., Foster, G., & Schoeninger, M. (1984) Burn bones and teeth: an experimental study of color, morphology, crystal structure and shrinkage. *Journal of Archaeological Science* **11**, 307-325.

Sillen, A & Kavanaugh, M. (1982) Strontium and palaeodietary research: a review. *Yearbook of Physical Anthropology* **25**, 67-90.

Sillen, A. & LeGeros, R. (1991) Solubility profiles of synthetic apatites and of modern and fossil bones. *Journal of Archaeological Science* **18**, 385-397.

Sillen, A. (1989) Diagenesis of the inorganic phase of cortical bone. in *The Chemistry of Prehistoric Human Bone* (ed. Douglas T. Price). Cambridge, 211-229.

Smith, P. R. & Wilson, M. T. (1990) Detection of haemoglobin in human skeletal remains by ELISA. *Journal of Archaeological Science* **17**, 255-268.

Sorokin, Yu. I. (1962). Experimental investigation of bacterial sulphate reduction in the Black Sea using ^{35}S. *Microbiology* **31**, 329-335.

Stamm, A.A., (1944) Surface properties of cellulosic materials. in *Wood Chemistry*, L.E. Wise ed. Reinhold. New York.

Stamm, A.A., (1970) Wood deterioration and its prevention. in *Proceedings of the 1970 IIC Conference on Waterlogged wood.*

Stead, I. M. & Brothwell, D. R. (1986) (ed.) *Lindow Man: The Body in the Bog*. British Museum Publications, London.

Stout, S. D. (1982) The effects of long-term immobilization on the histomorphology of human cortical bone. *Calcified Tissue International* **34**, 337-342.

Stout, S. D. (1983) The application of histomorphometric analysis to ancient human remains. *Anthropos* (Greece) **10**, 60-71. (Reported in Stout 1989).

Stout, S. D. (1989) Histomorphometric analysis of human skeletal remains. in Reconstruction of Life from the Skeleton. (Iscan, M. Y. & Kennedy, A. R. eds.) Alan R. Liss Inc., New York, 41-52.

Stumm, W. & Morgan, J. J. (1970). *Aquatic Chemistry*. John Wiley.

Termine, J. D., Eanes, ,E. D., Greenfield, D. S., Nylen, M. U. & Harper, R. A. (1973) Hydrazine-deproteinated bone mineral: physical and chemical properties. *Calcified Tissue Research* **12**, 73-90.

Termine, J. D. & Posner, A. S. (1966) Infrared Analysis of Rat Bone: Age Dependancy of Amorphous and Crystalline Mineral Components. *Science* **153**, 1523-1525.

Termine, J. D., Kleinman, H. K., Whitson, S. W., Conn, K. M., McGarvey, M. L. & Martin, G. R. (1981) Osteonectin, a bone specific protein linking mineral to collagen. *Cell* **26**, 99-105.

Traub, W. , Arad, T. & Weiner, S. (1989) Three-dimensional ordered distribution of crystals in turkey tendon collagen fibers. *Proceedings of the National Academy of Science, U. S. A.* **86**, 9822-9826.

Trudinger, P. A. & Swaine, D. J. (1979) Biochemical Cycling of Mineral Forming Elements. Elseiver Scientific Publishing.

Tuross, N, Behrensmeyer, A. K. & Eanes, E. D. (1989) Strontium increases and crystallinity changes in taphonomic and archaeological bone. *Journal of Archaeological Science* **16**, 661-672.

Tuross, N. (1989). Albumin preservation in the Taima-taima mastadon skeleton. *Applied geochem*istry **4**: 255-259.

van der Plicht, J., van der Wijk, A. & Barstra, G. J. (1989) Uranium and thorium in fossil bones: activity ratios and dating. *Applied Geochemistry* **4**, 339-342.

van Klinken, G. J. (1989) Note on the isolation of single amino acids from fossil bone. *Applied Geochemistry* **4**, 271.

Vaughan, J. M. (1975) *The Physiology of Bone*. Oxford.

Vincent, J. F. V. (1982) *Structural Biomaterials*. Macmillan Press, London.

von Meyer, H. (1867) *Die Architektur der Spongiosa*. u. Du Bois-Reymond's Archiv 1867, 615.

Vourinen, H. S., Tapper, U. & Mussalo-Rauhamaa, H. (1990) Trace and heavy metals in infants, analysis of long bones from Ficana, Italy, 8-6th Century BC. *Journal of Archaeological Science* **17**, 237-254.

Wainwright, S. A., Biggs, W. D., Currey, J. D. & Gosline, J. M. (1976) *Mechanical Designs in Organisms*. Wiley, New York.

Wakely, J., Manchester, K. & Roberts, C (1989) Scanning electron microscope study of normal vertebrae and ribs from early medieval human skeletons. *Journal of Archaeological Science* **16**, 627-642.

Waller, R. (1987) An experimental ammonia gas treatment method for oxidised pyritic mineral specimens. *Natural History Conservation, ICOM Committee for Conservation, 1987.*

Watkins, W. M. (1966) Blood-group substances. *Science* **152**, 172-181.

Watkins, W. M., Zarnitz, M.L. & Kabat, E. A. (1962) Development of H activity by human blood-group B substance treated with coffee bean a-galactosidase. *Nature* **195**, 1204-1206.

Watson, J. (1981) 'The application of freeze-drying on British hardwoods from archaeological excavations'. *Proeedings of ICOM Waterlogged Wood Working Group Conference*,237-242

Watson, J. (1984) 'Research into aspects of freeze-drying hardwoods between 1982 and 1984'. *Proceedings of 2nd ICOM Waterlogged Wood Working Group Conference*, 213-218.

Wedl, C. (1864) Ueber einen im zahnbein und knochen keimenden pilz. *Mineral. Biol. Erdkunde* **50**, 171-193.

Weiner, S. & Bar-Yosef, O. (1990) States of preservation of bones from Prehistoric sites in the near east. *Journal of Archaeological Science* **17**, 187-196.

Weiner, S., Arad, T. & Traub, W. (1991) Crystal organization in rat bone lamellae. *Federation of European Biochemical Societies, Letters* **285**, 1, 49-54.

Weiner, S. & Traub, W. (1992) Bone structure; from ångstroms to microns. *FASEB Journal* **6**, 879-885.

Wells, C. (1964) *Bones. Bodies and Disease*. London, Thames and Hudson.

Wells, C. (1967) Pseudopathology, in *Diseases in Antiquity*. (Ed. Brothwell, D. & Sandison, A.T.) Springfield, Ill. Charles C. Thomas, 5-19.

Wessen, G., Ruddy, F. H. Gustafson, C. E. & Irwin, H. (1978) Trace element analysis in the characterization of archaeological bone, in *Archaeological Chemistry II*, Advances in Chemistry Series No. 171 (ed. Carter, G. F.) Washington DC: American Chemical Society, 99-108.

White, E. M. & Hannus, L. A. (1983) Chemical weathering of bone in archaeological soils. *American Antiquity* **48**(2).

Wilby, P. (1992) As easy as getting blood from a stone. *New Scientist* 22 February, 1992; short report by Dave Martill.

Williams, C. T. (1988) Alteration of chemical composition of fossil bones by soil processes and groundwater. In (G. Gruppe ed.) *Trace Elements in Environment History*. Berlin: Springer-Verlag, 27-40.

Williams, C. T. & Potts, P. J. (1988) Element distribution maps in fossil bones. *Archaeometry* **30**, 237-247.

Wolff, J. (1892) *Das Gesetz der Transformation der Knochen*. Berlin.

Woodhead-Galloway, J. (1980) *Collagen: the Anatomy of a Protein*. The Institute of Biology's, Studies in Biology no. 117. London.

Yamada, H. (1970) *Strength of biological materials*. Waverly Press.

Yokoyama, Y., Quagebeur, J.-P., Bibron, R., Leger, C. Chappaz, N., Michelot, C., Shen, G.-J. & Nguyen, H.-V. (1983) ESR dating of stalagmites of the Caune de l'Arago, the Grotte de Lazarete, the Grotte du Vallonnet and the Abri Pie Lombard: a comparison with the U-Th method. *PACT* **9**, 381-389.

Young, J. Z. (1975) *Life of Mammals*, 1st ed. Clarendon Press, Oxford.

Zajic, J. (1969). *Microbial Biochemistry*, Academic Press.

Zivanovic, S. (1982) *Ancient Diseases: the Elements of Palaeopathology* (trans. Lovett F.) Edwards. London.

ZoBell, C.E. (1961). Importance of microrganisms in the sea. *Proc. Low Temp. Microbiol. Symp., Camden, N.J.*

Zymela, S., Schwartz, H. P., Grun, R., Stalker, A. M. & Churcher, C. S. (1988) ESR dating of Pleistocene fossil teeth from Alberta and Saskatchewan. *Canadian Journal of Earth Sciences* **25**, 235-245.